To the Graduate Council:

I am submitting herewith a thesis written by Steven J. Pawel entitled "The Sensitization Behavior of Cast Stainless Steels Subjected to Weld Repair." I have examined the final copy of this thesis for form and content and recommend that it be accepted in partial fulfillment of the requirements for the degree of Master of Science, with a major in Metallurgical Engineering.

E. Eugene Stansbury

E. Eugene Stansbury, Major Professor

We have read this thesis
and recommend its acceptance:

Accepted for the Council:

L Evans Roth

Vice Chancellor
Graduate Studies and Research

THE SENSITIZATION BEHAVIOR OF CAST STAINLESS STEELS SUBJECTED TO WELD REPAIR

A Thesis

Presented for the

Master of Science

Degree

The University of Tennessee, Knoxville

Steven J. Pawel

June 1983

DEDICATION

This thesis is dedicated to my family and friends, particularly the author's fellow graduate students. Without their support, research of this type is not possible.

ACKNOWLEDGEMENTS

The author would like to express his deep gratitude to his major professor, Dr. E. E. Stansbury, for his patience, guidance and support throughout the course of this research. Thanks are also extended to Dr. C. D. Lundin for his technical guidance and interest.

Financial support provided by research grants from the Steel Founders' Society of America and through teaching assistantships from the Department of Chemical, Metallurgical and Polymer Engineering are gratefully acknowledged.

The author is grateful to the departmental electronic shop led by Mr. Ted A. Long, Sr. and his efficient group, Mr. Stephen A. Steiner, Mr. Ronald L. Johnson and Mr. Michael R. Neal, for their work maintaining the corrosion lab equipment and heat treatment facilities.

Thanks are also extended to the departmental machine shop led by Mr. H. B. Thompson and his staff, Mr. Raymond Bellamy, Mr. Jack French, and Mr. Doug Fielden for their help with assorted sample preparations.

Special thanks are due to Mr. Bob L. McGill for his help with the scanning electron microscopy and to Mr. Albert W. J. Carter and Mrs. Aileen Cagle for procuring and distributing many of the materials necessary to this research.

The tireless support of the ladies in the departmental office, Mrs. Sancy Hail, Miss Jennifer Leslie and particularly the author's typist, Mrs. Phyllis Davis, is most gratefully acknowledged.

ABSTRACT

The sensitization behavior of CF and CFM type cast duplex stainless steels has been examined to provide a basis for the evaluation of potential sensitization damage due to weld repair thermal cycles. The major variables in the study include carbon content, ferrite number, molybdenum content (inherent in the choice of casting types) and heat treatment including simulated weld repair thermal cycles.

Two new electrochemical techniques, termed the EPR and JEPR tests, for assessing degree of sensitization (as a result of grain boundary chromium depletion) have been investigated and the results compared with those resulting from the standard oxalic acid etch test. The EPR test provides a sensitive quantitative measure of the degree of sensitization. For example, values for as-cast material exceed those for solution annealed material by approximately three orders of magnitude. Although molybdenum seemed to be the strongest compositional variable governing the EPR response, the test was also sensitive to carbon, chromium and ferrite content as well as heat treatment.

An adaptation of the EPR test, designed to be equally responsive to degree of sensitization but capable of reducing effects of variations in the bulk alloy content, was also investigated. This test, called JEPR, also detected the influence of carbon, chromium and molybdenum as they affected sensitization but not as they affected general passivation characteristics (general passivation controlled by total alloying present). This test indicated that molybdenum

retards carbide formation by indicating Mo bearing alloys are superior to alloys that do not contain Mo for short heat treatments.

The oxalic acid etch test was shown to be a very severe test for cast duplex stainless steels resulting, almost without exception, in etch structures "unacceptable" according to the ASTM standard. This test appears to be capable of providing only limited qualitative differences between low and high levels of sensitization in the cast duplex stainless steels.

Sensitization measurements on samples subjected to thermal cycles simulating weld repair indicate that for some alloys, the requirement of post weld repair heat treatment may be unnecessary from a sensitization standpoint. The effects of energy input (controlling the cooling rate), heat affected zone peak temperature, multiple thermal cycles and strain (simulating weld restraint) were studied. The results indicate that the Mo bearing CFM alloys with carbon contents less than .08% C may be reasonably immune to weld repair sensitization. The CF alloys with intermediate and high ferrite numbers, and with carbon contents less than .06% C, are only slightly sensitized by the simulated weld repair procedures. The low ferrite CF alloys appear to be the most susceptible to sensitization resulting from weld thermal cycles. However, this is at least in part related to a pitting phenomenon observed in these alloys which is not understood.

TABLE OF CONTENTS

LIST OF TABLES

LIST OF FIGURES

FIGURE PAGE

FIGURE PAGE

FIGURE PAGE

FIGURE PAGE

FIGURE PAGE

FIGURE PAGE

FIGURE PAGE

CHAPTER I

INTRODUCTION

Initial Scope of Research

Corrosion resistant stainless steel castings are of major importance to the chemical process industry. Although the large majority of corrosion resistant castings has performed adequately in service, incidences of premature failure occur and are of particular concern because of the enormous costs of unscheduled downtimes and breaks in production.

Based on a survey (1) of the chemical process industry, sensitization and the resultant intergranular corrosion was the cause of over half of the reported incidences of unsatisfactory performance. Sensitization is a process by which the corrosion resistance of stainless steel is dramatically reduced due to the formation of complex chromium carbides and resultant chromium depletion along the grain boundaries of the material. The behavior is typically brought about by inadequate control of the carbon content of the casting or by inadequate heat treatment (improper solution annealing) after casting or weld repair.

ASTM A743 (2) and A744 (3) specify the heat treatments for austenitic and duplex stainless steel castings following weld repair. These specifications define the need for a "post-repair" solution anneal based on the extent of repair necessary but do not state specifically the material composition; rather the specifications incorporate a wide variety of cast grades into single categories as

regards "post-repair" heat treatment needs. These specifications appear to overlook the possible benefits of low carbon grades or stabilized grades in mitigating sensitization. Thus the specifications may be requiring expensive and unnecessary solution heat treatments for some alloy compositions. The solution annealing requirement is a difficult one to meet for many foundries, particularly if the casting is large. In some instances, the casting is so large that heat treatment facilities are not available. Also, in many cases, the quenching stresses may cause such severe distortion that extensive machining may be required after quenching. Whether or not additional machining is required, solution annealing is an expensive, time consuming step.

In order to develop the data base necessary to justify possible alterations to the current specifications, the problem of measurement of sensitization susceptibility is encountered. Sensitization is not currently detectable by standard non-destructive testing techniques so the traditional measure of sensitization susceptibility is weight loss in a hot acid. Standard weight loss tests (ASTM A262 B,C,D) (4) have several disadvantages, foremost among which is the long testing time involved. Also, the tests were developed for wrought materials which have smaller grain sizes than do castings in general. Since the weight loss test is based on grain dropping tendency, the grain size is an important test factor. Large grained materials could be severely attacked intergranularly without dropping grains, which would of course yield an erroneously low sensitization indicator. In addition, these tests are

destructive and thus severely limited in potential for in the field or foundry testing. Another of the A262 tests, the oxalic acid etch test, is commonly used to indicate sensitization susceptibility; it can be non-destructive but is not quantitative (which sometimes makes it difficult to use as a specification).

A new test, called the Electrochemical Potentiokinetic Reactivation (EPR) test, is currently being examined as an ASTM standard and appears particularly promising for evaluation of castings. It is a rapid, quantitative examination of sensitization susceptibility (it basically measures passive film stability--see Literature Review) and its flexibility as a non-destructive test makes it a prime candidate for in the field testing.

A program of research has been pursued to examine the effects of composition and weld repair procedures on the sensitization behavior of cast stainless steels with the objective of accumulating data to evaluate the post-weld repair requirements of ASTM A743/4. The research has utilized the EPR method and a modification of the EPR method as the primary sensitization susceptibility evaluation techniques with the incorporation of other tests as appropriate.

Test Program Outline

The research effort focused on the "workhorses" of the cast stainless steels, i.e., CF and CFM types, which represent the bulk of the cast products now being produced. These alloy types represent the cast equivalents of AISI 304 and 316, respectively, for which much data are available in the literature on both wrought

material and weld metals concerning sensitization behavior. The only major compositional difference between CF and CFM type castings is the addition of about 2% Mo in the CFM types; thus this choice of material types inherently examined molybdenum as a major compositional variable.

Carbon content and ferrite content were also considered to be significant variables regarding sensitization. Accordingly, carbon contents spanning the common production range (.02 - .08% C) were examined. At least two ferrite contents at each carbon content were examined--all ferrite contents were selected to correspond to the normal production range (approximately 4-20 FN). Nitrogen content was carefully monitored but not specifically included as a variable.

Welding thermal cycles--corrosion studies were conducted to relate the sensitization behavior of the cast materials to weld repair. Welding conditions (energy input, preheat, interpass temperatures) were chosen to span the range of common industrial repair procedures. The Gleeble heat treatment device was used to simulate the thermal cycles seen by the heat affected zone during weld repair. The peak temperature(s) of the heat affected zone were chosen to reflect the sensitization temperature range anticipated to cause the maximum chromium carbide precipitation effect. The influence of strain on sensitization was evaluated to assess the significance of weld contraction/restraint on sensitization. Further, the influence of multiple thermal cycles representing multipass repair or multiple repairs was addressed.

The sensitization susceptibility developed during various isothermal holds in the classical sensitization temperature range (500 - 900°C) was also examined to develop a more fundamental understanding of the process of sensitization and the capability of the new corrosion tests that will be utilized with the practical result of deriving time-temperature-sensitization information for the various cast alloys.

In all of the above evaluation steps careful metallographic examination was carried out using optical and/or scanning electron microscopy (and EDAX) as appropriate.

CHAPTER II

LITERATURE REVIEW

Corrosion resistant, high alloy cast steels, commonly referred to as cast stainless steels, constitute a category of special steels which have grown steadily in technological and commercial importance during the past 40 years. The principal end-use applications for these steels are as materials of construction for chemical processing and power generating equipment involving corrosion service at temperatures normally below about 600°F, but in some instances the service temperature is as high as 1200°F (5).

Nomenclature

The cast stainless steels are most often specified on the basis of composition according to the classification system used by the Alloy Casting Institute (ACI). Briefly, the ACI nomenclature is as follows. The first letter of the alloy designation, either a "C" or an "H", denotes whether the casting is intended for corrosion service or heat resistant (high temperature) service respectively. The second letter of the designation indicates the nominal chromium-nickel type where generally the "A" level represents the highest Cr/Ni ratio (actually the lowest Ni level) and the "Z" level represents the lowest Cr/Ni ratio. The Cr/Ni ratio does not change linearly from the "A" designation to the "Z" designation but it is a general trend. Following the first two letters is a number that represents the maximum carbon content of the alloy in hundredths of a

weight percent. Any letter or letters that follow the carbon content indicate the presence of special alloying elements--the most common of these is the letter "M" indicating the addition of molybdenum to the alloy.

The CF grades constitute the most technologically important and highest tonnage segment of corrosion-resistant casting production (5). This grade is a 19Cr-9 Ni type that is the cast equivalent of AISI 304. (The cast equivalent of 304L would be CF3 by the ACI designation; similarly 304 = CF8, 316 = CF8M, 316L = CF3M, etc.) Although the compositions of the wrought grades and cast equivalents are similar, the differences are not trivial and are intentional to provide a special set of properties.

Properties of Duplex Stainless Steel

The major difference between the wrought AISI alloys and the CF grade counterparts is the end-use microstructure. The AISI wrought materials are fully austenitic alloys and the cast equivalents have a duplex microstructure, i.e., from about 5 - 40% ferrite in an austenite matrix. The reason for the presence of the ferrite is threefold (5): to provide strength, to improve weldability, and to improve resistance to corrosion in certain environments.

The strengthening comes about from the distribution of a second phase within a given matrix and these strength effects have been documented and presented in the literature (5,6). The corrosion resistant stainless steels cannot be hardened by heat treatment and cold working destroys some of the corrosion properties. Strengthening

by carbide precipitation also greatly compromises the corrosion resistance of the alloy. Some typical tensile property values for CF8 and CF8M and their wrought equivalents are shown in Table 1.

Fully austenitic materials typically suffer from a weldability problem termed "hot cracking" to which duplex austenite-ferrite alloys are nearly immune. The duplex alloys also may be less sensitive to sensitization and stress corrosion cracking relative to their single phase counterparts (these subjects discussed in a later section).

The amount of ferrite in the casting is controlled principally by the composition (the balance of austenite stabilizing elements to ferrite stabilizing elements). The major austenite stabilizers are Ni, C, N and Mn and the major ferrite stabilizers are Cr, Si, Mo, and Cb. Schoefer (7) derived a one line constitution diagram for cast stainless steels with the aid of previous work by Schaeffler (8). The diagram (shown in Figure 1) may be used to estimate the average ferrite content of a stainless steel casting from its composition by finding the "Cr equivalent" from the amount of ferrite stabilizers as indicated on the diagram and likewise the "Ni equivalent" from the austenite stabilizers. Within certain overall compositional limits, the Schoefer diagram has proven to be a fairly reliable indicator of average ferrite content. Of course, uncertainty in chemical analysis, prior thermal history (including cooling rate) and segregation during casting are the major sources of error in this approximation.

Table 1. Typical tensile properties of selected stainless steels. (All material in solution annealed condition; CF8/CF8M have approximately 10 vol. % ferrite.)

MATERIAL	Tensile Strength ksi	Tensile Strength MN/m^2	0.2% offset yield ksi	0.2% offset yield MN/m^2	Elongation % in 2"	Young's Modulus psi	Young's Modulus KN/m^2
CF8	77	531	37	255	55	28×10^6	193
CF8M	80	552	42	290	50	28×10^6	193
304	84	579	42	290	50		
316	84	579	42	290	50		

Source: Handbook of Stainless Steels, Peckner, D., and Bernstein, I.M., eds., McGraw-Hill, Inc., (1977).

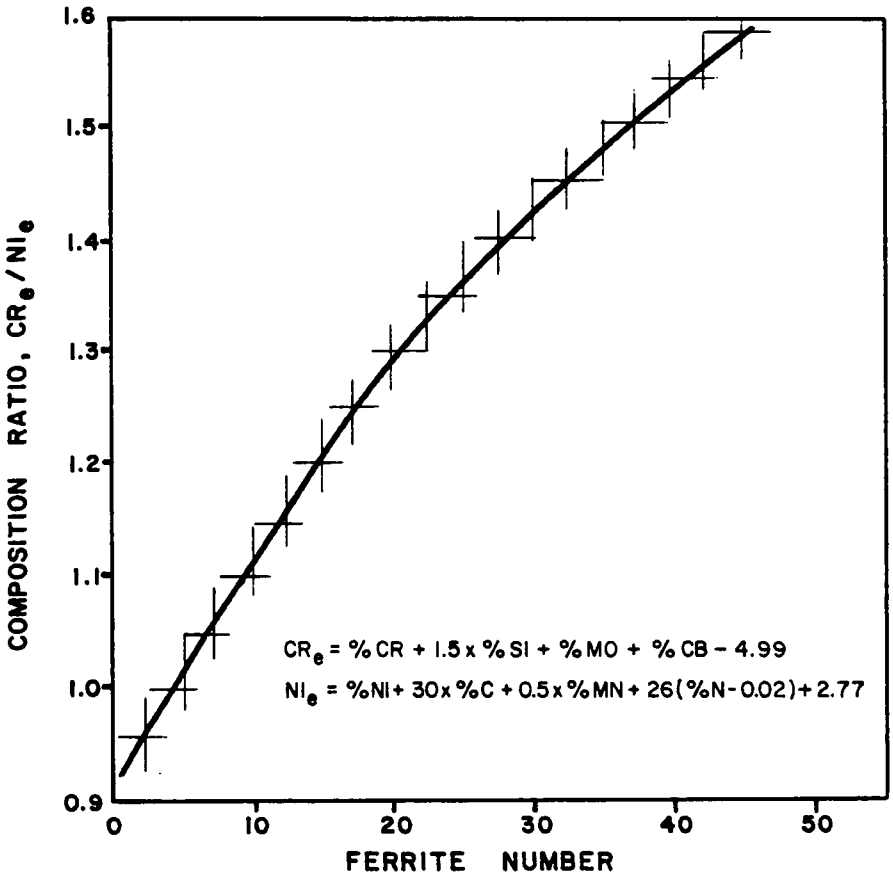

Figure 1. Constitution diagram for stainless steel castings (Schoefer Diagram). Crosshatching indicates uncertainty band.

Source: Schoefer, E., "Appendix to Mossbauer-Effect Examination of Ferrite in Stainless Steel Welds and Castings," Weld. Res. Supp., Vol. 39, p. 10-s, (1974).

Another useful tool for predicting the microstructures of these alloys is of course the phase diagram. Unfortunately, no entirely adequate diagram exists that incorporates all the elements commonly found in a stainless steel. One can, however, obtain constant iron vertical sections of the iron-chromium-nickel system such as those shown in Figure 2. These are pseudo-binary phase diagrams that, although still not exact, represent useful qualitative approximations in many instances. Since the diagrams are representative of equilibrium states, there are questions concerning their applicability to casting and welding. Nevertheless, diagrams of this type are often used in welding or solidification studies (9-13) to help explain the presence, amount and morphology of ferrite in various stainless steel welds and castings. It has been noted (11) that the CF and CFM cast grades have composition ranges that stradle the eutectic reaction in Figure 2a. As a consequence of the chemical segregation and variable cooling and solidification rates within the average casting, these diagrams are of only qualitative value when applied to castings.

Sensitization of Austenitic and Duplex Stainless Steel

The most important aspect of the corrosion behavior of stainless steels is that they derive their corrosion resistance from a chromic oxide type of passive film that is generally less than approximately 100 angstroms thick (14). It is usually considered necessary to have about 12% chromium (14) in the bulk metal substrate in order to have a generally corrosion resistant oxide film. In the absence of this

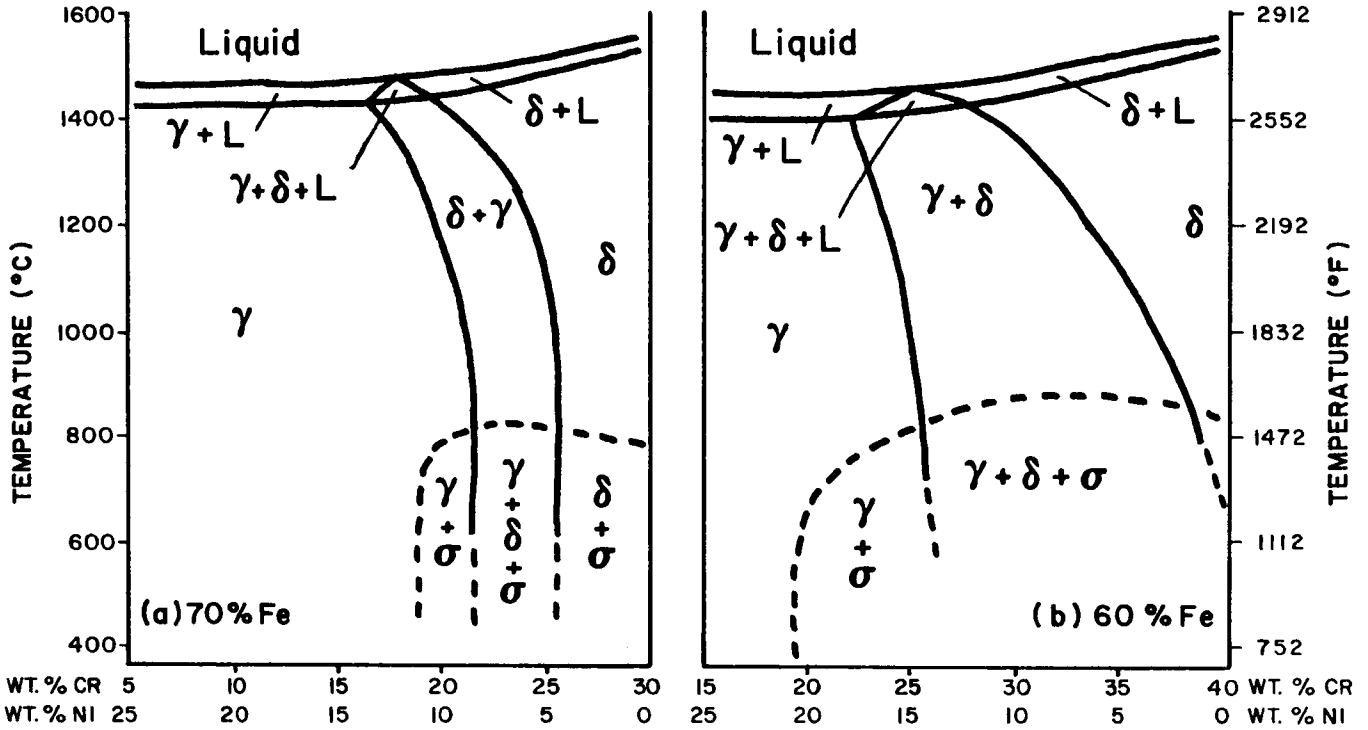

Figure 2. Constant iron vertical sections of the iron-chromium-nickel system for (a) 70% Fe and (b) 60% Fe.

Source: Brooks, J. A., et al., "STEM Analysis of Primary Austenite Solidified Stainless Steel Welds," Metall. Trans. A., Vol. 14A, p. 23, (1983).

film, stainless steels may corrode at very high rates, and this is particularly significant when relatively small areas of passive film have been altered or destroyed. This allows very deep localized attack at the points of film instability as opposed to fairly shallow and uniform general corrosion (attack over the whole exposed surface) if the entire passive film has been destroyed.

Stainless steels and other high alloy materials can become susceptible to selective (localized) attack at the grain boundaries through a process called sensitization. The detailed aspects of this phenomenon vary from alloy to alloy and there are several different theories that attempt to explain sensitization, but in general, typical observations that characterize the intergranular attack in high alloy materials are as follows (15):

1. The time at temperature in the range 500 - 900°C (932 - 1652°F) controls the degree of sensitization. The particular alloy composition controls the temperature at which sensitization occurs most rapidly, but for many alloys, this temperature is 650 - 700°C.
2. A characteristic feature of sensitized alloys is the presence of a complex carbide (usually of a form similar to $(Cr_{.76}\ Fe_{.24})_{23}\ C_6$) at the grain boundaries.
3. There are heat treatments that restore the intergranular corrosion resistance of the alloys, including continued heating at the temperature that initially caused sensitization. This later phenomenon is referred to as healing.

Any theory that attempts to explain sensitization and the resultant intergranular corrosion must explain each of these observations (as well as others).

There are basically three major models that have been proposed to explain sensitization behavior; they are commonly referred to as the chromium depletion theory, the noble carbide theory, and the segregation theory. (A somewhat detailed review of these appears in Reference 15 and was used as an outline for some of the following discussion.) Of these theories, the chromium depletion theory is the oldest and enjoys the widest acceptance within the scientific community. It appears to offer the best explanation to fit the observations although each model is applicable in certain cases. A short description of each follows.

Chromium Depletion Theory

This model (for wrought austenitic stainless steels) was proposed by Bain, Aborn, and Rutherford (16) in 1933 and is based on the generally acknowledged fact that a minimum chromium level (something near 12% Cr) is required to maintain a protective passive film on stainless steels. This theory contends that in the temperature range of 500 - 900°C, complex chromium carbide formation is favorable and that this carbide precipitation takes place (nucleates and grows) most rapidly at the grain boundaries. Figure 3 is an adaption of the now famous schematic representation of the chromium depletion theory. The chromium rich carbide particle may contain up to 90 - 95% Cr whereas the bulk alloy may be only 18 - 20% Cr. Thus, the region immediately adjacent to the carbide particle is depleted

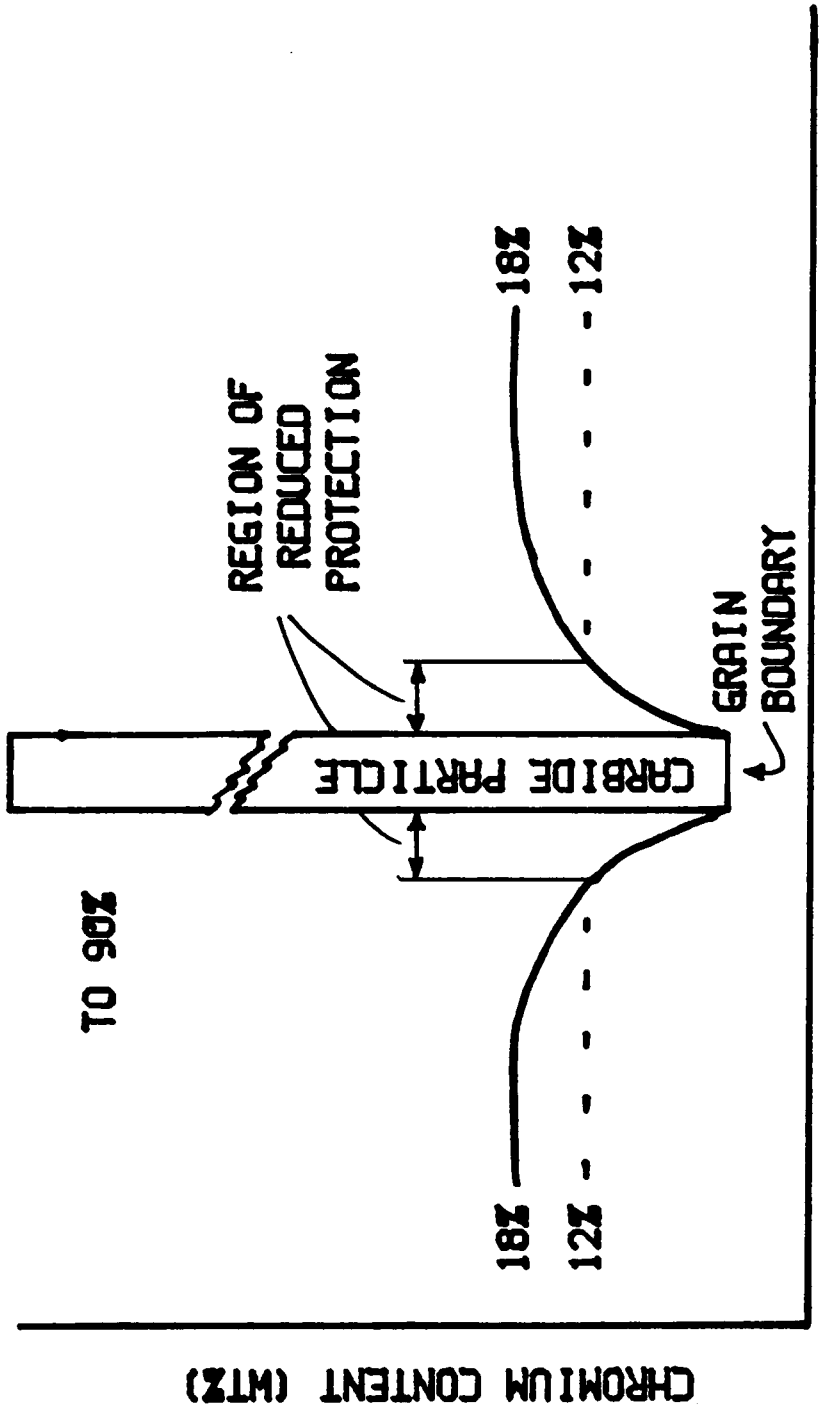

Figure 3. Schematic diagram representing the chromium depletion theory of sensitization.

Source: Bain, E. C., Aborn, R. H., and Rutherford, J. B., "Intergranular Corrosion of Austenitic Stainless Steels," Trans. Am. Soc. Steel Treating, Vol. 21, p. 481, (1933).

in chromium (carbide particle "absorbed" it) and this depletion may be sufficiently advanced to reduce the local chromium concentration to below the level (~12% Cr) required to provide protection. This can lead to intergranular attack if the stainless steel is exposed to a suitable corrosive environment.

The diffusion of chromium is the controlling factor in this scenario. The diffusion of chromium is much slower than the carbon migration rate (rapid interstitial diffusion) in the bulk alloy and only at the grain boundaries (high energy-misfit regions) is the diffusion rate of chromium fast enough to accumulate the necessary amount of chromium to form carbides of up to 95% Cr. The bulk diffusion of chromium is too slow to adequately replenish the amount of chromium in the region immediately adjacent to the carbide particle (grain boundary).

This theory is in excellent agreement with the observed facts about sensitization. The theory predicts that reducing the carbon content of the alloy should reduce sensitization susceptibility (as measured by one of several corrosion tests to be discussed later) as there would be less carbon, fewer carbides, and therefore less chromium depletion in general. Experience and experiments have indeed shown this to be the case. The literature (1,6,14-19) is replete with data that illustrate this behavior very clearly. Figures 4-6 are different example representations of the effect of carbon content on sensitization. Two of these curves indicate that the time required in the carbide formation temperature range to "sensitize" the material increases exponentially as the carbon content is decreased from 0.1% C. From a pragmatic viewpoint, this means that the

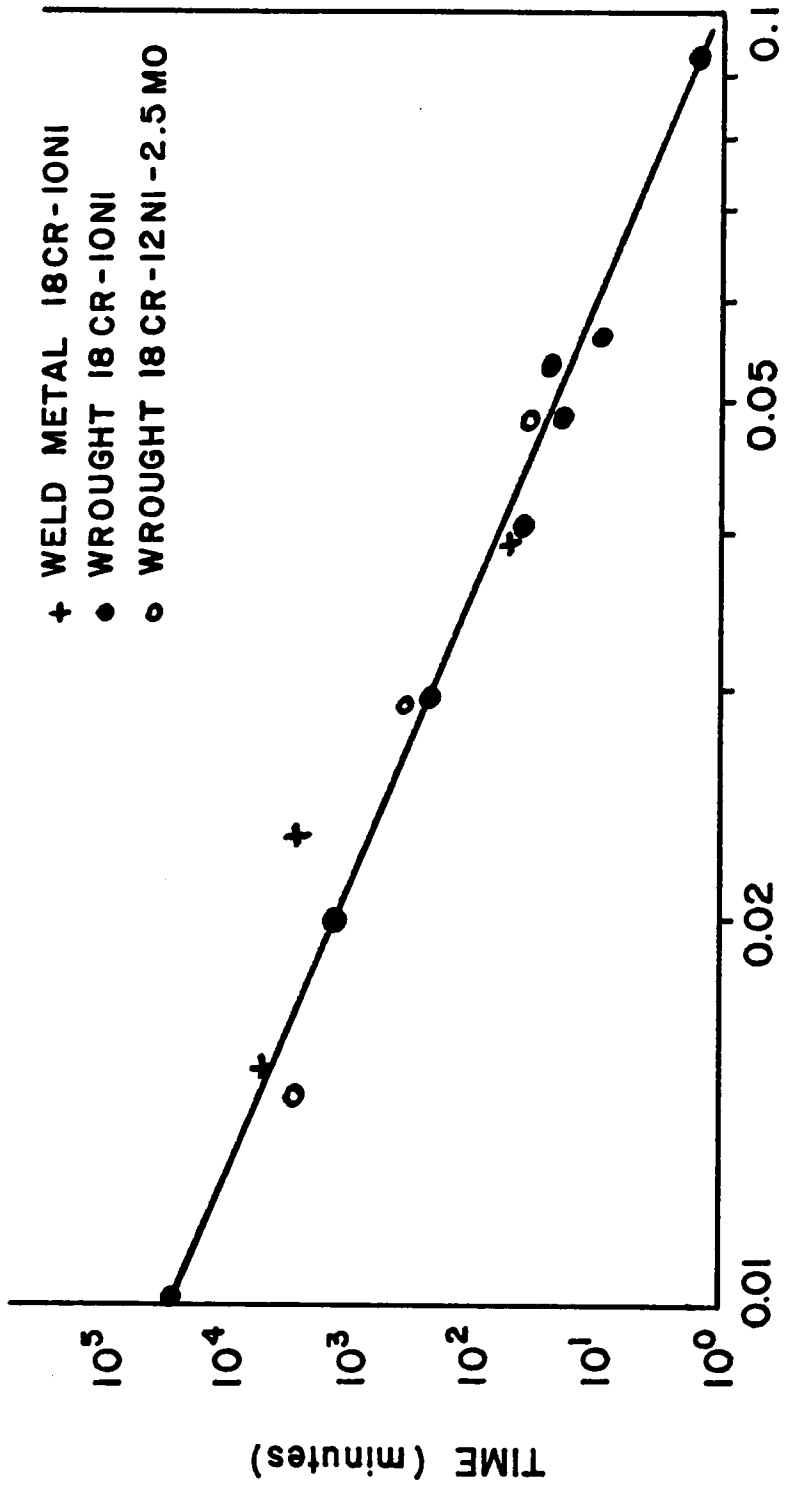

Figure 4. Cumulative time to sensitize at 550 - 750°C as a function of carbon content. (Evaluated by Strauss Test.)

Source: Polgary, S., "Stainless Steel Welding," Metal Construction, Vol. 8, (1976).

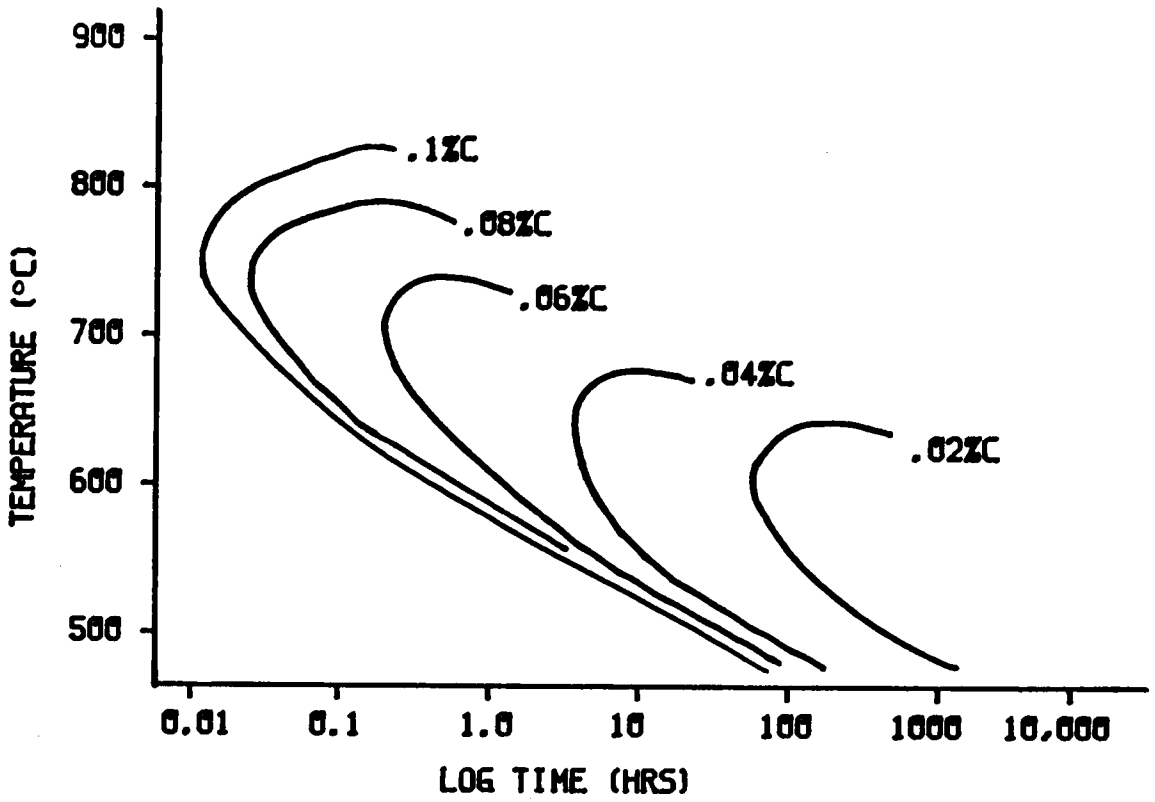

Figure 5. Time-temperature sensitization curves as determined by the Strauss Test for 18Cr-8Ni stainless steel.

Source: Hishida, M., and Nakada, H., "Critical Cooling Rate of 18Cr-8Ni Stainless Steel for Sensitization and Subsequent Intergranular Stress Corrosion Cracking in High Temperature Water," Corrosion, Col. 34, p. 338, (1978).

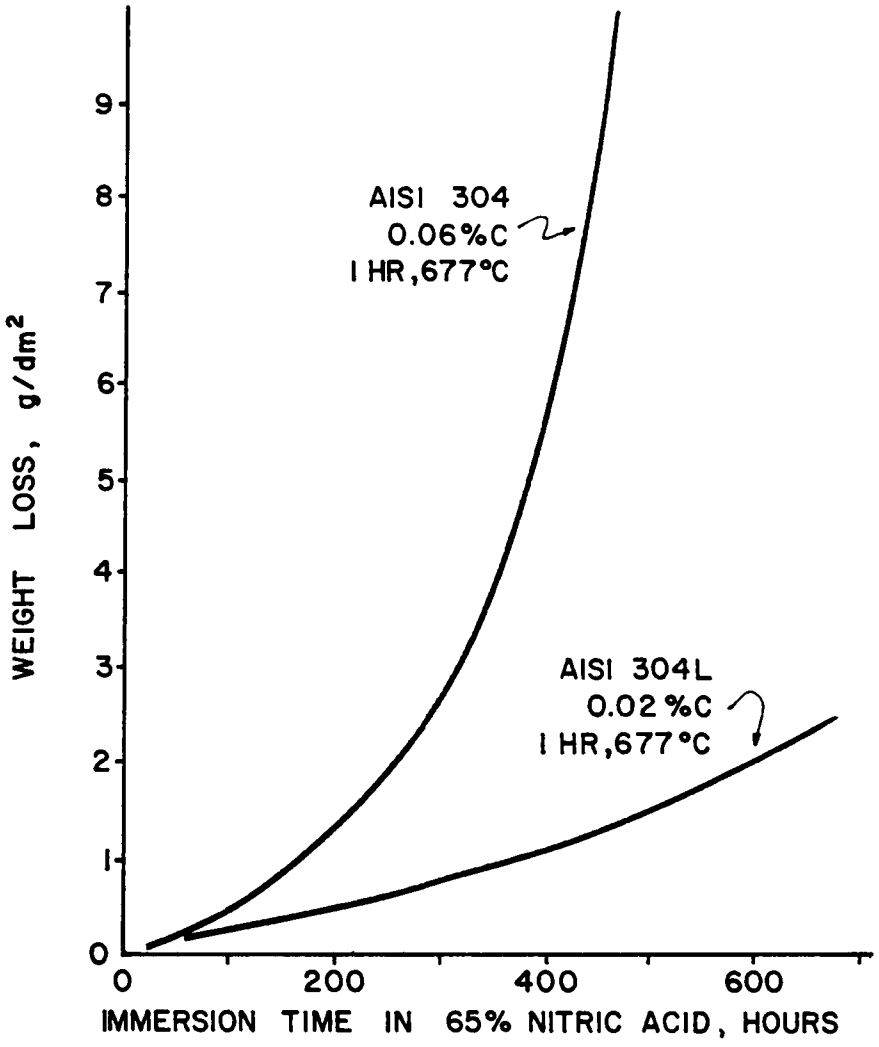

Figure 6. Representative data for corrosion of AISI 304 and 304L in the nitric acid weight loss test.

Source: Streicher, M. A., "Theory and Application of Evaluation Tests for Detecting Susceptibility to Intergranular Attack in Stainless Steels and Related Alloys - Problems and Opportunities," in Intergranular Corrosion of Stainless Alloys, ASTM STP 656, Steigerwald, R. F., ed., p. 3-84, ASTM, (1978).

thermal cycles imposed by welding or post weld heat treatment conditions are less likely to sensitize the material as the carbon content decreases. The trend seems to be that below about .03% C or so, the susceptibility to sensitization has been decreased dramatically (thus the "L" grades of stainless steel). The theory also predicts reduced corrosion rates for increasing the bulk chromium content of the alloy, which has also been shown experimentally (20).

The chromium depletion theory predicts that if the chromium in a carbide particle could be returned to the matrix, the corrosion resistance of the material would return. This is in fact the basis for solution annealing stainless steels after casting, welding or working. Holding at a high temperature (typically 1000 - 1150 °C) dissolves chromium carbides and returns the carbon and chromium to solid solution in the matrix. Water quenching the material from this temperature retains the chromium and carbon in solid solution and there is no chromium depletion. The resulting austenite, however, is supersaturated in carbon (low carbon solubility in austenite) and this supersaturation is the driving force for carbide precipitation in the temperature range 500 - 900 °C.

Also inherent in the chromium depletion theory is the prediction that the addition of "carbon getters" to the alloy, i.e., elements that form carbides more stable than chromium rich carbides, should reduce sensitization by tying up carbon and thus reducing the amount of chromium carbides and the resulting chromium depletion. This has been borne out (6,16,21-23) and is in fact the basis of what is

known as the stabilized grades of stainless steel. Small additions of titanium or columbium are the most common elements added to the alloy to form carbides preferentially over chromium carbides. Figure 7 is a schematic diagram of the relative temperature regions where columbium carbides and chromium carbides are likely to form and it indicates that columbium carbides form at higher temperatures than chromium carbides. This is the basis for "stabilization" heat treatments. Holding a stainless steel containing Cb or Ti (in amounts balanced with the carbon content and appropriate carbide stoichiometry) in the temperature range above 900°C dissolves chromium carbides and forms columbium or titanium carbides such that there is little carbon remaining in solid solution to form chromium carbides upon subsequent exposure to the temperature range 500 - 900°C. (Stabilized stainless steels may fail in an intergranular manner due to a phenomenon called knife-line attack--this will be discussed in a later section.)

Until recently, one of the major criticisms of the chromium depletion theory was that there was no direct evidence of a chromium depleted zone in sensitized materials. A recent investigation (24), using a thin film energy dispersive x-ray analysis coupled to a scanning transmission electron microscope, revealed Cr-depleted zones of the order of 50 - 100 nm in width adjacent to grain boundaries. The authors claim that due to its minute size, no other experimental technique was previously able to detect its presence. Quantitative theoretical calculations (25,26), based on thermodynamics and diffusion models give the width of this zone to be 100 nm or less.

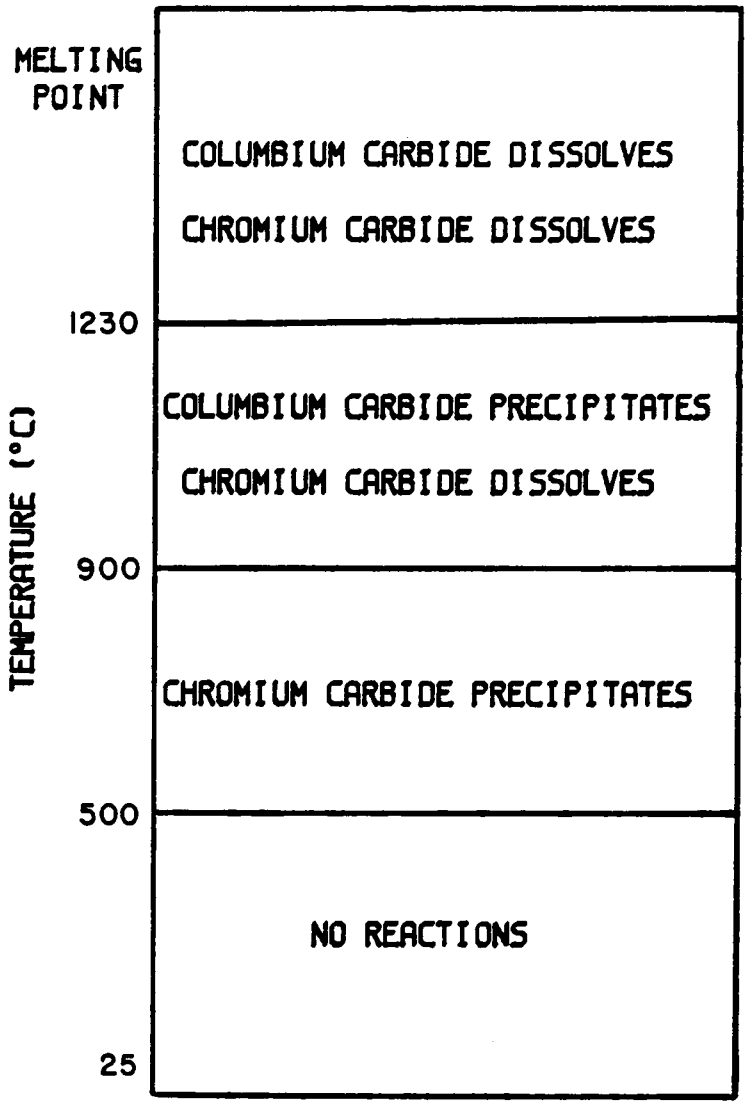

Figure 7. Schematic diagram of stability regions for chromium carbide and columbium carbide.

Source: Cowan, R. L., and Tedmon, C. S., Jr., "Intergranular Corrosion of Iron-Nickel-Chromium Alloys," in Advances in Corrosion Science and Technology, Vol. 3, Fontana, M. G., and Staehle, R. W., eds., Plenum Press, New York, (1973).

These calculations, using Cr-C-$Cr_{23}C_6$ equilibria, showed that the chromium content in the vicinity of carbide particles is a strong function of the temperature and the carbon and alloy content. Actual data and the calculations (Figure 8) show generally good agreement. In addition, one of the treatments (26) also showed that chromium concentrations within the grain boundaries between particles can lead to the irregular or discontinuous type of intergranular corrosion often observed.

These treatments also predict that given a sufficient time at temperatures that initially cause sensitization, the alloy will desensitize, or "heal". (See Figure 9.) This is due to the fact that chromium diffusion from the bulk alloy will eventually replenish the chromium content in the vicinity of the carbides to a protective amount. (Recall that chromium diffusion is slow compared to carbon diffusion and the time required to form carbides at the grain boundaries.) This healing phenomenon has been observed in many instances (20,25,27,28), but typically only after very long heat treatments as indicated schematically in Figure 9.

This particular model also predicts that carbide morphology should not be directly related to sensitization because the mere existence of the carbide particles is sufficient to cause chromium depletion. Studies have been done (29-32) on carbides and their morphologies in sensitized stainless steels that point out that the carbides tend to assume many complex shapes (dendritic, flakelike, geometric) and are very thin (in general). The shapes of the carbides are controlled to a large extent by the location of the precipitation

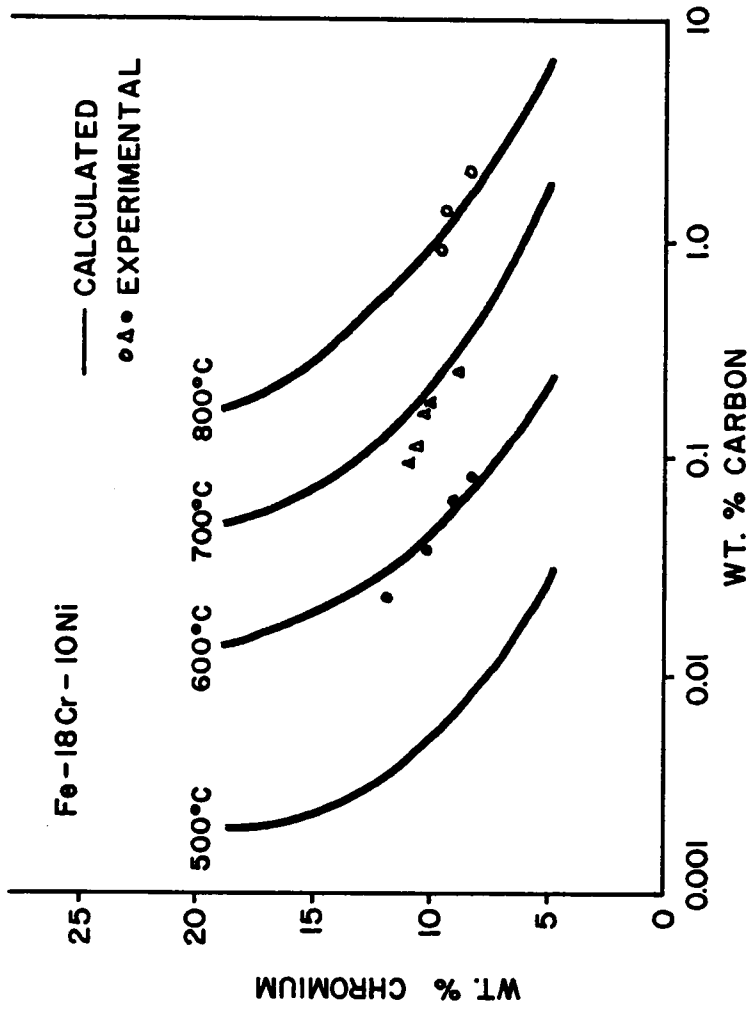

Figure 8. Comparison of Cr-C-$Cr_{23}C_6$ equilibrium data for type 304 stainless steel with experimentally obtained corrosion data.

Source: Stawstrom, C., and Hillert, M., "An Improved Depleted-Zone Theory of Intergranular Corrosion of 18-8 Stainless Steel," J. Iron and Steel Inst., Vol. 207, p. 77, (1969).

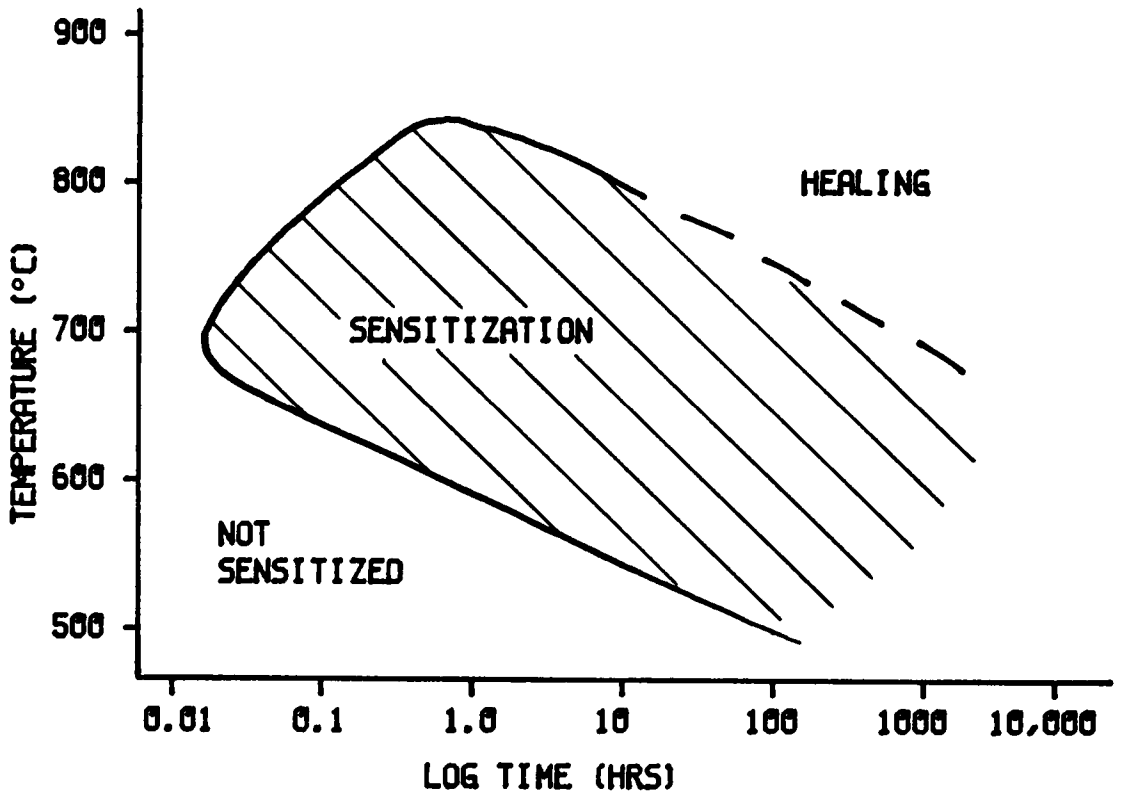

Figure 9. Schematic diagram indicating the approximate onset of healing for many stainless steels.

reaction, i.e., grain boundaries, twin boundaries, etc., as well as the temperature at which the carbides nucleate and grow. (Good review on carbides in Reference 6.) These precipitation sites control the sensitization kinetics as shown in Figure 10. The carbides tend to be in discontinuous particle form at the grain boundaries and of the general composition $(Cr_{\sim.75}\ Fe_{\sim.25})_{23}\ C_6$ or $M_{23}\ C_6$. In the absence of strong carbide forming elements, $M_{23}\ C_6$ is the stoichiometry of the carbides formed (6). When Mo is present, small amounts may substitute for Cr. In support of the chromium depletion theory, the studies by Cihal and Kasova (29) and Mahla and Nielsen (30) have shown that intergranular corrosion was independent of carbide morphology. Their presence was sufficient to cause chromium depletion along the grain boundaries and between the particles along the grain boundary.

In summary, there is much experimental evidence to support the predictions of the chromium depletion theory of sensitization, with no major flaws developing in the theory since its origin 50 years ago.

Noble Carbide Theory

In one study of grain boundary carbides (31), the corrosion data obtained led the authors to state that intergranular corrosion in sensitized austenitic stainless steels could be explained without postulating grain boundary chromium depletion. Stickler and Vinckier (31) observed that good intergranular corrosion resistance was associated with isolated dendritic carbide particles (long sensitization heat treatment or high temperatures) and poor intergranular

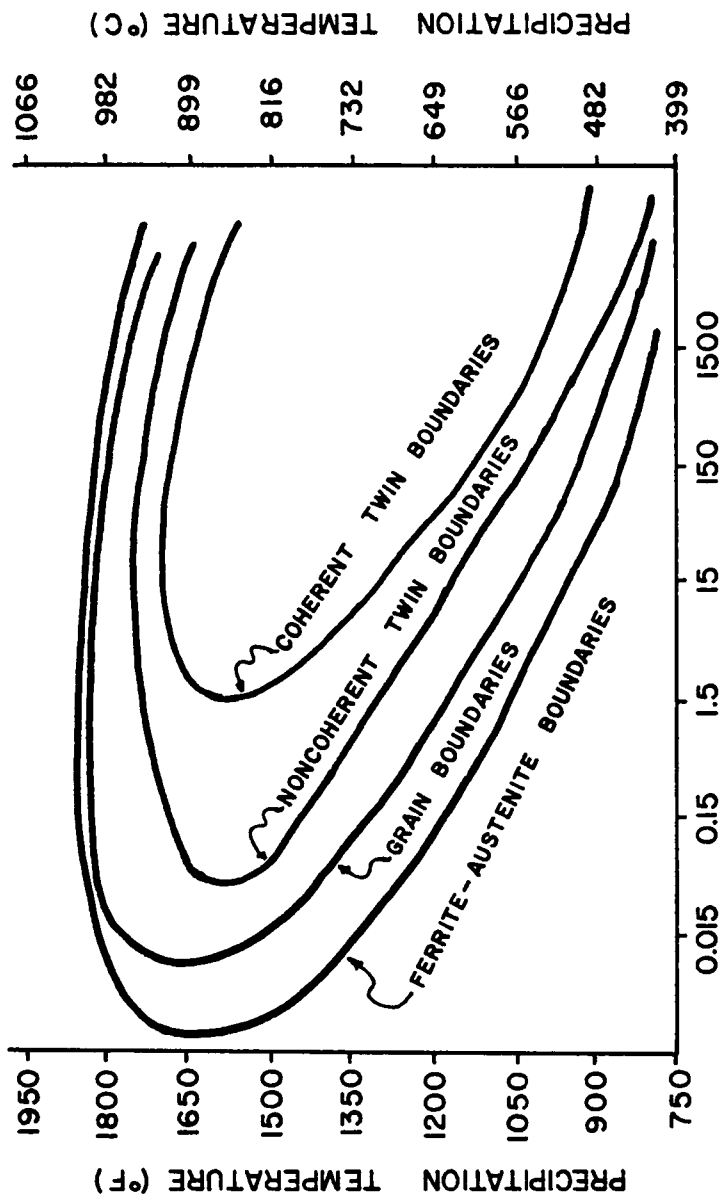

Figure 10. Precipitation kinetics of $M_{23}C_6$ carbide in 18Cr-9Ni stainless steel. (.038% C, quenched from 1260°C.)

Source: Handbook of Stainless Steels, Peckner, D., and Bernstein, I. M., eds., McGraw-Hill, Inc., (1977).

corrosion resistance was associated with sheets of connected particles (short sensitization times or lower temperatures). In both cases, the matrix around the particle was partially dissolved and this indicated an electrochemical corrosion mechanism to the authors. The authors concluded that the carbide particle was noble to the surrounding matrix and this provided for rapid penetration along the grain boundaries when there were continuous carbide sheets at the grain boundaries. No chromium depletion is required by this model. Proof that the carbides were noble to the matrix was the observation that corrosion attack occurred when isolated carbides were brought into contact with solution annealed material. The authors point out that the corrosion process due to this galvanic couple may be accelerated by some degree of residual stress on the matrix as a result of the formation of the particle itself (33). According to the noble carbide theory, the phenomena of healing is explained by their observation that at higher sensitizing temperatures or longer heating times, the carbides become isolated dendrites and continuous corrosion along the grain boundaries can no longer take place.

Among the chief criticisms of the noble carbide theory is that the matrix and the carbide are at the same potential in the passivated state in many aqueous oxidizing environments. Furthermore, it is not always necessary to have a continuous grain boundary precipitate in order to have intergranular corrosion because chromium depletion between particles in the grain boundary may occur as well (20), which could account for the observed corrosion.

Another factor that indicates that the noble carbide theory may not be a valid model in most cases is that it does not explain the

benefit of adding carbide stabilizing elements such as Ti or Cb. In chemically stabilized stainless steels, these "noble" carbides exist and are noble to the metal matrix but do not cause intergranular corrosion. Also, it is interesting to note the work of Gellings and deJongh (34) who attempted an experiment to differentiate between the chromium depletion theory and the noble carbide theory. They postulated that (due to the difficulty of differentiation between these theories by experimentation in an electrolyte solution) the oxidation rate in air at high temperatures would enable them to make a choice between the two theories as the noble carbide theory does not predict an increased oxidation rate along the grain boundaries as does the chromium depletion theory. Their data showed increased oxidation along the grain boundaries where chromium carbides had precipitated in unstabilized stainless steel and no preferential oxidation in stabilized stainless steels. Thus, their experiment supports the chromium depletion theory over the noble carbide theory. In addition, Osozawa, et al. (35) dispute the notion that galvanic coupling between a carbide and the surrounding matrix is responsible for intergranular corrosion based on their potential measurements in a Strauss solution and the fact that their data indicated that the corroded zones in the sensitized material had considerably less chromium than the bulk matrix. At very high potentials ($\geq$1200 mv vs. SHE) they found that the solution annealed material was attacked intergranularly at equivalent or even higher rates than the sensitized material. (Above 1500 mv

vs. SHE, no intergranular attack was noted on sensitized steels.) Their conclusion was that below the transpassive region for these steels, the chromium depletion theory adequately accounted for the intergranular corrosion and that at high potentials, some other mechanism may be coming into play.

It seems then, in general, that the noble carbide theory does not explain as much of the observed data on sensitization as the chromium depletion theory, although it is possible that this mechanism could contribute under certain circumstances.

Segregation Theory

Several corrosive environments are now known (36-39) to cause intergranular corrosion of solution treated stainless steels. To explain this observation, Aust et al. (36) proposed a solute segregation theory that associates the intergranular corrosion observed with a continuous grain boundary path of either second phase or soluble segregate. This model does not attempt to explain the carbide-sensitized case specifically, although the formation of carbides is part of the model. The argument is, however, limited to applicability in highly oxidizing solutions (such as nitric-dichromates) as this is the only type of data available to support this theory.

During high temperature non-sensitizing heat treatments (solution annealing) impurity elements, particularly sulfur, phosphorus and silicon, apparently segregate to grain boundaries as supported by Auger electron spectroscopy (40-41) and microhardness measurements (38,42). Ferrite-austenite boundaries have also been

shown to adsorb sulfur and phosphorus in duplex materials (43). Proponents of this theory contend that the segregation results in a chemical difference type of driving force between the matrix and the grain boundary to support accelerated corrosion. Studies (44) on high purity steels that indicate no preferential grain boundary attack in highly oxidizing solutions tend to support the chemical difference driving force idea as opposed to the contention that grain boundaries preferentially corroded because they are high energy regions. Also, high temperature "stabilizing" treatments (36,42), i.e., a few hours at 800°C to intentionally form isolated carbides at grain boundaries, interrupted the continuity of corrosion attack at the grain boundaries. The investigators (36,42) concluded that the isolated carbides had incorporated or absorbed some of the impurities, leaving behind "clean" grain boundary that was not susceptible to preferential corrosion. Treatments that form continuous networks of carbides (a few hours at 600°C) again promote susceptibility to continuous grain boundary attack, probably due to continuous paths of chromium depletion. If the continuous second phase is sigma, the nature of the corrodent is critical as to whether preferential grain boundary corrosion susceptibility is indicated.

Another major study (Armijo (39)) aimed at the examination of grain boundary susceptibility of solution annealed material showed that the rate of attack (in a solution containing nitric acid and dichromate ions--i.e., very oxidizing) at grain boundaries in 304

is a maximum near 1100°C and decreases with higher or lower temperature treatments. References cited by Armijo (39) suggest that preferential attack of grain boundaries in solution annealed material is due to crystallographic factors or orientation differences between adjacent grains, but Armijo's work indicated that adsorbed impurities were responsible. He explained that low temperature solutionizing (900 - 1000°C) decreased grain boundary susceptibility by the formation of globular carbides or other precipitates that agglomerate many of the adsorbed impurities. At higher temperatures (1300 - 1420°C) the energy of the impurities is too high for a grain boundary site to "trap" the impurity. Near 1100°C, continuous impurity films were postulated to exist. Armijo also found that dislocations also weakly (compared to grain boundaries) absorb impurities.

In conclusion, it appears that although no unanimous agreement has been reached on the chromium depletion theory, it does fit the available experimental observations more readily than any other theory proposed to date. It is possible or even probable that under special conditions a mechanism predicted by some other theory may contribute to the sensitization behavior of austenitic stainless steels, but the chromium depletion theory, as has been shown, has the widest acceptance among the scientific community because it explains the observations the most adequately.

Compositional Factors that Affect Sensitization

So far, the discussion has centered on theories that attempt to explain some of the major observations concerning sensitization in austenitic stainless steels. Aside from the addition of carbide

formers such as Ti and Cb, changing the carbon content and changing the chromium content, there are several ways in which the alloy composition is known to affect the sensitization behavior of austenitic stainless steels. A short review of some other factors that have been found to influence the sensitization behavior in austenitic stainless steels follows.

In general, it appears that 2 - 3% Mo is beneficial with regard to intergranular corrosion resistance (15,45-47) in that it retards carbide formation somewhat. It does, however, promote the formation of sigma phase and in some environments or applications, this could be detrimental.

Increasing the nickel content is usually considered somewhat detrimental to intergranular corrosion resistance as this tends to decrease the solubility of carbon in austenite (15,46), thus promoting carbide formation. Manganese additions appear to behave similarly to nickel additions (Mn has been used as a substitute for Ni during Ni shortages) and in fact slightly increase the nitrogen solubility (46). One effort (47) indicates that additions of Mn for any given carbon content delay sensitization.

It is unclear as to the exact role nitrogen plays in the sensitization behavior of austenitic stainless steels. Nitrogen is typically added to increase the strength of the low carbon stainless steels or as a potent austenitizer to replace Ni. Studies have been done (48) that indicate that nitrogen additions of up to .16% (with .05% C) retard intergranular carbide precipitation. Some data (15) indicates that the maximum nitrogen content that is beneficial is

lower than .16%. This could be due to differences in total (C+N) amounts or other interactions. Work by Briant, et al. (47) showed a profound effect of nitrogen in retarding the onset of sensitization in 304 and 316 type alloys, presumably by simply slowing carbon migration. A similarly large effect of nitrogen in delaying sensitization was found by Akashi, et al. (49). No nitrides have been found in association with the apparent role of nitrogen in delaying sensitization in unstabilized stainless steels. High nitrogen steels cannot be effectively stabilized with Ti or Cb as the nitrogen reacts with these elements to form nitrides and excess carbon could remain to form chromium carbides at lower temperatures (46).

It appears that high silicon levels are also detrimental to intergranular corrosion resistance (15,46). Its tendency to form inclusions and its involvement with segregation to grain boundaries (already discussed) in even non-sensitized stainless steels points to the need to closely control silicon levels.

Sulfur has been shown (50) to have little effect on the intergranular corrosion of type 304 stainless steel, except at very high potentials (highly oxidizing conditions) that have been discussed in relation to the solute segregation theory. Phosphorus likewise has very little effect on intergranular corrosion except in the Huey test (50).

Another way that the composition can greatly alter the sensitization behavior is by allowing the formation of ferrite within the austenite matrix (called a duplex stainless steel). As indicated earlier (6), carbides will form preferentially (faster) on

austenite-austenite grain boundaries within a duplex stainless steel. (In general, austenite within a ferrite matrix is beneficial as well (51,52).) Henthorne (46) reviewed the probable reasons for the beneficial role of ferrite and listed them as follows:

1. The total area of grain boundaries and phase interfaces is increased in the presence of ferrite, thereby reducing the quantity of carbide precipitates per unit area.
2. The ferrite is significantly higher in chromium than is the austenite. Therefore, it can lose chromium to a precipitate and not become sufficiently depleted to be preferentially attacked.
3. Chromium diffuses more readily in ferrite than austenite so there is less chromium depletion.
4. The islands of ferrite present minimize the formation of continuous grain boundary precipitates in the austenite grain boundaries.

Item 4 above was considered to be the most important factor. Other workers (47,48) have found similar benefits of ferrite. Beck, et al. (53) have found ferrite beneficial to intergranular corrosion resistance for CF3 and CF8 cast grades (304L, 304 equivalents) but found it detrimental in the Mo containing CF-3M and CF-8M grades (316L and 316 equivalents). It is also known that Mo promotes sigma formation in duplex alloys, and this author feels that the Huey test used by Beck attacked the sigma phase preferentially and did not necessarily indicate the true sensitization (degree of chromium depletion) behavior. Testing with another corrosive (one that does not attack sigma phase) most probably would have indicated beneficial effects of

ferrite in the CF-3M and CF-8M grades as well. (More on testing in another section.) Henthorne (46) has noted the same trend in his literature review.

Devine (54) found that the sensitization resistance of wrought duplex 308 is related to the amount and distribution of the ferrite-austenite boundary and that above a critical ferrite content, chromium carbides always formed at the ferrite-austenite boundary. Wholly austenitic material was found to be highly susceptible to sensitization (as measured by the Strauss test) due to the formation of continuous chromium depleted grain boundary paths that did not exist in the duplex material above the critical fraction of ferrite as the ferrite (and thus the ferrite-austenite boundaries) was predominantly in isolated pools. Devine noted that the carbide precipitation process transforms ferrite into cellular austenite (sometimes referred to as γ_2) and $M_{23}C_6$ at the ferrite-austenite interfaces. A similar observation was made by Tedmon, et al. (55). Tedmon noted that on aging at 750°C, small carbide particles formed extremely quickly (less than 1 min.) at ferrite-austenite boundaries and that on continued aging the carbides tended to remain at the position of precipitation and that the ferrite-austenite boundary migrated toward the center of the ferrite pool. No evidence to suggest dragging of the carbides by the boundary was noted and only occasional pinning of the boundary by the carbides was noted. This isolation of the carbides and chromium depletion zone further diminishes the likelihood of continuous chromium depletion.

If the composition is adjusted such that high ferrite fractions are realized, the ferrite may become an interconnected, continuous matrix again approximating grain boundaries and the beneficial effect of ferrite may level off or reverse (actually become detrimental).

In a related phenomenon, it appears that duplex microstructures are also very beneficial regarding resistance to stress corrosion cracking (which may be exaserbated by sensitization). There are a few references (56-58) available which attempt to document this additional benefit of ferrite in cast duplex stainless steels.

Other Factors that Affect Sensitization

Another factor which influences the sensitization behavior is the degree of cold work in a stainless steel prior to sensitization. Its beneficial effect was noted as early as the work by Bain, et al. (16) and by Tedmon (59) and others (60). A commonly proposed mechanism to explain this behavior states that the increased dislocation density introduced by the cold work provides more nucleation sites (dislocation pile-ups and tangles) for carbides within grains (precipitation sites other than grain boundaries) which tends to make the carbides and the chromium depletion associated with them more discontinuous in nature. This precipitation mode precludes extended chromium depletion zones and increases intergranular corrosion resistance. Recrystallization of a cold worked material can also improve the sensitization behavior through grain boundary migration (59). The carbides are evidently not as mobile as the prior grain boundaries on which they precipitated at recrystallization temperatures and recrystallization would tend to remove any continuous

grain boundary network of chromium depletion that existed before recrystallization. A few authors have apparently noted deleterious effects of cold work on the corrosion resistance, but this has been attributed (46,59) to the formation of martensite (from austenite) during deformation and this martensite is subsequently attacked preferentially.

Briant and Ritter (61) showed (using modified Strauss test) that 304L was immune to intergranular attack in the solution annealed condition whether or not martensite (55 vol%) was present. (The martensite was formed by applying a tensile load to an electro-polished solution annealed sample.) Samples containing martensite that were subsequently exposed to isothermal treatments between 450 - 650°C were sensitized much faster than the same samples without martensite. Transmission electron microscopy showed that in the wholly austenitic samples, carbides formed at the grain boundaries. In samples which contained martensite the carbides precipitated primarily in the transgranular laths and along lath boundaries (all carbides $M_{23}C_6$). Even a 304L sample containing .005%C and about 60 vol% martensite was sensitized in less than 5 minutes at 600 - 650°C. The authors also showed that the sensitization temperature range (classically ≈500 - 900°C) could be extended to lower temperatures if the sample contained martensite.

Relatively little work has been done on the influence of strain during sensitization on the sensitization process. In a recent paper by Solomon and Lord (62), it was found that mechanical strains (over

and above thermal strains) of as low as .8% could enhance the sensitization process. It was not clear as to the mechanism involved, but this was found to be a trend for both tensile and compressive strains.

Solomon (63) found that strains of 2.4% (thermal strains subtracted by computer) did not alter the sensitization behavior of 304 specimens but that at 5% strain, the accelerating effect of strain had saturated, and strains as large as 25% did not further enhance sensitization. Adachi, et al. (64) found that welding stresses increase sensitization susceptibility of 304, principally in the temperature range of 700 - 800°C, where sensitization kinetics are already quite rapid.

There is some disagreement in the literature as to the effect of grain size on sensitization susceptibility. It appears that there is a slightly greater susceptibility to sensitization for a large grained material (46), possibly because there is less total boundary area for the carbide precipitation to take place, thus increasing the likelihood of a continuous chromium depletion region. As Streicher (65) points out, however, small grains are more easily dislodged so that a weight loss test is not a good technique for measuring this phenomenon (and these are the techniques used predominantly).

Another interesting observation on the sensitization behavior of austenitic stainless steels involves a phenomenon termed "Low Temperature Sensitization" or LTS. Povich (66) found that it was possible to relatively quickly cool (samples were not quenched) type

304 through the sensitizing region (considered generally as 500 - 900°C) and nuclate some very small carbides but not produce detectable chromium depletion zones. Isothermal holds at temperatures as low as 400°C then produced severe intergranular attack susceptibility in as few as 100 days. His study involving nucleation time and temperature dependence kinetics suggested that once the carbide is nucleated (from a high temperature) it may grow at temperatures lower than those predicted by most isothermal time-temperature-sensitization diagrams. In fact, very few studies involving continuous cooling have been done, but in general they (63,64,67,68) suggest that isothermally derived diagrams underestimate the severity of continuous cooling through the sensitization region. Adachi, et al. (63) found sensitization in 304 stainless steel in as little as four seconds, for example. Jominy bars (69) and the Gleeble (63,64,67, 68) have been used to evaluate continuous cooling sensitization. Also, various investigators (63,64) have found that for continuous cooling studies (such as weld simulation) that the most damaging peak temperatures are 800 - 900°C and that in multiple thermal cycle simulation, peak temperatures above this range effectively erase the damage of the previous cycles.

Sensitization of Ferritic Stainless Steels

Although not expected to be a major consideration in this research, a few words on the sensitization behavior of ferritic stainless steels are in order.

The phenomenology of sensitization in ferritic stainless steels is much different from that of austenitic stainless steels.

Sensitization is caused in ferritics by the high temperature heat treatments used to remove sensitization from the austenitics, and sensitization in ferritics is relieved at the same temperatures that cause sensitization in the austenitics. The ferritics are particularly sensitive to carbon and nitrogen content, and since the solubility of these interstitials is much lower in ferrite than austenite, the time to sensitize is shorter in ferritic stainless steels (and it occurs at a higher temperature at least partially for the same reason). Despite the apparent differences in behavior, the chromium depletion theory is applied to ferrite stainless steels by several workers (5,46,70) with some success. Hodges (70) showed (with very low %C, %N samples) that water quenching from 1000°C produces material immune to intergranular corrosion (this is in contrast to alloys of conventional purity) while air cooling from the same temperature produced severely intergranularly attacked samples. Furnace cooling from the same temperatures produced more resistance to intergranular attack than the air cooled samples. This behavior was explained as follows. In the water quenched alloys, the amount of diffusion time is short and the amount of (C+N) is small so that the diffusion distances to form carbides and nitrides are large and insufficient time is allowed for precipitation. In the air cooled samples, the cooling rage was slow enough to sensitize the material and furnace cooling allowed the samples to sensitize and then "heal" themselves. The effect of molybdenum was to slightly increase the tendency of the furnace cooled specimens to reach room temperature in the sensitized

condition. It was postulated by Hodges that Mo slowed nitrogen diffusion and thus delayed sensitization. This delay did not allow sufficient time for the re-diffusion of chromium to "heal" the material.

Adding weight to the applicability of the chromium depletion theory to ferritic stainless steels is the fact that preferential carbide formers such as Cb and Ti can minimize the sensitization tendency of the ferritics (21,71,72).

Compared to austenitic stainless steels, much less research has been done on ferritics and they are correspondingly less understood. More work is required on ferritic stainless steels but in general it appears that the chromium depletion theory may explain sensitization in these materials as well.

Welding Sensitization

Studies on sensitization are useful because they may be used to predict potential corrosion problems associated with service conditions at elevated temperatures or with the thermal cycles imposed by welding. There are basically two types of sensitization problems associated with welding and they are generally referred to as weld decay and knifeline attack. A short discussion of each follows with emphasis on austenitic stainless steels.

As a weld bead is moved through a material, the temperature distribution perpendicular to the weld centerline requires a band of material in the base metal be heated into the sensitizing range (500 - 900°C) for a period of time controlled by the heat input of

the welding process (volts, amps, travel speed), the specimen thickness and the preheat temperature employed. If this sensitizing time is great enough, the part could preferentially corrode in this narrow band parallel to the weld upon exposure to an aggressive environment. The most common remedy for this problem is to solution anneal the weldment or to employ low carbon or stabilized grades of material. Solution annealing is an expensive, time consuming step and it may not even be possible on some large structures that cannot be heated to these high temperatures or because the distortion incurred during quenching may be detrimental to the service performance of the structure. The most probable cause of the rapid formation of a sensitized region in the heat affected zone in the short times allowed by a welding thermal cycle has been mentioned previously. Carbides nucleated at high temperatures in the sensitizing range can grow relatively easily at lower temperatures (similar to the LTS phenomenon) and this probably explains the discrepancy between the degree of sensitization predicted by isothermally derived diagrams and actual welding practice. (Very few studies have been done involving continuous cooling type behavior, as previously mentioned.)

The use of low carbon stainless steels to minimize this problem has been somewhat successful, but often times the strength of the weldment or base material has been lowered greatly by the reduction in carbon. It may be possible in some instances to restore this strength with nitrogen additions.

Knifeline attack is the name of the phenomenon given to a corrosion failure adjacent to the weld bead of a Ti or Cb stabilized

stainless steel. (See Reference (73).) It occurs because the region immediately adjacent to the weld bead is heated above the temperature at which Ti and Cb carbides are stable and it cools too quickly through this region for these carbides to reform (i.e., Ti and Cb still in solid solution). Subsequent reheating (service temperature or multi-pass welding) into the temperature range of 500 - 900°C forms chromium carbides preferentially and this narrow region may become sensitized. A stabilization heat treatment of 1950°F, cool to 1650°F for 1/2 hour, then cool to room temperature (at any rate) produces Ti and Cb carbides and renders the alloy immune to knifeline attack. Again, this heat treatment may not be possible.

Review of Experimental Techniques

Traditionally, there are several methods to measure or estimate the susceptibility to sensitization. Here, susceptibility to sensitization means that the potential for developing a sensitized material exists (due to heat treatment, alloy type, etc.) and it is desired to predict the likely service behavior of the material in the given condition for a given (or possibly unknown) service environment. An indication of sensitization susceptibility does not necessarily imply poor service behavior; likewise, an indication of low sensitization susceptibility does not necessarily imply that the material is not sensitized or that the material will perform adequately in service. The results of such tests are merely guidelines for making material selections or similar decisions.

The susceptibility to sensitization and intergranular corrosion will depend somewhat on the method used to detect this susceptibility. ASTM A262 (4) contains five standardized tests for determining susceptibility to intergranular corrosion and these tests (or slightly modified versions thereof) have been used for many years by consumers, producers and scientists. A discussion of each follows, as well as a discussion of some more recently developed tests that are as yet not standardized.

ASTM A262--Practice A--Oxalic acid etch test. This test is used as a rapid method to examine susceptibility to intergranular corrosion. Those samples that pass this test are usually deemed "not susceptible" and are screened from the need for further testing. Those that do not pass are tested further.

Basically, the test involves electrolytically etching a sample for 1.5 minutes at 1 amp/cm^2 in 10% oxalic acid solution and then evaluating the resultant microstructure as one of the following conditions:

1. Step Structure: In the absence of chromium carbides (or nitrides), differences in the rate of etching of variously oriented grains results in steps at the grain boundaries. No ditching (wide grooves) present.
2. Ditch Structure: One or more grains completely surrounded by ditches. Ditches are caused by excessive attack at the grain boundaries due to sensitization and the presence of high chromium carbides.
3. Dual Structure: A combination of ditches and step structure with no single grain completely surrounded by ditches.

Other similar etch structure classifications include isolated ferrite, interdendritic ditches and end grain pitting. These are the classifications common in castings and welds. The standard classifies which microstructures are acceptable for many different compositions. An unacceptable structure calls for a hot acid test to further judge the material and does not fail the material outright. The reason is, as Figure 11 shows, that the rates of corrosion of specimens with a ditch structure could be very different, i.e., representing mildly or very sensitized structures, and a hot acid test can possibly differentiate. Both Curve B and Curve C probably represent acceptable corrosion rates in this hot acid test, yet one shows a step structure and one is a ditch structure in the oxalic acid test. Curves A and B each have ditch structures but very different hot acid corrosion rates. Thus, after further testing, material B would likely "pass", yet material A would fail despite the same etch structure classification.

The oxalic acid test primarily attacks chromium rich phases such as chromium carbides (20). Some sample data from Devine and Drummond (20) that led to this conclusion are shown in Table 2. Oxalic acid does not specifically attack sigma phase, which means that the ditching revealed by the oxalic acid test is almost certainly dissolved carbides (20). Among the major advantages of the oxalic acid test are that it is fast and it can be economical if a large fraction of material can be screened from further testing. Practical experience (74) shows that this is sometimes not the case particularly for rod and tube stock. Among the major disadvantages

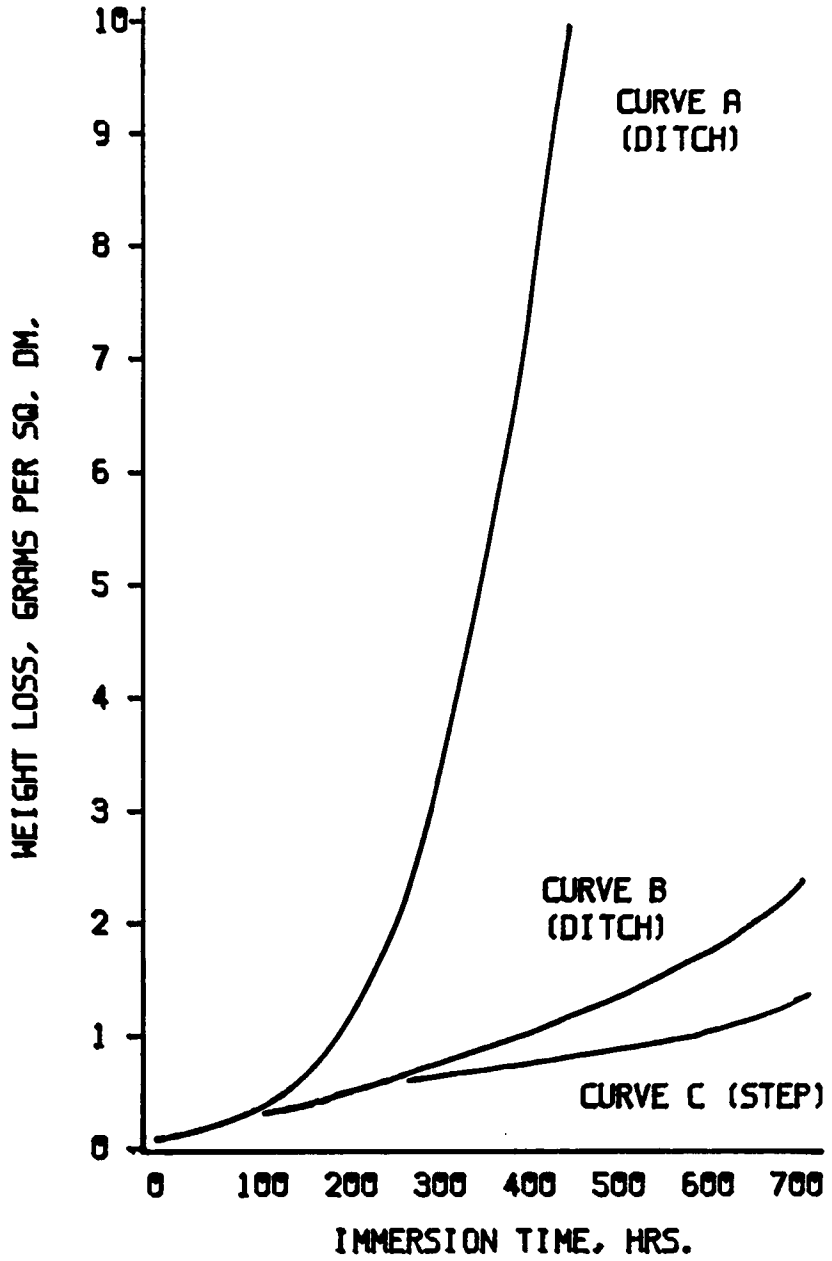

Figure 11. Schematic diagram showing a potential relationship between A262A etch structure and corrosion rate in a hot acid.

Source: Streicher, M. A., "Theory and Application of Evaluation Tests for Detecting Susceptibility to Intergranular Attack in Stainless Steels and Related Alloys - Problems and Opportunities," in Intergranular Corrosion of Stainless Alloys, ASTM STP 656, Steigerwald, R.F., ed., p. 3-84, ASTM, (1978).

Table 2. Sample data indicating that the oxalic acid etch test primarily attacks chromium rich phases.

COMPOSITION	TIME TO TOTAL DISSOLUTION (MIN)
FE	1060
FE-5%CR	690
308 SS (20%CR)	97
CR	32

Source: Devine, T. M., and Drummond, B. J., "Use of Accelerated Intergranular Corrosion Tests and Pitting Corrosion Tests to Detect Sensitization and Susceptibility to Intergranular Stress Corrosion Cracking in High Temperature Water of Duplex 308 Stainless Steel," Corrosion, Vol. 37, p. 104, (1981).

of the test are the facts that it is not a quantitative test and it does not detect healing. (The carbides are still present--and attacked--even if chromium redistribution has taken place.)

Another way to compare the various evaluation tests is through the electrochemical potentials each applies. Figure 12 indicates the various approximate potentials superimposed on a schematic polarization curve for type 304 stainless steel in many media.

ASTM A262--Practice B--Streicher Test. This is a hot acid test for further evaluation of those materials that do not show acceptable etch structures after the oxalic acid screening test. The test consists of placing a small sample (known mass) in a boiling ferric sulfate-sulfuric acid mixture for 120 hours and then determine the weight loss or corrosion rate. This test attacks chromium depleted regions (associated with carbides) and sigma phase in stabilized stainless steel but not in the Mo bearing grades. The test does not detect susceptibility associated with end grain attack.

Among the major advantages of this test are the facts that it requires half of the time as one of the other weight loss tests and the corrosion products do not accelerate the corrosion rate in this test. Among the major disadvantages are the facts that it is a 120 hour test and no quantitative guide as to the significance of the weight loss or corrosion rate numbers is known.

ASTM A262--Practice C--Huey Test. This is another boiling acid (65% nitric acid) weight loss test to which materials that are not screened by the oxalic acid test are exposed. It is a 240 hour

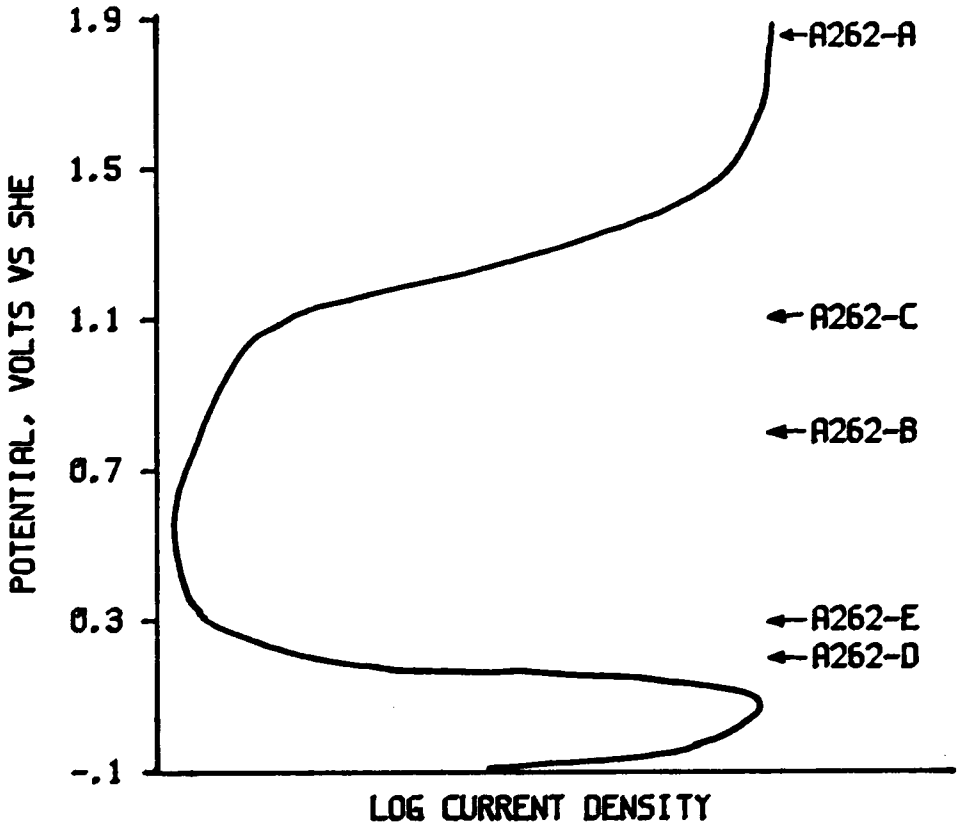

Figure 12. Schematic diagram indicating the relative potentials of the A262 evaluation tests.

Source: Henthorne, M., "Intergranular Corrosion in Iron and Nickel Base Alloys," in Localized Corrosion-Cause of Metal Failure, ASTM STP 516, p. 66, ASTM, (1972).

(five 48 hour periods) test that, with the exception of the fact that nitric acid service is fairly common, has very few advantages now that many other tests are available.

This test is known to attack chromium depletion areas as well as chromium carbides to a lesser extent. It also attacks sigma phase or its sub-microscopic precursor. The significance of the attack on sigma phase is that, as regards intergranular corrosion resistance, it is not detrimental in any media except extremely oxidizing ones (74), such as nitric acid. Thus, if the material is intended for service in such an environment, this is a good test. Otherwise, if sigma phase exists (particularly in Mo bearing stainless steels), the corrosion rates determined will be erroneously high and not particularly applicable. It is also known that the buildup of corrosion products (Cr^{+6}) accelerates the rate of attack in the test solution. This could affect the reproducibility of the test somewhat but it might be looked on as slightly advantageous as this would tend to increase the spread in the results between unsensitized and sensitized specimens (15). The test takes a long time (240 hours) and is expensive (46). It is also somewhat sensitive to surface preparation and end grain attack (46). Devine and Drummond (20) found this test to be incapable of differentiating between unsensitized and mildly sensitized samples. Also, as with many of these tests, no guide is given as to the significance of the corrosion rates found in this test as they relate to service behavior.

ASTM A262--Practice D--Nitric-Hydrofluoric acid test. This test is a four hour weight loss test in a solution of 10% HNO_3

and 3% HF at 70°C. The test solution attacks chromium depleted zones only (not sigma phase or carbides) and as such is a good test for the Mo bearing stainless steels. The duration of this test is the shortest among the weight loss tests. The results are reported in terms of ratios of corrosion rates of the test material versus the same material type known not to be susceptible to intergranular corrosion (i.e., solution annealed).

A special disadvantage of this test is the unusually dangerous acid employed. The vapors are extremely noxious and special containers are needed for the hydrofluoric acid (no glass can be used). The test is also extremely sensitive to chromium content (even in the range of 16 - 18%) and thus care must be taken in choosing the baseline material for the ratio calculation. A ratio of greater than 1.5 is considered to indicate susceptibility in this test.

ASTM A262--Practice E--Strauss Test. This test is an upgrade of ASTM A393. The original test solution was a mixture of copper sulfate and sulfuric acid, and the improvement was to add metallic copper to the test solution to increase the severity of the test. The copper functions to maintain the potential in a region more aggressive to chromium depletion regions. The test does not detect the presence of carbides or sigma phase specifically. After a 24 hour exposure in boiling solution, the sample is removed and bent to a standard radius. Intergranular cracking in the bend is then taken as evidence of susceptibility to potential intergranular corrosion.

Disadvantages to this test center around the need for careful metallographic examination. The amount of cracking in the bend is the quantitative measure of the test and this could depend on the effort the observer puts into finding cracks.

Electrochemical Tests

Various attempts have been made to develop an electrochemical measurement that quantifies the degree of sensitization. Interpretation of anodic polarization curves has been popular and a review of several of these appears in a survey by Cowan and Tedmon (15). In summary of these techniques it appears that the anodic peak current density is controlled principally by the alloy composition and the degree of sensitization plays a very minor role. Attempts have been made to analyze the second anodic current maximum of polarization curves in sulfuric acid as related to sensitization but this phenomenon has been shown (75,76) not to be related to sensitization. The passive range current density at a given potential has been correlated to sensitization behavior, but overall alloy composition, surface finish, and the time necessary to establish equilibrium give no real advantage to this particular method.

A new test has been developed largely by General Electric (27, 77) in this country (Cihal (78) and others in Europe) and the details of the technique are discussed by Clarke, et al. (27). It is called the Electrochemical Potentiokinetic Reactivation (EPR) test and is currently under investigation as an ASTM standard. Basically, the EPR test is a quantitative evaluation of the degree of sensitization

of a stainless steel based on assessing the stability of the passive film on a polished sample. (See schematic of Figure 13.) The test solution is 1N sulfuric acid and .01M KSCN (as an activator) at 30°C with a two minute deaeration prior to testing. The sample is allowed to equilibrate at its open circuit potential in the test solution and then it is quickly changed to .445 volts (SHE), which is in the middle of the passive range in this solution for stainless steels. After two minutes at this potential (time to form a reproducible passive film) the potential is changed in a negative direction (toward the active range) at a known scan rate (terminating at the open circuit potential) while the current response of the sample is noted. If the passive film is everywhere stable, the current density should not change from the passive current density value for the entirety of the downscan all the way back to the open circuit potential. If there are low chromium regions in the sample, such as those expected adjacent to carbides that may form due to thermal cycling of the material, the passive film is not everywhere stable and will break down to degrees representative of the degree of sensitization of the sample. As the film breaks down, the current density will increase.

Since the downscan is at a known rate, the potential-current density plot is equivalent to a time-current density plot. The area under this curve is total coulombs of charge passed (seconds x amps/cm^2). The sample is observed after the test and the type of interface attacked is determined. The charge density (C/cm^2) is then divided by the total susceptible grain boundary area (with some conversions from ASTM grain size developed by Clarke for wrought

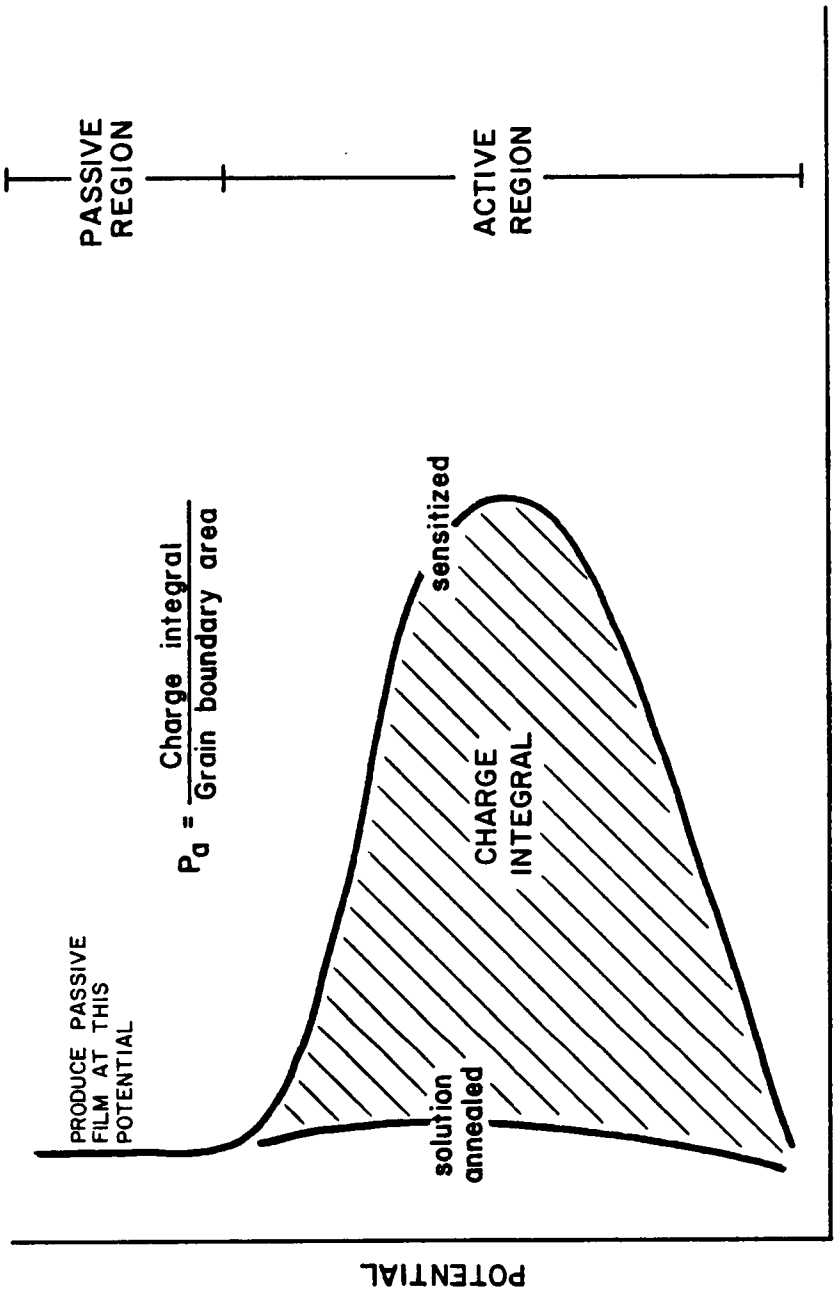

Figure 13. Standard EPR evaluation method.

material) to determine the coulombs/unit boundary area. The larger this number, the greater the susceptibility to interface corrosion.

A slight modification of the EPR test developed by the Japanese (49) (Cihal (78) and others in Europe use a fundamentally similar test) has reached the literature. Akashi, et al. (49) point out that the reactivation peak of the standard EPR test is influenced significantly by alloying elements, most notably Mo content. The goal of their effort was to adapt the EPR test into an evaluation method for susceptibility to intergranular corrosion which is not influenced by bulk composition. Since some data already generated by the standard EPR test indicate a substantial effect of Mo (for example) for equivalent heat treatments, it is evident that a method to remove bulk composition effects from the EPR test would be beneficial.

The solution chemistry and temperature, sample preparation and scan rate are identical in the Japanese EPR test (referred to hereafter as JEPR) and the standard EPR test. The differences are the initiation of the controlled potential scan and the method of quantitative analysis. In the JEPR test, the potential scan begins at the open circuit potential and sweeps anodically (up-scale) to the passivation potential of the standard EPR test. Immediately upon reaching this passivation potential, the scan direction is reversed and, like a standard EPR test, the remainder of the test is a downscan from the passive to the active region. (See schematic curve of Figure 14.) The measure of sensitization sensitivity is reported as the reactivation ratio Ir/Ia where Ir is the maximum reactivation current density and

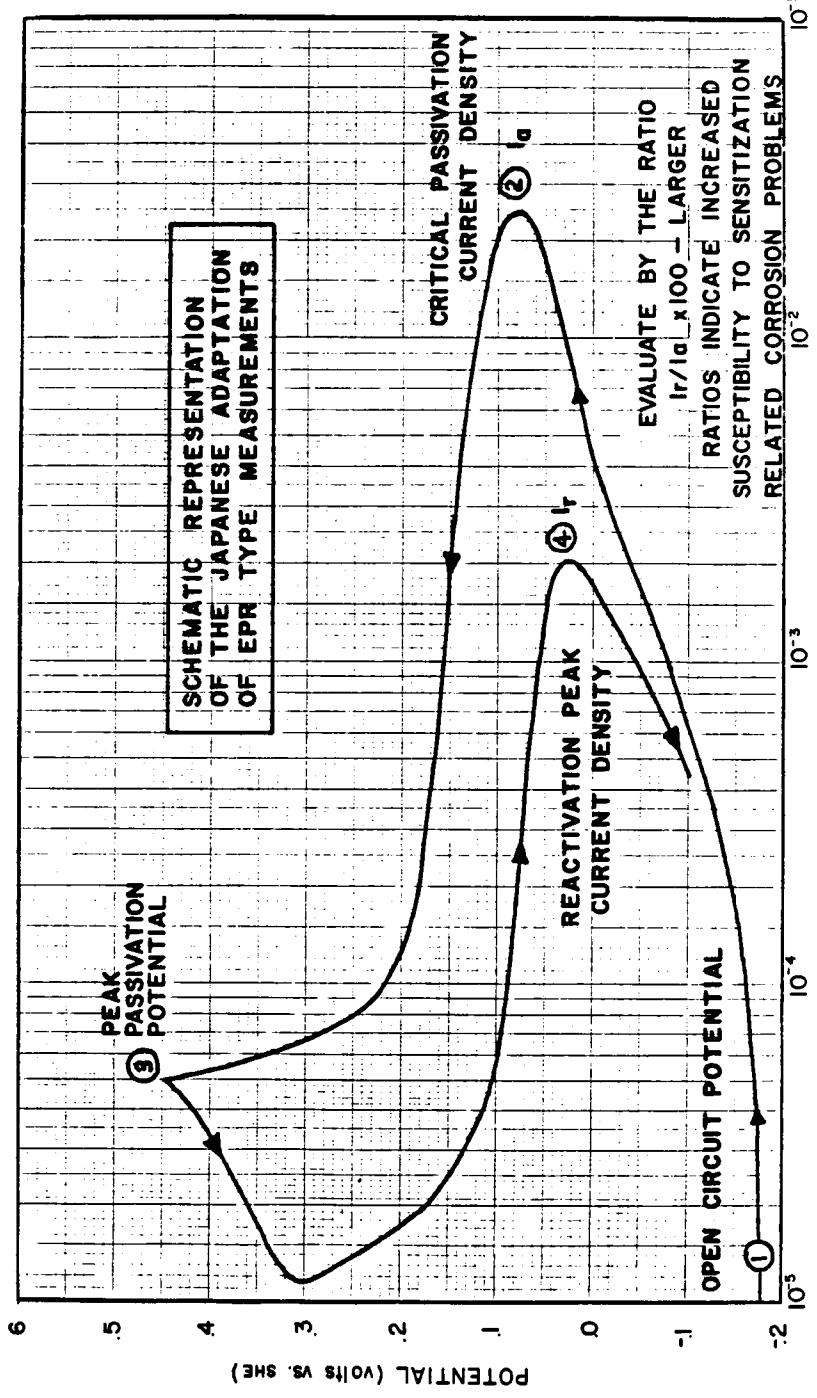

Figure 14. Schematic representation of the Japanese adaptation of EPR type measurements.

Ia is the critical passivation current density of the anodic sweep. The larger this number, the higher the susceptibility to intergranular corrosion. A potential advantage in reporting this ratio over the standard EPR test may be described as follows.

Ia measures the active dissolution of the whole test piece as determined principally by its composition and only slightly by the degree of sensitization. Included among the elements to which this peak is very sensitive are Cr and Mo. (For example, increasing Mo content decreases Ia--in fact, 2 - 3% Mo may make an order of magnitude difference in Ia.) On the other hand, Ir is affected by the degree of sensitization (Cr-deficient regions in the passive film) as well as general dissolution. Thus, by using the reactivation ratio Ir/Ia, the effect of alloy composition is decreased and the JEPR results can lead to a better comparison of the relative sensitization susceptibilities of different alloys. Although not developed for this purpose, observations seem to indicate that the JEPR test reduces the importance of sample surface finish because this effect appears in both the upscan and downscan curves, and thus is effectively cancelled out of the quantitative values. There are, of course, other research tools available to study sensitization, but the aforementioned tests are the major evaluation methods that have been used to date.

There have been a few studies (References (20,27,79-82)) that compare several of the methods mentioned above. Devine and Drummond (20) found A262E to be the best correlation to stress corrosion cracking problems related to sensitization and Clarke, et al. (27)

found the EPR test to be the most sensitive test for detecting all levels of sensitization below some "very severe" levels. Majidi and Streicher (79) found the EPR test to be very sensitive to the low to medium levels of sensitization but found A262B to be the most sensitive at high levels of sensitization.

Streicher (19) comments that the weight loss tests were really developed for (and are most readily applicable to) wrought products. Castings generally have a much larger grain size than wrought materials and as a result, the time required to undermine and dislodge grains (register effectively in a weight loss measurement) is much longer for castings. If a weight loss test for a casting is employed, it is likely that the standard immersion time would need to be doubled or tripled for the test to be effective. (See schematic of Figure 15.) Streicher (18) also comments that testing actual welds would not be easily accomplished since in general the damaged zones would be very small. Bend testing (for fissures) was suggested as a more sensitive test for weldments. However, Vyas and Issacs (83) have used a scanning reference electrode technique to locate and quantify sensitization behavior on stainless steel weldments. It is apparent than an electrochemical method such as the EPR test (or its modification) has a great potential for evaluating cast duplex materials.

In general, then, most of the literature on sensitization behavior has focused on the chromium depletion theory using isothermal (relatively long time) holds on wrought materials (principally 304 types). Relatively little work has been done toward simulating actual weldments and studying corrosion behavior, particularly involving cast

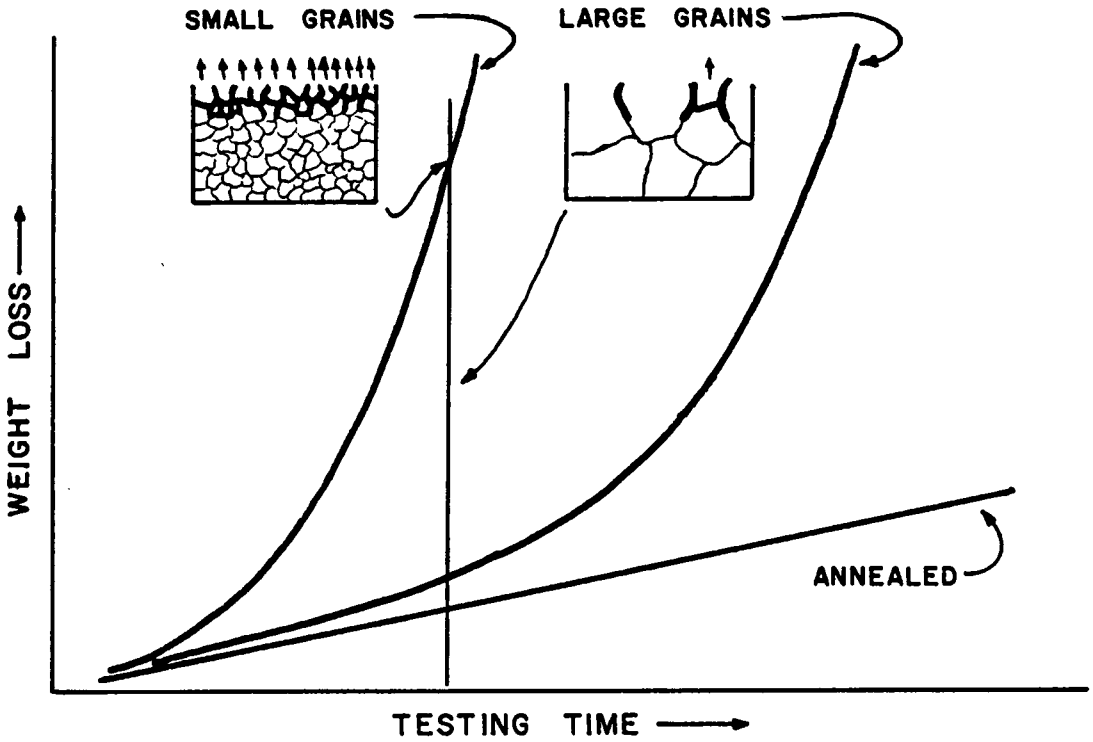

Figure 15. Effect of grain size on weight loss test results (schematic).

Source: Streicher, M. A., "Theory and Application of Evaluation Tests for Detecting Susceptibility to Intergranular Attack in Stainless Steels and Related Alloys - Problems and Opportunities," in Intergranular Corrosion of Stainless Alloys, ASTM STP 656, Steigerwald, R. F., ed., p. 3-84, ASTM, (1978).

duplex type material. Also, the EPR and JEPR techniques are gaining acceptance in the technical community (reference (80) shows at least six different countries involved by Reference list in addition to U.S.A. and Canada) but have yet to be used to evaluate cast duplex material. Among the goals of this research is to address these needs.

CHAPTER III

EXPERIMENTAL PROCEDURE

Materials

All of the castings used in this study were supplied in the as-cast condition by member foundries of SFSA. These materials had been in induction furnace melted and cast in sodium silicate molds in test blocks roughly 15 cm (6 in) deep, 38 cm (15 in) long and tapered from 3 cm (1.2 in) to 2.5 cm (1.0 in) from top to bottom of the casting. The compositions reported in Table 3 were determined by wet chemical analysis. Included in this table are the average ferrite numbers after solution annealing as determined by the Magne Gage. In most cases, series of alloys were prepared by dividing a single initial heat and adjusting the Cr/Ni ratio to give a range of ferrite numbers in the resulting alloys; this minimized the difference in residual elements from alloy to alloy.

Heat Treatments

When solution annealing treatments were required, the castings were heat treated at 1120°C (2050°F) for approximately one hour followed by a water quench. In most instances, no special precautions against decarburization such as encapsulating samples in Vycor (under vacuum or inert backfill) or special furnace atmospheres were used. Following heat treatment, each sample (common size about 1.3 cm x 1.3 cm x .5 cm) was ground on 120 grit paper to remove heat treatment scale as well as 2 - 10 mils of each exposed

Table 3. Composition of research alloys.

MATERIAL	%C	%MN	%SI	%P	%S	%CR	%NI	%MO	%N	FN
CF8 LO	.058	.60	1.52	.012	.013	18.53	9.98	.02	.02	4
CF8 INT	.086	.84	1.10	.031	.012	19.90	8.73	.50	.02	11
CF8 HI	.066	.79	1.25	.031	.011	20.81	8.85	.45	.02	20
CF8M LO	.063	.94	1.21	.011	.014	18.26	11.17	2.28	.02	5
CF8M INT	.083	1.20	1.20	.030	.013	19.78	9.53	2.21	.02	12
CF8M HI	.071	1.19	1.16	.030	.011	19.92	9.40	1.95	.02	21
CF3 LO	.016	.98	1.12	.010	.008	17.36	10.10	.10	.04	2
CF3 INT	.023	.68	1.24	.011	.009	19.35	10.27	.10	.06	5
CF3 HI	.015	.67	1.09	.013	.006	19.82	8.73	.10	.04	8
CF3M LO	.027	.96	.85	.011	.010	17.55	12.00	2.18	.04	5
CF3M INT	.027	1.04	1.02	.009	.009	18.78	10.79	2.12	.03	9
CF3M HI	.022	.94	1.14	.012	.007	19.85	10.08	2.26	.02	16

surface. This was found to be adequate protection against testing a non-representative sample due to decarburization or other surface phenomenon.

Based on measurements on samples with thermocouples imbedded near the center of the sample, it required approximately 9 - 14 minutes for each sample to reach the furnace temperature (for temperatures from 600°C - 1120°C). All isothermal heat treatments report the time at temperature allowing for this heating period. Unless otherwise stated, all samples were water quenched following heat treatment.

Sample Preparation for Testing

After the samples had been ground on 120 grit paper to remove heat treatment scale, a brass screw was soldered to each specimen. The expended soldering flux was carefully scraped from the solder joint and the sample was then mounted (so that at least half of the brass screw protruded from the mount) in Maraglas plastic epoxy (see Figure 16). Unless otherwise specified, each sample mount was then ground and polished through 1μ micron paste. The same sample mount, repolished before each test, was used for the EPR, JEPR, and oxalic acid tests.

Ferrite Measurement

Ferrite measurements were made on surfaces polished through 600 grit paper and prior to testing with an Aminco-Brenner Magne Gage. This instrument was calibrated with the NBS variable thickness coating standards to AWS A4.2 - 74 (84). Because of lack of

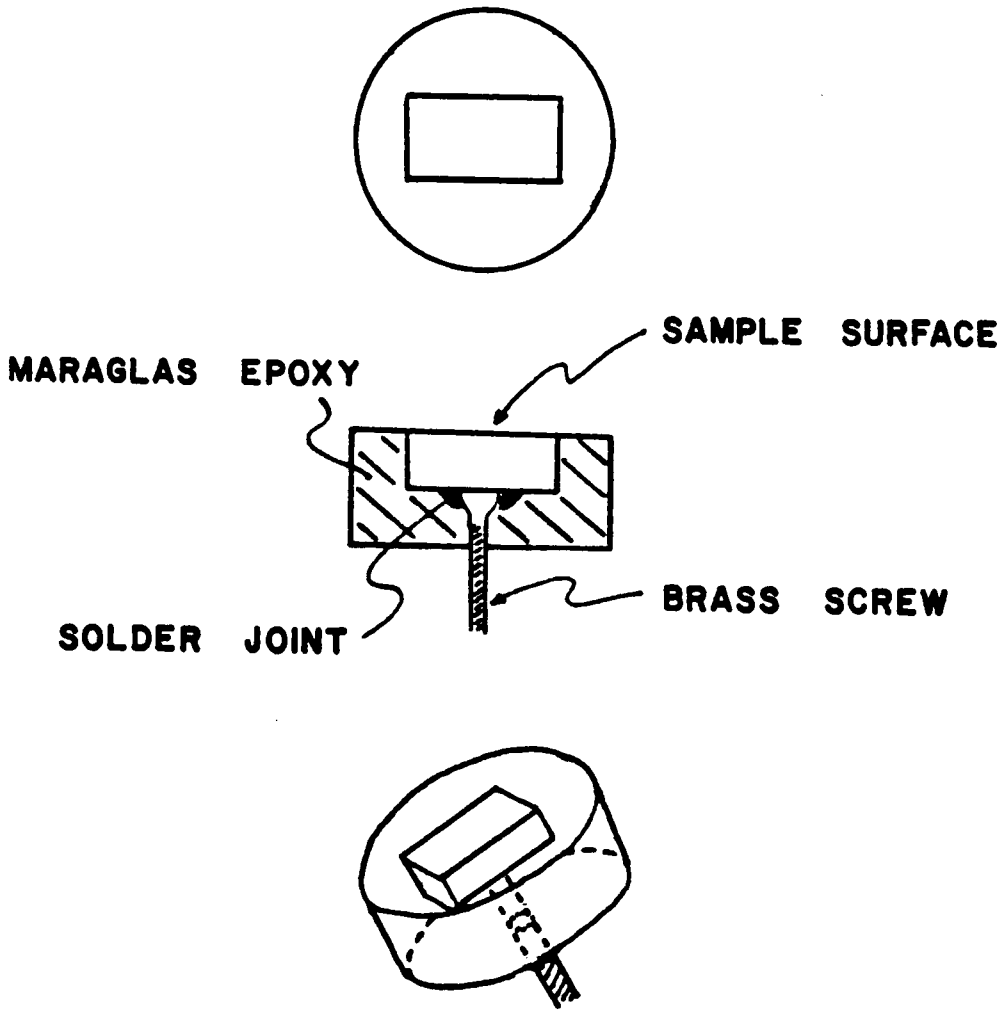

Figure 16. Schematic of sample mount.

availability, a No. 3 magnet (usually designated for stainless steel weld metals) was used for all ferrite determinations instead of a No. 2 magnet (usually designated for stainless steel castings). The difference between the two magnets should be negligible for the accuracy required (± 1-2 FN) in this work. All reported ferrite numbers represent the average of at least five measurements made at various locations on the test surface of the sample.

Polarization Cell

The polarization cell used for the EPR and JEPR corrosion tests has been described in some detail elsewhere (85) and will be described only briefly here. (See Figures 17 and 18.)

The lid to the 2 liter test cell contained several drilled and tapped holes for various sizes of bulkhead fittings. Through these entries, the various electrodes and equipment were introduced into the test cell as indicated in the sketch of Figure 17.

Brass screws near the edges of the lid were used to compress an O-ring between the vessel lid and the flange of the 2 liter vessel, thus sealing off the test cell from the atmosphere.

EPR Test

After some initial testing to examine the sensitivity of the test to a number of experimental variables (see Results and Discussion) the following EPR test procedure was adopted for the remainder of the research effort. The test procedure is essentially that described by Clarke (27) and is summarized here for the convenience of the reader.

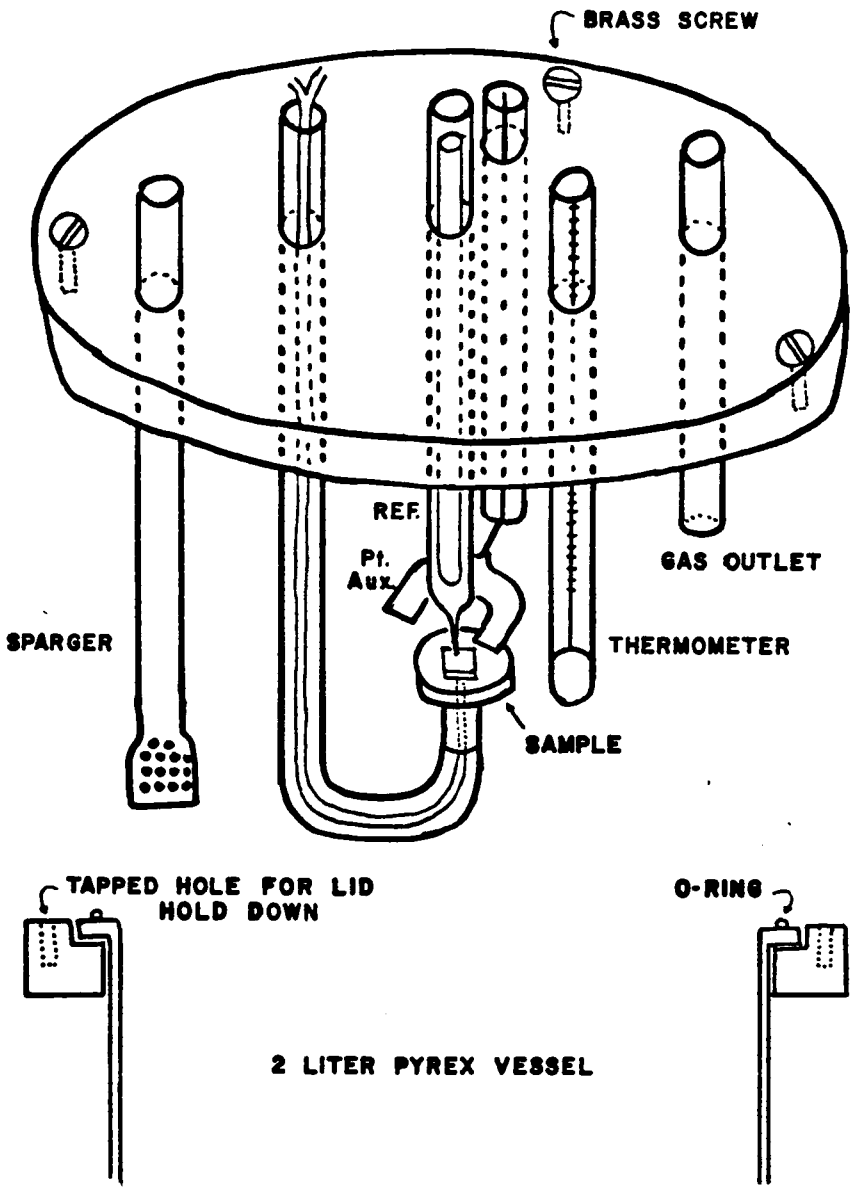

Figure 17. Schematic of polarization cell.

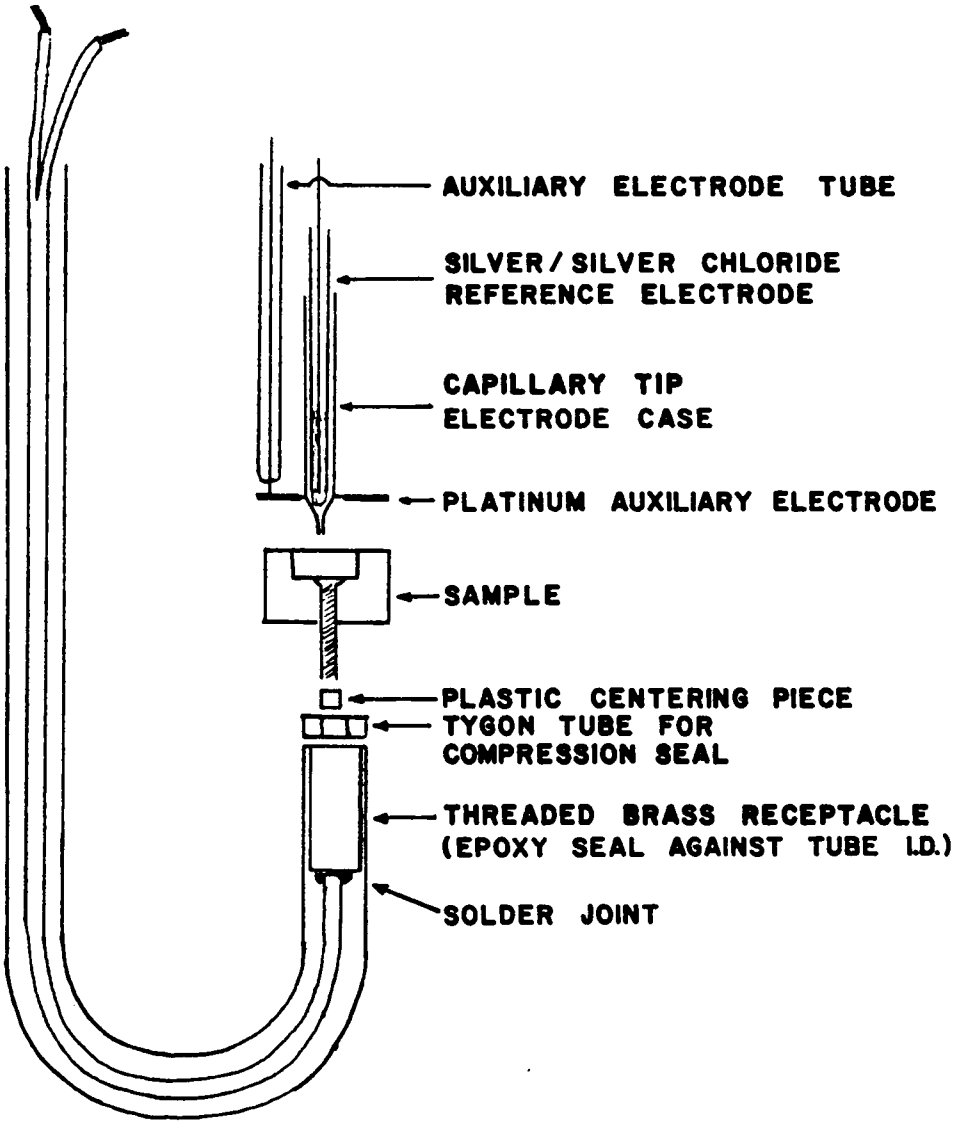

Figure 18. Detail of sample relationship to reference electrode and polarization equipment.

The test solution was 1.0 N sulfuric acid and 0.01 M potassium thiocyanate made from reagent grade chemicals and distilled water. The solution volume of about 1500 ml was maintained at 30°C ±1 and was agitated slightly by a continuous nitrogen sparge. The reference electrode used was a saturated silver-silver chloride electrode contained in a capillary tipped casing and positioned about 1 - 2 mm from the surface of the sample (at least 1 cm^2 surface area exposed).

Immediately prior to testing, the sample was repolished on the 1μ diamond paste cloth to remove any atmosphere induced films or tarnishes. One minute after immersion in the test cell, the open circuit potential of the sample was recorded. If it was not within the usual range (-375 to -405 mv vs. Ag/AgCl for 304/CF8 types and -350 to -375 mv vs. Ag/AgCl for 316/CF8M types) the specimen was cathodically charged at -600 mv vs. Ag/AgCl for 1 - 2 minutes and then after a one minute wait, the open circuit potential was rechecked. (The reader should note that, although most potentials were measured vs. Ag/AgCl, the results were plotted vs. the standard hydrogen electrode. Reporting data vs. SHE has become a convention and to convert the potentials vs. Ag/AgCl to SHE, simply add 196 mv to the Ag/AgCl values.) Repolishing the sample is an alternative to cathodic charging. After the open circuit potential was deemed acceptable, a nitrogen sparge of approximately 200 cm^3/min (not critical) was begun and continued throughout the test. After a two-minute wait for deaeration, the sample was then quickly moved to +245 mv vs. Ag/AgCl to passivate the surface. This potential was maintained for two minutes (passivation is assured by a current

density of 10^4 amp/cm^2 or less). The reactivation scan (cathodic direction) was then started using a potentiodynamic scan rate of 6 V/hr. The current response during the reactivation scan was recorded on semilogarithmic paper with potential as the ordinate and current as the abscissa with a Honeywell 560 xy recorder. The test was terminated when the sample reached its prior open circuit potential.

Based on data reviewed in the Results and Discussion section, the peak reactivation current density was reported in lieu of the entire EPR curve in most instances. When appropriate, microstructural observations were also recorded.

When consecutive tests were performed, 200 ml of test solution were replaced with fresh (unused) solution for each new sample tested. Stock solution may be used for up to a few weeks if it has been in a sealed (limited access to oxygen) in a container.

JEPR Test

The test conditions and procedures for the JEPR test were identical to those of the EPR test up to and including the two minute wait during the initial nitrogen sparge. At this point, instead of passivating the sample at +245 mv (Ag/AgCl), an activation scan (anodic direction) was begun at the open circuit potential and the potential was potentiodynamically changed toward +245 mv at 6 V/hr. Upon reaching +245 mv and with no time delay, the sweep direction was reversed and a reactivation scan (cathodic direction) was performed at 6 V/hr. The test was terminated when the sample reached

its original open circuit potential. The results recorded included Ia (peak anodic current density during activation scan), Ir (peak current density during reactivation scan) and the JEPR ratio, i.e., (Ir/Ia) X 100.

Oxalic Acid Etch Test

The exact procedures for execution of this test appear in ASTM A262--Practice A (4). Basically, the sample was electrolytically etched in 10% oxalic acid at 1 amp/cm^2 (dimensions of sample measured to nearest .5 mm) for 90 seconds and the appearance of the microstructure then noted. The brass screw served for electrical contact to the sample and a stainless cathode completed the circuit in the etching solution.

Deviations from the standard procedure include the fact that each specimen was polished through 1μ diamond paste (finer than the 600 grit finish required by the specification) and that in many instances 45 seconds or less of etching was sufficient to note the outcome of the test.

Gleeble Testing

Gleeble model 510, with a reference generator model 734 and model 766 programmer, was used for all weld simulation studies. A chromel-alumel .025 cm (.010 in) diameter wire thermocouple was percussion welded to the sample with equipment provided with the Gleeble and placed in the water cooled copper jaws as shown in Figure 19. When the strain capability of the Gleeble was desired,

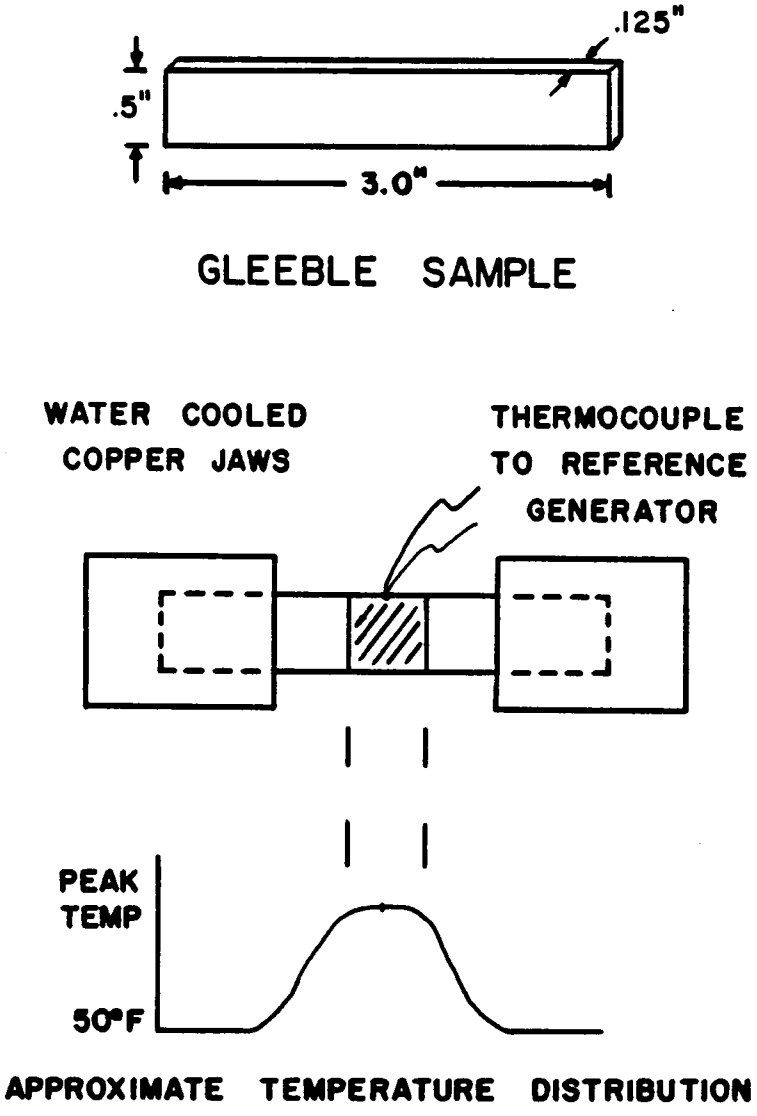

Figure 19. Schematic of Gleeble sample.

3/16 in. diameter holes were drilled near the ends of the samples so that a steel pin could fit through these holes into matching holes recessed in the copper jaws. While one set of jaws remained fixed, the other set of jaws could be pulled away from the fixed jaws, thus providing strain in the center, or "hot zone," of the sample. (See Figure 20.)

All thermal cycles were calculated to simulate weld repair passes on 3.8 cm (1.5 in) thick stainless steel with no preheat. Tabulated values of the solutions to the differential equation relating temperature to time and distance for arc weld thermal cycles on 3.8 cm stainless steel were taken from the literature (86).

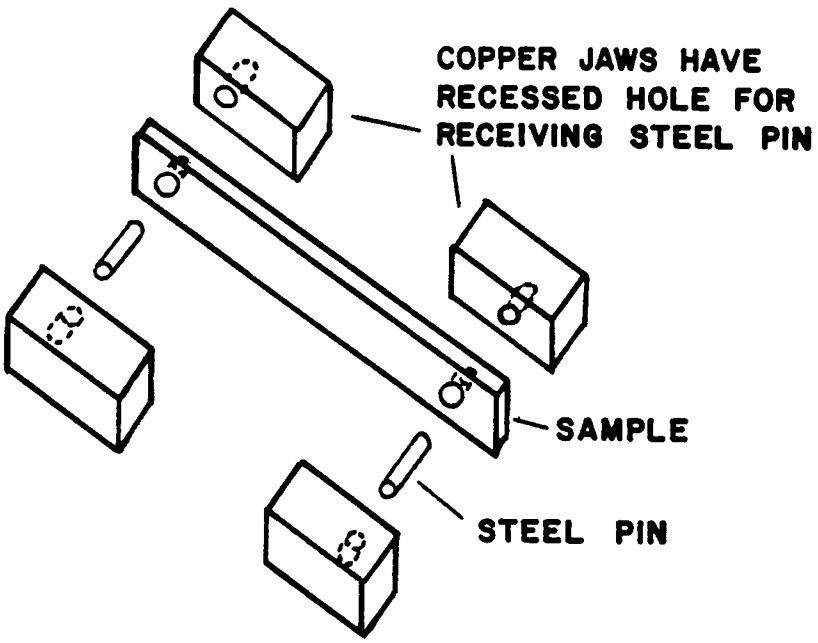

Figure 20. Schematic of adaptation of Gleeble sample to utilize the strain capacity of the Gleeble.

CHAPTER IV

RESULTS AND DISCUSSION

The EPR Test--Introduction

Stainless steels derive their passivity from the formation of a protective oxide film (generically Cr_2O_3) on the surface of the steel and this passive film forms when the solid solution chromium content of the substrate metal is maintained above or near 12% Cr. During exposures to the temperature range 500 - 900°C (900 - 1600°F), chromium rich carbides (usually of the type $M_{23}C_6$) precipitate at grain boundaries and at other interface locations such as ferrite-austenite interfaces in duplex stainless steels. Adjacent to these chromium rich carbides a narrow chromium depletion zone forms; this region may be sufficiently depleted in chromium that its local solid solution chromium content may be lowered to a level below that required for passivation of the alloy. These chromium depleted zones are susceptible to localized corrosion in many media and a stainless steel in this condition is said to be sensitized.

The Electrochemical Potentiokinetic Reactivation (EPR) test was developed

> "because of an industrial need for a rapid, non-destructive quantitative field test which could be used for assessing sensitization in reactor components and . . . all tests used by the industry to detect degree of sensitization are considered deficient . . . ." (77).

This reactivation method is based on the phenomenon that the passive film (once it has formed) of a stainless steel may remain "intact," i.e., protective of the substrate, for a limited time even at a

potential that is in the active potential range for the alloy. Because the presence of a passive film in the active potential range is not a stable state, any defect in the passive film (such as that found near the chromium depleted areas adjacent to carbides in the substrate metal) will cause the surrounding film to breakdown and the substrate metal to be attacked. Thus, if a non-sensitized stainless steel is passivated (noble potentials) and then the potential is changed into the active region, the passive film would be expected to remain relatively stable everywhere, at least for short periods of time. However, if a sensitized stainless steel is passivated (noble potentials) and then the potential is changed into the active region, the passive film would be expected to breakdown at or near regions of chromium depletion in the substrate and remain relatively intact over the regions having at least 12% chromium in solid solution. The degree of passive film breakdown upon changing a stainless steel from the passive potential region to the active potential region could then be considered to be representative of the degree of sensitization (chromium depletion) in a stainless steel. It is this stability of the passive film that the EPR test was designed to measure.

Figure 21 is a schematic diagram of the EPR test reactivation polarization curve for three different conditions. From the passive potential at position "1" of this curve the potential is changed at a relatively fast (6 V/hr) dynamic potential scan rate in the active direction toward the open circuit potential (position "3" of Figure 21). For the solution annealed condition (no chromium carbides) the

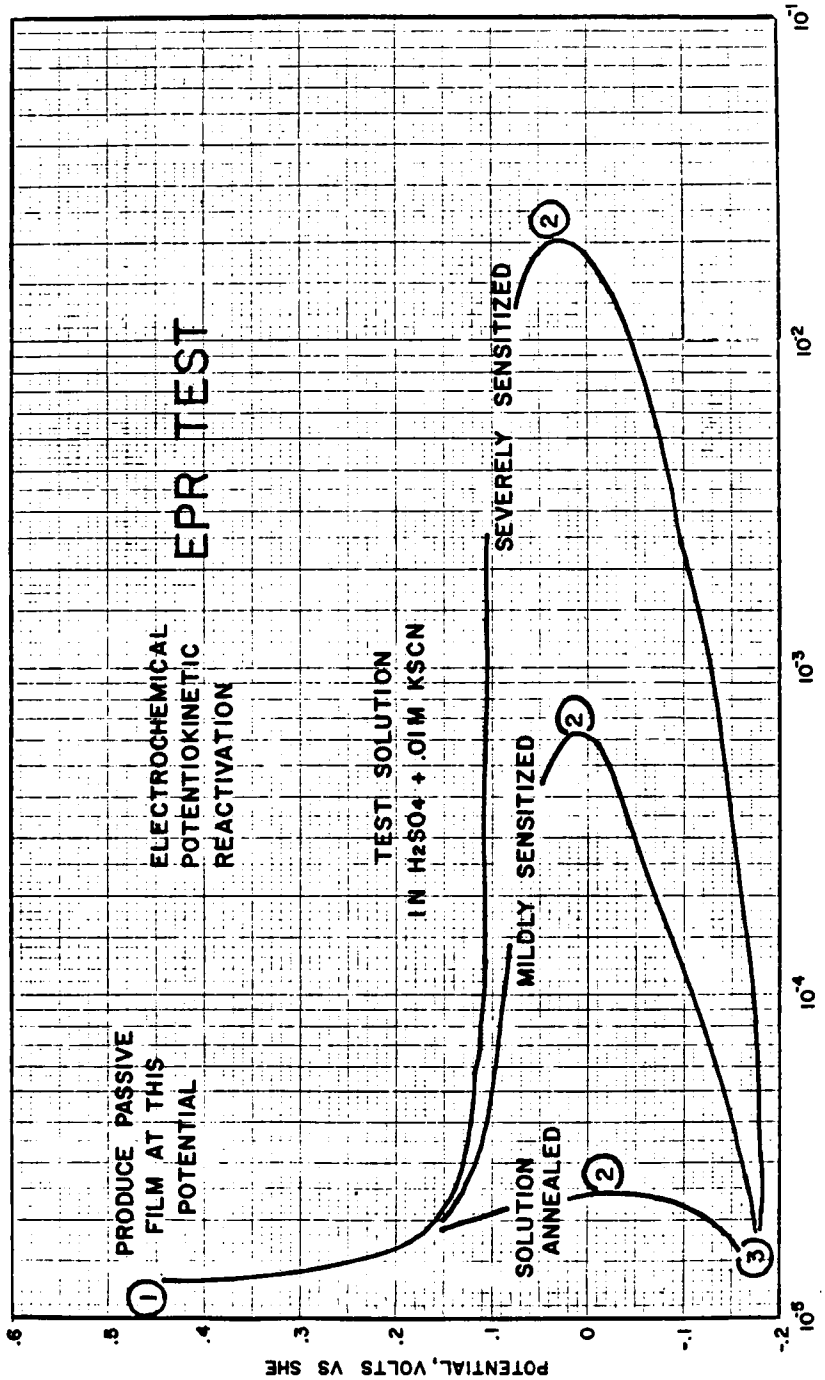

Figure 21. Schematic of EPR results for three different degrees of sensitization.

reactivation peak current density (position "2") would be expected to be quite small, i.e., not much different from the current density at position "1." Also as shown in Figure 21, the reactivation peak current density would be expected to increase in magnitude as the degree of sensitization increases because the total area of chromium depleted regions (total number of carbides) that is dissolving at potentials in the active region is increasing as the degree of sensitization increases.

As originally developed, the measure of sensitization from the EPR test was designated Pa, the integrated charge passed over the potential range scanned expressed as coulombs/cm^2 of attacked depleted zone along grain boundaries, and it was derived from the area under the reactivation polarization curve as shown in Figure 13 (page 55). Since the downscan from the passivation potential is at a known and constant rate, the potential axis of Figure 13 may be considered as a time axis with units of seconds and thus the cross-hatched integrated area of Figure 13 (page 55) has the units of amps/cm^2 multiplied by seconds, or coulombs/cm^2. The resulting coulombs/cm^2 were then "normalized" to account for various grain sizes from material to material, i.e., the total amount of grain boundary area per square centimeter of sample surface. This was accomplished by dividing the coulombic charge integral (the cross-hatched area of Figure 13) by a grain size factor and a factor accounting for the width of the grain boundary attack as derived for AISI 304 type materials (and described by Clarke (77)).

Many of the details of the evolution of the EPR test parameters for wrought materials are described by Clarke in the developmental work by General Electric (77) and it is not the purpose of this research effort to evaluate the choice of the individual test parameters per se. Rather, the EPR test as detailed in the recent literature by Clarke, et al. (27) was taken more or less at face value and applied to duplex cast stainless steels to investigate the applicability of the EPR test to this grade of materials. The following paragraphs report the results of the EPR test as it characterizes duplex cast stainless steels with the eventual application to the evaluation of sensitization during weld repair.

EPR Test--Initial Evaluation and High Carbon Alloys

Material for this investigation was supplied in the form of cast blocks (see Experimental Procedure). Due to the nature of the solidification process during casting, the chemical composition of the test blocks cannot be homogeneous. In order to study the possible effects that this inhomogeneity could have on the EPR test results it was decided that the initial EPR testing would obtain results from a variety of sample positions and orientations from sections of as-cast material (where the inhomogeneity is at a maximum) as well as some solution annealed and furnace cooled conditions. Samples were taken from the test blocks in patterns similar to those shown in Figures 22 and 23. Specimens were cut from the cast blocks so that the exposed faces represented three different depths from the sand wall face of the casting (Figure 22) as well as mutually perpendicular directions within the casting (Figure 23).

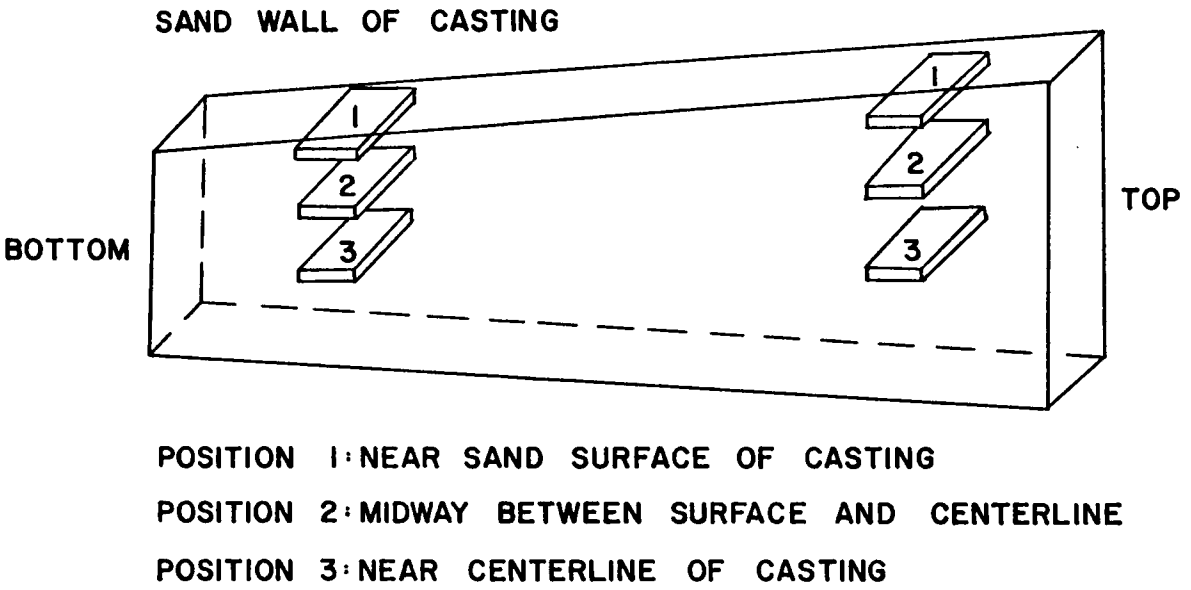

Figure 22. Schematic diagram of sample position pattern.

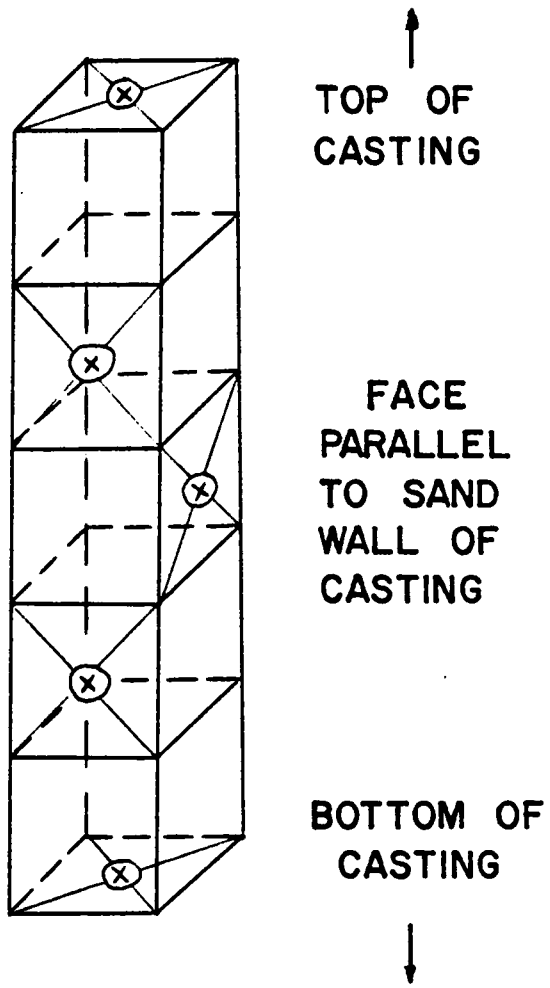

Figure 23. Schematic diagram of sample orientation pattern.

The data generated in this manner showed that for a particular alloy, each EPR curve was remarkably similar. The initial open circuit potentials, the passive current densities, and the shape and position of the reactivation peak were all more or less identical; only the peak reactivation current density varied significantly for various alloys and heat treatments. Some sample data from the aforementioned testing scheme for the high carbon (.06 - .08%C) content material are shown in Figure 24. For each alloy and heat treatment a scatter bar is shown indicating the entire range of the peak current densities (each curve was corrected for the individual sample area) obtained for all sample positions and orientations. Note that the peak current densities all occurred in the range of 0 - .1 V vs. SHE but for ease of comparison the data have been shown on a single plot.

The data of Figure 24 point out several significant factors. Unlike EPR values for wrought materials, no factor exists for normalizing the area under an EPR curve to account for the equivalent of grain size and therefore total susceptible exposed interface are for duplex stainless steels. This area is a combination of the austenite-austenite grain boundaries and the interface boundaries between the ferrite and the austenite matrix. The amount of susceptible interface between the ferrite and the austenite is a complex function of the total ferrite present and the ferrite morphology. As this research shows (and will be discussed later) the fraction of the total ferrite-austenite boundary area that is susceptible to attack as well as the degree of attack at susceptible interface areas is

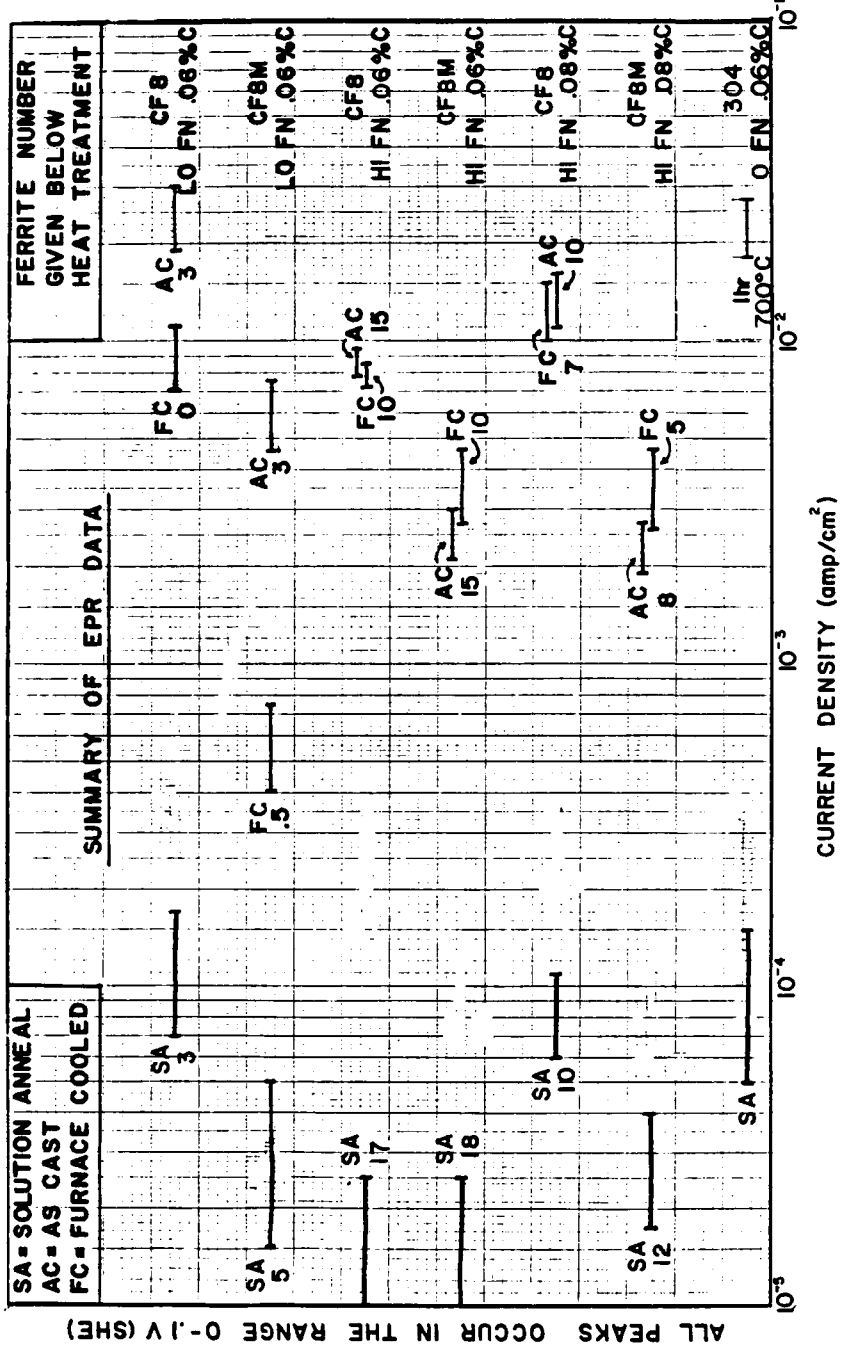

Figure 24. Summary of EPR data for initial test results.

variable from alloy to alloy. It was, however, noted that the coulombic area (integrated area under each EPR curve) was linearly related to the peak reactivation current density as shown in Figure 25. This was not an unexpected correlation as the maximum contribution to the area under an EPR curve should come from the region of the curve near the peak current density since the current response is recorded on a log scale. Until some correlation is found for normalizing to an exposed susceptible grain boundary interface area from sample to sample (various ferrite contents and morphologies will greatly complicate this), the peak reactivation current density will be reported as a measure of susceptibility to sensitization as indicated by the EPR test. (Higher peak current densities indicate greater levels of chromium depletion--i.e., more susceptible to sensitization.) Where appropriate, microstructural observations that indicate the location and extent of attack after EPR testing will be noted.

In order to determine whether or not an orientation effect was indicated within each spread bar of Figure 24, some samples were selected and were EPR tested six times each--repolished after each test--to examine the reproducibility of the results for a particular sample. Some sample data of this type are shown in Figure 26. Note that the uncertainty in peak current density measurement for each alloy is of the same order of magnitude as the "spread" bars of Figure 24. Because the range of EPR measurements for a particular sample is the same as the range of EPR measurements representing the same alloy and heat treatment but from various sample orientations

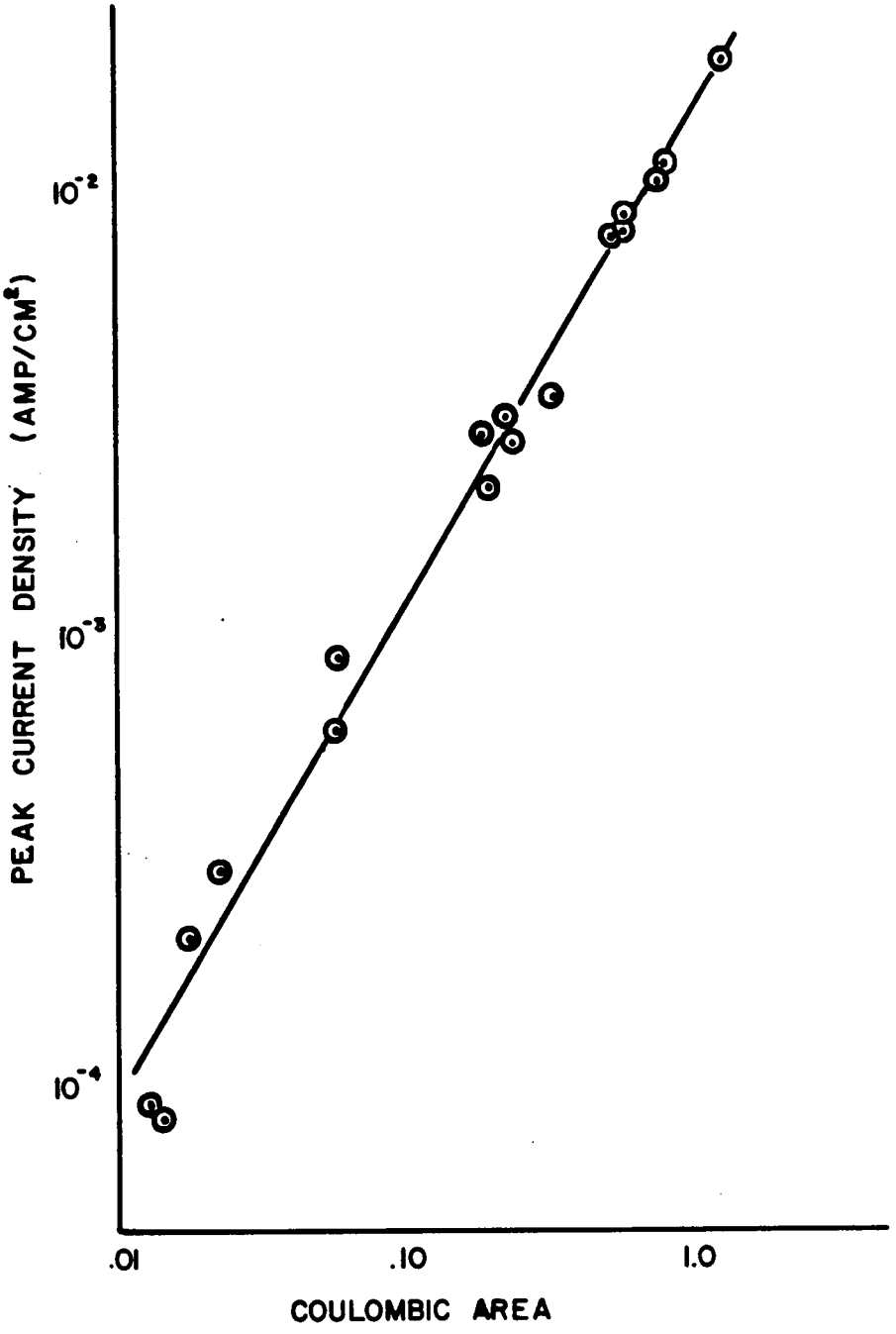

Figure 25. Relationship between EPR peak current density and the area under an EPR curve.

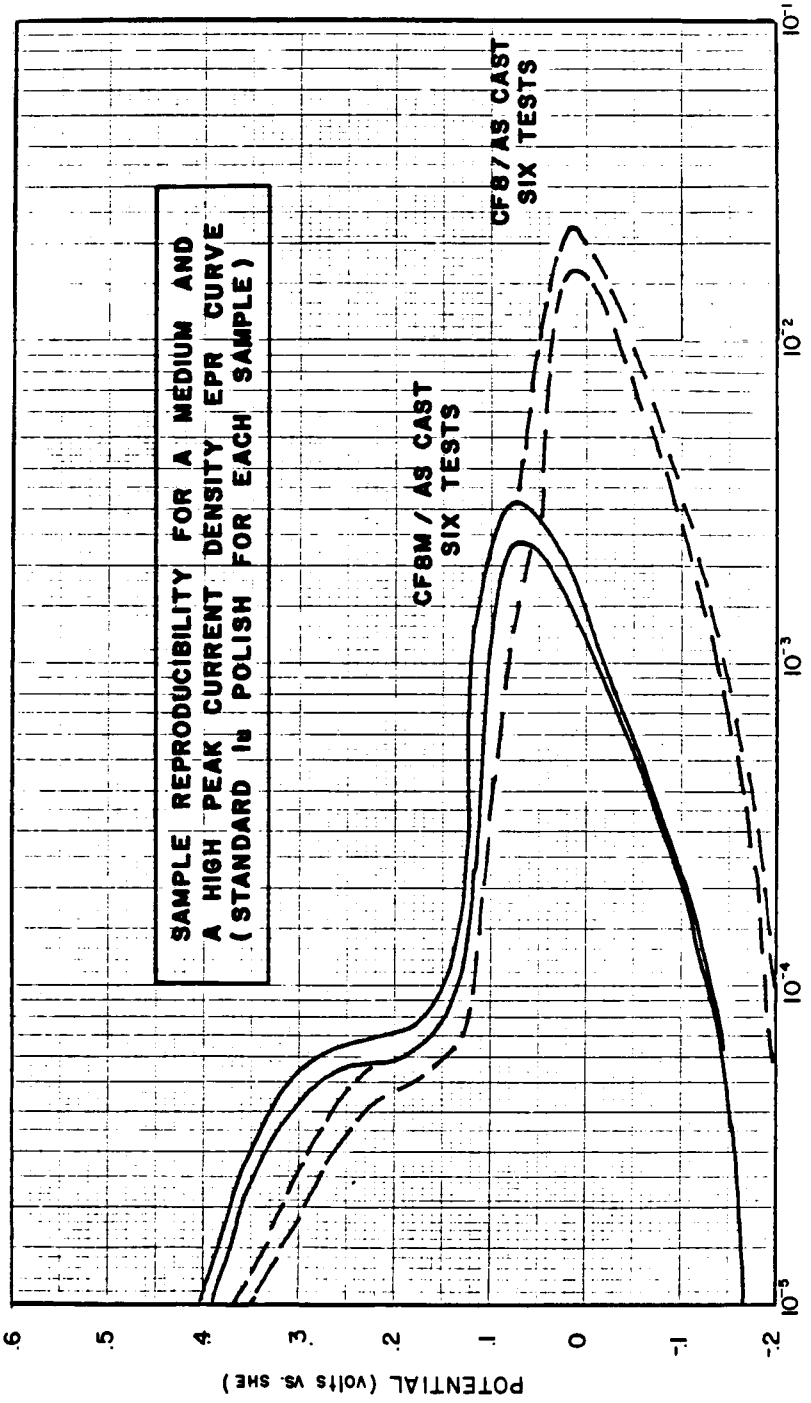

Figure 26. Reproducibility of the EPR test for selected samples.

and positions within the casting, it was concluded that no effect of sample position or orientation is measured by the EPR test and that future testing need not be concerned with this factor.

The solution annealed condition (approximately one hour at 1120°C followed by a water quench) was studied in some detail to provide a "baseline" condition with which to compare all other heat treatments. Immediately evident from Figure 24 is the fact that the solution annealed materials often exhibit a small reactivation peak. The reactivation peak for the solution annealed condition (particularly the CF8 alloys) is not as reproducible as the reactivation peak for the other conditions examined. This is possibly due to the low overall current densities involved but it is more likely that at these low overall current densities, small variation in sample preparation, edge effects and other factors may be detected whereas samples with higher peak current densities are not influenced by the small current contributions from the same factors that may affect the solution annealed sample data. (More on this in a later paragraph.)

It has been indicated that attack on the ferrite in the duplex structure probably does not contribute to the reactivation peak for a solution annealed material in the EPR test by noting the following:

1. Microstructural examination after EPR testing shows no signs of preferential attack on the ferrite although in some cases the ferrite is slightly stained or lightly outlined.
2. CF8M alloys with ferrite contents similar to those in the CF8 alloys show smaller reactivation peaks (or even none

at all) than for the corresponding CF8 alloys in the solution annealed condition.

3. Similar (but sometimes smaller) peaks are found in solution annealed fully austenitic castings as well as solution annealed 304 and 316.

Likewise, it does not appear that segregation (chromium) is a contributing factor since the reactivation peaks still exist in material solution annealed for six days at 1120°C (2050°F). If this peak had not been present after the lengthy solution anneal, chromium segregation from the melt which was too severe to be removed by a short (approximately 90 minutes) anneal would have been suspected. Also, since the quenching procedure for the solution annealed samples produced specimens that reached room temperature in less than three seconds from removal from the furnace, it is unlikely that significant carbide precipitation (and associated chromium depletion) could take place in this amount of time and contribute to the reactivation peak.

As a result of the uncertainty concerning the exact position of the reactivation peak for solution annealed materials, three particular EPR test technique variables were examined: surface finish, edge effects and solution strength.

The effect of surface finish on a selected CF8 alloy in the solution annealed condition is shown in Figure 27. As one can clearly see, the EPR response of the CF8 alloy is a strong function of the surface finish of the alloy. The CF8M alloy chosen was unaffected

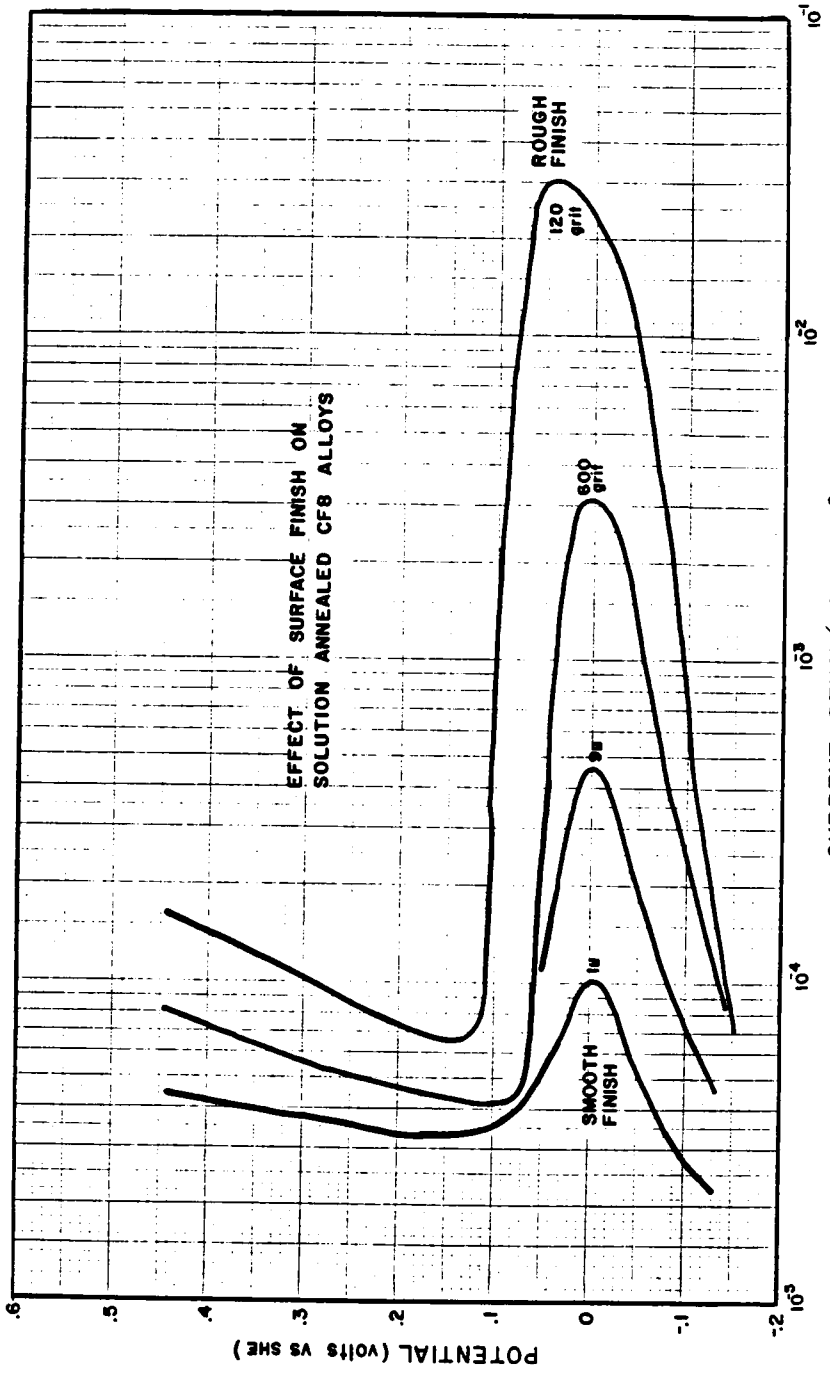

Figure 27. Effect of surface finish on EPR results for the solution annealed condition.

by surface finish in the solution annealed condition. This behavior may possibly be explained by consideration of the following phenomenon. As the surface roughness of a sample increases, the actual surface area of the sample increases over the apparent surface area (obtained from macroscopic dimensions of the sample) due to the ridges and valleys created on the metal surface during coarse grit grinding. The current densities shown for the CF8 alloy in Figure 27 were derived by dividing the total current passed at any potential by the apparent surface area of the sample and not the actual surface area, which is considerably larger than the apparent surface area for the rough surface finishes. If the actual surface area had been measured (this is a somewhat difficult and time consuming measurement) and used as the divisor for the total current passed at any potential, the reactivation peak for the solution annealed CF8 alloy might not show such a strong relationship to the surface finish. The fact that the solution annealed CF8M alloy is not affected in the same manner as the CF8 alloy (although the dependence of the surface area on the degree of finish remains the same) indicates that another factor besides actual surface area may be involved. One possibility is that the CF8M alloys have lower reactivation peaks than the CF8 alloys in the solution annealed condition; so much lower that increasing the surface area dramatically still does not yield a high enough apparent current density to be measured on the scale of Figure 27. A more likely possibility to explain the difference in behavior of the CF8 and CF8M alloys is to postulate that the nature of the oxide film formed at the passivation potentials of

the EPR test is not readily altered by surface finish variations in the CF8M alloy as it may be for the CF8 alloy. In either case, this sensitivity to surface finish may explain the slightly erratic EPR test results on the solution annealed CF8 alloys.

The effect of surface finish on sensitized samples is shown in Figures 28 and 29. The rough finish indicated is a 120 grit finish and the smooth finish is a standard 1μ diamond paste finish. Several graduations between these two finishes are also indicated. As one can see from these data, surface roughness appears to affect solution annealed and sensitized samples differently. This behavior may be explained by considering that on a sensitized sample at least two factors are competing to cause the observed effect of surface finish. As the surface finish becomes more rough, the amount of disturbed metal increases dramatically and in fact, the small chromium depleted regions can be covered or masked by material that is free of chromium depletion, thus reducing the EPR peak current density. Also, as already mentioned, as the surface roughness increases, the actual surface area of the sample exposed to the test solution increases which tends to increase the apparent EPR peak current density (unless this increase in area is taken into account). Apparently, the masking of areas that could potentially make large contributions to the peak current density is the overriding factor because the apparent peak current density decreases with increasing surface roughness for the sensitized CF8 and CF8M alloys. Again notice that the Mo bearing alloy is less sensitive to surface preparation than the corresponding CF8 alloy. As a result of the sensitivity to surface finish

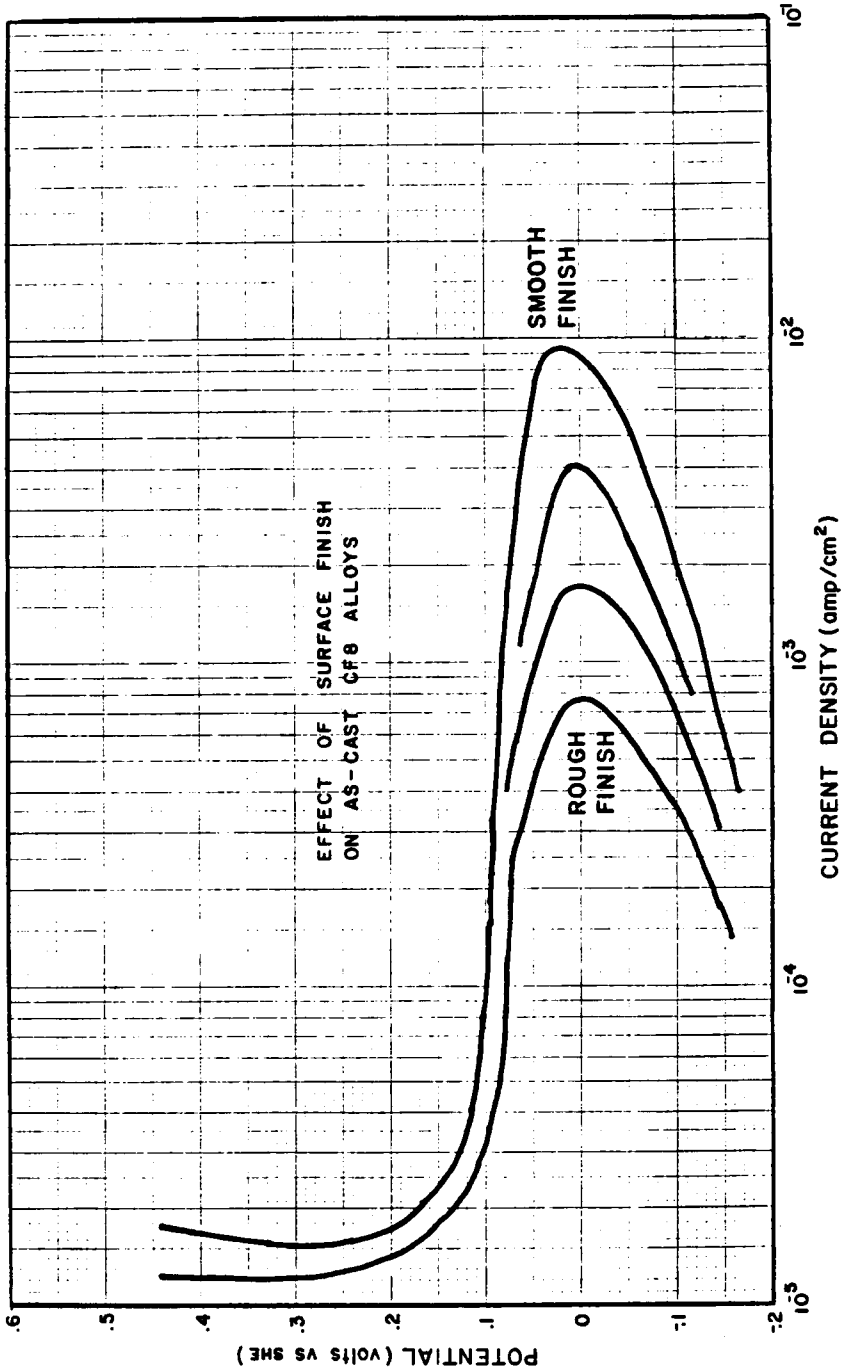

Figure 28. Effect of surface finish on EPR results on an as-cast CF8 alloy.

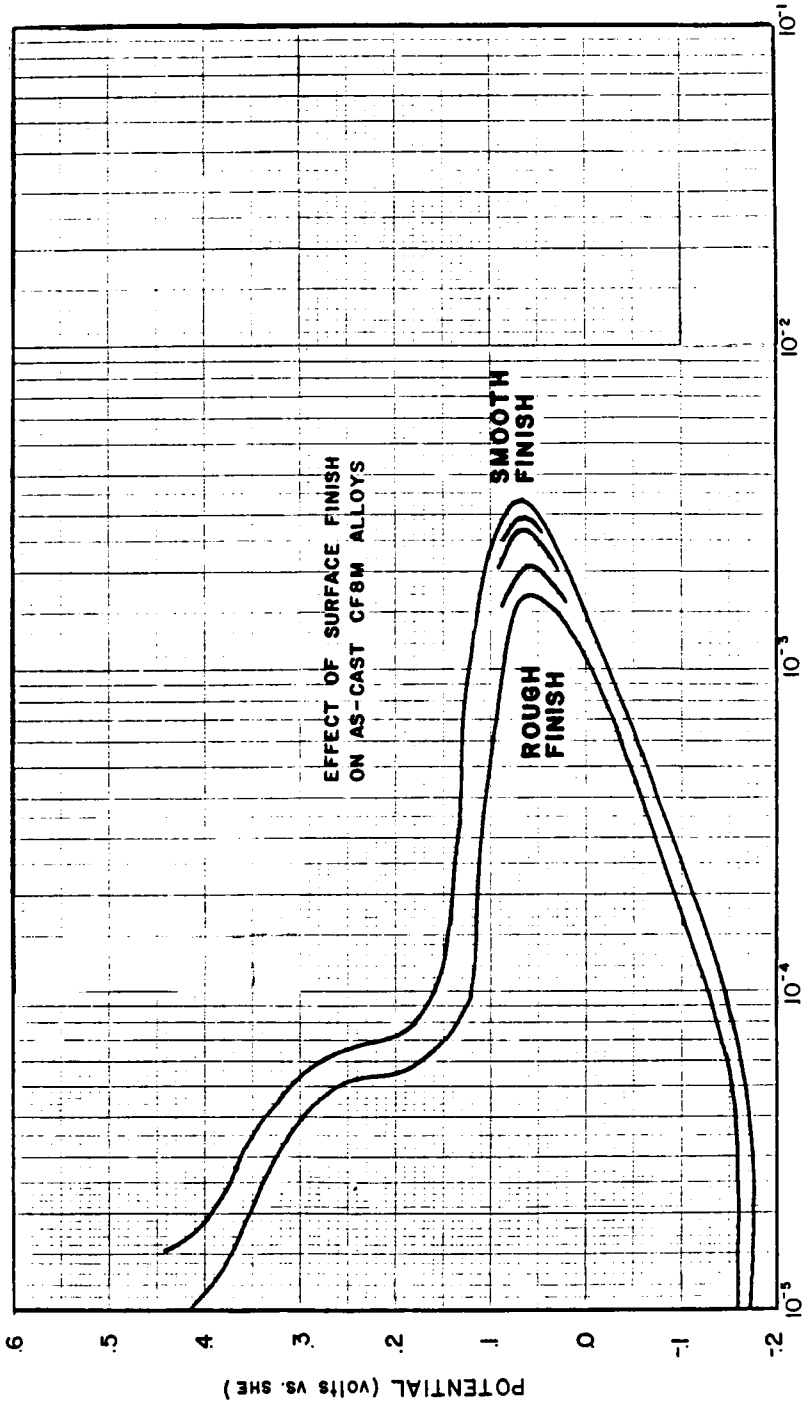

Figure 29. Effect of surface finish on EPR results on an as-cast CF8M alloy.

of the CF8 alloys, it was decided that a 1 micron diamond paste polish would be the surface finish for testing for all samples unless otherwise noted.

It was also found that edge effects of the sample can contribute to the observed EPR peak for the solution annealed materials. Specifically, if heat treatment scale is not removed from the edges of the sample (those faces perpendicular to the face exposed to the test solution) the activation of this scale, no matter how thin, can contribute to the apparent peak current density in the neighborhood of 10^{-4} amp/cm^2. This effect is too small to be detected on samples sensitized sufficiently to produce peak current densities much larger than 10^{-4} amp/cm^2.

The effect of aging of the 1N H_2SO_4-.5M KSCN test solution on the EPR results was examined briefly. In short, it appears that a solution that is bottled and standing can age in a relatively short time, i.e., a week or two, and become less aggressive than a freshly mixed EPR solution. Although not documented for the purposes of reporting, it is further suspected that solution contact with oxygen can accelerate solution decomposition. It appears that only the solution annealed materials are particularly sensitive to this variable as the solution needs to be at full strength to reactivate a material with no chromium depletion zones and may not need to be at full strength to be aggressive enough to reactivate a sensitized material. In this light, all EPR testing was performed in solution that was less than 24 hours old.

Based on the above discussion, the possibility of a small reactivation peak for solution annealed material may be inherent electrochemically in the EPR test or due in part to some aspect of the sample preparation but this peak relatively small when it occurs and does not represent senstization of any kind.

For most of the solution annealed alloys tested, insufficient etching took place during the EPR test for significant detail of the microstructure to be visible. When visible (generally the lower ferrite CF8 alloys) the ferrite pools were slightly stained and no discernable "step" structures between the ferrite pools and austenite matrix were noted. No other microstructural detail was noted.

The data of Figure 24 (page 83) indicate that, in general, the as-cast and furnace cooled conditions of the high carbon (.06 - .08% C) alloys have EPR responses (peak magnitude higher than the corresponding solution annealed alloys. Microstructurally the attacked regions (chromium depleted zones) leading to the high peak current densities of the as cast and furnace cooled materials are readily apparent. The ferrite-austenite interface is the preferred location for the precipitation of chromium carbides (see Literature Review) and the associated chromium depletion zones--which are dissolved by the EPR test--surround the carbides. Figure 30a is a low magnification optical micrograph indicating attack (deep grooves that appear dark) that is confined to the ferrite-austenite boundary regions in an as cast CF8 alloy with a ferrite number of approximately four. The austenite matrix is immune to attack in most cases. Figures 30b and

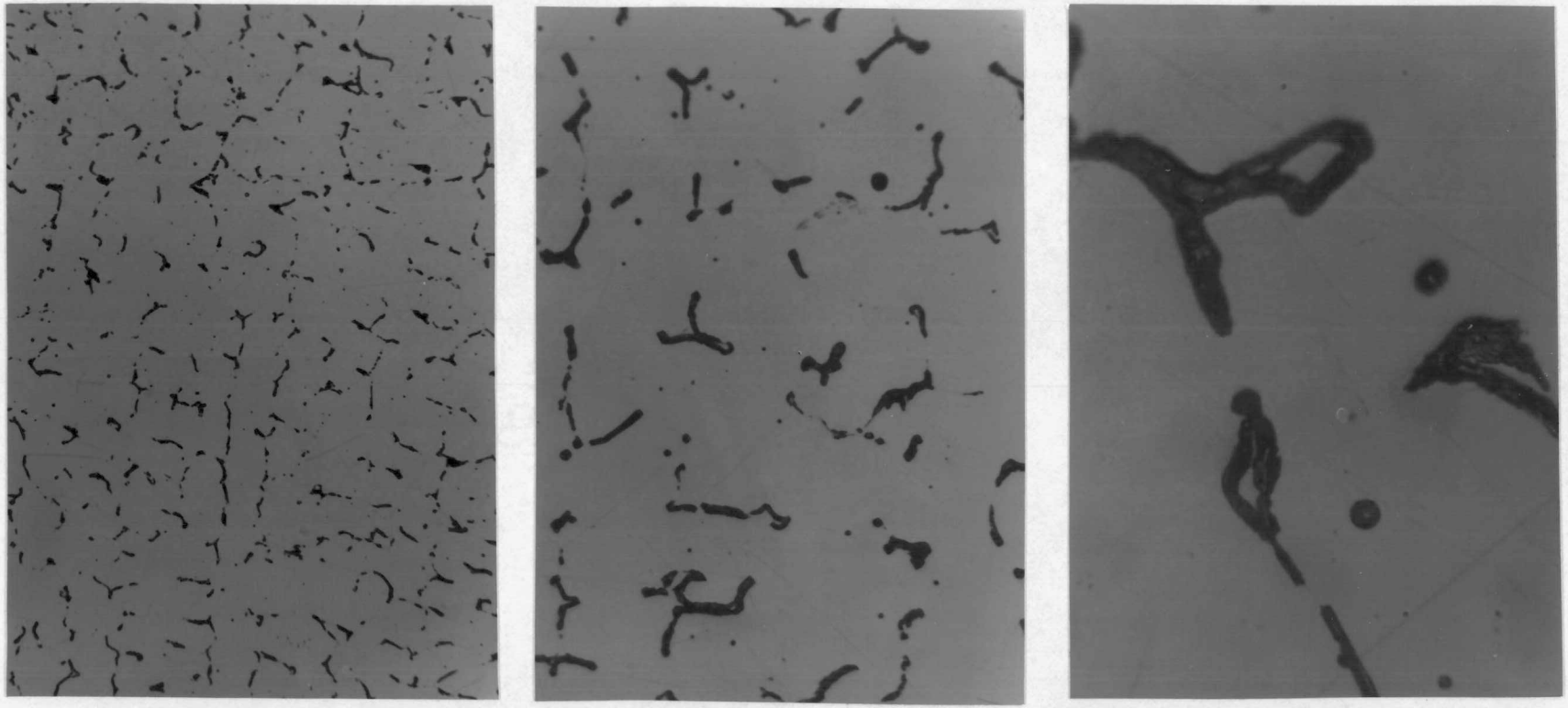

(a) 100 X (b) 250 X (c) 1000 X

Figure 30. Low ferrite (FN ≈ 4) CF8 alloy in the as-cast condition, as EPR tested.

30c are optical photographs of the same alloy at increasing magnification. The attack at the ferrite-austenite boundary is very extensive (nearly 100% of the available interface has deep grooves associated with it) and has obliterated the detail of the ferrite-austenite boundary. Also, the wide grooves at the boundary make the alloy appear to have more ferrite than is actually present.

Figure 31 points out an interesting fact about these alloys. Despite the data that indicates no substantial overall orientation effect for the alloys, Figure 31 shows that some grains within a test piece may not be attacked to the same degree as the majority of the sample. This indicates (as expected) that sampling sizes should not be so small as to incorporate only a few grains of material.

Figure 31 also points out that even for ferrite numbers in the range of 3 - 4, the austenite-austenite grain boundaries are not totally immune to attack. As indicated at the boundary between the austenite grains of Figure 31 the continuous and near continuous grooves (of which ferrite pools are a part) indicate that some chromium depletion has taken place at the austenite-austenite boundaries. It may be significant that this behavior at the austenite grain boundaries was noted only adjacent to grains that showed a relatively small amount of attack at the ferrite-austenite boundaries.

Figure 32 is an SEM photograph of the ferrite-austenite boundary in the low ferrite CF8 alloy that shows the deep grooving at the ferrite-austenite interface and some dendritic carbides at the ferrite-austenite interface. Figures 30 - 32 represent typical appearances

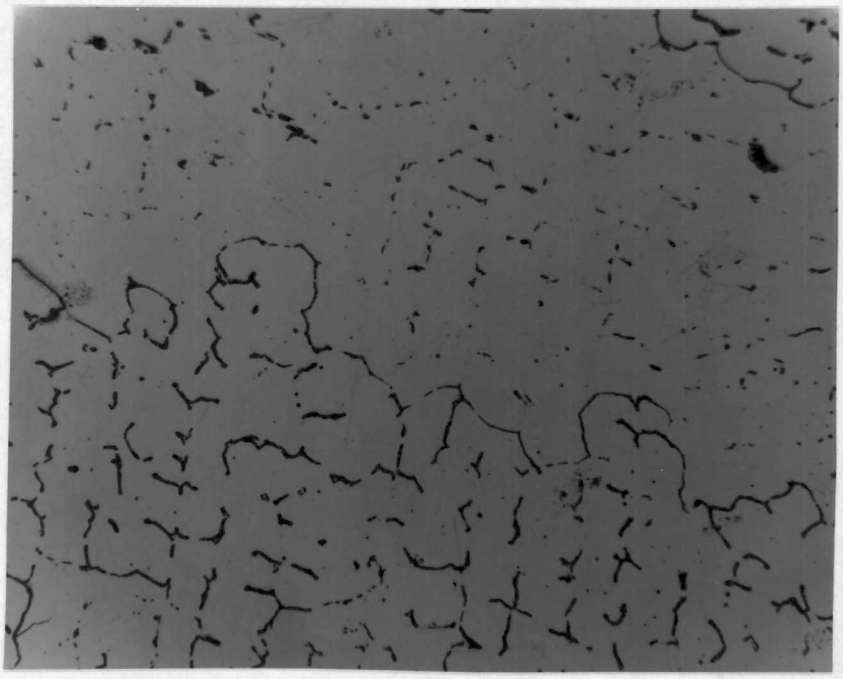

Figure 31. Low ferrite (FN ≈ 4) CF8 in the as-cast condition, as EPR tested, indicating variability of attack in adjacent grains. 100 X.

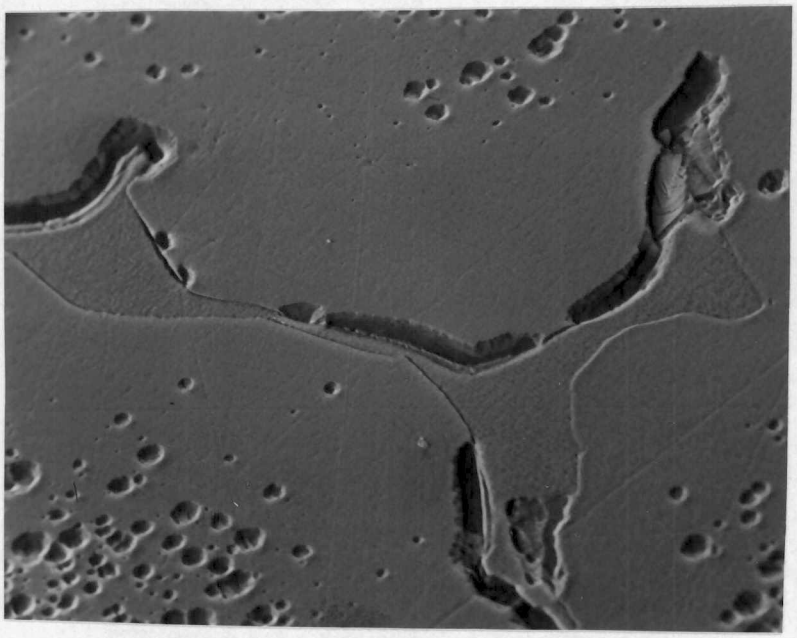

Figure 32. Low ferrite (FN ≈ 3) CF8 in the as-cast condition indicating ferrite-austenite boundary nature of attack in the EPR test. SEM, 5000 X.

of as cast and furnace cooled CF8 alloys with a ferrite content greater than about 2 percent. In some instances, the austenite matrix was severely pitted by the EPR test. In these instances, the pitting was confined to the centers of the austenite grains with a "denuded zone" around each ferrite pool that was free of pitting. Figure 33 is representative of this type of behavior. The cause of this pitting tendency is not understood at present, however it has been noted that it seems to occur only in particular alloys after specific heat treatments. In the high carbon (.06% C - .08% C) alloys, only the low ferrite CF8 alloy tends to exhibit occasional austenite pitting in the as cast condition. Pitting has not been observed in any other high carbon alloy. Many samples of the low ferrite CF8 material in the as cast condition were evaluated by the EPR test and only a few exhibit pitting. The pitting is not particularly reproducible--i.e., occasionally a low ferrite CF8 alloy will pit in the EPR test but in the majority of cases it does not pit. The pits also vary in depth and density so that it is not feasible to predict their contribution to the EPR peak current density. In the as cast condition, the pitting contribution to the peak current density seems to be small compared to the contribution from the grooves at the ferrite-austenite boundary (based on comparison of results with and without pitting) but as will be noted later this pitting tendency does appear in low ferrite CF8 samples with different heat treatments where the pitting constitutes the majority of the peak current density for the sample. It is possible that this behavior indicates a special susceptibility

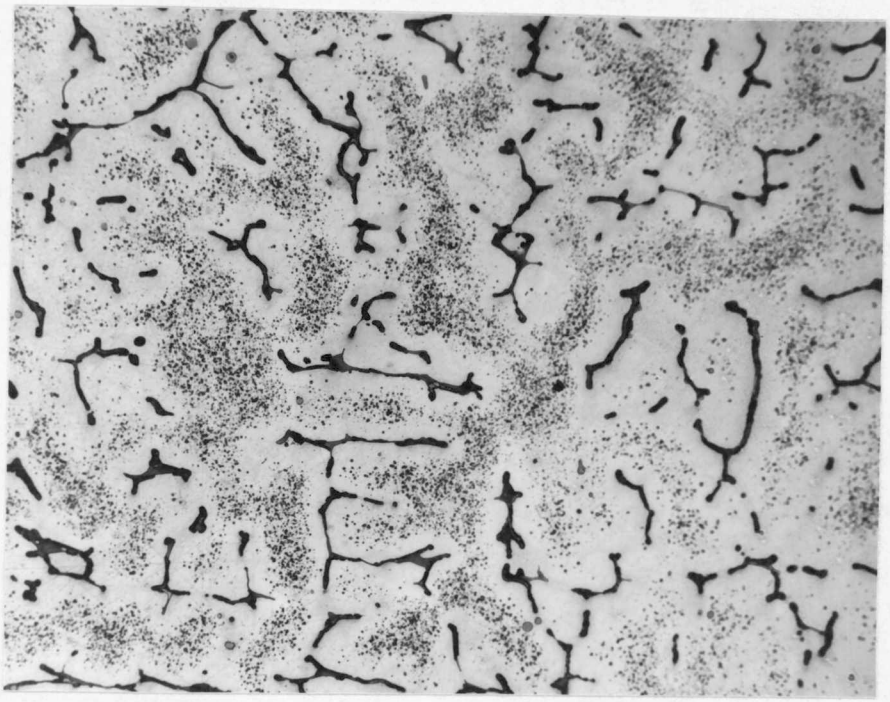

Figure 33. Low ferrite (FN ≃ 5) CF8 in the as-cast condition indicating pitting behavior in addition to ferrite-austenite boundary ditching in the EPR test. 250 X.

to surface preparation variables for the low ferrite CF8 alloys but in a later section it will be indicated that surface preparation may not be the controlling variable.

Figure 34a represents the typical appearance of the high carbon CF8 alloys with a high ferrite content in the as-cast condition. As with the low ferrite samples, the austenite matrix is virtually immune to attack. With the high ferrite samples, there is enough ferrite-austenite interface available to "absorb" all of the carbide precipitation and the austenite-austenite boundaries are free from attack associated with carbide formation and chromium depletion. Figure 34b is a high magnification photograph of the same alloy. Note the small, unetched particles that seem to be surrounded by the ditching (dark). These particles are the carbides that are responsible for the chromium depletion. Various etching and staining techniques indicated that a few of these particles may be sigma phase but very few such particles were found in the CF8 alloys.

Occasionally a region such as that shown in Figure 35 was observed on CF8 alloys following EPR testing. Note the flakelike dendritic carbides associated with the ferrite-austenite interface as well as the eutectic looking carbide situated on (or in) the ferrite pool. The occurrence of carbides in this type of eutectic network and orientation was relatively rare.

During the sensitizing treatment, if the ferrite content of the alloy is less than FN = 1 - 2, there is insufficient ferrite-austenite boundary to "absorb" all of the carbide precipitation and the

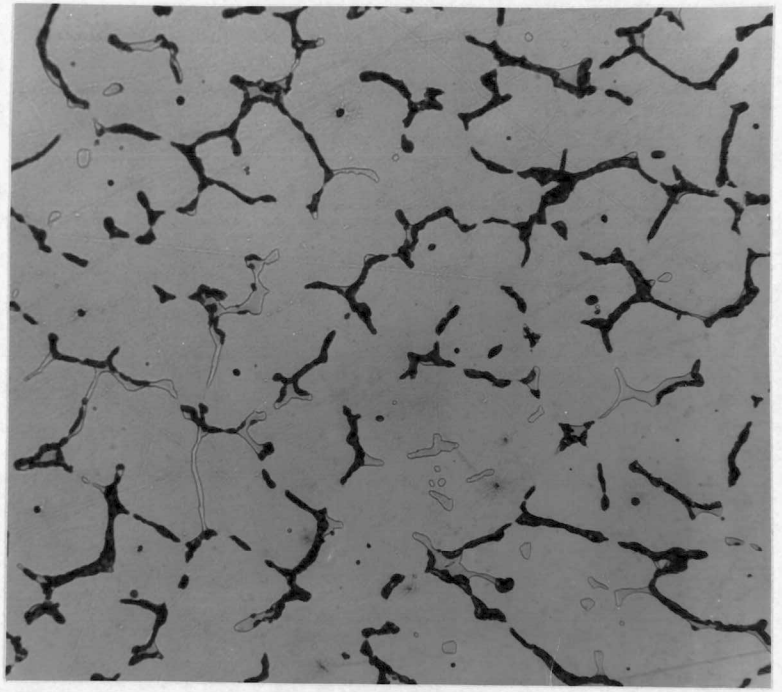

(a) 250 X

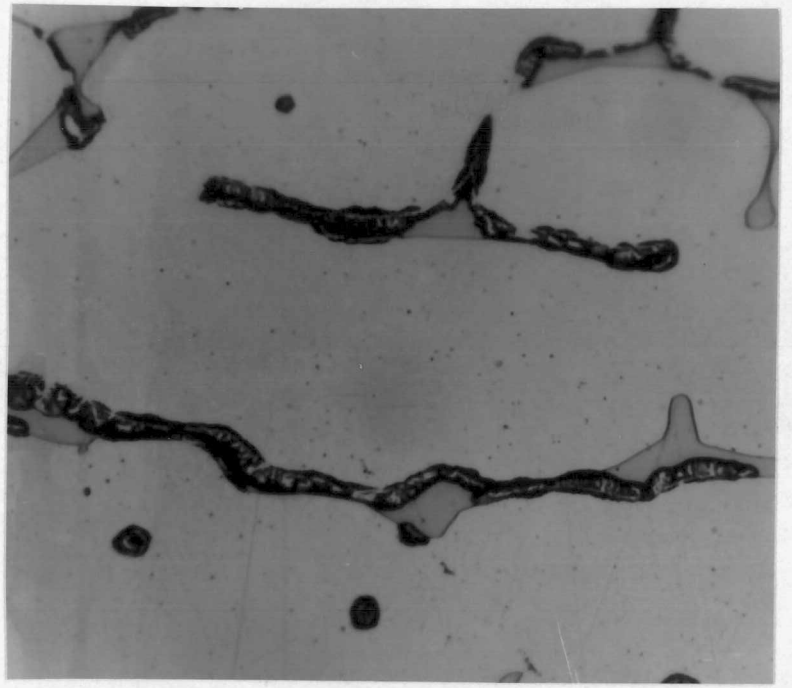

(b) 1000 X

Figure 34. High ferrite (FN ≈ 15) CF8 alloy in the as-cast condition, as EPR tested.

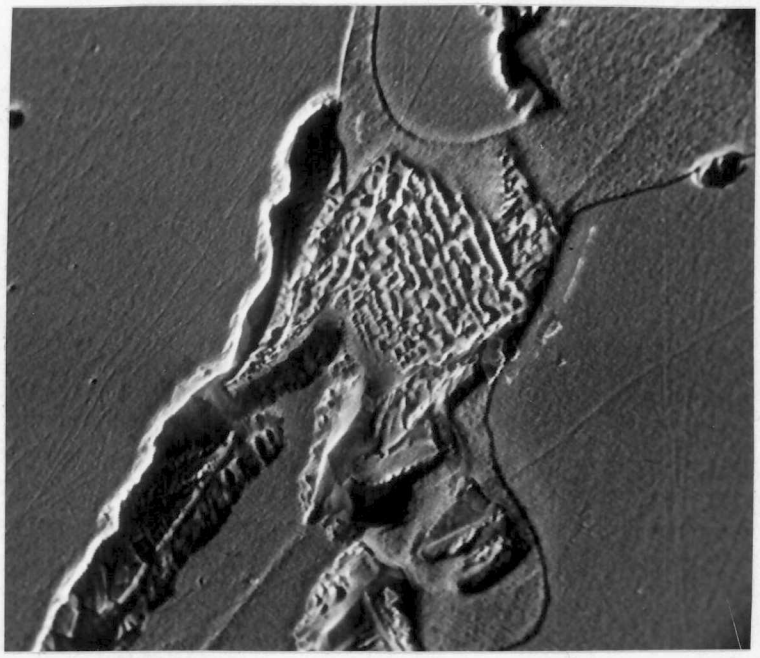

Figure 35. Low ferrite CF8 alloy, as EPR tested, indicating carbides associated with ferrite pool. SEM, 2100 X.

austenite-austenite boundaries (as well as the austenite matrix to a small degree) become susceptible to carbide precipitation and associated chromium depletion. Figure 36a shows a low magnification optical micrograph indicating grain boundary ditching after the EPR test for a ferrite content near zero. At higher magnification (Figure 36b) dendritic carbides may be observed at the bottom of the grain boundary.

The sensitized (as cast, furnace cooled) CF8M samples have a somewhat more complicated etching pattern after EPR testing and this appears due to the presence of some sigma phase as well as carbides in an around the ferrite pools. Figure 37a indicates a typical appearance of a low ferrite as cast CF8M alloy. Note that, in general, the ferrite-austenite boundaries are not ditched to the extent that the boundaries were ditched in the CF8 alloys. Higher magnification (Figure 37b) shows that the particles responsible for the chromium depletion are located predominantly in the ferrite pool as opposed to on the ferrite-austenite boundary in the CF8 alloys. Based on the results of other staining and etching techniques, most of the particles that are outlined in the ferrite are carbides. Sigma particles can occasionally be observed at various locations within the ferrite (usually near the center of the ferrite pool) but they are difficult to identify positively; this is due to their small size and proximity to carbide particles.

Another important result indicated by the EPR data of Figure 24 (page 83) for the as cast and furnace cooled conditions is that the CF8M alloys have a reactivation peak current density that is an

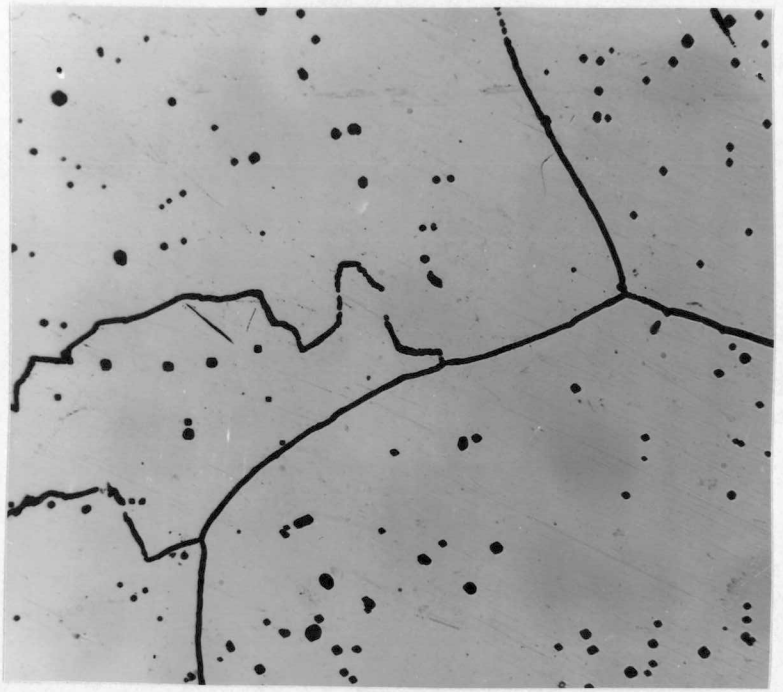

(a) 100 X

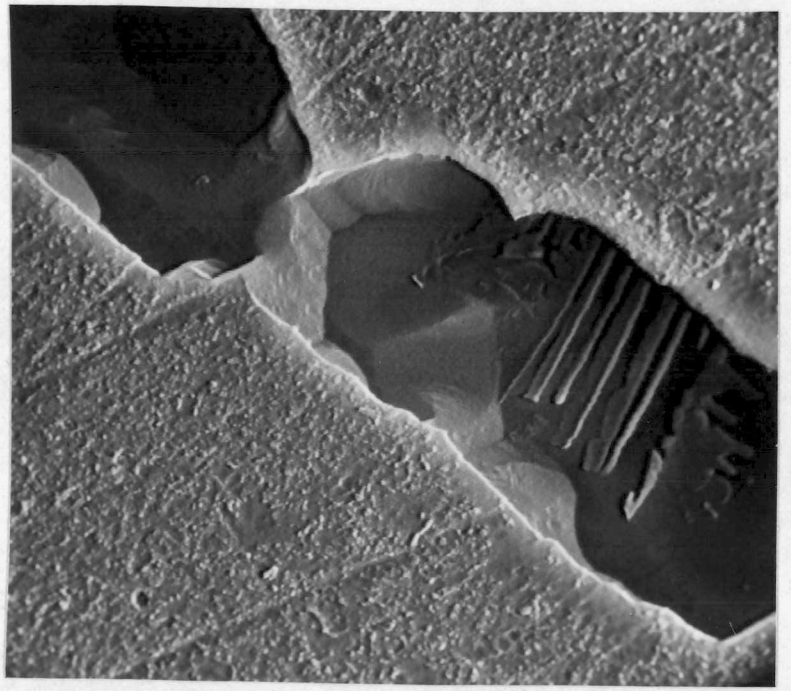

(b) SEM, 5000 X

Figure 36. Furnace cooled CF8 alloy (FN ≈ 0 after heat treatment) after EPR testing indicating grain boundary attack.

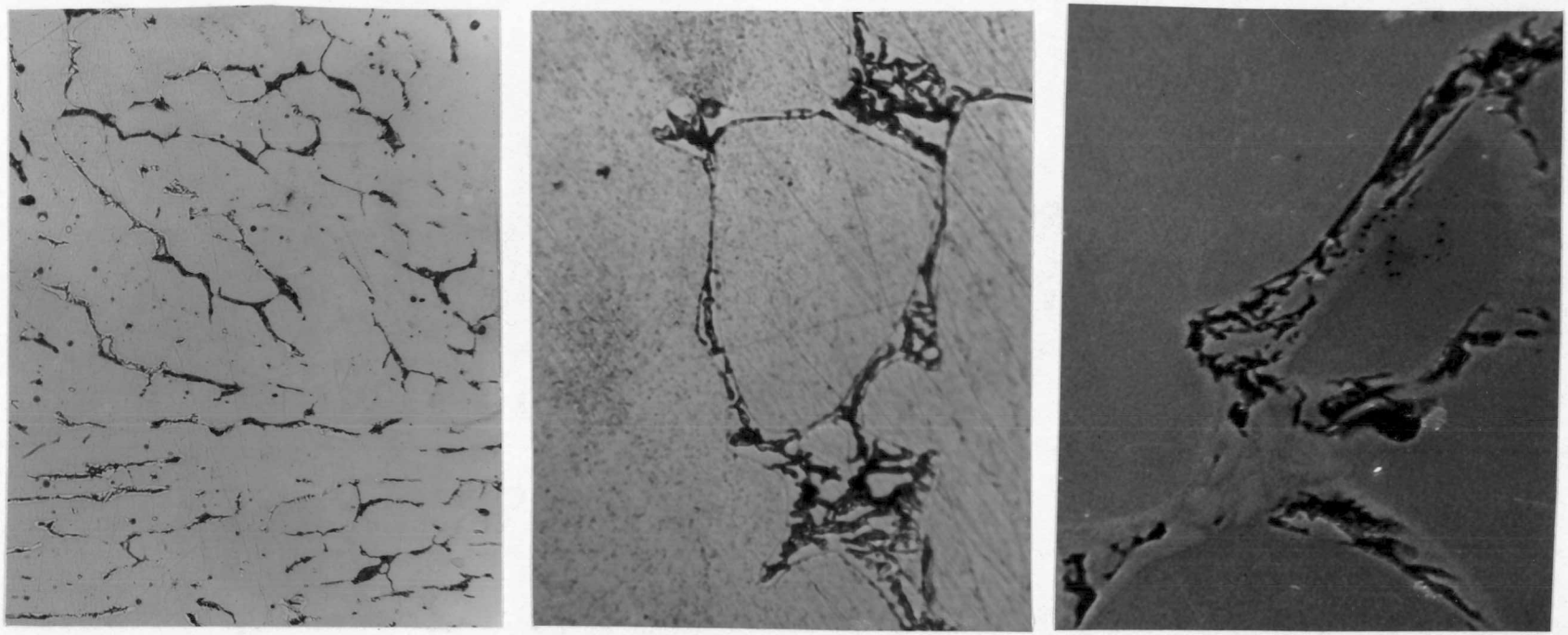

(a) 100 X (b) 1000 X (c) SEM, 2000 X

Figure 37. Low ferrite (FN ≈ 5) CF8M alloy in the as-cast condition, as EPR tested.

order of magnitude smaller than the peak current density for the corresponding CF8 alloy for equivalent heat treatments at both the .06 and .08% C carbon contents and all ferrite levels. The only compositional difference between the CF8 and CF8M alloys is that the CF8M alloys contain about 2% Mo and the CF8 alloys contain much smaller amounts (generally below about .1% Mo).

Having laid the groundwork for the evaluation of the sensitization characteristics of duplex stainless steels with the EPR test, the test program was expanded to evaluate the various degrees of sensitization utilizing isothermal hold data in the temperature range 550 - 875°C and for times from 20 minutes - 48 hours.

Table 4 is a collection of the isothermal hold EPR data for the high carbon alloys with some representative EPR data for the solution annealed, as cast, and furnace cooled conditions for comparison. Several important trends are indicated by these data and representative data are graphed in Figures 38 - 45.

It appears that, in general, the EPR test does not detect a significant difference between alloys containing .06% C (high and low ferrite levels) and .08% C (intermediate ferrite level). This is manifest by the fact that, for both CF8 and CF8M, the .08% C alloy does not sensitize appreciably faster (reach high peak curent density in shorter isothermal holds) than the low ferrite CF8 or CF8M alloys, respectively. In fact, for many heat treatments, the .08% C alloys have lower EPR response than the corresponding low ferrite .06% C alloys. (See Figures 38 - 42.) This trend is particularly true for

Table 4. Summary of EPR data for high carbon alloys. Peak current density x 10^5 amp/cm given.

HEAT TREATMENT		CF8 LO FN	CF8 INT FN	CF8 HI FN	CF8M LO FN	CF8M INT FN	CF8M HI FN
SOLUTION ANNEALED		10	8	2	3	2	1
AS CAST		900	1200	900	600	200	250
FURNACE COOLED		2000	1200	800	60	350	450
550°C	20 MIN	170	29	19			
	1 HR	830	130	71	.10	.10	.10
	6 HR	1100	520	550	11	40	92
	48 HR	3000	2500	2200	150	450	600
600°C	1 HR	1400	760	910	2	5	3
650°C	20 MIN	630	1100		5	9	
	1 HR	970	1500	450	22	150	130
	6 HR	1200	830	31	250	100	16
	48 HR	1700	530	62	95	120	90
725°C	20 MIN	290	150	80	100	200	47
	1 HR	400	150	110	200	330	18
	6 HR	220	90	100	23	7	60
	48 HR	350	70	120	100	130	62
800°C	20 MIN						
	1 HR						
	6 HR	820	32	23	22		36
	48 HR	190	36	130	110	85	36

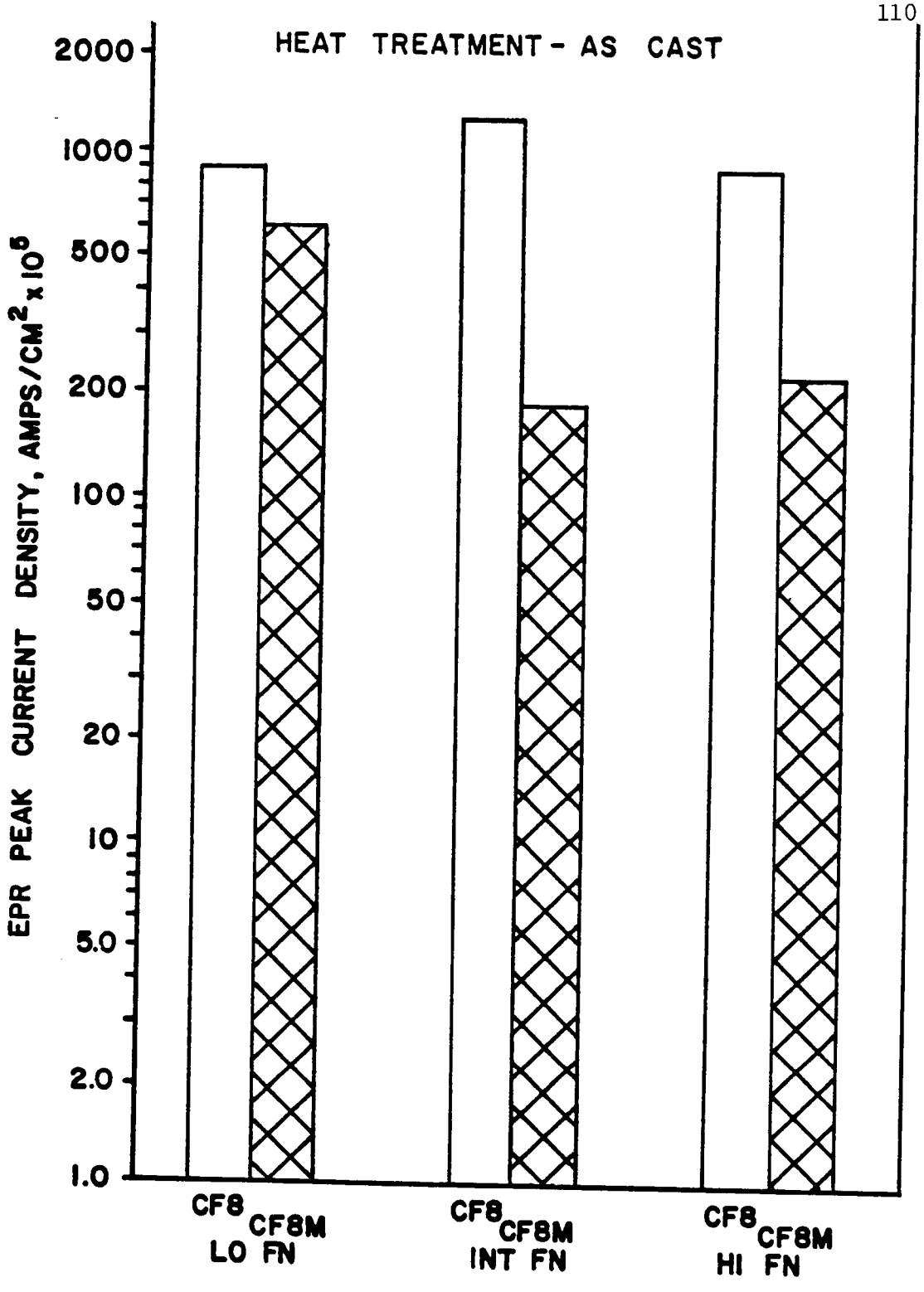

Figure 38. EPR data for CF8 and CF8M as a function of ferrite for as-cast condition.

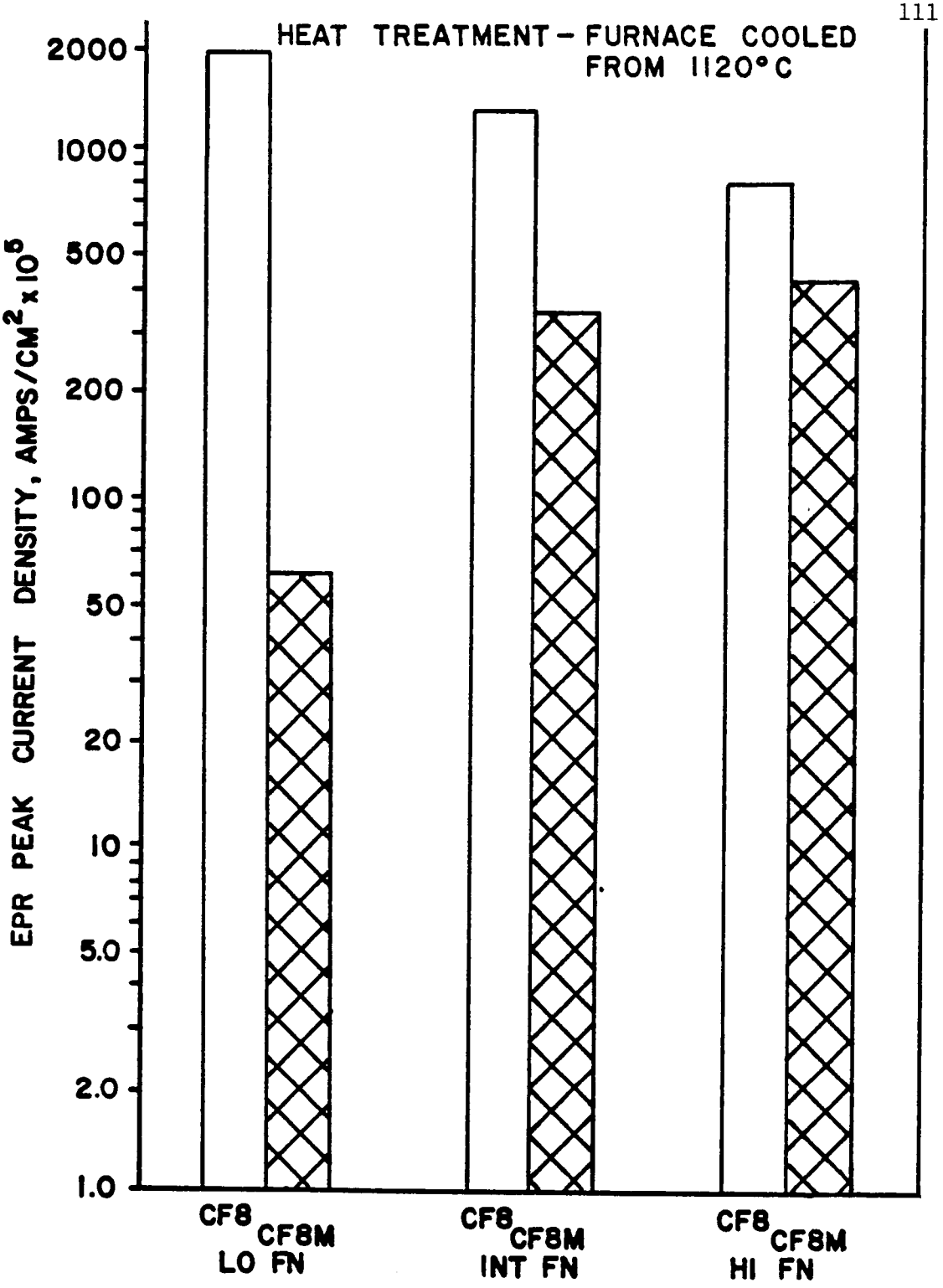

Figure 39. EPR data for CF8 and CF8M as a function of ferrite for furnace cooled condition.

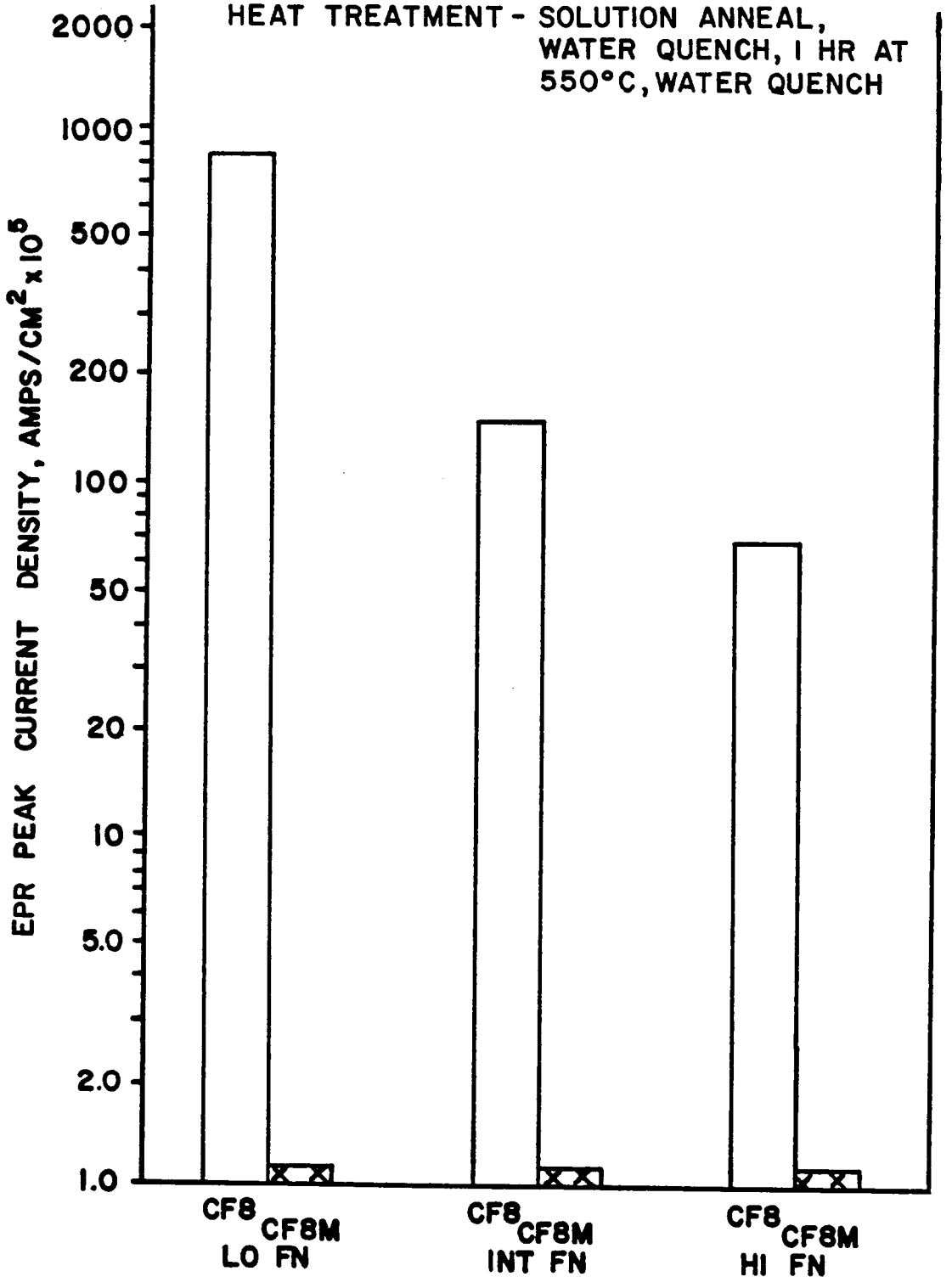

Figure 40. EPR data for CF8 and CF8M as a function of ferrite for heat treatment at 550°C.

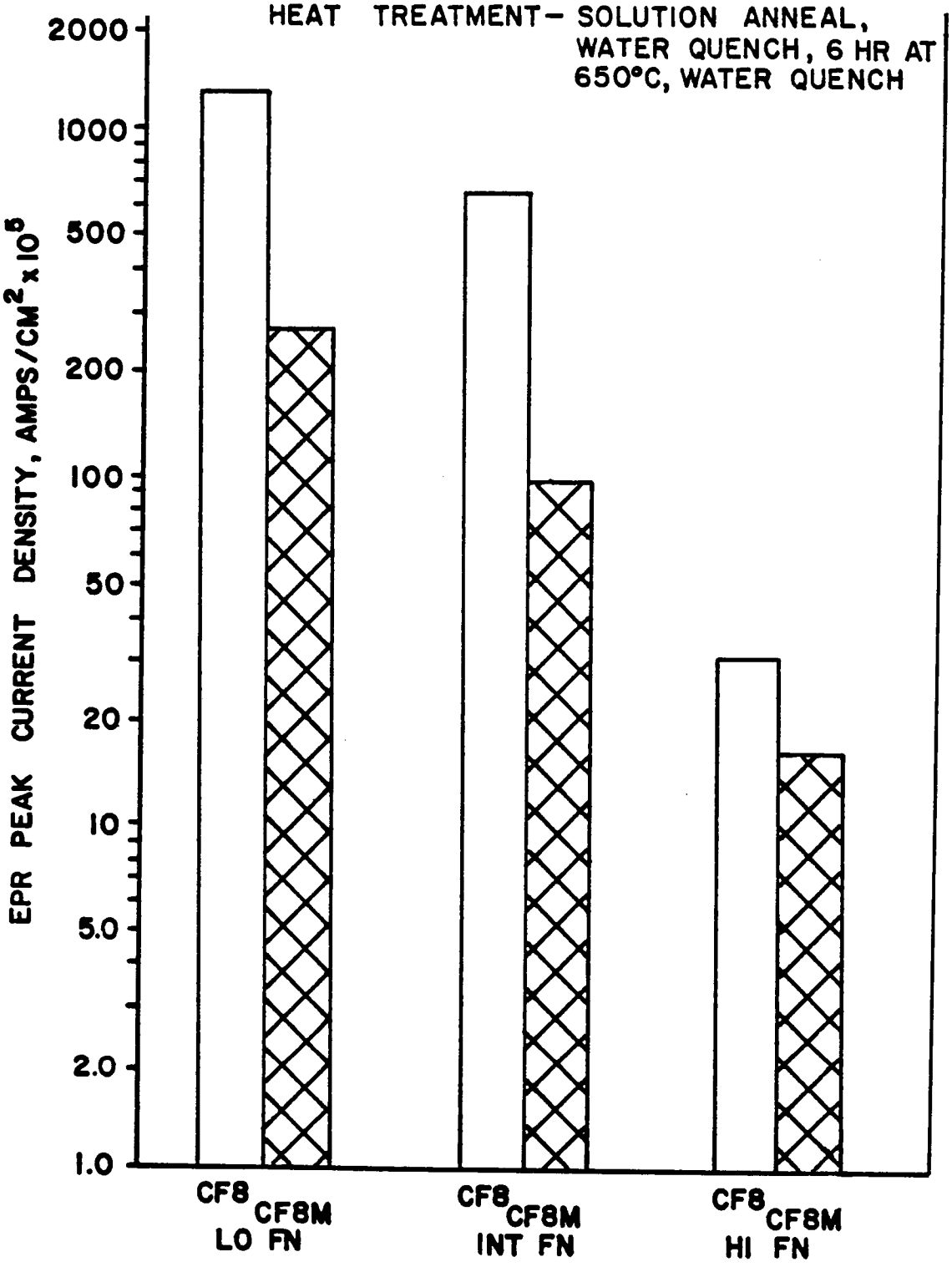

Figure 41. EPR data for CF8 and CF8M as a function of ferrite for heat treatment at 650°C.

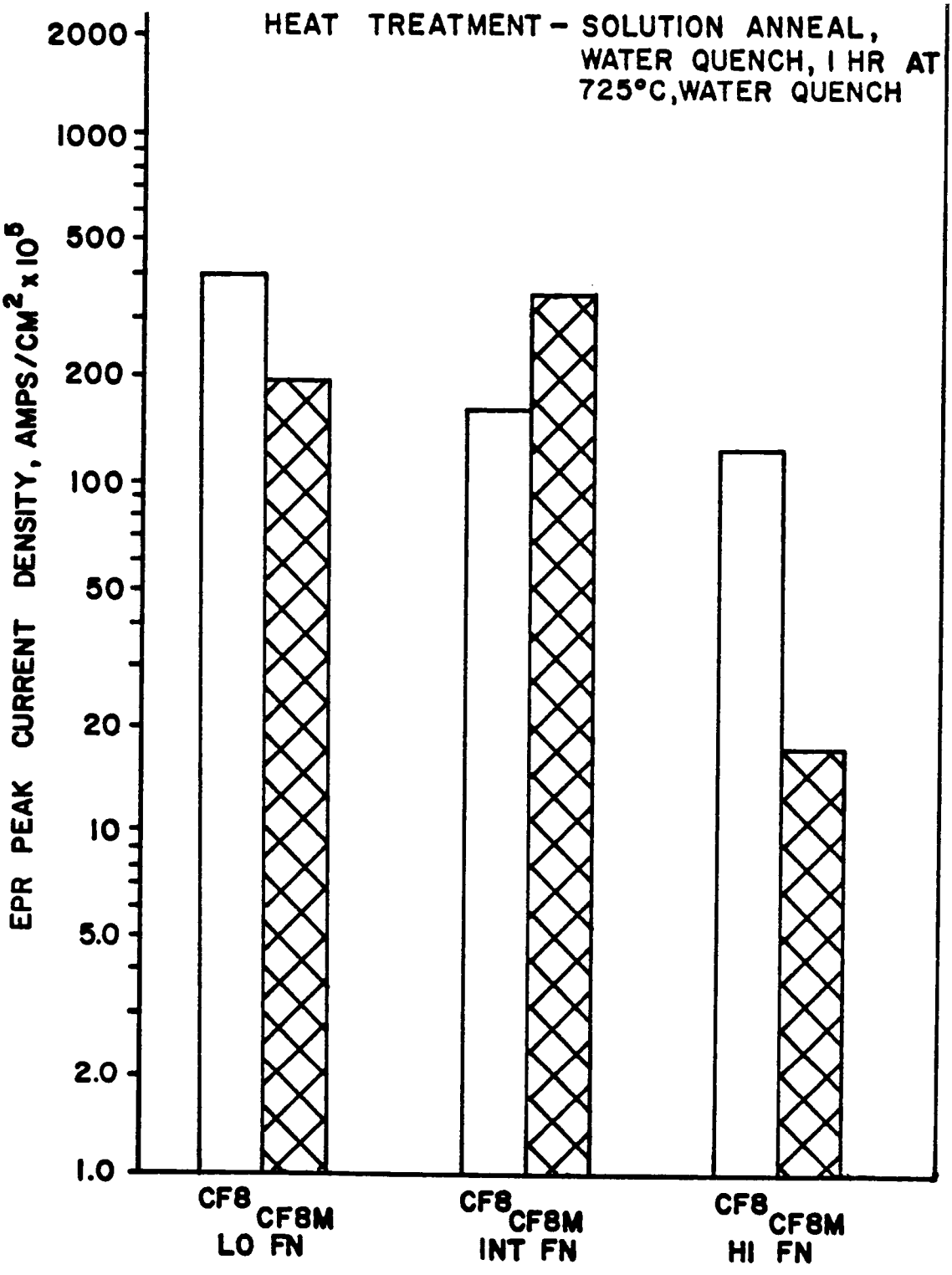

Figure 42. EPR data for CF8 and CF8M as a function of ferrite for heat treatment at 725°C.

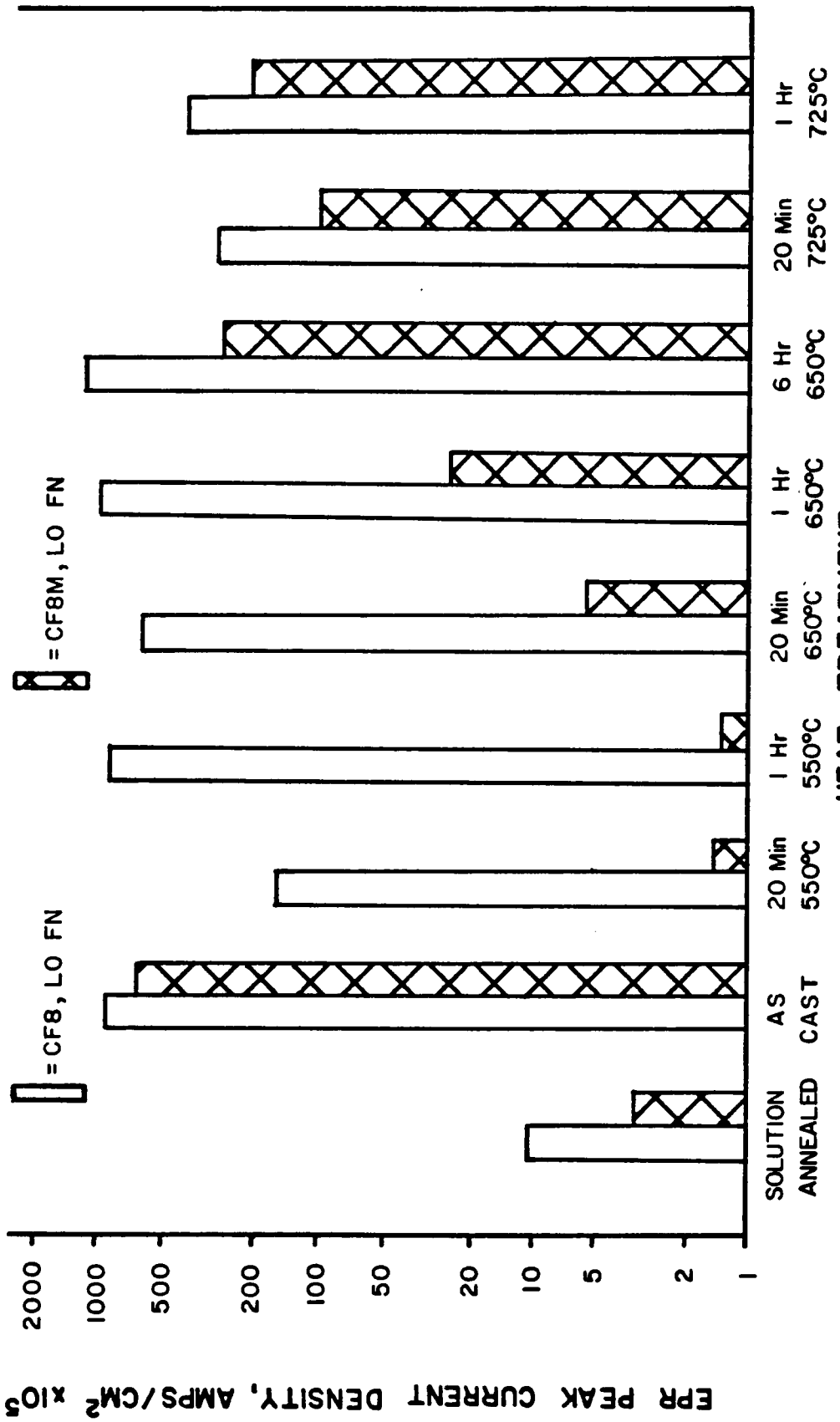

Figure 43. Representative EPR data for CF8 and CF8M at the low ferrite level for various heat treatments.

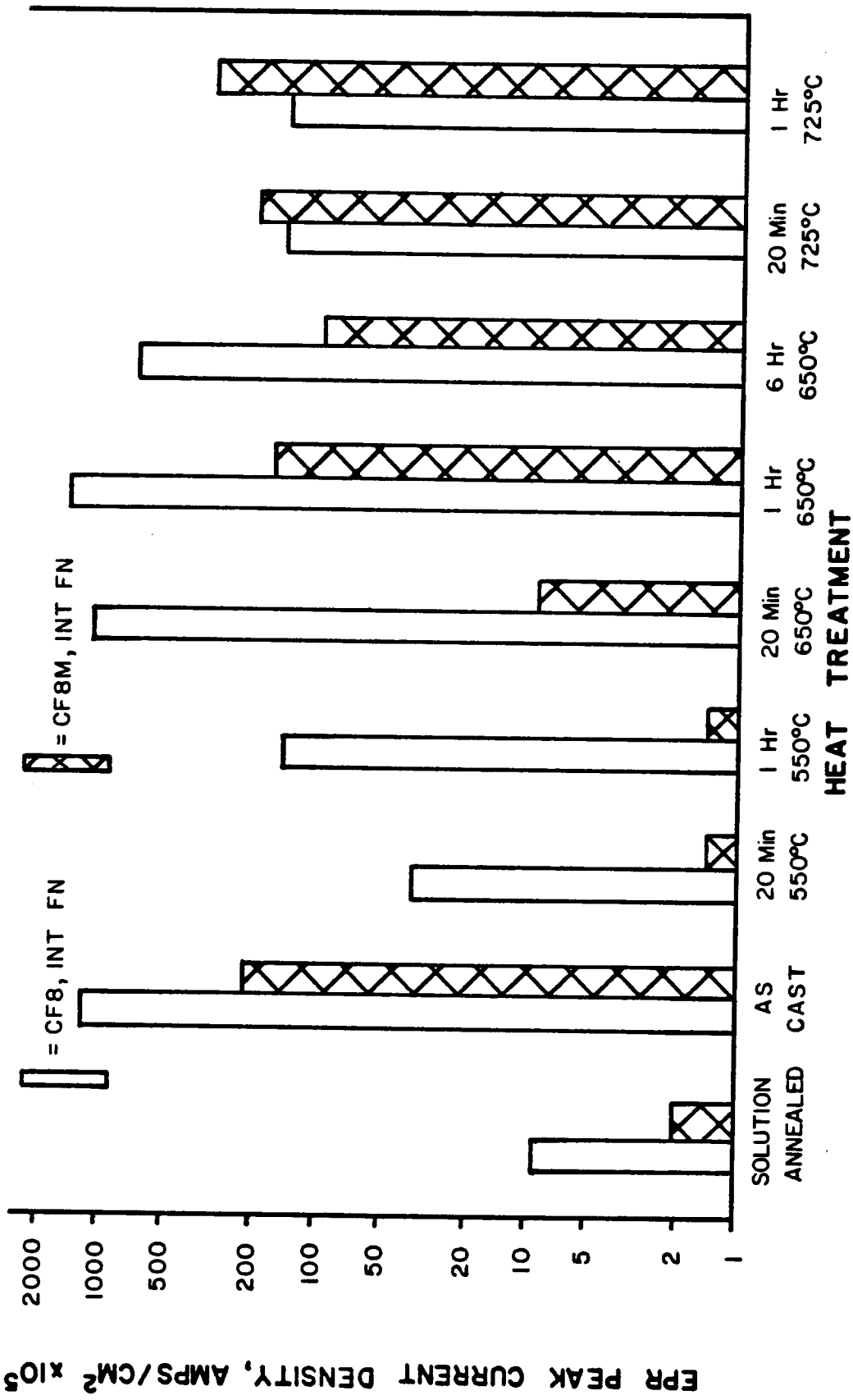

Figure 44. Representative EPR data for CF8 and CF8M at the intermediate ferrite level for various heat treatments.

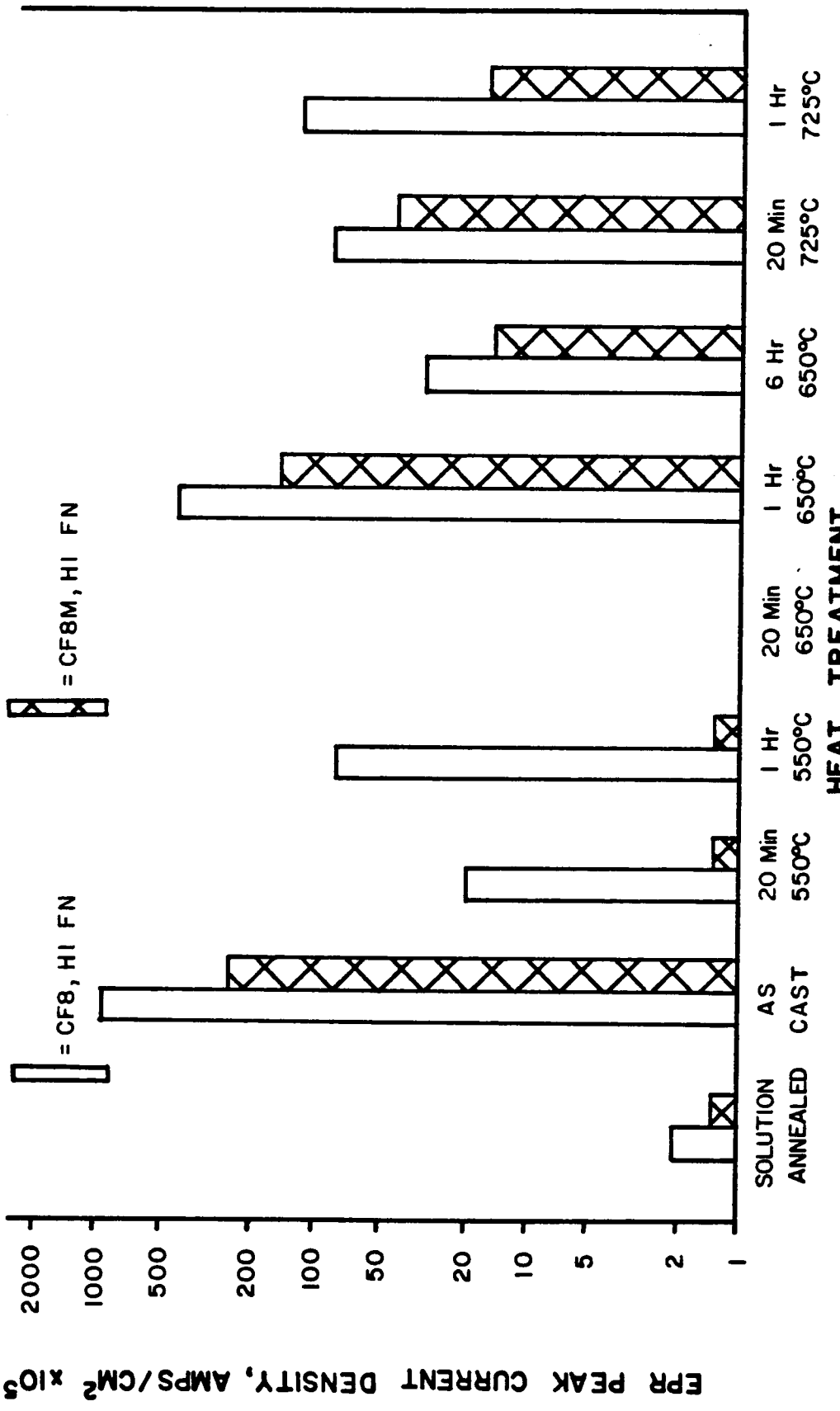

Figure 45. Representative EPR data for CF8 and CF8M at the high ferrite level for various heat treatments.

the CF8 alloys. Close inspection of Table 4 indicates that, particularly for the CF8 alloys, the ferrite content appears to be a very important variable. Although not true in every case, the trend seems to be that the higher the ferrite content, the lower the peak EPR response for a given heat treatment within an alloy class. This trend is again indicated by Figures 38 - 42. (As will be discussed in detail in another section, this effect may actually be related to the bulk chromium content of the alloy as opposed to the ferrite content per se.)

The isothermal hold data also indicate that (compared to the solution annealed condition) the CF8 alloys are particularly susceptible to sensitization at all temperatures examined but the maximum sensitization damage appears to occur in the lower half of the classical sensitization temperature range, i.e., 550 - 650°C. According to the literature (29 - 32) the temperature range of 550 - 650°C roughly corresponds to the temperature range at which the maximum chromium depletion occurs due to the morphology of the carbides that form at these temperatures. Also, the most rapid sensitization seems to occur in the 600 - 650°C temperature range for the CF alloys which is significantly lower than the temperature range predicted by A262 B - E tests (6). Temperatures near 725°C seem to sensitize the CFM alloys the most readily. Representative data as a function of heat treatment are shown in Figures 43 - 45.

As was discussed earlier for the as cast and furnace cooled conditions for the high carbon alloys, the isothermal hold data also

indicate that the Mo bearing CF8M alloys seem to be far less susceptible to sensitization than the CF8 alloys. This is particularly true for the short duration or low temperature heat treatments, where the difference can be as large as two orders of magnitude or more. In Figures 38 - 45, this is shown clearly as all CF8 alloys (except two heat treatments at 725°C) are more susceptible to sensitization as measured by the EPR test than the equivalent CF8M alloy. This indicates that the degree (amount and extent) of chromium depletion in the Mo bearing alloys is considerably smaller than in the CF8 alloys that contain only very small (<.1%) amounts of Mo. It is known (6) that when Mo is present it may substitute for Cr in small amounts in the carbide but it is unlikely that this could account for the signficant differences in EPR response between the CF8 and CF8M alloys. It is possible that molybdenum may slow chromium diffusion such that the number and size of the carbides that form in the CF8M alloys are more limited than for the CF8 alloys for short heat treatments in the sensitizing temperature range. It is also probable that the presence of Mo in some way "makes up for" chromium depletion, i.e., the chromium level at which "chromium depletion" is detected by the EPR test is somewhat lower in the presence of molybdenum. This effect is also very evident microstructurally following the EPR test. The CF8 alloys show extensive (greater than 50%) ditching at the ferrite-austenite boundaries for all of the heat treatments for which the EPR peak current density exceeds about 1.0×10^{-3} amp/cm^2 (i.e., 100 in Table 4). The CF8M alloys very

seldom showed ditching at all, even for the few heat treatments where the corresponding peak EPR response was greater than 1.0×10^{-3} amp/cm^2. The etching (when there was enough to detect with the optical microscope) was limited to very thin regions adjacent to carbides that appeared to be contained predominantly in the ferrite pools and some very light etching of the ferrite-austenite boundaries. Carbides may be located at the ferrite-austenite boundary where light etching occurs but they are too small (or insufficient etching has occurred) to be detected. Thus, the EPR test is very sensitive to the presence of molybdenum.

The data of Table 4 also point out that, as expected, the peak EPR response generally increases as the length of isothermal exposure in the sensitizing temperature range increases. This would be expected because as the carbides grow in size with increasing isothermal hold time, chromium is depleted from the area adjacent to the carbide faster than chromium can diffuse from the bulk matrix to the chromium depleted zone. One might expect that after a very long isothermal hold that the material would tend to become desensitized, or "heal," due to rediffusion of chromium from the bulk matrix to the chromium depleted zones. Since the EPR peak current densities of Table 4 for the long isothermal holds do not show a regular decrease compared to the other isothermal hold data--in fact, after 48 hours the EPR response is still increasing for some alloys--healing is not occurring to any significant extent in these alloys even after 48 hours at temperature. (A possible exception could be the CF8M alloys heat treated at 725°C.) The "healing" process is

commonly found in wrought stainless steels but the time required is on the order of 100 - 1000 hours depending on the isothermal hold temperature and the carbon and chromium content of the alloy.

As a final note concerning the isothermal hold data for the high carbon alloys, it was noted that the low ferrite CF8 alloy showed a tendency toward pitting in the austenite matrix between ferrite pools during the EPR test. This tendency was mentioned previously in connection with the as-cast material of the same alloy. This tendency was only noticed on the alloys treated at 550 - 650°C and only for the case of the sample treated for 20 minutes at 550°C did the pitting seem to contribute a significant fraction (specifically, more than half for this alloy) of the total EPR response.

EPR Test--Low Carbon Alloys

Alloys with carbon contents of .015 - .027% C (cast equivalents of the "L" grades of wrought stainless steel) were also evaluated with the EPR test for a variety of heat treatment conditions. Table 5 summarizes the EPR data for the low carbon alloys. (The carbon content of the CF3M alloys ranges from .022 - .027% C; the low and high ferrite CF3 alloys have .015 - .016% C and the intermediate ferrite CF3 contains .023% C.) Representative data are shown graphically in Figures 46 - 55. As is immediately evident from the representative data of Figures 46 - 48, the low carbon alloys have significantly lower EPR peak current densities than the corresponding high carbon alloys for most heat treatments. Of particular importance is the fact that in the as-cast and furnace

Table 5. Summary of EPR data for low carbon alloys. Peak current density x 10^5 amp/cm given.

HEAT TREATMENT		CF3 LO FN	CF3 INT FN	CF3 HI FN	CF3M LO FN	CF3M INT FN	CF3M HI FN
SOLUTION ANNEALED		52		9.6	1.3		0.8
AS CAST		720	1100	50	13	11	2.0
FURNACE COOLED		430	270	100	9.0	11	2.4
	20 MIN						
550°C	1 HR	710		58	1.9		1.0
	6 HR	1600		180	4.1		1.0
	20 MIN						
650°C	1 HR	1400		66	11		1.0
	6 HR	1500		36		35	16
	20 MIN						
725°C	1 HR	280	14	10	3.2	1.1	3.2
	6 HR	130	7.7	50	5.2	1.0	1.0

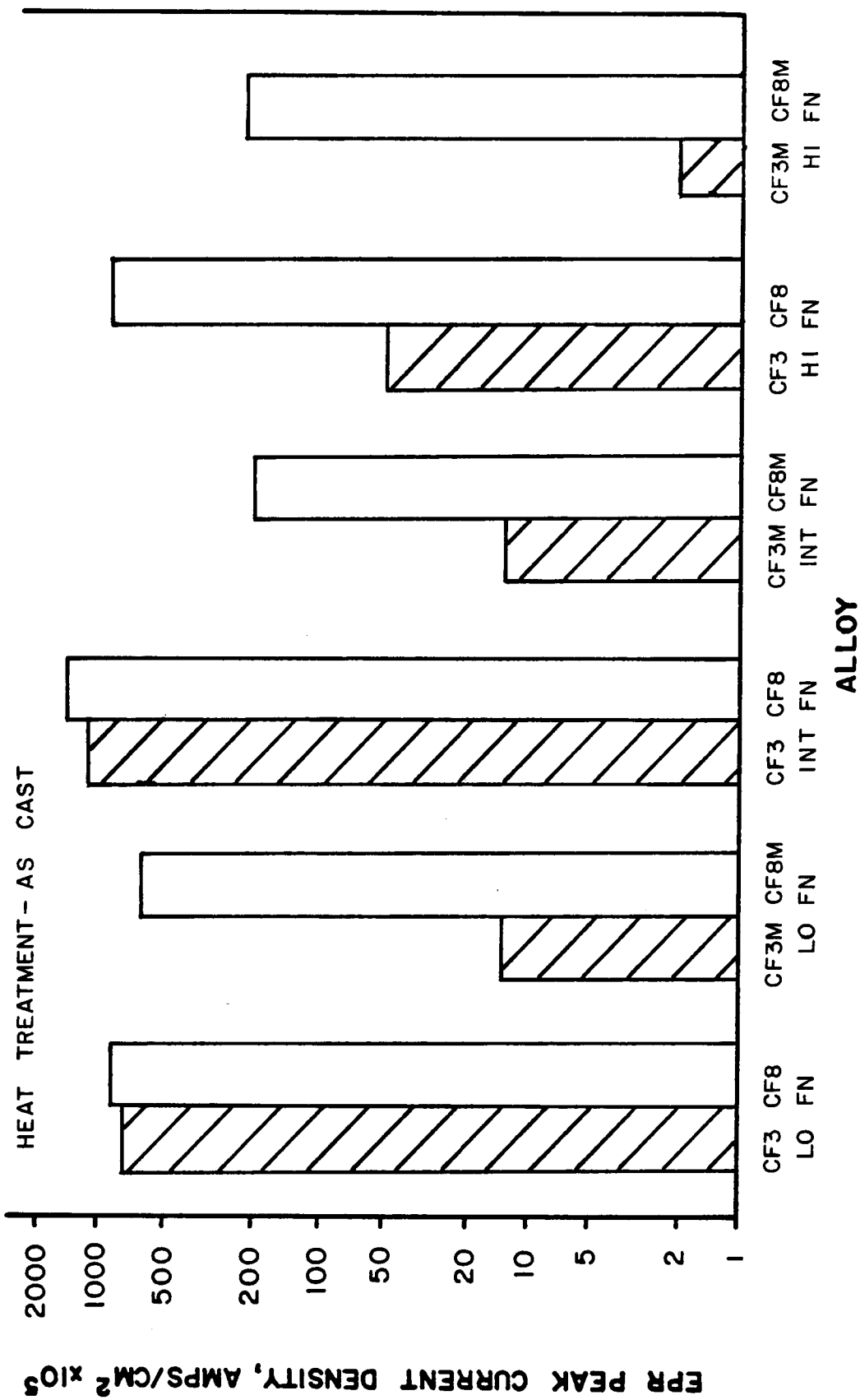

Figure 46. Comparison of EPR results as a function of carbon content for CF and CFM alloys in the as-cast condition.

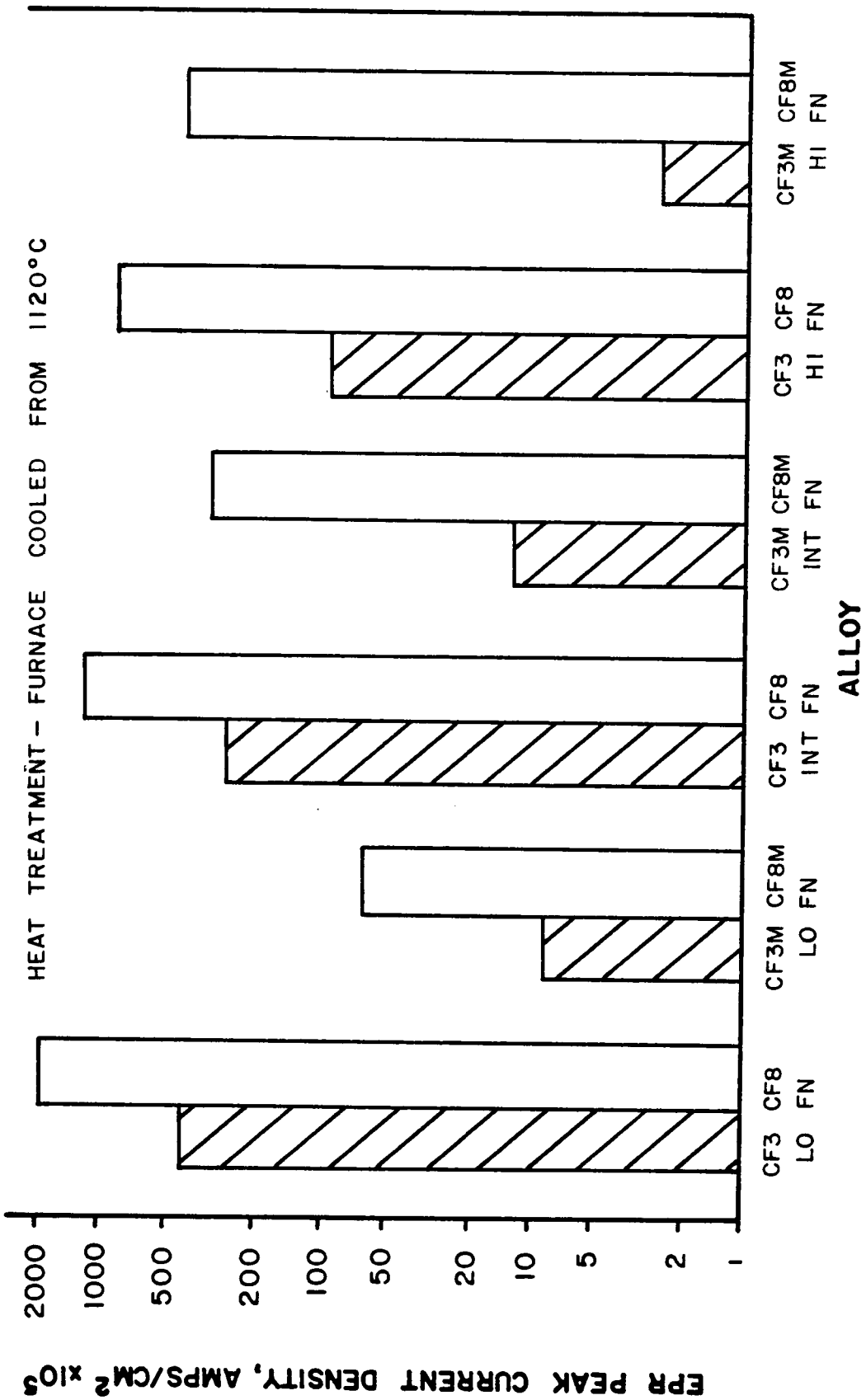

Figure 47. Comparison of EPR results as a function of carbon content for CF and CFM alloys in the furnace cooled condition.

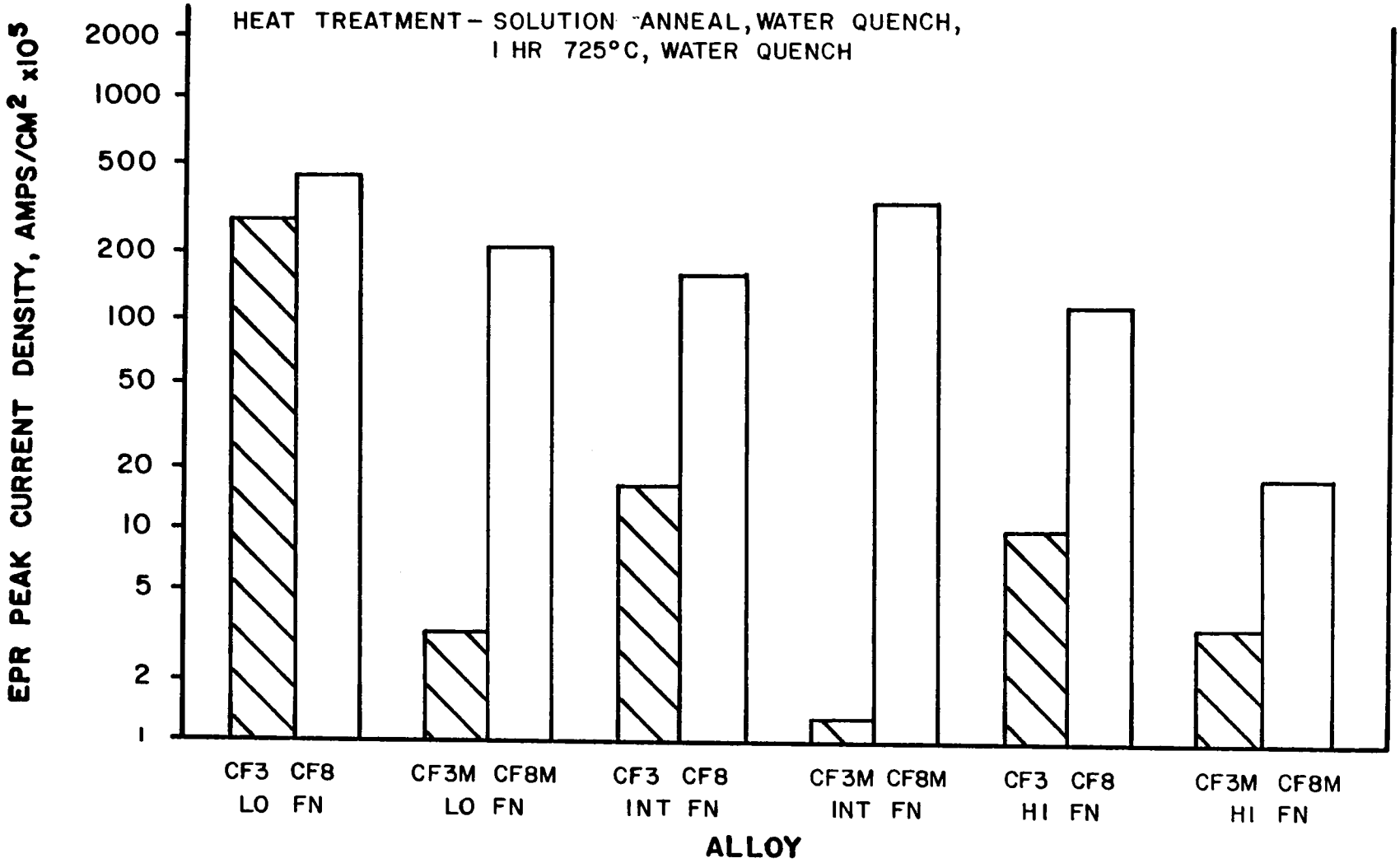

Figure 48. Comparison of EPR results as a function of carbon content for CF and CFM alloys for heat treatment at 725°C.

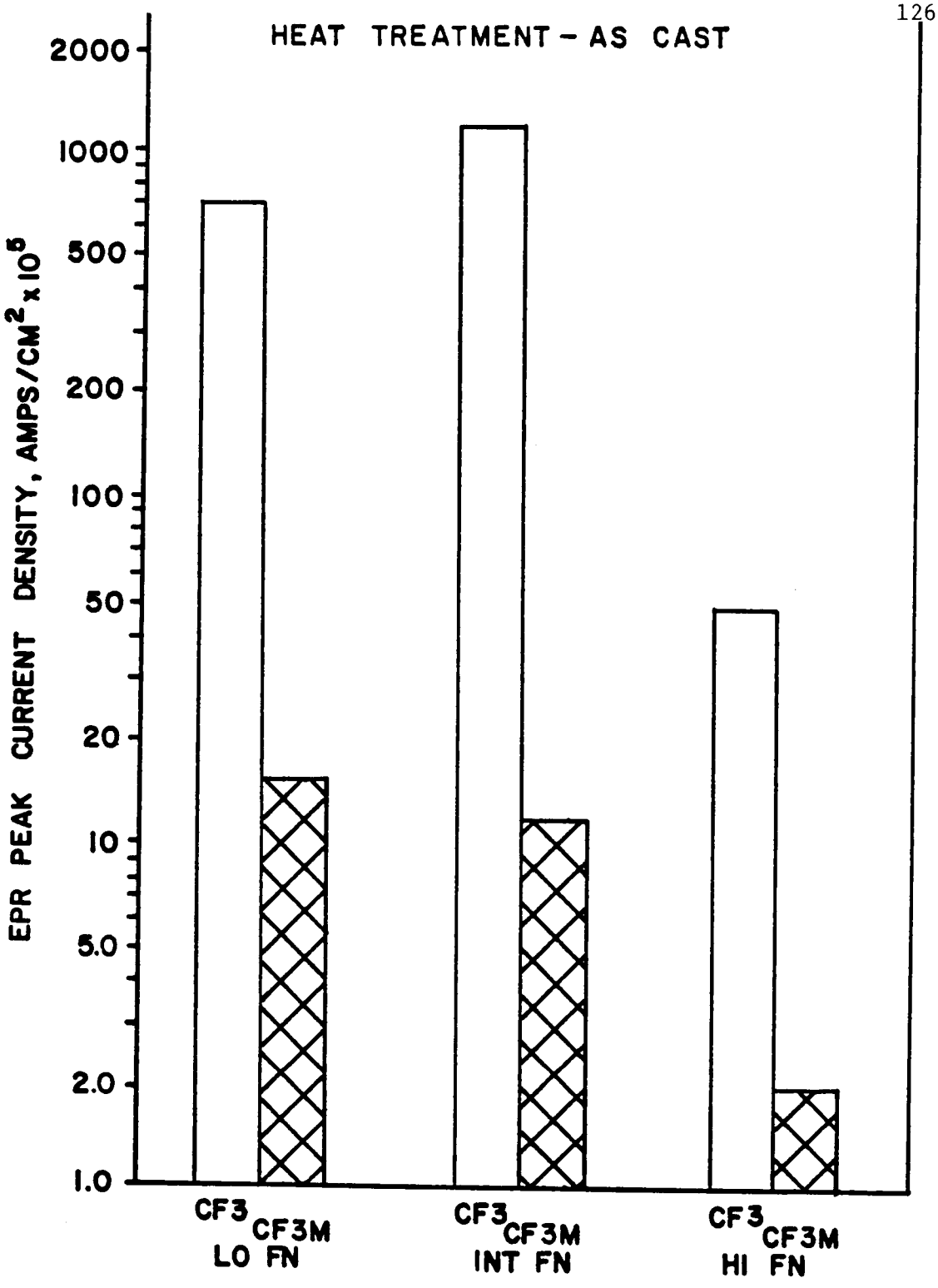

Figure 49. EPR data for CF3 and CF3M as a function of ferrite for the as-cast condition.

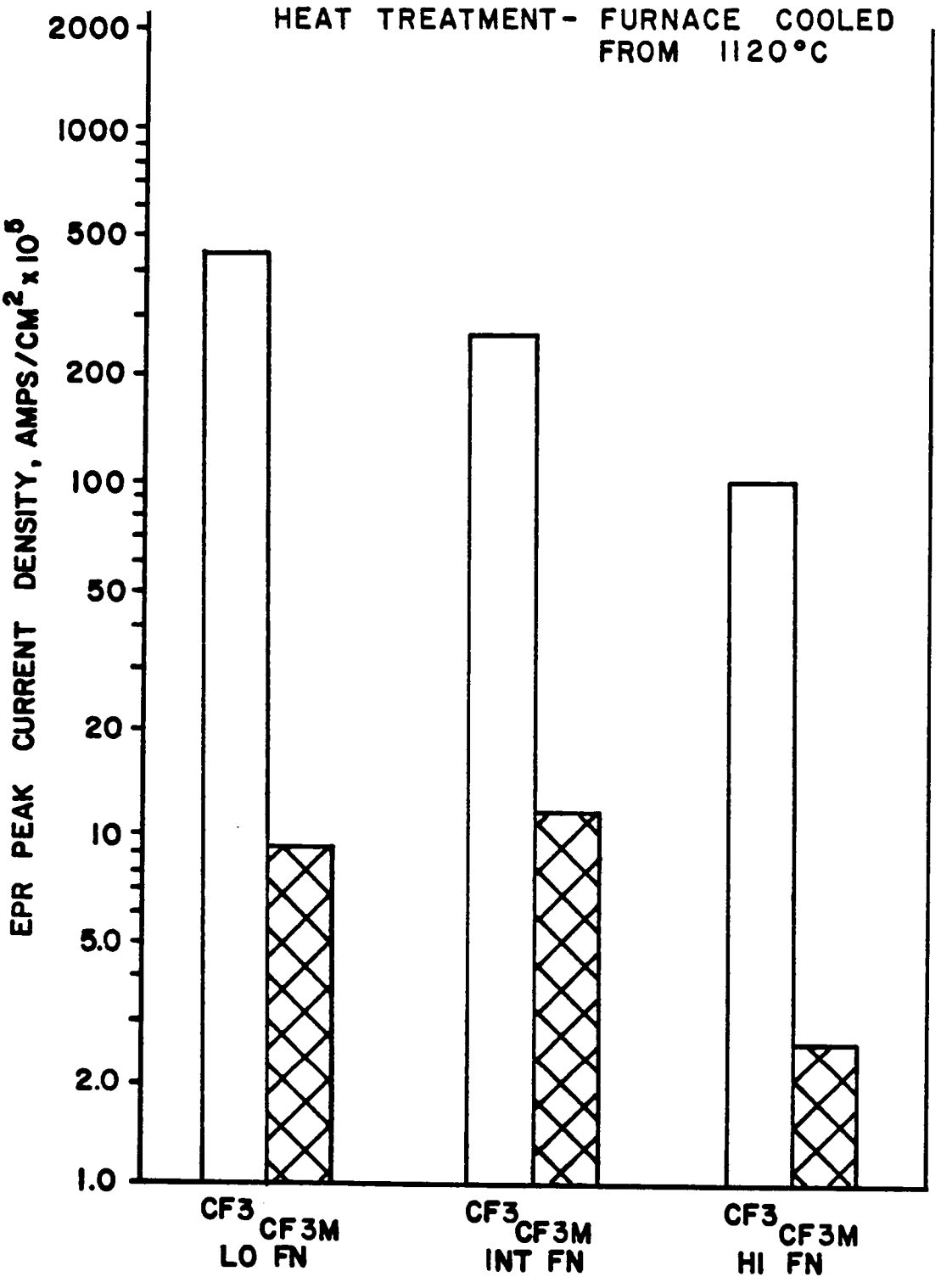

Figure 50. EPR data for CF3 and CF3M as a function of ferrite for the furnace cooled condition.

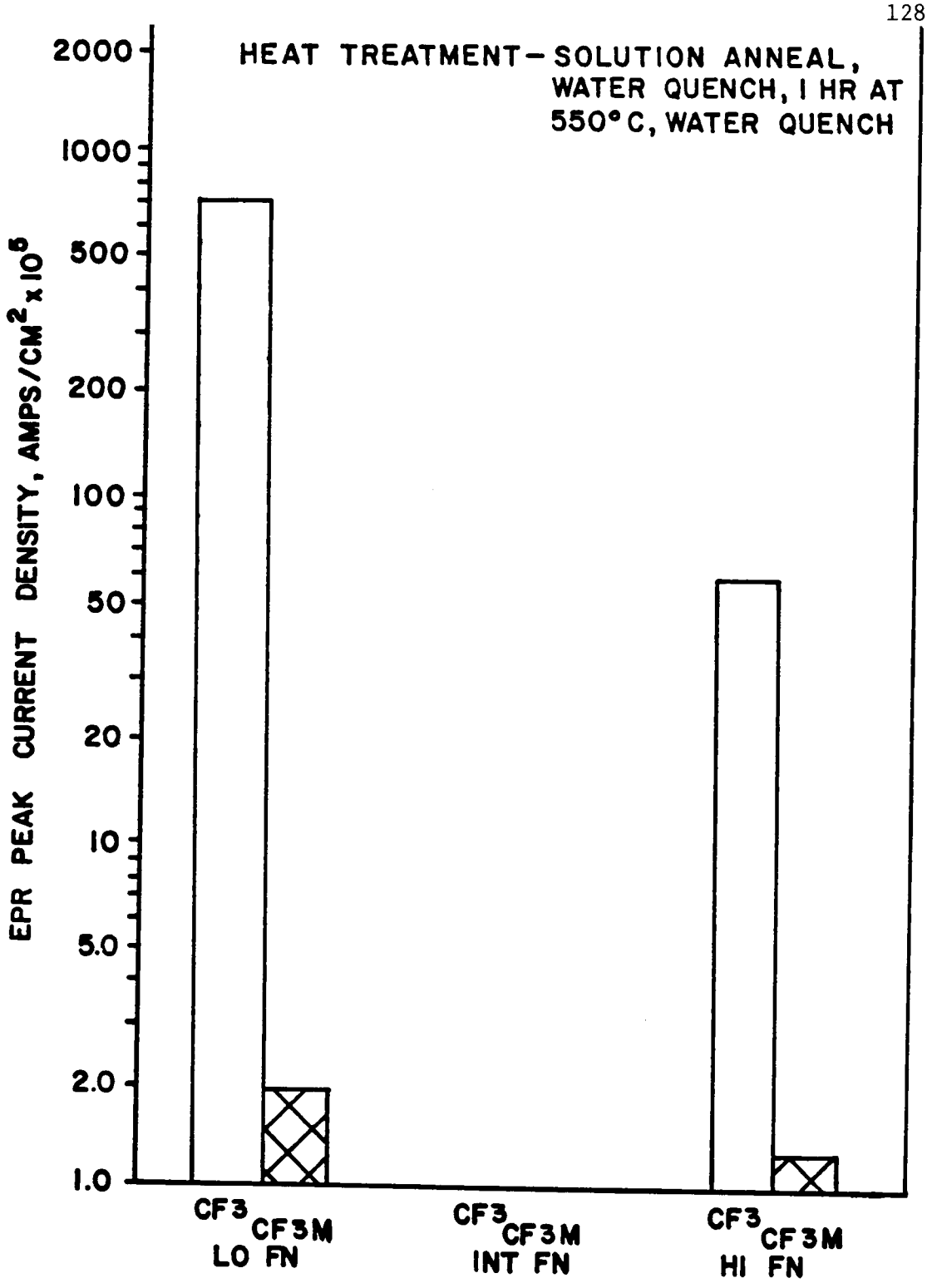

Figure 51. EPR data for CF3 and CF3M as a function of ferrite for heat treatment at 550°C.

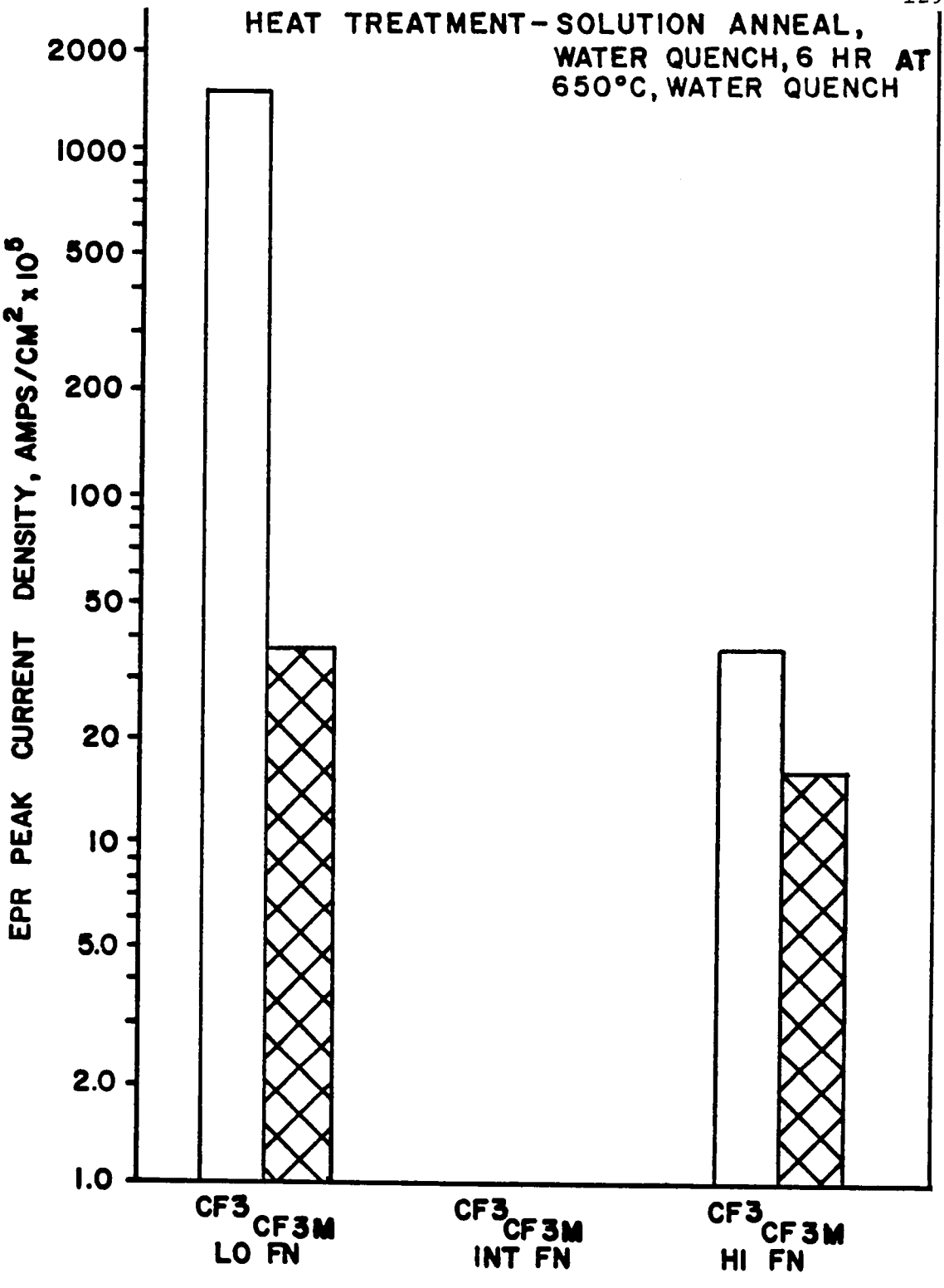

Figure 52. EPR data for CF3 and CF3M as a function of ferrite for heat treatment at 650°C.

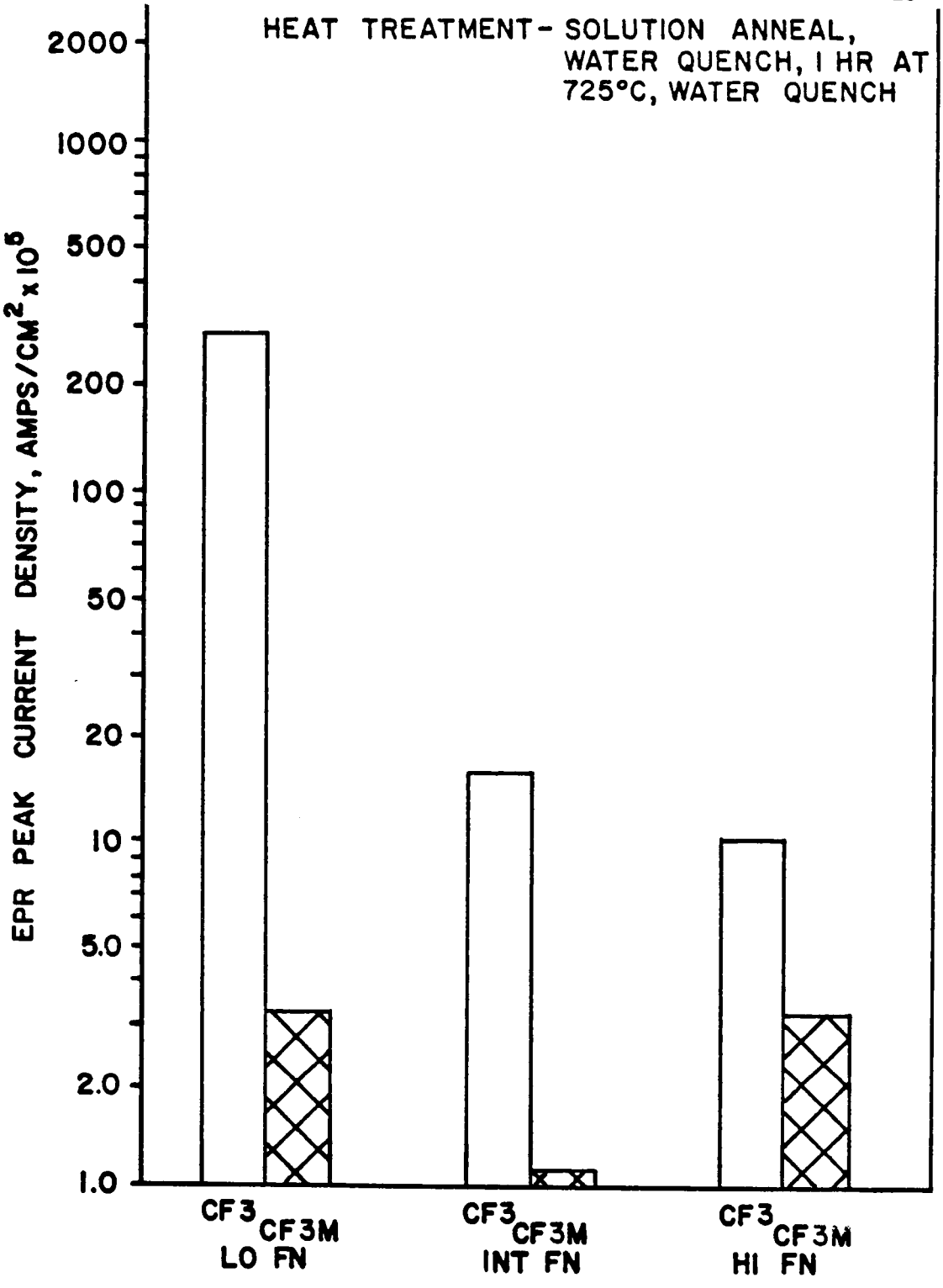

Figure 53. EPR data for CF3 and CF3M as a function of ferrite for heat treatment at 725°C.

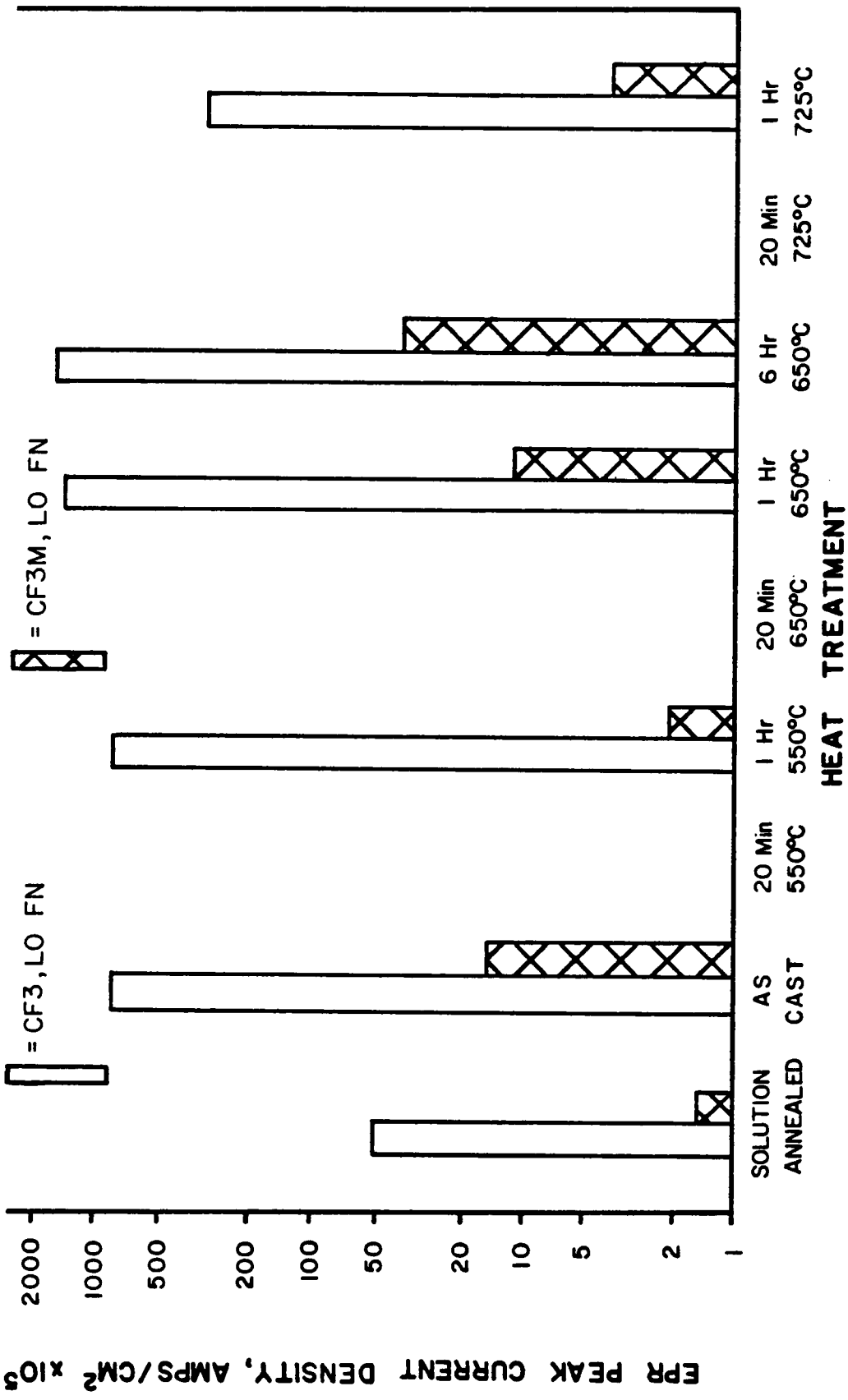

Figure 54. Representative EPR data for CF3 and CF3M at the low ferrite level for various heat treatments.

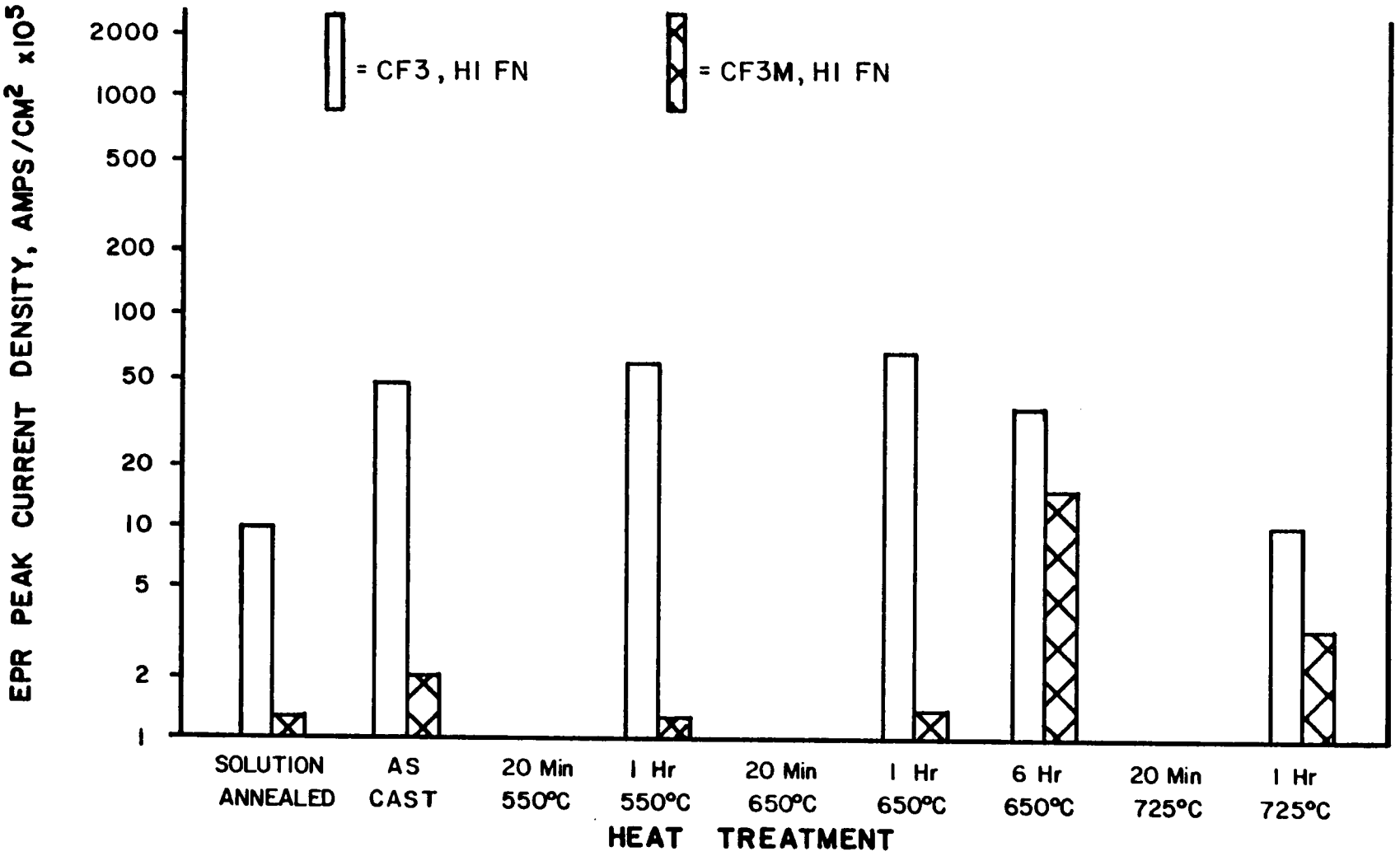

Figure 55. Representative EPR data for CF3 and CF3M at the high ferrite level for various heat treatments.

cooled conditions the CF3 and CF3M alloys have much lower EPR responses than for the higher carbon alloys under the same conditions. Again notice (see Figures 49 - 55) that the Mo bearing CF3M alloys have uniformly smaller EPR responses when compared to the CF3 alloys. The CF3M alloys have EPR responses similar to the value for the solution annealed CF3M alloy for all heat treatment examined indicating very low susceptibility to sensitization. After EPR testing, the microstructures of the CF3 and CF3M indicate that overall fewer carbides are present in the low carbon alloys but those that have formed seem to be of similar size to those formed in the high carbon alloys. A representative microstructure of the CF3 alloys is shown in Figure 56. There is not much detail present in the photomicrograph of Figure 56 but it is included to indicate the limited size and number of chromium depleted zones in the low carbon material. The CF3M alloys did not etch enough in the EPR test to show any significant detail. The CF3 alloys at the intermediate and low ferrite levels seem to be particularly susceptible to austenite matrix pitting as mentioned earlier and the cause for this trend is not known at present. The pitting in the low ferrite CF3 alloy seems to be responsible for a large portion of the EPR peak current density for many heat treatments because of the frequent lack of ferrite-austenite or austenite-austenite boundary ditching.

JEPR Test--Introduction

It is possible that this "order of magnitude" effect of Mo in reducing the EPR peak current density is related to the potential

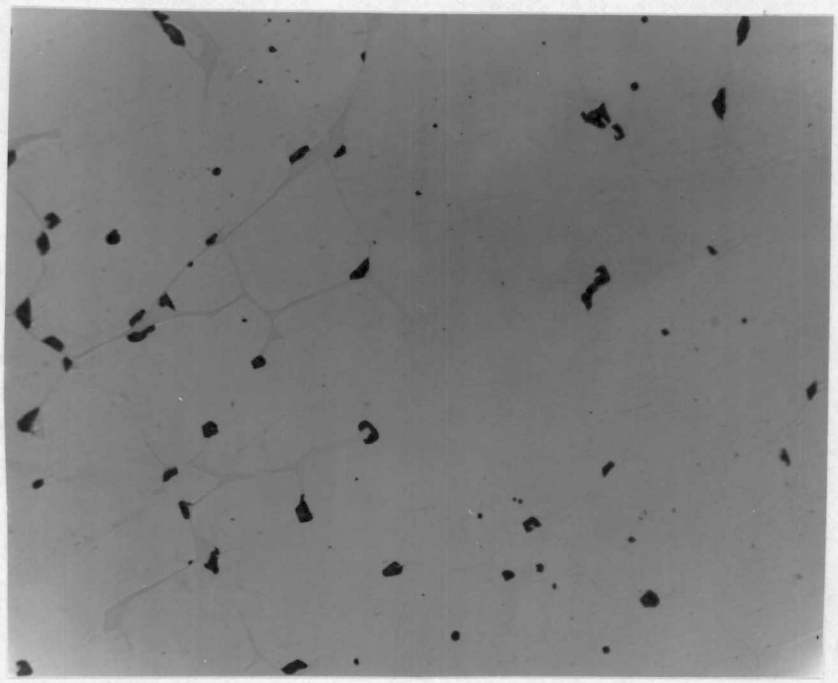

Figure 56. High ferrite (FN ≃ 8) CF3 alloy in the as-cast condition, as EPR tested. 250 X.

scan rate of the test. In the development of the test (77) it was found that the EPR peak current density was very sensitive to the particular scan rate chosen for the test. The scan rates of 6 V/hr for 304 alloys and 3 V/hr for 316 alloys were found to be the most sensitive to the whole spectrum of possible results for these alloys although Clarke (27) does not mention this distinction of scan rates in his review paper. A slower potential scan rate (all of the aforementioned testing utilized 6 V/hr scan rate regardless of the particular alloy being tested) for the Mo bearing alloys would certainly increase the reactivation peak for alloys that are sensitized by allowing more time for the breakdown of the passive film in the active potential range. However, adhering to the philosophy of changing the scan rate to obtain an expected or desired result severely compromises the significance of the results for several reasons, the most important of which is that it implies that the composition of the alloy must be known before the EPR test can be performed. Many elements besides Mo--for instance, Cr, Ni and Si, affect the passivation characteristics of the alloy and it may be discovered that small variations in each of these elements may significantly affect the EPR results. If this were the case, it would certainly restrict the applicability of the EPR test. Thus, a potential improvement over the EPR test would be an evaluation technique that was less sensitive to the overall composition of the alloy.

Akashi, et al., (49) attempted to develop a version of the EPR test that was less sensitive to overall composition (notably the

effect of Mo). They pointed out that the active dissolution of the entire specimen (no passive film present) was determined principally by the overall composition of the alloy and only to a very minor extent by the degree of sensitization. Included among the elements to which this peak is very sensitive are Cr and Mo; for example the addition of 2 - 3% Mo to an 18Cr-8Ni stainless steel will reduce the active dissolution peak approximately an order of magnitude in the EPR test solution (and many others). On the other hand, the reactivation peak (passive film initially present) of an EPR test is affected by the degree of sensitization (chromium deficient regions in the passive film) as well as general dissolution characteristics. Akashi, et al., (49) combined these ideas into a new type of EPR test (referred to by this author as the JEPR test) that measures the degree of sensitization of the alloy while "dividing out" compositional differences such as the effect of Mo.

Basically, the JEPR test is very similar to the EPR test (see Experimental Procedure) with the following exceptions. (Note the schematic diagram of Figure 14, (page 57).) The initiation point of the controlled potential scan is at the open circuit potential of the alloy and the potential is dynamically increased (6 V/hr) to the passivation potential of the standard EPR test. During this anodic polarization, the alloy exhibits a critical passivation current density (called Ia) that is representative of the overall composition of the alloy and is relatively unaffected by the degree of sensitization. Immediately upon reaching the passivation potential of the standard EPR test, the scan direction is reversed and the

remainder of the test is a reactivation (from passive to active regions) scan identical to the standard EPR test. The reactivation peak (called Ir) is controlled by both the degree of sensitization and the overall composition of the alloy. The method of quantitative analysis is called the reactivation ratio (R) and is numerically (Ir/Ia) x 100. This ratio is intended to "divide out" the influence of overall composition (which affects both Ir and Ia) and leave a number representative of the degree of sensitization (principally affects Ir only). The larger the reactivation ratio, the more susceptible the material is to sensitization. Another way to think of the reactivation ratio is to consider that it represents how much the passive film is reducing the current passed from the sample as a percentage of its general dissolution value. Thus, low reactivation ratios indicate that the passive film (on reactivation) is protecting the sample more than on a sample with a high reactivation ratio.

JEPR Test--High Carbon Alloys

To test the above idea, the high carbon (.06 - .08% C) alloys were evaluated by the JEPR test and some sample data appear in Figure 57 and Table 6. As can be noted in Figure 57, the reactivation ratio for the as-cast CF8 alloy is about the same as that for the as-cast CF8M alloy. Both the activation peak (Ia) and the reactivation peak (Ir) are nearly an order of magnitude smaller for the CF8M alloy compared to the CF8 alloy. Thus, contrary to the EPR test which judged the as-cast CF8M superior to the as-cast CF8

Table 6. JEPR data (Ia, Ir, R) for some high carbon alloys. Ia, Ir in amps/cm^2; R = (Ir/Ia) x 100.

MATERIAL	HEAT TREATMENT: SOLUTION ANNEAL		HEAT TREATMENT: AS CAST		HEAT TREATMENT: FURNACE COOLED	
CF8 LO FN	$Ia = 1.4 \times 10^{-1}$ $Ir = 1.8 \times 10^{-4}$	R = .13	$Ia = 1.1 \times 10^{-1}$ $Ir = 1.1 \times 10^{-2}$	R = 10	$Ia = 1.2 \times 10^{-1}$ $Ir = 6.4 \times 10^{-3}$	R = 5.6
CF8 INT FN	$Ia = 3.5 \times 10^{-2}$ $Ir = 3.6 \times 10^{-5}$	R = .10	$Ia = 4.5 \times 10^{-2}$ $Ir = 8.5 \times 10^{-3}$	R = 19	$Ia = 4.8 \times 10^{-2}$ $Ir = 7.8 \times 10^{-3}$	R = 16
CF8 HI FN	$Ia = 3.6 \times 10^{-2}$ $Ir = 4.2 \times 10^{-5}$	R = .12	$Ia = 4.8 \times 10^{-2}$ $Ir = 5.5 \times 10^{-3}$	R = 11	$Ia = 4.9 \times 10^{-2}$ $Ir = 6.9 \times 10^{-3}$	R = 14
CF8M LO FN	$Ia = 1.2 \times 10^{-2}$ $Ir = 1.2 \times 10^{-5}$	R = .10	$Ia = 1.7 \times 10^{-2}$ $Ir = 2.2 \times 10^{-3}$	R = 13	$Ia = 1.3 \times 10^{-2}$ $Ir = 3.3 \times 10^{-4}$	R = 2.5
CF8M INT FN	$Ia = 4.6 \times 10^{-3}$ $Ir = 1.3 \times 10^{-5}$	R = .29	$Ia = 1.2 \times 10^{-2}$ $Ir = 1.0 \times 10^{-3}$	R = 8.8	$Ia = 1.1 \times 10^{-2}$ $Ir = 1.2 \times 10^{-3}$	R = 11
CF8M HI FN	$Ia = 8.2 \times 10^{-3}$ $Ir = 2.9 \times 10^{-5}$	R = .35	$Ia = 1.8 \times 10^{-2}$ $Ir = 1.6 \times 10^{-3}$	R = 9.1	$Ia = 1.8 \times 10^{-2}$ $Ir = 1.5 \times 10^{-3}$	R = 8.6

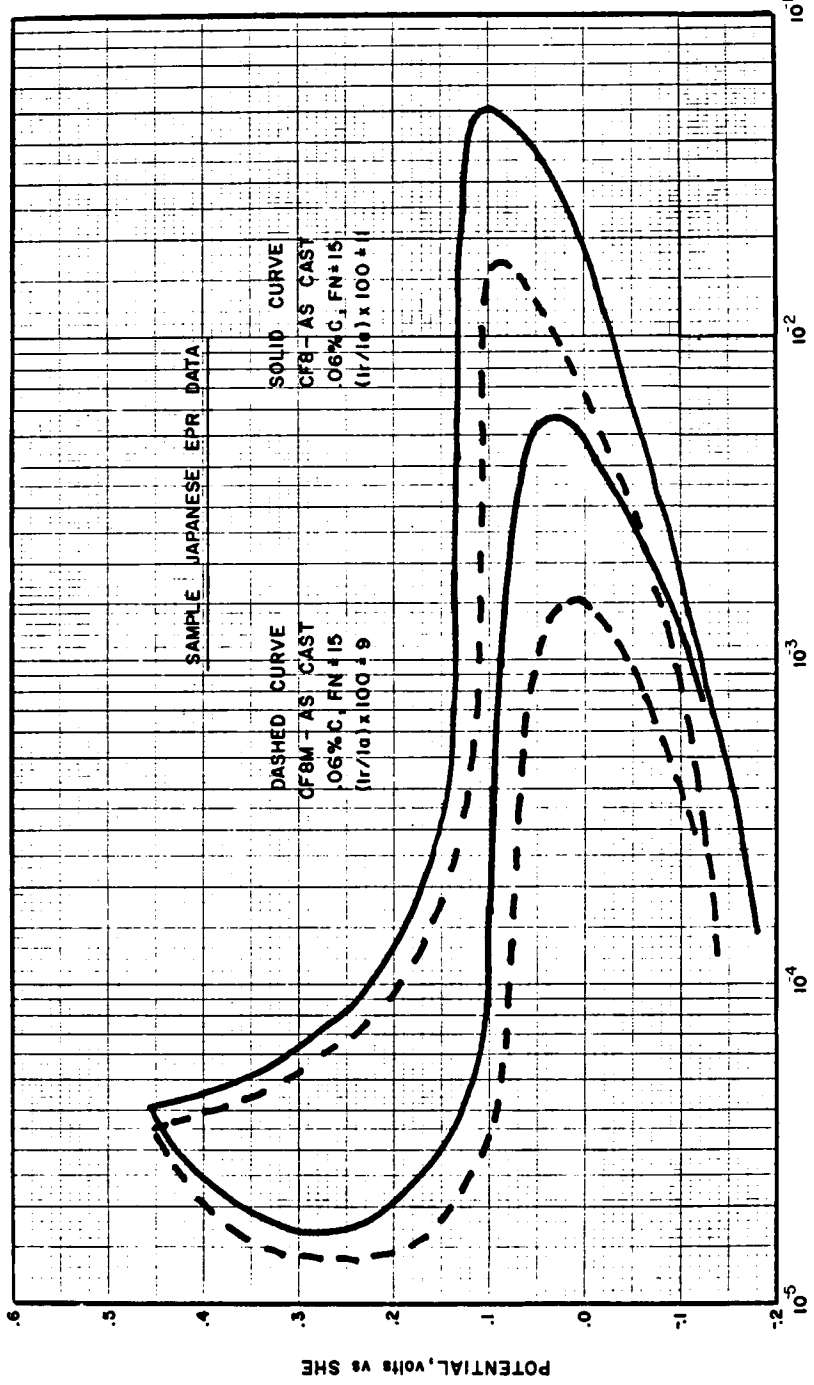

Figure 57. Sample JEPR data comparing CF8 and CF8M in the as-cast condition.

as regards sensitization, the JEPR test has apparently "divided out" the effect of Mo on the passivation characteristics and yielded a ratio that indicates that CF8 and CF8M are approximately equally sensitized in the as-cast condition.

Table 6 indicates JEPR ratios for some of the high carbon alloys tested and it shows that for the solution annealed, as-cast and furnace cooled conditions, CF8 and CF8M are evaluated as approximately equivalent in degree of sensitization as measured by the JEPR test. Generally the CF8M alloys show JEPR ratios of 1.5 - 2 less than the corresponding CF8 alloy as opposed to factors of 8 - 12 less as evaluated by the EPR test.

The data of Table 6 also show that, like the EPR test, the as-cast and furnace cooled conditions are often two orders of magnitude more sensitized than the solution annealed condition (baseline condition). This indicates that the possible range of JEPR ratios is large enough to be able to discriminate between fairly small differences in sensitization.

Also note from Table 6 that, as predicted, the degree of sensitization affects the activation peak current (Ia) only slightly; factors of usually less than 1.5 between the solution annealed condition and the as-cast condition, for example, as compared to ranges of 2 - 3 orders of magnitude for the reactivation peaks (Ir).

Although very limited data is available concerning the effect of surface finish on the JEPR test results, indications are that this effect may also "divide out" of the ratio in a similar manner

to the effect of Mo. Since both Ia and Ir are likely to be affected in similar ways by surface preparation, this effect may indeed be factored out by the reactivation ratio. The limited data of this research indicate that this is approximately the case and the JEPR test may be less sensitive to surface finish than the EPR test.

Regarding the surface condition of the sample the data of Table 6 and Figure 24 (page 83) indicate that Ir of the JEPR test is often slightly smaller than Ir recorded during the EPR test. The only difference between the EPR result and Ir of the JEPR test (as far as test technique is concerned) is that the EPR test sample is in the polished condition when reactivation occurs and the JEPR test specimen has already been exposed to high anodic dissolution current densities prior to passivation and reactivation. As will be discussed more later, the samples that show matrix pitting in the EPR test often have much lower Ir values in the JEPR test compared to the EPR test. Apparently, in many cases, the material susceptible to pitting in the EPR test has been at least partially dissolved prior to reactivation in the JEPR test.

Table 7 and Figures 58 - 64 summarize the JEPR data on the high carbon alloys including results from some of the isothermal hold samples. In addition to the trends already discussed, the JEPR data indicates other trends similar to the EPR results. The JEPR results for the isothermal hold samples generally show increased sensitization as the time at temperature increases with no appreciable "healing" indicated. (See Figures 58 - 60). For the

Table 7. Summary of JEPR data for the high carbon alloys. Values are (Ir/Ia) x 100.

HEAT TREATMENT		CF8 LO FN	CF8 INT FN	CF8 HI FN	CF8M LO FN	CF8M INT FN	CF8M HI FN
SOLUTION ANNEALED		.13	.10	.12	.10	.29	.35
AS CAST		10	19	11	13	8.8	9.1
FURNACE COOLED		5.6	16	14	2.5	11	8.6
550°C	20 MIN	.21	.24	.35	.33	.22	.04
	1 HR	4.8	1.4	1.7	.10	.22	.08
	6 HR	16	17	20	.22	1.8	2.4
	48 HR						
600°C	1 HR	11	12	12	.15	.43	.12
650°C	20 MIN	7.7	17	9.7	.19	.65	3.8
	1 HR	10	19	14	.67	5.4	8.8
	6 HR	14	21	9.5			
	48 HR	21	20	10	17	13	3.8
725°C	20 MIN	4.1	5.0	3.2	4.0	8.0	2.4
	1 HR	5.0	4.1	.90	5.5	11	2.4
	6 HR						
	48 HR	2.8	1.0		2.2	4.1	

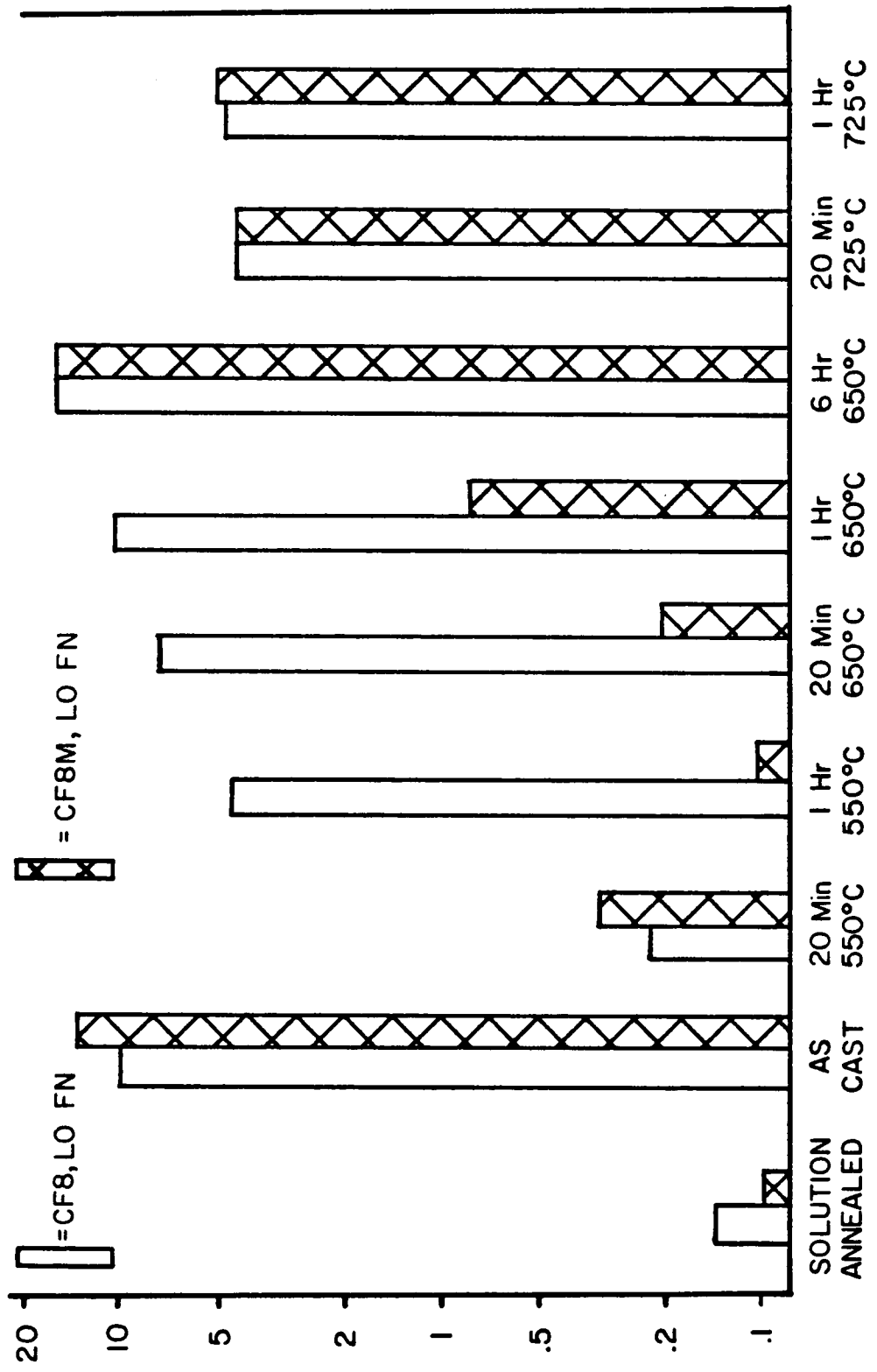

Figure 58. Representative JEPR data for CF8 and CF8M at the low ferrite level for various heat treatments.

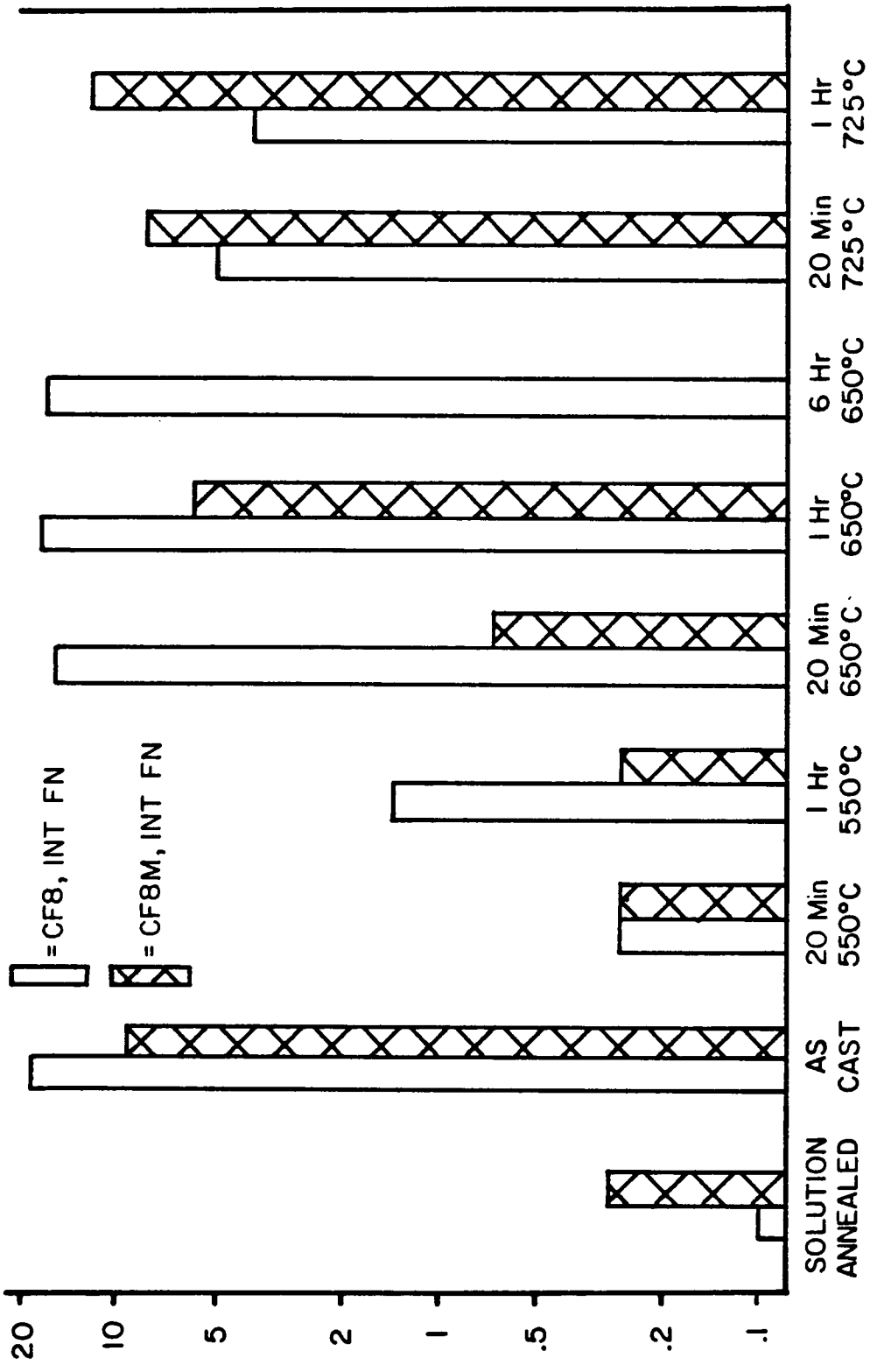

Figure 59. Representative JEPR data for CF8 and CF8M at the intermediate ferrite level for various heat treatments.

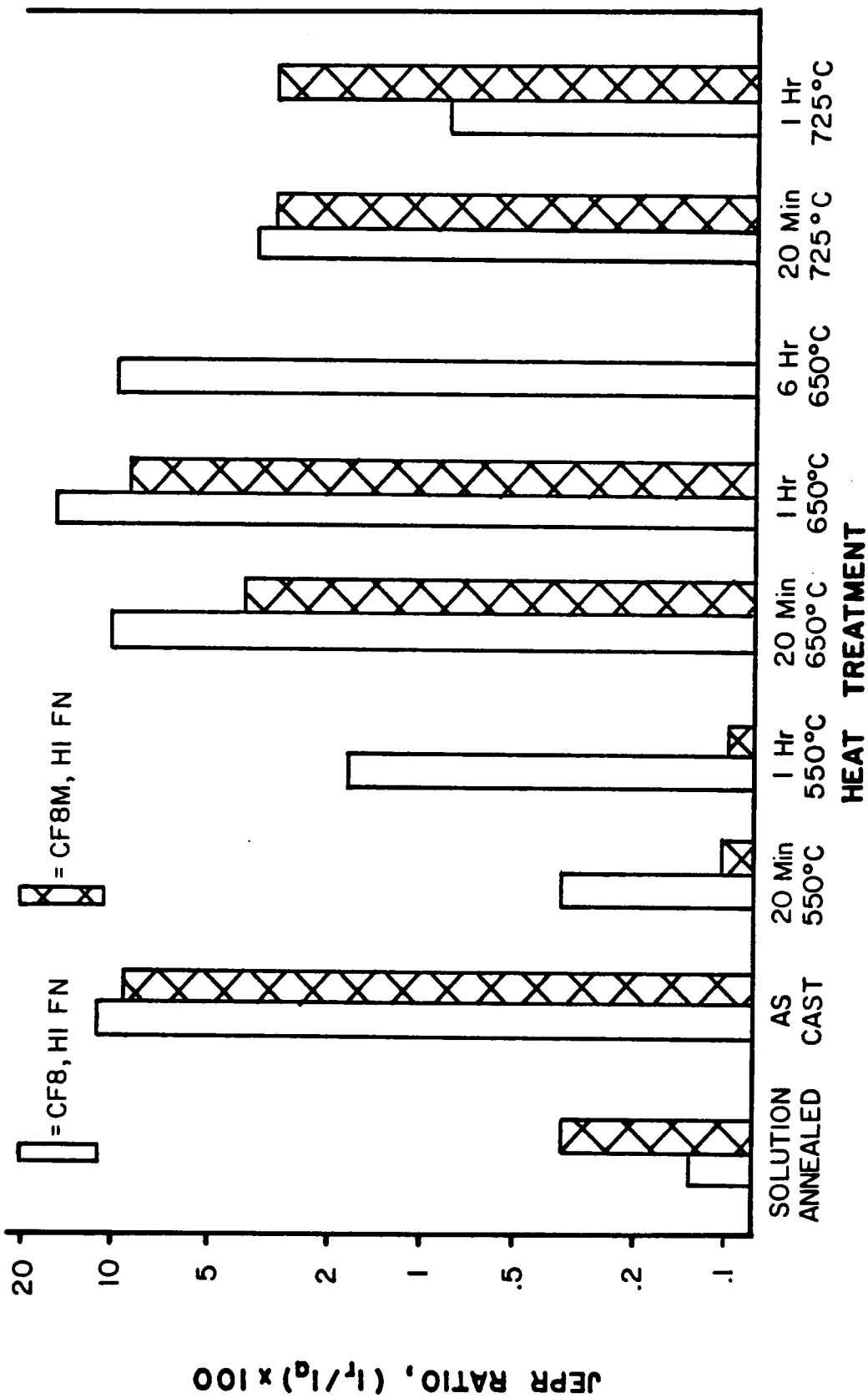

Figure 60. Representative JEPR data for CF8 and CF8M at the high ferrite level for various heat treatments.

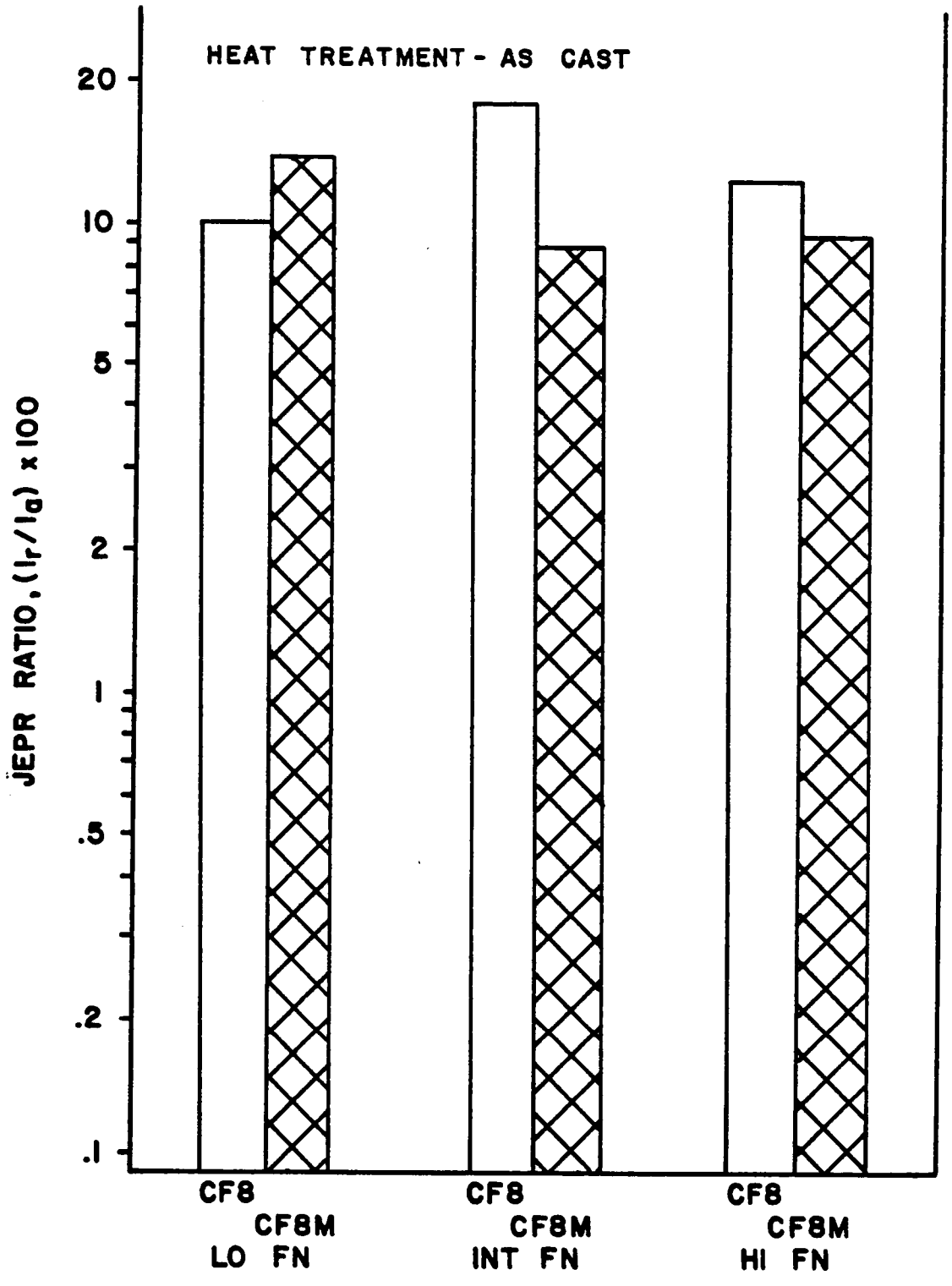

Figure 61. JEPR data for CF8 and CF8M as a function of ferrite for the as-cast condition.

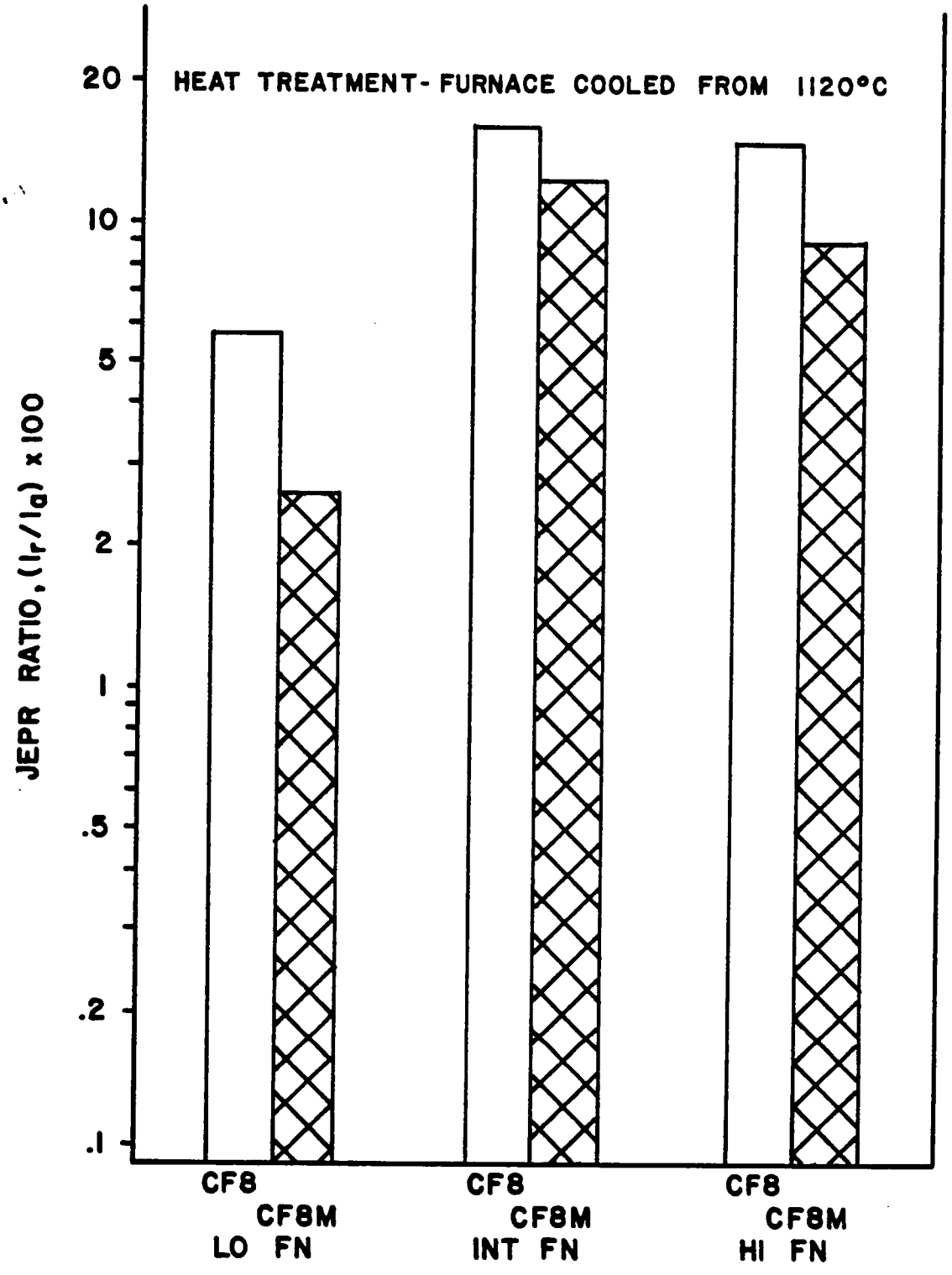

Figure 62. JEPR data for CF8 and CF8M as a function of ferrite for the furnace cooled condition.

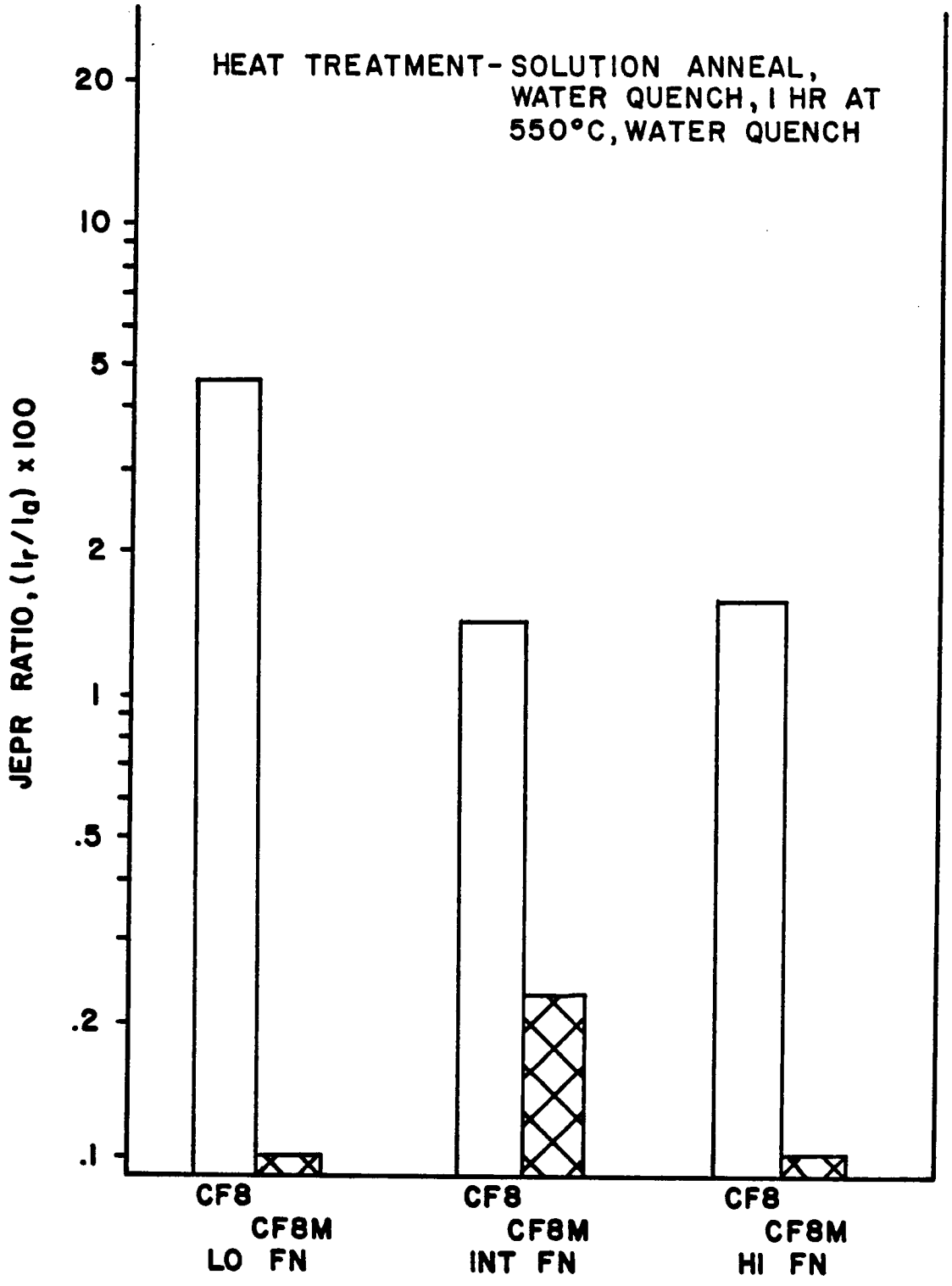

Figure 63. JEPR data for CF8 and CF8M as a function of ferrite for heat treatment at 550°C.

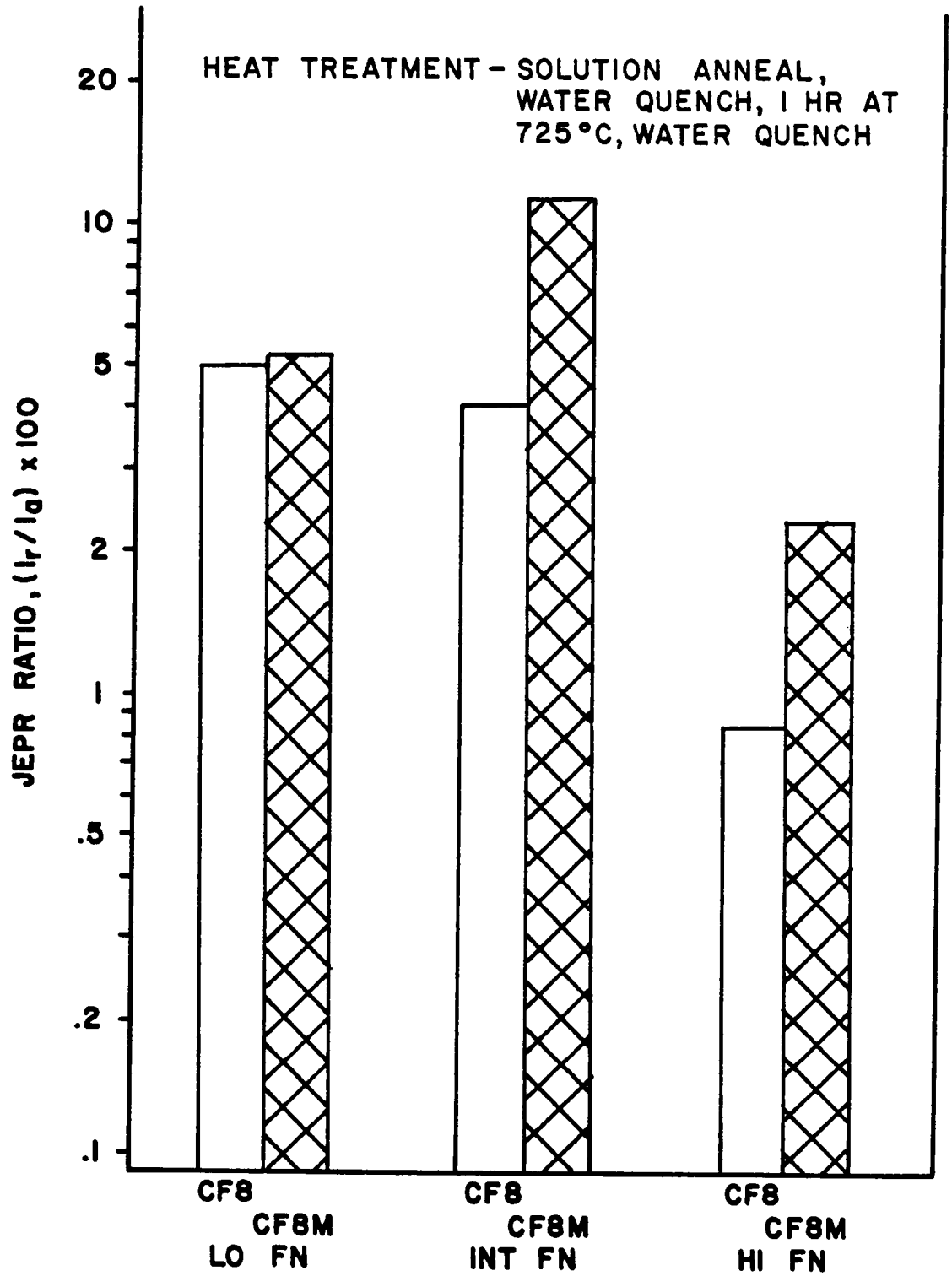

Figure 64. JEPR data for CF8 and CF8M as a function of ferrite for heat treatment at 725°C.

isothermal heat treatments investigated, the JEPR test evaluates the Mo bearing CF8M alloys as approximately an order of magnitude less susceptible to sensitization than the corresponding CF8 alloys except for some very long and/or relatively high temperature ($\geq$ 725°C) treatments. Figures 58 - 64 all indicate this trend. This indicates that for isothermal sensitizing treatments the effect of Mo on the sensitization behavior does not entirely "divide out" in the JEPR test and that Mo may actually retard carbide precipitation for relatively short isothermal holds. This effect of Mo seems to disappear for long isothermal holds and for the continuous cooling conditions of the as-cast and furnace cooled heat treatments for the high carbon alloys.

Table 7 also shows that the effect of ferrite observed in the EPR data for the high carbon alloys tends to be "divided out" by the JEPR data. (See Figures 61 - 64.) This is manifest by the fact that, for a given heat treatment, each ferrite level within an alloy class (CF8 or CF8M) has approximately equal JEPR ratios. This suggests that the observed effect of ferrite may actually be an effect of the bulk chromium content of the alloy. Since this would affect both the peak anodic current density (Ia) and the peak reactivation current density (Ir) and thus would tend to "divide out" of the JEPR results.

JEPR Test--Low Carbon Alloys

Table 8, for direct comparison with Table 6, is a summary of the JEPR data (including Ia and Ir values) for the low carbon

Table 8. JEPR data (Ia, Ir, R) for some low carbon alloys. Ia, Ir in amps/cm^2; R = (Ir/Ia) x 100.

MATERIAL	HEAT TREATMENT: SOLUTION ANNEAL		HEAT TREATMENT: AS CAST		HEAT TREATMENT: FURNACE COOLED	
CF3 LO FN	$Ia = 9.2 \times 10^{-2}$ $Ir = 7.4 \times 10^{-4}$	R = .81	$Ia = 1.0 \times 10^{-1}$ $Ir = 2.4 \times 10^{-3}$	R = 2.4	$Ia = 1.0 \times 10^{-1}$ $Ir = 1.1 \times 10^{-3}$	R = 1.1
CF3 INT FN	Ia = Ir =	R =	$Ia = 1.1 \times 10^{-1}$ $Ir = 6.1 \times 10^{-4}$	R = .57	$Ia = 8.0 \times 10^{-2}$ $Ir = 2.1 \times 10^{-4}$	R = .26
CF3 HI FN	$Ia = 8.0 \times 10^{-2}$ $Ir = 6.0 \times 10^{-5}$	R = .08	$Ia = 9.1 \times 10^{-2}$ $Ir = 1.5 \times 10^{-4}$	R = .16	$Ia = 7.8 \times 10^{-2}$ $Ir = 5.2 \times 10^{-4}$	R = .67
CF3M LO FN	$Ia = 1.7 \times 10^{-2}$ $Ir = 3.0 \times 10^{-5}$	R = .20	$Ia = 2.1 \times 10^{-2}$ $Ir = 5.6 \times 10^{-5}$	R = .27	$Ia = 1.8 \times 10^{-2}$ $Ir = 7.5 \times 10^{-5}$	R = .43
CF3M INT FN	Ia = Ir =	R =	$Ia = 1.8 \times 10^{-2}$ $Ir = 1.0 \times 10^{-4}$	R = .57	$Ia = 1.3 \times 10^{-2}$ $Ir = 1.0 \times 10^{-4}$	R = .80
CF3M HI FN	$Ia = 1.0 \times 10^{-2}$ $Ir = 2.0 \times 10^{-5}$	R = .20	$Ia = 1.4 \times 10^{-2}$ $Ir = 1.3 \times 10^{-5}$	R = .09	$Ia = 1.1 \times 10^{-2}$ $Ir = 2.0 \times 10^{-6}$	R = .02

alloys in the solution annealed, as-cast and furnace cooled conditions. Table 8 indicates that the peak anodic current densities (Ia) are very similar for all of the alloys for their respective alloy class (Mo bearing or not) and ferrite content, indicating no measured effect of carbon content on Ia. Note that for the intermediate and high ferrite content CF3/8 type, Ia for the low carbon alloys is about a factor of two higher than the corresponding Ia for the high carbon alloys. The major compositional variable between these, (besides the carbon content, which does not seem important based on the other alloys) is Mo--the high carbon alloys have 4 - 5 times the amount of Mo that the low carbon CF3/8 alloys contain (.45 - .50 vs. .10)--this factor seems to manifest itself here also.

Contrary to the high carbon alloys, the as-cast and furnace cooled conditions for the low carbon alloys do not have JEPR ratios more than an order of magnitude higher than the solution annealed condition; in fact, in many instances the JEPR ratios are very similar for the solution annealed and slowly cooled conditions. Although not very comprehensive data, the JEPR results on the isothermal hold low carbon samples (see Table 9) indiate a similar trend, i.e., that the low carbon alloys, particularly the CF3M alloys, are very difficult to sensitize based on the very low JEPR ratios for most heat treatments. Figures 65 - 70 indicate graphically representative data of Table 9.

The JEPR test sample is often very difficult to evaluate microstructurally because of the high degree of general attack on the

Table 9. Summary of JEPR data for low carbon alloys. Values are (Ir/Ia) x 100.

HEAT TREATMENT	CF3 LO FN	CF3 INT FN	CF3 HI FN	CF3M LO FN	CF3M INT FN	CF3M HI FN
SOLUTION ANNEALED	.81		.08	.20		.01
AS CAST	2.4	.57	.16	.27	.57	.09
FURNACE COOLED	1.1	.26	.67	.43	.80	.02
550°C 20 MIN						
550°C 1 HR	2.3		1.5	.10		.10
550°C 6 HR						
650°C 20 MIN						
650°C 1 HR	.20		.15	.08		.20
650°C 6 HR	3.5		.84		.63	.44
725°C 20 MIN						
725°C 1 HR	.63					
725°C 6 HR	1.1		.22	.01		.04

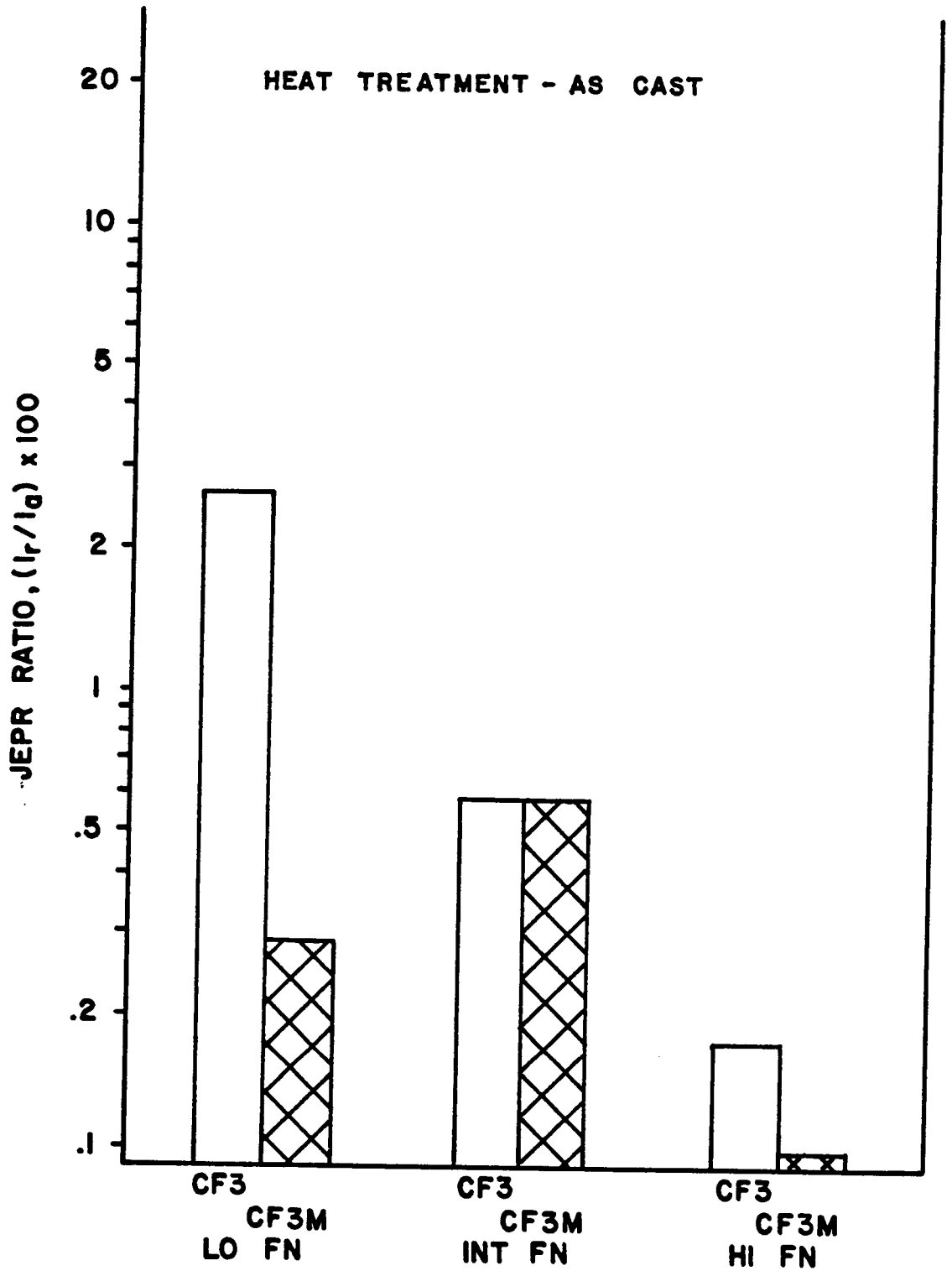

Figure 65. JEPR data for CF3 and CF3M as a function of ferrite for the as-cast condition.

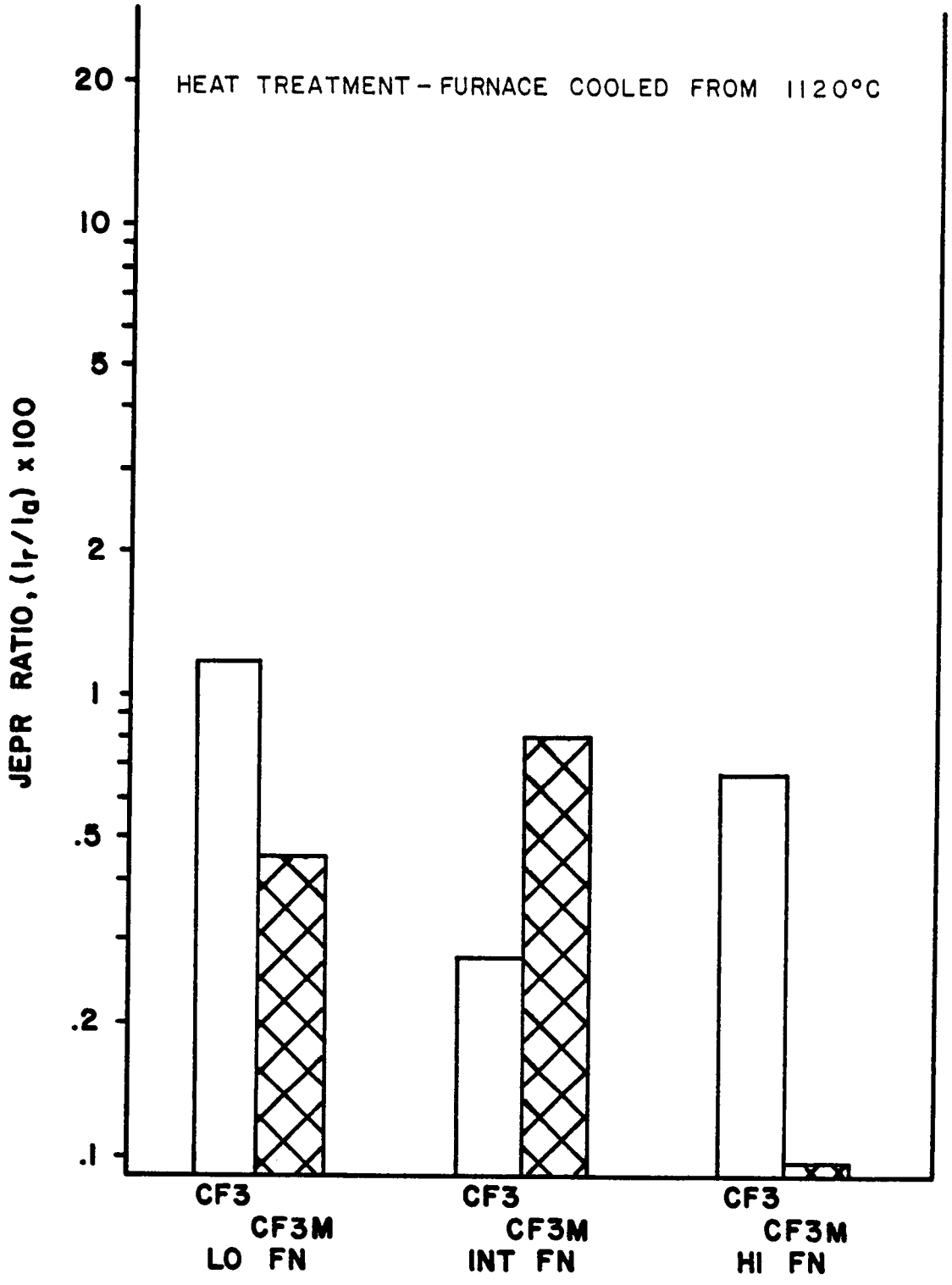

Figure 66. JEPR data for CF3 and CF3M as a function of ferrite for the furnace cooled condition.

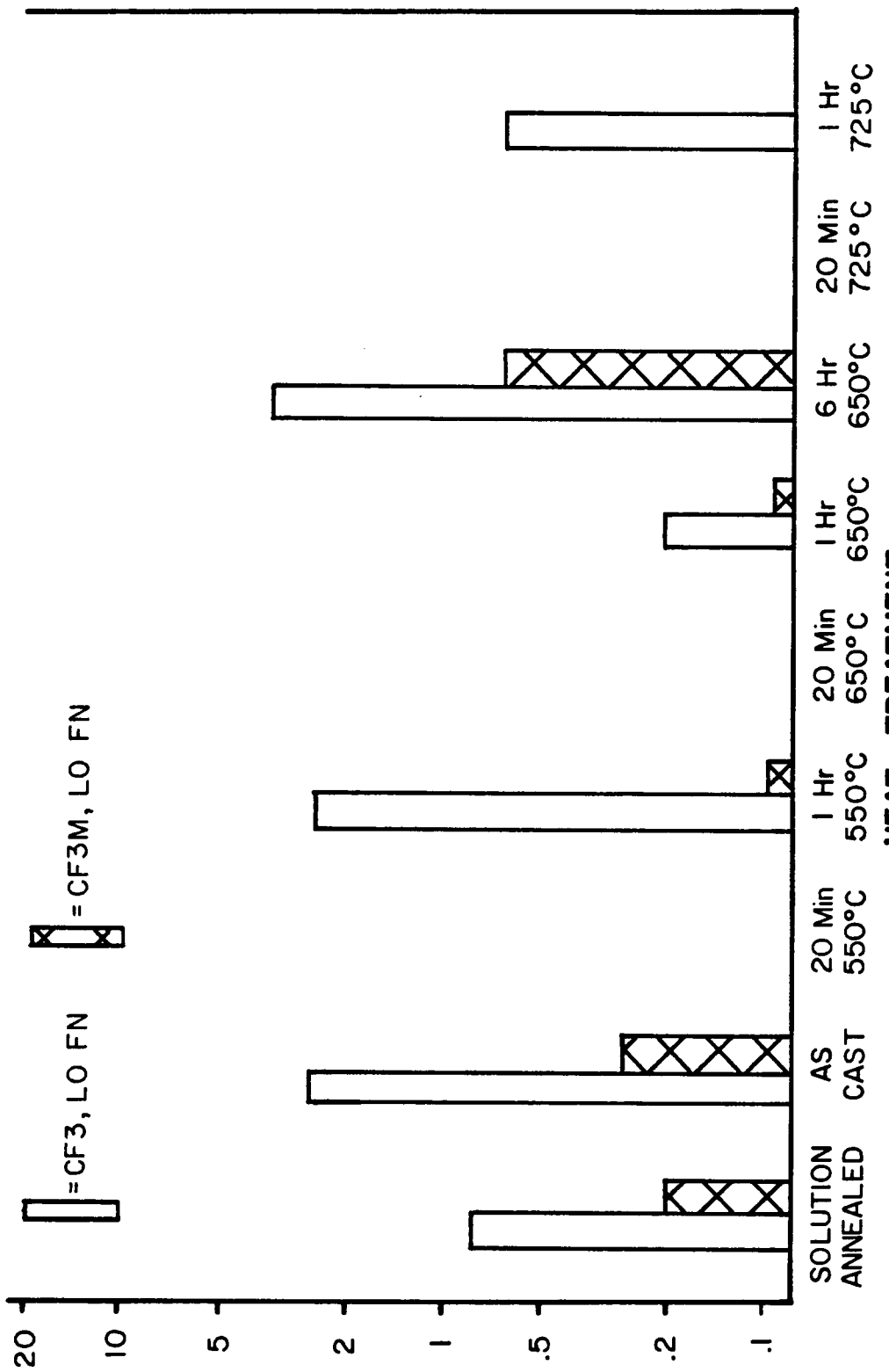

Figure 67. Representative JEPR data for CF3 and CF3M at the low ferrite level for various heat treatments.

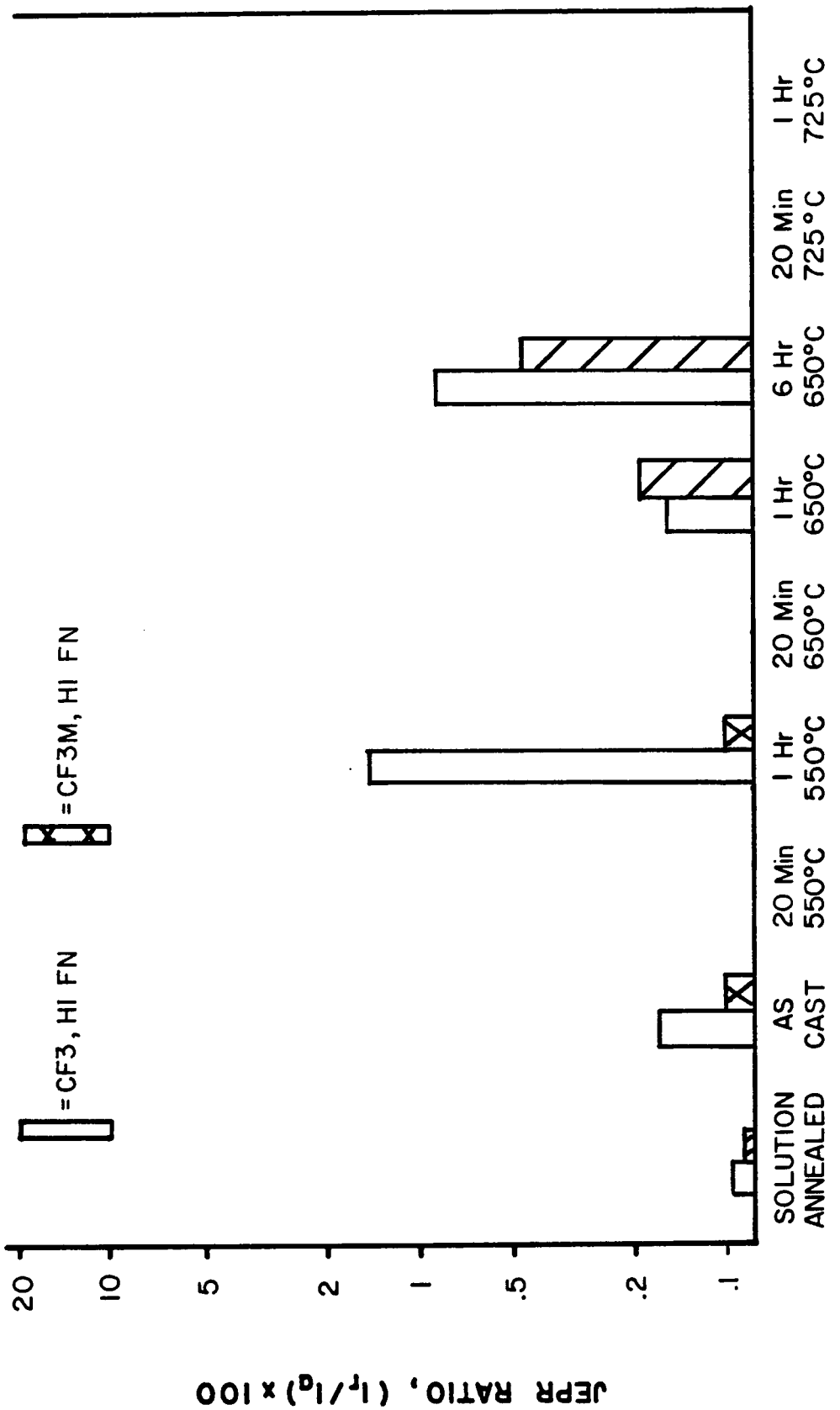

Figure 68. Representative JEPR data for CF3 and CF3M at the high ferrite level for various heat treatments.

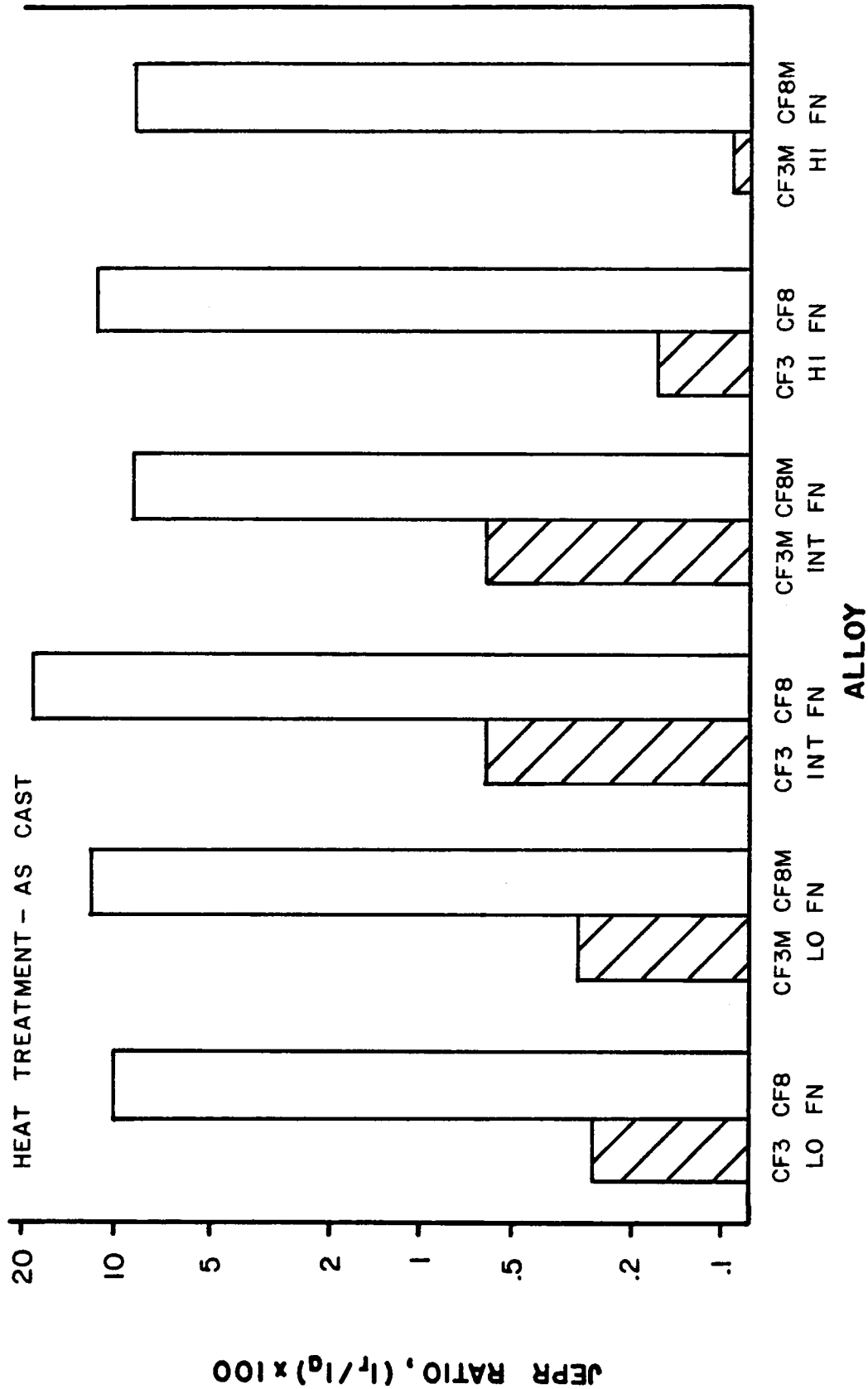

Figure 69. Comparison of JEPR results as a function of carbon content for CF and CFM alloys in the as-cast condition.

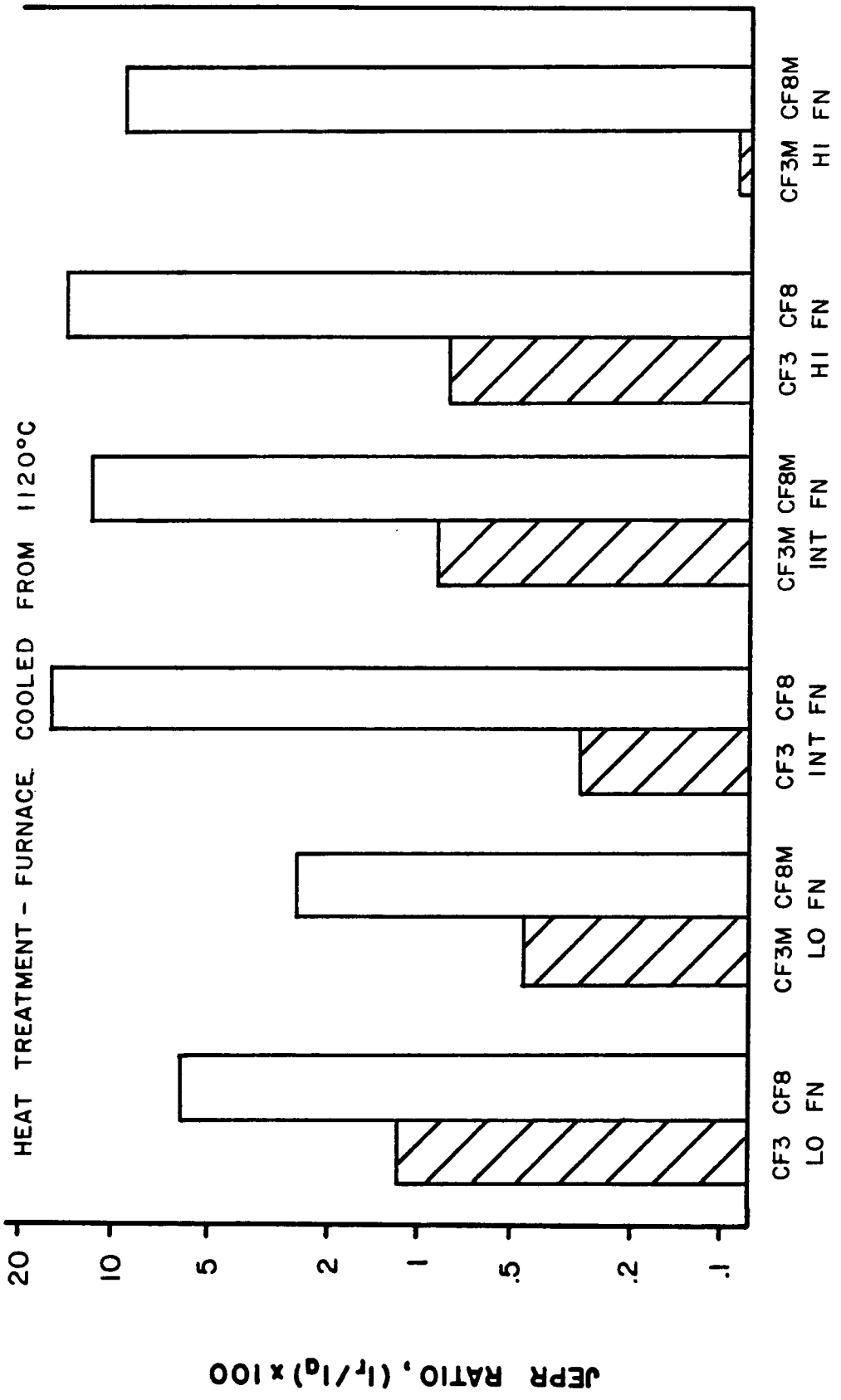

Figure 70. Comparison of JEPR results as a function of carbon content for CF and CFM alloys in the furnace cooled condition.

sample during the anodic sweep of the test. The general attack obscures most microstructural detail, even at high magnification.

Oxalic Acid Etch Test

The oxalic acid etch test was also used to evaluate the high carbon material in the solution annealed, as-cast and furnace cooled conditions. This test is a standardized test (also known as ASTM--A262 Practice A) for the detection of susceptibility to sensitization. (The specific test characteristics are outlined in the Literature Review section.) As indicated in the specification the solution attacks chromium carbides and leaves a groove or ditch where the carbide was located prior to the etch test. Evaluation of the microstructure following the etch test by comparison of the resulting microstructure with those given in the specification allows one to decide if the material is potentially sensitized. If the microstructure indicates potential sensitization, then, by specification, the material is not "failed" on the basis of this test; rather, a weight loss test or simulated service environment test is utilized if the oxalic acid test yields an "unacceptable" microstructure.

As expected, the solution annealed material (all carbon contents) is representative of the "isolated ferrite" or "step structure" condition of the specification, i.e., no (or very few) ditches in the structure due to the presence of carbides. Figure 71a shows the smooth "step" at the ferrite-austenite interface (indicating no carbide precipitation) that was found in all solution annealed samples.

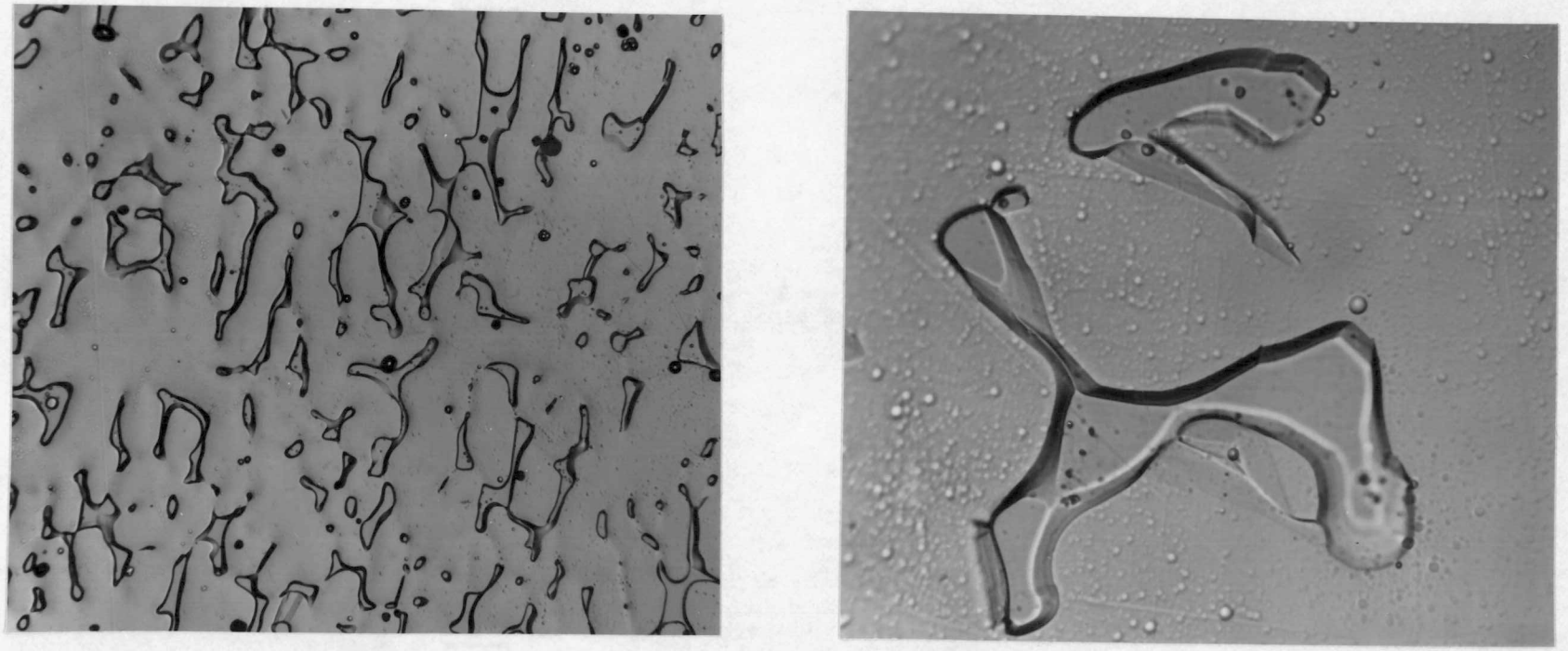

(a) 200 X

(b) 1000 X

Figure 71. Representative structure of solution annealed alloys following oxalic acid testing.

Also notice that no austenite-austenite boundaries have been etched, again indicating no carbide precipitation at this location. Note, particularly in the high magnification photo of Figure 71b, that the ferrite is in relief (stands higher in the microstructure) compared to the austenite matrix. This result is somewhat surprising since indications in the literature (19) suggest that the average corrosion rate increases as the chromium content increases at the potential of the oxalic acid etch test. If this were uniformly the case (i.e., independent of crystal structure, etc.) the austenite in these microstructures might be expected to be higher relative to the ferrite. This is a minor point of course, and the etch structures published in the specification also show the ferrite "standing up" in the microstructure for the solution annealed sample.

In contrast, the as-cast and furnace cooled high carbon alloys reveal interdendritic ditching in the microstructure after the EPR test. Representative examples of this observation are shown in Figures 72 and 73. Note that no austenite-austenite boundaries were attacked although high ferrite content tends to make the attack look continuous in some portions of the microstructure. Also note that in the CF8M the ferrite itself seems to contain the carbides that led to the attack in oxalic acid (as was indicated by the EPR test microstructure) and the CF8 alloy shown indicates that the carbides are more localized at the ferrite-austenite boundary (as was also indicated by the EPR test microstructure). When sensitized samples (such as as-cast CF8 and CF8M) are etched for the full 90 seconds

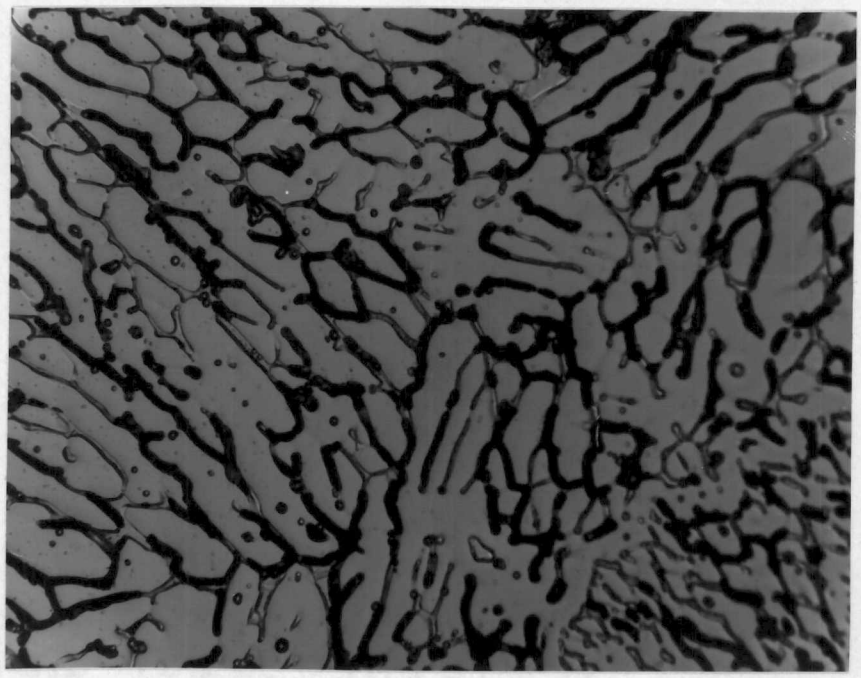

Figure 72. Representative microstructure of CF8 alloy in the as-cast condition following oxalic acid testing. 200 X.

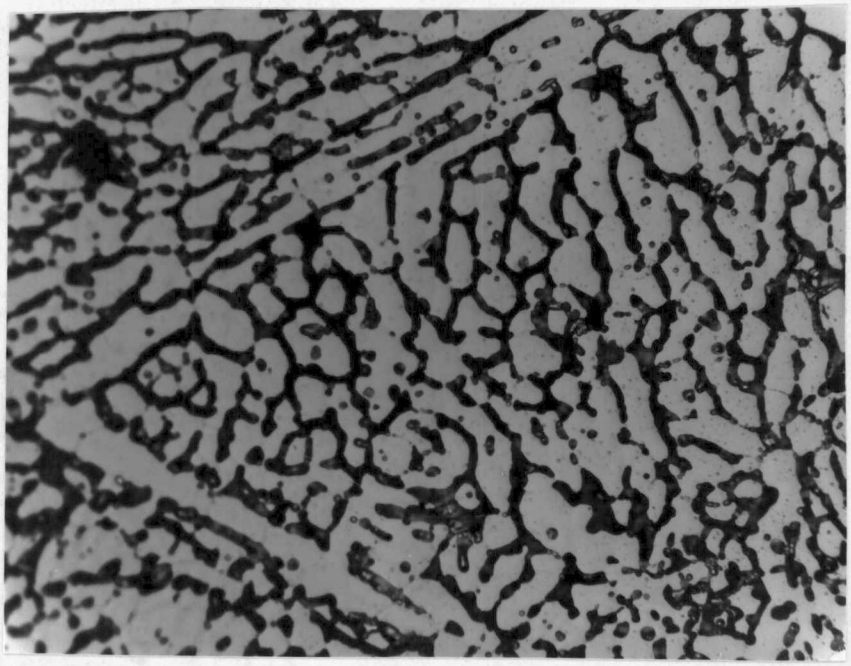

Figure 73. Representative microstructure of CF8M alloy in the as-cast condition following oxalic acid testing. 200 X.

called for by the specification, the ferrite appears as if it has been dissolved in most instances. In this research, alloys that show this complete "interdendritic ditching" behavior are interpreted to have unacceptable etch structures as indicated by the specification. In the discussion that follows, samples are considered sensitized as measured by A262A that show interdendritic ditching. In some instances, however, the microstructures shown were produced by etching only 20 - 30 seconds to show the initiation sites of the ditching.

As the oxalic acid etch test data was expanded to include the high carbon and low carbon isothermal hold samples, it was found that with very rare exception, extensive interdendritic ditching (ditching of the ferrite-austenite interface) occurred in all samples that were not in the solution annealed condition. This includes both the high and low carbon samples as well as the samples with and without molybdenum. This etch structure, according to the specification, is "unacceptable" and indicates potential sensitization and an "appropriate" weight loss test is then called for by the specification to determine if the material is indeed sensitized. That the oxalic acid etch test is a very severe test is acknowledged in the specification and that is why a second "referee" test is used in cases where the oxalic acid etch test yields an unacceptable microstructure. A probable explanation for the EPR test and the JEPR test indicating low degrees of sensitization and the oxalic acid etch test indicating potential sensitization can be found in the phenomena that the different tests measure: the EPR and JEPR

tests evaluate the degree of "chromium depletion" within an alloy where the oxalic acid etch test dissolves chromium carbides. It is entirely possible that carbides may exist without chromium depletion of sufficient magnitude to be detected by the EPR and JEPR tests, particularly if molybdenum affects the level of "chromium depletion" that may be tolerated by the alloy before sensitization has actually occurred. Carbides also exist in a stainless steel that has "healed" without having regions of chromium depletion adjacent to these carbides. Unless the material were to be exposed to a service environment in which carbides themselves are attacked, the carbides are not harmful. Thus, this disparity between the EPR and JEPR test results and the oxalic acid etch test results may or may not indicate an inadequacy of any of the tests. This result will be discussed again in a later section.

Weld Simulation

The thermal cycles for the weld simulation studies were calculated from the published (86) values of the solutions to the differential equation relating temperature to time and distance for the arc welding of 1-1/2 in. thick stainless steel. In the welding of 1-1/2 in. stainless steel, an energy input of 70 kJ/in is a typical value. In order to simulate the thermal cycle experienced by the heat affected zone of stainless steel subjected to a 70 kJ/in energy input, the complete thermal history including the cooling rate from a peak temperature of 870°C (1600°F) for this energy input was calculated and programmed into the Gleeble. It was also

desired to employ welding conditions producing a faster and a slower cooling rate in the weld simulation studies. The "fast cool" cycle was obtained with gas accelerated cooling from the peak temperature. The slower rate was characteristic of a 140 kJ/in energy input to 1-1/2 in. stainless steel. For the simulated 70 kJ/in and 140 kJ/in thermal cycles, both single and multiple thermal cycles (3 cycles) were imposed. All cast alloys subjected to the Gleeble cycles had been solution annealed at 1120°C (2050°F) for approximately 45 minutes.

The thermal cycles chosen for the weld simulation study are summarized in Figure 74 (the approximate time in the sensitizing range is given by the number in parentheses). A peak temperature of 870°C (1600°F) was chosen because it is most commonly taken as the maximum temperature in the sensitizing range; a higher peak temperature would probably have little effect as it would lead to no additional carbide precipitation and may, in fact, dissolve some carbides (although the ferrite number might change slightly) and a lower peak temperature would decrease the time in the sensitizing range. Also, in order to check the validity of the choice of 870°C (1600°F) as the temperature inducing maximum sensitization, autogenous welds were made on the edge of 1/4" thick wrought 304 and 316 plate and on 1/4" cut slabs of high and low ferrite CF8 (all samples .05 - .06% C level). The temperature/time history at various locations in the HAZ was determined by thermocouple techniques. From these cycles a plot of peak temperature vs. distance from the fusion line was developed. Samples were sectioned, polished and etched to find the region of maximum carbide precipitation (sensitized zone)--this

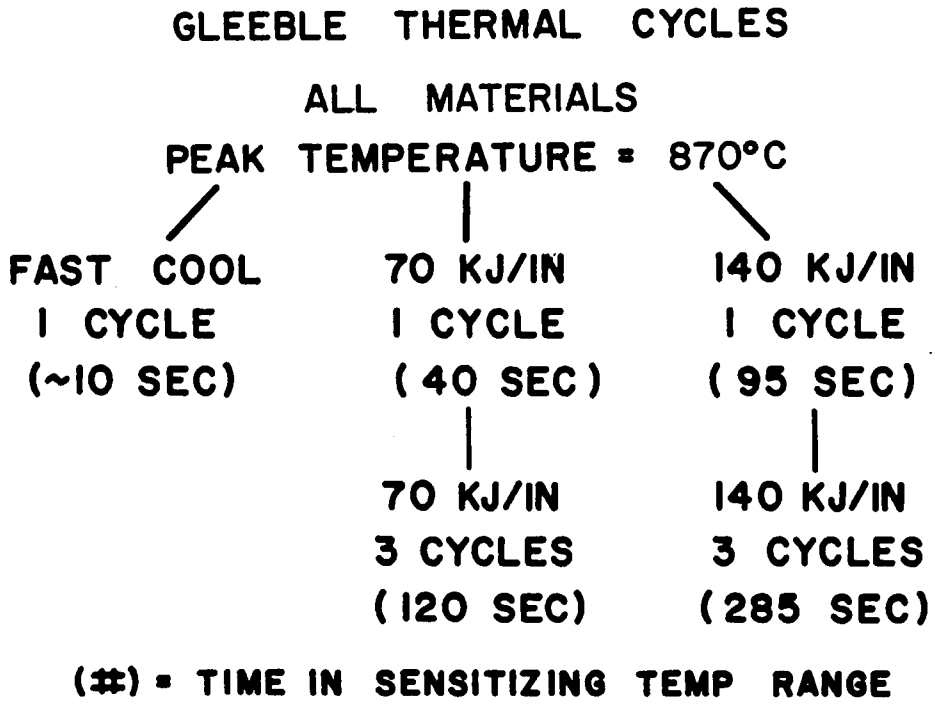

Figure 74. Schematic of weld simulation thermal cycles.

procedure is shown in Figure 75. The region of maximum precipitation (when precipitation occurred at all--the region in the HAZ adjacent to the fusion line showed little or no precipitation) corresponded to the position at which the peak temperature was 867°C (1592°F) for 304 stainless steel.

Some investigators (63,64) have indicated that weld thermal cycle peak temperatures above 800°C (1450°F) erase prior thermal cycle damage in wrought material due to the tendency of the carbides to go back into solution above 800°C. Appropriately, some thermal cycles were simulated that reached 870°C (1600°F) on the first cycle and 790°C (1450°F) on each of two subsequent cycles. In addition, on some selected samples, a strain of about 20% was applied at the peak temperature of the thermal cycle to simulate restraint during welding.

EPR results on the high carbon (.06 - .08% C) alloys that simulate weld repair are shown in Figure 76. Recalling that the higher peak current density represents greater sensitization (within an alloy class) in the EPR test, one can note that each lot of CF8M (.06% C, FN = 4; .08% C, FN = 12; .07% C, FN = 20) and the high ferrite CF8 alloy (.06% C, FN = 20) have very low EPR responses indicating very low sensitization damage due to the welding HAZ thermal cycle exposure. Only the low ferrite CF8 (.06% C, FN = 4) and the intermediate ferrite CF8 (.08% C, FN = 10) seem to give a large EPR response. It is particularly significant that the response for each alloy was not a strong function of the thermal cycle it received after the solution annealing treatment. This means that for these

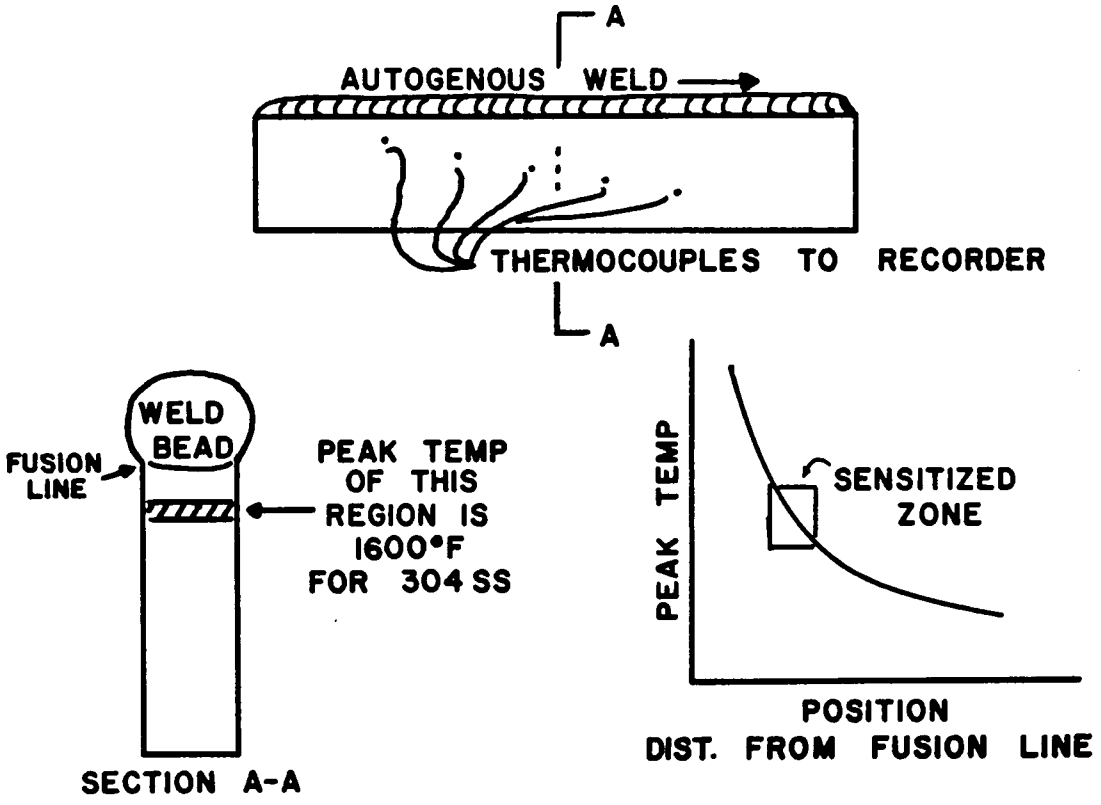

Figure 75. Locating the region of maximum sensitization.

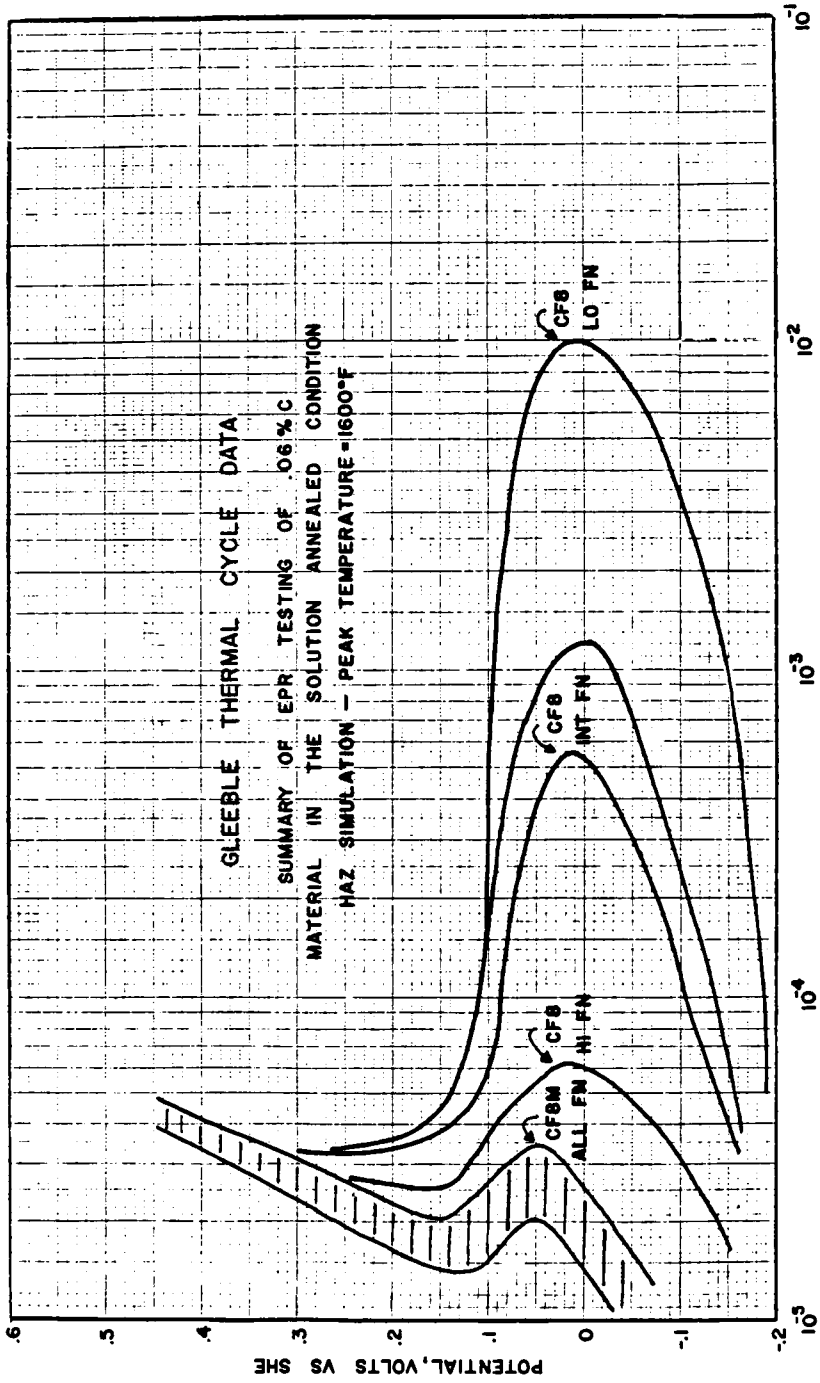

Figure 76. Representative summary of weld simulation data for EPR testing the high carbon alloys.

alloys, the position of each EPR curve did not change appreciably whether the sample received the "fast cool" cycle or the slow cool (140 kJ/in) cycle.

The CF8M material was found to be unaffected by any of the thermal cycles imposed, i.e., from a sensitization standpoint the CF8M alloys had not been changed from the solution annealed condition by the weld simulation. Microstructurally (as EPR tested), no evidence of attack or sensitization of any kind was observed in the CF8M alloys--only occasional slight staining of the ferrite pools. The low ferrite CF8 appeared to have the highest susceptibility to sensitization as EPR tested and microstructurally (Figure 77) it was found that at low magnification with an optical light microscope the alloy seems to be relatively free of sensitization damage, i.e., very few ditches and some light etching of the ferrite-austenite boundaries. At higher magnification (see Figures 78 and 79), small particles have formed over a large fraction of the ferrite-austenite interfaces. Notice that, for the most part, no ditching is associated with these carbides. This indicates that the carbides that have formed have created a very small "chromium depletion" zone that is difficult to detect or that does not etch an extraordinary amount or that there may be very little "chromium depletion" as detected by the EPR test. The EDAX technique was used to obtain a qualitative feel for the amount of chromium in the carbides. The counting time was normalized to 4000 counts maximum for any one channel. The results indicate less chromium in the carbides than was expected. Given the small size of the carbides, it was

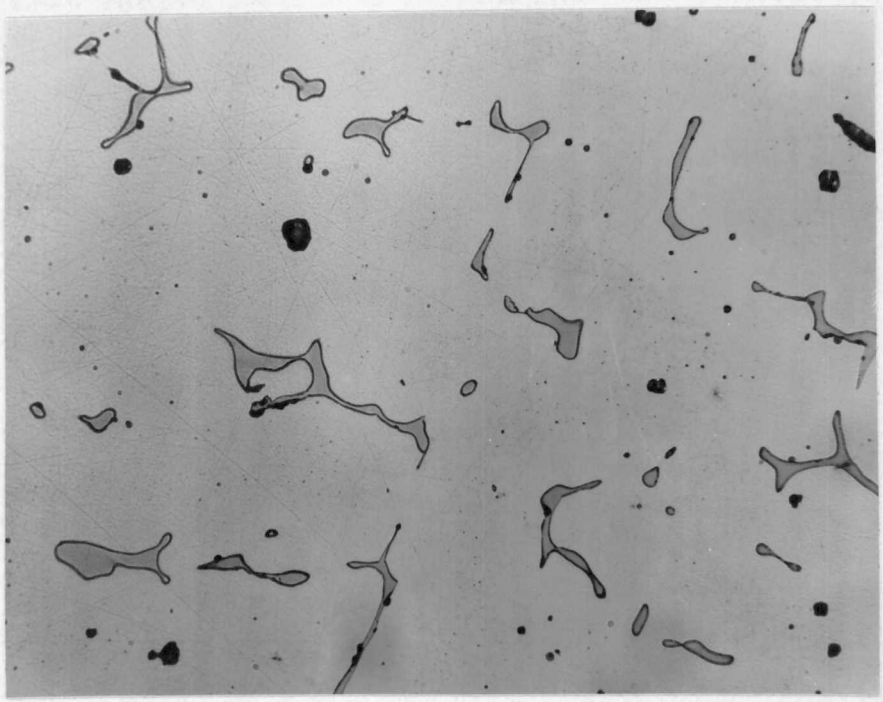

Figure 77. High carbon, low ferrite CF8 alloy following weld simulation and EPR testing at low magnification. 140 kJ/in, 3 cycles. 200 X.

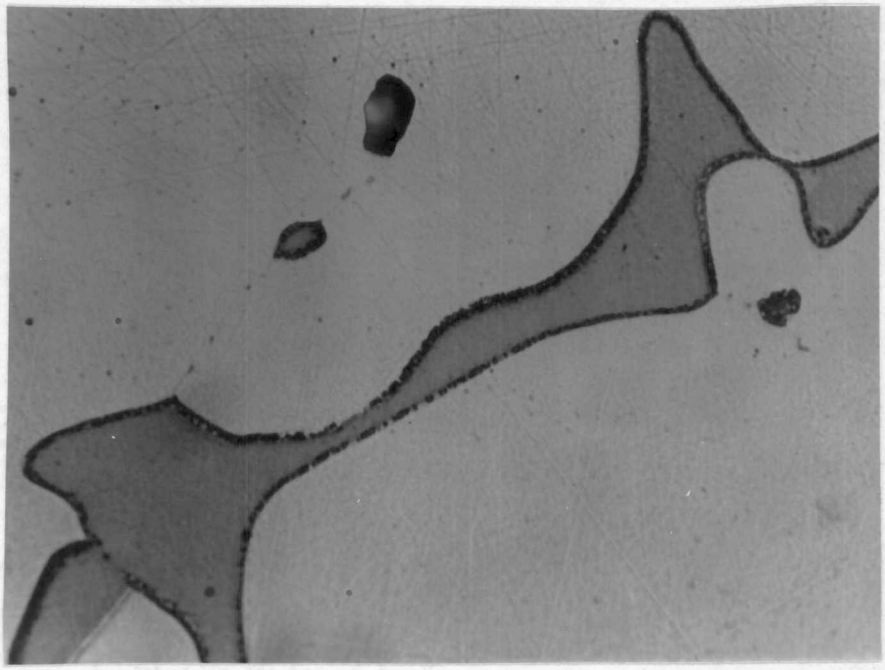

Figure 78. High carbon, low ferrite CF8 alloy following weld simulation and EPR testing at high magnification. 140 kJ/in, 3 cycles. 1000 X.

Figure 79. SEM photograph of particles at ferrite-austenite boundary. CF8, high carbon, low ferrite. 140 kJ/in, 3 cycles. 8500 X.

difficult to set the x-ray probe such that no other material near the carbide was included in the analysis; even so, the chromium content of the carbides was still lower than expected. The relative counts for the Kα peaks for each of Fe, Cr, and Ni are shown in Table 10. These do not indicate composition--simply a qualitative idea of the relative amounts of each element. As expected, the ferrite contains more Cr and less Ni than the austenite but the carbides (whose composition is often assumed to be $(Cr_{.75}\ Fe_{.25})_{23}C_6$) do not contain the large fraction of chromium expected based on the chromium-rich carbide stoichiometry. This may be due to a much larger volume of material contributing to the analysis. It may, however, indicate that carbides that form in a very short time do not have as much chromium as some carbides that are given more time to form and grow (time to "absorb" chromium). This could possibly explain the small amount of ditching observed near these carbides. The larger carbides observed on other samples with much longer exposures to the sensitizing temperature range tend to have Fe and Cr EDAX counts that indicate much higher Cr. (Again, this may be due partially to their size.) It is also possible that these particles are sigma phase but not particularly likely, especially since these particles are predominantly, although not exclusively, found in the CF8 (no Mo) alloys most readily.

Occasionally, the low ferrite CF8 alloys that were subjected to weld simulation thermal cycles exhibited extensive pitting in the austenite matrix away from the ferrite pools (as previously described in this text). When the low ferrite CF8 did not exhibit pitting, the

Table 10. Relative composition (EDAX counts) of phases in Figure 79.

	COUNTS FOR Kα OF EACH ELEMENT		
	IRON	CHROMIUM	NICKEL
AUSTENITE	4000	1860	420
FERRITE	4000	2220	290
PARTICLES (CARBIDES?)	4000	2630	290

EPR response was approximately an order of magnitude lower. The low ferrite CF8 was the only high carbon alloy that exhibited pitting after weld simulation and as previously noted, it is unknown at present why this alloy tends to be susceptible to pitting.

The intermediate ferrite level CF8 alloy gave the greatest delineation of response with regard to the different thermal cycle conditions and microstructurally (as EPR tested) it showed only attack at the ferrite-austenite boundaries as shown in Figure 80. Figure 81 is representative of the behavior of the high ferrite CF8 samples. Note the lack of ditching and pitting in this sample.

Based on the weld simulation study results from the high carbon materials and the extensive isothermal hold data for all materials, it was decided that testing a low ferrite (~2FN) and a high ferrite (~8FN) CF3 alloy as well as a low ferrite (~5FN) CF3M alloy would adequately represent the low carbon (.015 - .027% C) alloys in the weld simulation testing.

The EPR testing of the low carbon weld simulation samples yielded results similar to the results from the high carbon alloys, i.e., the low ferrite CF3 alloy gave the highest EPR response, an indication of susceptibility to sensitization, but again the austenite matrix was severely pitted in some cases and the ferrite-austenite boundaries relatively free of attack. The high ferrite CF3 alloy was nearly free from any ferrite-austenite boundary ditching and yielded a very low peak current density in the EPR test as did the low ferrite CF3M alloy, which was not etched at all by the EPR test.

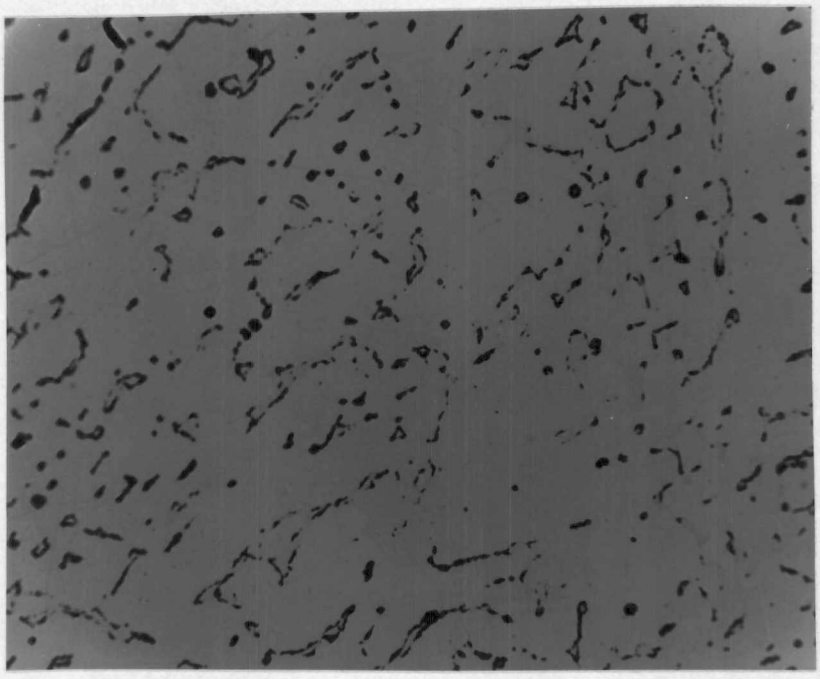

Figure 80. High carbon, intermediate ferrite CF8 alloy following weld simulation and EPR testing. 140 kJ/in, 3 cycles. 200 X.

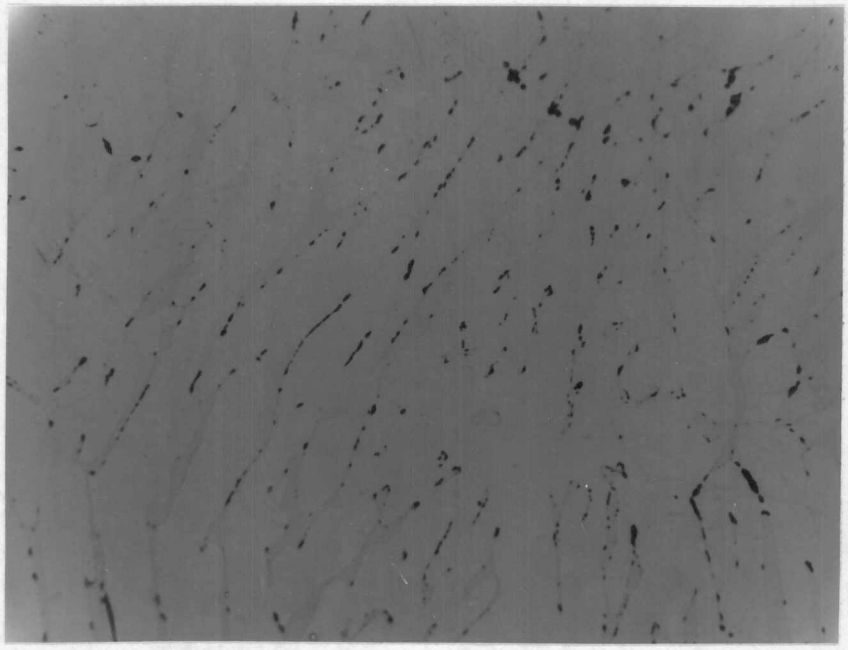

Figure 81. High carbon, high ferrite CF8 alloy following weld simulation and EPR testing. 140 kJ/in, 3 cycles. 200 X.

In order to attempt to further distinguish between CF8 and CF8M, each weld simulation sample was evaluated using the JEPR test. Table 11 gives representative data from the JEPR testing of the Gleeble samples and it generally supports the trends seen in the EPR data. Specifically it shows that the CF8M alloys are about an order of magnitude superior to the CF8 alloys in all conditions except the solution annealed condition, where the difference is not as great. It also shows that for very short times in the sensitizing temperature range the CF8 alloys are changed markedly from the solution annealed condition where the CF8M alloys are not changed from the solution annealed condition significantly. Since the effect of Mo does not appear to "divide out" of the data for the short sensitizing times this data implies that Mo may have a beneficial effect in slightly retarding sensitization. If only the passivation behavior was affected by the Mo content, the JEPR test would "divide out" this compositional effect and the JEPR ratios for CF8 and CF8M alloys would be approximately equal--which is the case for some of the more severe (long times) sensitizing treatments. The low carbon samples indicated uniformly low JEPR values.

The JEPR data also show that, for the CF8 alloys, the effect of .08% C versus .06% C may be detected by this test based on the higher JEPR ratios for the intermediate ferrite level CF8 alloy (.08% C) compared to the other CF8 alloys. The JEPR data of Table 11 also seem to be more sensitive to the thermal cycle imposed, i.e., the JEPR ratios are higher for slower cooling through the sensitizing range.

Table 11. Representative JEPR data from high carbon weld simulation samples.

	POST SOLUTION ANNEAL HEAT TREATMENT (PEAK TEMP = 870°C)			
MATERIAL	FAST COOL	1 CYCLE 70 KJ/IN	3 CYCLES 140 KJ/IN	NONE
CF8, LO FN	0.31	1.5	3.1	0.12
CF8, INT FN	1.1	3.9	3.8	
CF8, HI FN	0.50	0.50	1.2	
CF8M, ALL FN	0.05	0.09	0.11	0.05

(NUMBERS ABOVE ARE $I_r / I_a \times 100$ RATIOS)

In an effort to further characterize the behavior of the weld simulation samples, the oxalic acid test was performed on each. For the high carbon samples, the test was unable to distinguish (heat treatment or alloy type) between the samples because extensive interdendritic ditching occurred in all samples. Figure 82 is representative of the range of ditching observed (60 - 100% of ferrite-austenite boundary) in these samples. These results seem to contradict the results of the EPR and JEPR tests by indicating large degrees of sensitization for all samples, including the CF8M alloys. This apparent incongruity may possibly be explained by recalling that oxalic acid attacks carbides specifically and the EPR and JEPR test are designed to attack chromium depletion zones. Small particles (probably carbides) located on the ferrite-austenite boundaries in the low and intermediate ferrite CF8 samples may be present, but much smaller, on the ferrite-austenite boundaries in the other CF8 and CF8M alloys. These carbide networks have yet to be observed in the CF8M alloys. The oxalic acid etching of the low carbon alloys exposed to the HAZ weld simulation thermal cycles yielded step structures for all samples. This fact seems to imply that carbides are indeed responsible for the ditching in oxalic acid observed in the high carbon alloys.

In addition to the thermal cycles with a peak temperature of 870°C (1600°F), a multiple thermal cycle condition with an HAZ peak temperature of 870°C (1600°F) for the initial cycle and 790°C (1450°F) for the subsequent two thermal cycles was investigated. The results

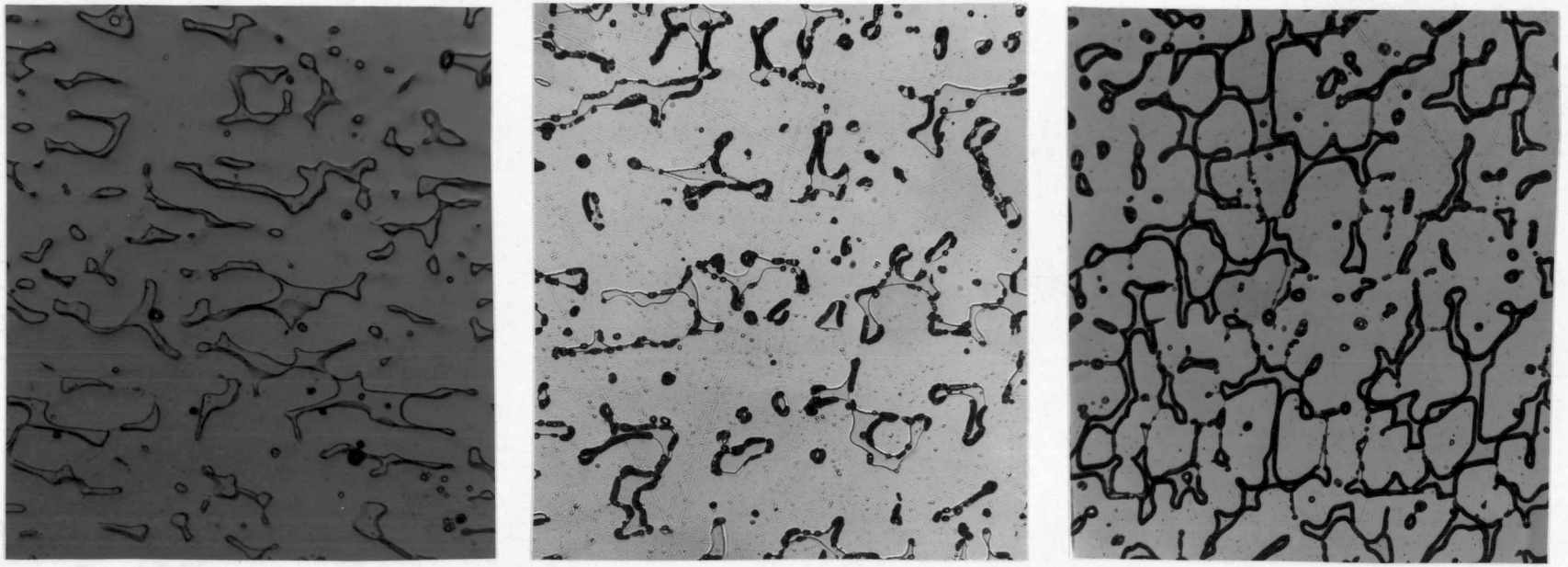

(a) solution annealed; no ditching. 200 X.

(b) 60% ditching after weld simulation. 200 X.

(c) 100% ditching after weld simulation. 200 X.

Figure 82. Oxalic acid etch test results from weld simulation samples.

are shown graphically in Figures 83 - 84. As one can see, the lower peak temperature may be slightly more damaging (from a sensitization standpoint) than the peak temperature of 870°C (1600°F). Limited JEPR data indicate a similar slight increase. This is probably a result of reduced tendency for the carbides to go back into solution at 800°C compared to 870°C, although it is expected that even for the small carbide sizes involved that the kinetics to carbide dissolution are sufficiently sluggish at these temperatures that this would be a rather small effect.

The application of 20% strain (to simulate weld restraint) at the peak temperature of 870°C (for single thermal cycles) increases the EPR and JEPR responses of the CF8 alloys somewhat with no appreciable change in the CF8M or low carbon alloys. Representative data are shown in Figures 85 - 86.

These data on the weld simulation samples imply that the low carbon alloys may not be sensitized after common weld repair procedures and that from a specific service enviornment perspective the high carbon Mo bearing alloys, due to low EPR and JEPR indications of chromium depletion, may also be essentially in the "unsensitized" condition following weld repair. Table 12 summarizes the weld thermal cycle data for all materials for the convenience of the reader.

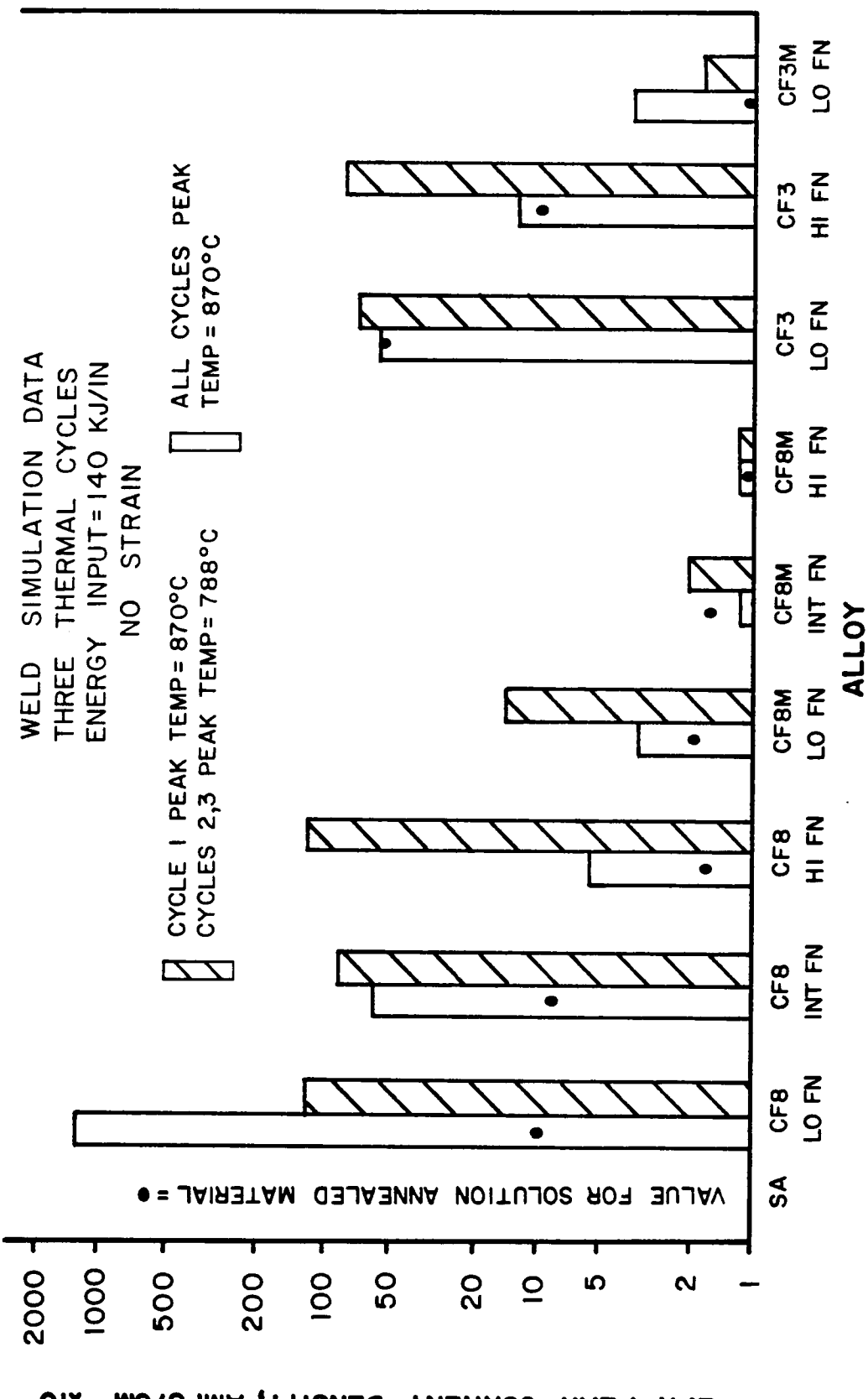

Figure 83. EPR weld simulation data examining the effect of thermal cycle peak temperature.

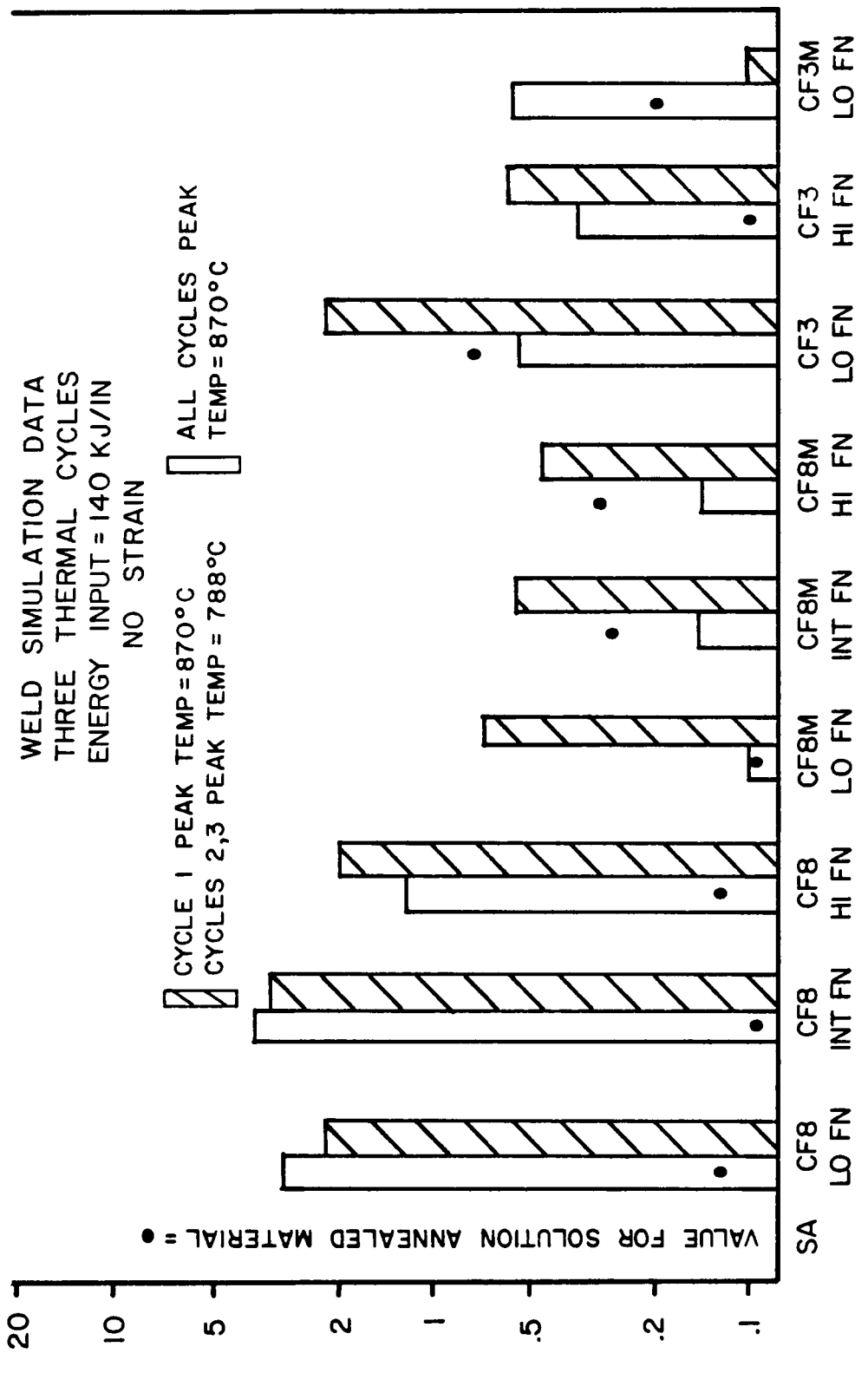

Figure 84. JEPR weld simulation data examining the effect of thermal cycle peak temperature.

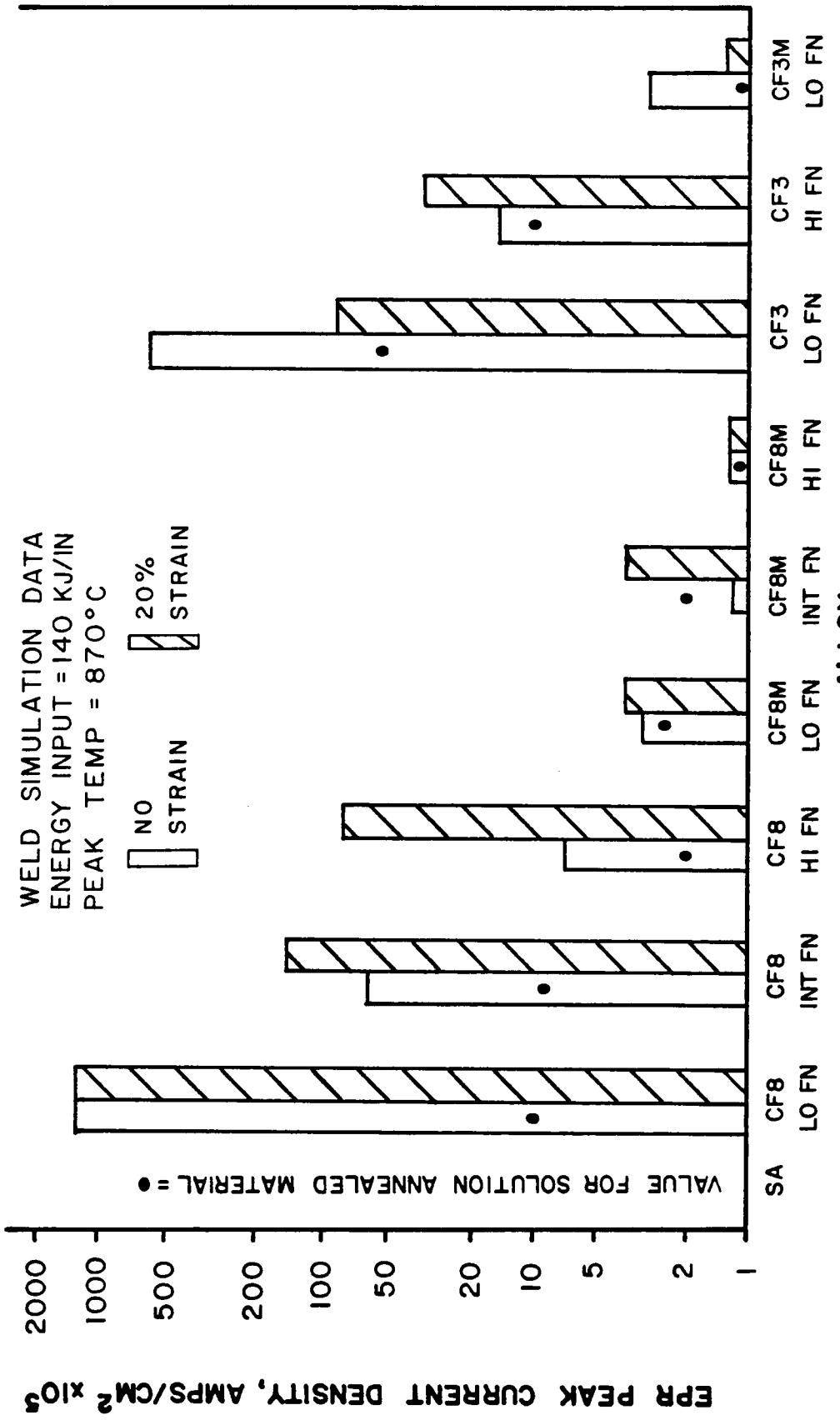

Figure 85. EPR weld simulation data examining the effect of strain.

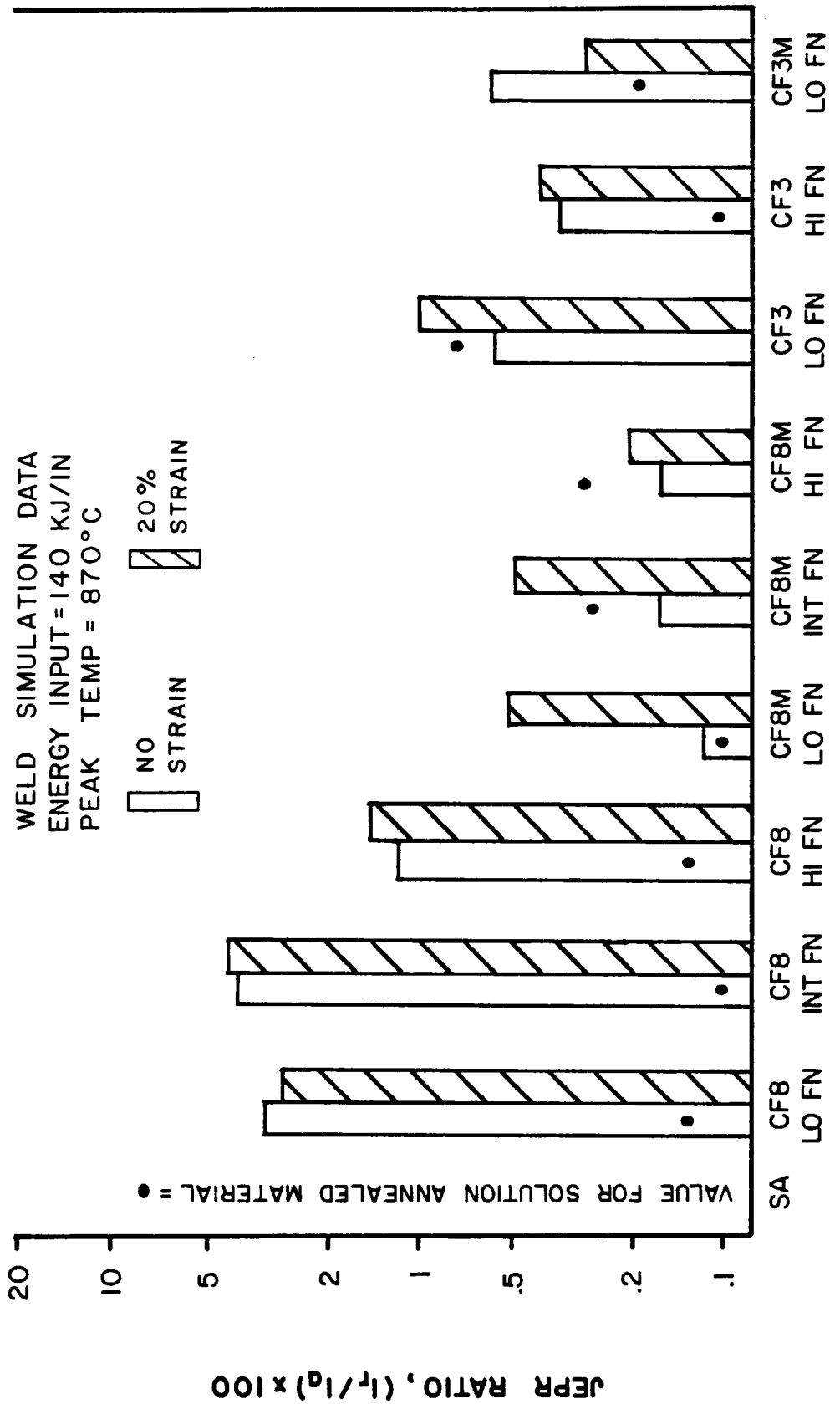

Figure 86. JEPR weld simulation data examining the effect of strain.

Table 12. Summary of weld simulation data.

	no. cycles = 3 no strain peak temp(°F) = 1600(1), 1450(2) energy input = 140 KJ/IN			no. cycles = 3 no strain peak temp(°F) = 1600(3) energy input = 140 KJ/IN			no. cycles = 1 20% strain peak temp(°F) = 1600 energy input = 140 KJ/IN		
	EPR amp/sq cm	JEPR ratio	A262A structure	EPR amp/sq cm	JEPR ratio	A262A structure	EPR amp/sq cm	JEPR ratio	A262A structure
CF8 LO	1.2×10^{-3}	2.2	ditch	1.2×10^{-2}	3.1	ditch	1.2×10^{-2}	2.7	ditch
CF8 INT	9.1×10^{-4}	3.3	ditch	5.5×10^{-4}	3.8	ditch	1.4×10^{-3}	4.1	ditch
CF8 HI	1.2×10^{-3}	2.0	ditch	6.2×10^{-6}	1.2	ditch	6.9×10^{-4}	1.6	ditch
CF8M LO	1.5×10^{-4}	.81	ditch	3.0×10^{-5}	.11	ditch	4.2×10^{-5}	.50	ditch
CF8M INT	2.2×10^{-5}	.53	ditch	1.0×10^{-5}	.15	ditch	3.7×10^{-5}	.50	ditch
CF8M HI	1.0×10^{-5}	.48	ditch	1.0×10^{-5}	.15	ditch	1.0×10^{-5}	.21	ditch
CF3 LO	6.8×10^{-3}	2.1	step	5.8×10^{-3}	.52	step	8.2×10^{-4}	1.0	step
CF3 HI	8.3×10^{-4}	.54	ditch	1.7×10^{-4}	.33	step	3.9×10^{-4}	.38	ditch
CF3M LO	1.7×10^{-5}	.11	step	2.9×10^{-5}	.54	step	1.0×10^{-5}	.30	step

CHAPTER V

CONCLUSIONS

The sensitization behavior of CF and CFM type cast duplex stainless steels has been examined for correlation with sensitization that may result from weld repair thermal cycles. The EPR, JEPR and oxalic acid etch tests were used for the evaluation of degree of sensitization and the following major conclusions may be drawn from this research effort.

1. The standard specification of the susceptible interface area for single phase stainless steels in the EPR test does not apply to the duplex materials. However, it was noted that the reactivation peak current density was an adequate measure of the degree of sensitization.
2. The EPR peak current densities are very sensitive to carbon, chromium and molybdenum content as well as ferrite number and heat treatment, varying more than three orders of magnitude for the heat treatments and alloys tested.
3. The EPR test indicates that the .03% C alloys are more difficult to sensitize than the .06% C or .08% C alloys, thus confirming that the effect of carbon is to enhance formation of chromium depletion zones adjacent to the chromium rich carbides.
4. In general, the higher the ferrite number, the greater the resistance to sensitization as measured by the EPR test.

It was indicated that this was related to the bulk chromium content or the Cr/Ni ratio as opposed to the ferrite content per se (above FN = 2 - 3).

5. Microstructurally, the EPR test attacks chromium depleted regions adjacent to chromium rich carbides. These carbides are located exclusively at the ferrite-austenite boundaries for ferrite numbers above about FN = 2 - 3. For ferrite numbers less than FN = 2 - 3, the austenite-austenite boundaries are susceptible to carbide precipitation and associated local chromium depletion.
6. Molybdenum seems to be the most important compositional variable governing the EPR response of each alloy. CFM alloys containing about 2% Mo have EPR responses approximately an order of magnitude lower than similar CF alloys (%Mo <0.2 in general) for equivalent heat treatments.
7. The JEPR test technique was shown to be less sensitive to bulk alloy composition (particularly Mo content) than the EPR test for the alloys tested. The active dissolution peak current density of the JEPR test was very sensitive to bulk composition but very insensitive to degree of sensitization. Like the EPR test, the reactivation peak current density was very sensitive to degree of sensitization.
8. For long sensitizing times such as those represented by an as-cast microstructure, the effect of Mo is related primarily to the passivation characteristics of the alloy and the JEPR test often "divides out" the compositional

difference between CF and CFM (at all ferrite levels) and indicates essentially equivalent sensitization rankings for equivalent thermal histories.

9. For short sensitizing times such as those representative of weld repair, the JEPR test does not "divide out" the compositional difference between CFM and CF alloys, with the CFM alloys having a considerably smaller EPR response for equivalent heat treatments. This indicates that Mo actually retards the onset of sensitization.

10. The JEPR test ranks the .03% C alloys more difficult to sensitize than the .06% C alloys. Further, the JEPR test also ranks the .06% C alloys more difficult to sensitize than the .08% C alloys.

11. The oxalic acid etch test is a very severe test for duplex stainless steel castings. The solution annealed samples yield a "step" structure but most other heat treatments produce a "ditch" structure which is unacceptable according to the ASTM specification. Apparently the oxalic acid test does not differentiate between low and high levels of sensitization.

12. Because of the inability of the oxalic acid etch test to differentiate between various levels of sensitization, a disparity exists between this test and the EPR and JEPR tests. Specifically, the oxalic acid test indicates extensive ditching (and thus "unacceptable microstructure"

according to the specification) for almost all alloys and heat treatments where for the same alloys a wide range of sensitization response is indicated by the EPR and JEPR tests.

13. From a sensitization standpoint, the most detrimental peak temperature in the simulated weld thermal cycles was approximately 800°C (1470°F). Peak temperatures of 870°C (1600°F) yield only slightly lower peak current densities and JEPR ratios for all alloys.

14. The effect of energy input in the weld thermal cycle simulation on sensitization was examined and within the limits studied (≈20 to 140 kJ/in) had only a small influence. Alloys (CF8, FN ≈ 4; CF8, FN ≈ 11; CF3, FN ≈ 2) susceptible to sensitization under these conditions became sensitized (at least somewhat) at all energy inputs. Other alloys (all CF8M; CF3M; CF8, FN ≈ 20) were not susceptible to sensitization for any energy input.

15. The effect of multiple thermal cycles was studied to simulate multiple pass repair techniques. The alloys that were susceptible after one thermal cycle to sensitization were not appreciably damaged by two additional thermal cycles. Some alloys (all CF8M; CF3M; CF8, FN ≈ 20) were not sensitized after all three thermal cycles.

16. The effect of strain applied at the peak temperature of the thermal cycle was examined to simulate the effect of

restraint during welding. Up to 20% strain, no appreciable effect was measured with any test technique.

The original goal of this research program was to evaluate the post-weld repair heat treatment requirements of ASTM - A743/4 for the cast duplex stainless steels. It appears that, for the simulated welding conditions considered, the Mo bearing CFM alloys may be immune to sensitization for carbon contents below .08% as measured by the EPR and JEPR tests. However, this trend was not clearly shown with the oxalic acid etch test. The CF alloys (no Mo) are slightly more susceptible to sensitization during weld repair. The low carbon (< .03%) CF alloys appear to be relatively free from sensitization after weld repair simulation. At the higher carbon level (.06% C), only the high ferrite CF alloy appears to be free from sensitization following weld repair simulation. The intermediate and low ferrite content CF alloys are at least marginally sensitized following the weld repair simulation thermal cycles. However, this is at least in part related to a pitting phenomenon observed in these alloys which is not understood at present.

The interest in this type of corrosion testing is growing steadily in the casting industry and this research has opened doors to continuation of research in this area. For example, some preliminary results have shown that nitrogen may have a substantial effect in retarding the onset of sensitization in cast stainless steels and research in this area is expected to be pursued.

LIST OF REFERENCES

LIST OF REFERENCES

1. Roach, D. B., and Beck, F. H., "Performance and Reliability of Corrosion Resistant Castings: MTI Project #4/Phase II," Battelle Columbus Labs., (May 1981).

2. ASTM A 743-77: Standard Specification for Corrosion-Resistant Iron-Chromium, Iron-Chromium-Nickel, and Nickel-Base Alloy Castings for General Application.

3. ASTM A 744-77: Standard Specificaiton for Corrosion-Resistant Iron-Chromium-Nickel and Nickel-Base Alloy Castings for Severe Service.

4. ASTM A 262-77a: Standard Recommended Practices for Detecting Susceptibility to Intergranular Attack in Stainless Steels.

5. Steel Castings Handbook, 5th Edition, Wieser, P.F., ed. Steel Founders' Society of America, Rocky River, Ohio, (1980).

6. Handbook of Stainless Steels, Peckner, D., and Bernstein, I.M., eds., McGraw-Hill, Inc., (1977).

7. Schoefer, E., "Appendix to Mossbauer-Effect Examination of Ferrite in Stainless Steel Welds and Castings," Weld. Res. Supp., Vol. 39, p. 10-s, (1974).

8. Schaeffler, A., "Constitution Diagram for Stainless Steel Weld Metal," Metal Progress, p. 68-B, (1949).

9. Brooks, J. A., et al., "STEM Analysis of Primary Austenite Solidified Stainless Steel Welds," Metall. Trans. A., Vol. 14A, p. 23, (1983).

10. Ritter, A. M., et al., "Precipitation in CF-8M Duplex Stainless Steel Welds," Metall Trans. A., Vol. 14A, p. 37, (1983).

11. Cieslak, M. J., and Savage, W. F., "Weldability and Solidification Phenomenon of Cast Stainless Steel," Weld. J., Vol. 59, p. 136-s, (1980).

12. Suutala, N., et al., "Ferritic-Austenitic Solidification Mode in Austenitic Stainless Steel Welds," Metall. Trans. A., Vol. 11A, p. 717, (1980).

13. Lippold, J. C., and Savage, W. F., "Solidification of Austenitic Stainless Steel Weldments: Part II - The Effect of Alloy Composition on Ferrite Morphology," Weld. J., Vol. 59, p. 58-s, (1980).

14. Metals Handbook, Vol. 10, 8th ed., "Failure Analysis and Prevention," American Society for Metals, (1975).

15. Cowan, R. L., and Tedmon, C. S., Jr., "Intergranular Corrosion of Iron-Nickel-Chromium Alloys," in Advances in Corrosion Science and Technology, Vol. 3, Fontana, M. G., and Staehle, R. W., eds., Plenum Press, New York, (1973).

16. Bain, E. C., Aborn, R. H., and Rutherford, J. B., "Intergranular Corrosion of Austenitic Stainless Steels," Trans. Am. Soc. Steel Treating, Vol. 21, p. 481, (1933).

17. Polgary, S., "Stainless Steel Welding," Metal Construction, Vol. 8, (1976).

18. Hishida, M., and Nakada, H., "Critical Cooling Rate of 18Cr - 8Ni Stainless Steel for Sensitization and Subsequent Intergranular Stress Corrosion Cracking in High Temperature Water," Corrosion, Vol. 34, p. 338, (1978).

19. Streicher, M. A., "Theory and Application of Evaluation Tests for Detecting Susceptibility to Intergranular Attack in Stainless Steels and Related Alloys - Problems and Opportunities," in Intergranular Corrosion of Stainless Alloys, ASTM STP 656, Steigerwald, R. F., ed., p. 3-84, ASTM, (1978).

20. Devine, T. M., and Drummond, B. J., "Use of Accelerated Intergranular Corrosion Tests and Pitting Corrosion Tests to Detect Sensitization and Susceptibility to Intergranular Stress Corrosion Cracking in High Temperature Water of Duplex 308 Stainless Steel," Corrosion, Vol. 37, p. 104, (1981).

21. Dundas, H. J., and Bond, A. P., "Niobium and Titanium Requirements for Stabilization of Ferritic Stainless Steels," Intergranular Corrosion of Stainless Alloys, ASTM STP 656, Steigerwald, R. F., ed. p. 154-178, ASTM (1978).

22. Samans, C. H., "Further Observations on Sensitization of Chemically Stabilized Stainless Steels," Corrosion, Vol. 33, p. 271, (1977).

23. Streicher, M. A., "Effect of Heat Treatment, Composition and Microstructure on Corrosion of 18Cr - 8Ni - Ti Stainless Steels in Acids," Corrosion, Vol. 20, p. 57t, (1964).

24. Pande, C. S., et al., "Direct Evidence of Chromium Depeletion Near the Grain Boundaries in Sensitized Stainless Steels," Scripta Met., Vol. 11, p. 681, (1977).

25. Stawstrom, C., and Hillert, M., "An Improved Depleted-Zone Theory of Intergranular Corrosion of 18-8 Stainless Steel," J. Iron and Steel Inst., Vol. 207, p. 77, (1969).

26. Tedmon, C. S., Vermilyea, D. A., and Rosolowski, J. H., "Intergranular Corrosion of Austenitic Stainless Steel," J. Electrochem. Soc., Vol. 118, p. 192, (1971).

27. Clarke, W. L., Cowan, R. L., and Walker, W. L., "Comparative Methods for Measuring Degree of Sensitization in Stainless Steel," in Intergranular Corrosion of Stainless Alloys, ASTM STP 656, Steigerwald, R. F., ed., p. 99-132, ASTM, (1978).

28. Chung, P., and Smialowska, S. S., "The Effect of Heat Treatment on the Degree of Sensitization of Type 304 Stainless Steel," Corrosion, Vol. 37, p. 39, (1981).

29. Cihal, V., and Kasova, I., "Relation Between Carbide Precipitation and Intercrystalline Corrosion of Stainless Steels," Corr. Sci., Vol. 10, p. 875, (1970).

30. Mahla, E. M., and Nielsen, N. A., "Carbide Precipitation in Type 304 Stainless Steel - An Electron Microscope Study," ASM Trans. Quart., Vol. 43, p. 290, (1951).

31. Stickler, R., and Vinckier, A., "Morphology of Grain Boundary Carbides and its Influence on Intergranular Corrosion of 304 Stainless Steel," Trans. ASM, Vol. 54, p. 362, (1961).

32. DaCasa, C., Nileshwar, V. B., and Melford, D. A., "$M_{23}C_6$ Precipitation in Unstabilized Austenitic Stainless Steel," J. Iron and Steel Inst., p. 1325, (1969).

33. Kinzel, A. B., "Chromium Carbide ($Cr_{23}C_6$) in Stainless Steels," J. of Metals, Vol. 4, p. 469, (1952).

34. Gellings, P. J., and deJongh, M. A., "Grain Boundary Oxidation and Chromium Depletion Theory of Intercrystalline Corrosion of Austenitic Stainless Steels," Corr. Sci., Vol. 7, p. 413, (1967).

35. Osozawa, K., Bohnenkamp, K., and Engell, H. J., "Potentiostatic Study on the Intergranular Corrosion of an Austenitic Chromium-Nickel Stainless Steel," Corr. Sci., Vol. 6, p. 421, (1966).

36. Aust, K. T., Armijo, J. S., and Westbrook, J. H., "Heat Treatment and Corrosion Resistance of Austenitic Type 304 Stainless Steel," Trans. ASM., Vol. 59, p. 544, (1966).

37. Aust, K. T., et al., "Intergranular Corrosion and Electron Microscopic Studies of Austenitic Stainless Steels," Trans. ASM, Vol. 60, p. 360, (1967).

38. Joshi, A., and Stein, D. F., "Chemistry of Grain Boundaries and Its Relation to Intergranular Corrosion of Austenitic Stainless Steel," Corrosion, Vol. 28, p. 321, (1972).

39. Armijo, J. S., "Impurity Adsorption and Intergranular Corrosion of Austenitic Stainless Steel in Boiling HNO_3 - $K_2Cr_2O_7$ Solutions," Corr. Sci., Vol. 7, p. 143, (1967).

40. Park, J. Y., and Danyluk, S., "An Intergranular Fracturing Technique for Grain Boundary Segregation Studies of Austenitic Stainless Steels," Corrosion, Vol. 33, p. 304, (1977).

41. Hanninen, H., and Minni, E., "On Grain Boundary Segregation in Austenitic Stainless Steels," Metall. Trans. A., Vol. 13A, p. 2281, (1982).

42. Armijo, J. S., "Intergranular Corrosion of Nonsensitized Austenitic Stainless Steels - 1. Environmental Variables," Corrosion, Vol. 21, p. 235, (1965).

43. Lumsden, J. B., and Stocker, P. J., "Grain Boundary Composition of Unsensitized and Sensitized Stainless Steel," Corrosion, Vol. 37, p. 60, (1981).

44. Armijo, J. S., "Intergranular Corrosion of Non-Sensitized Stainless Steels - 2. Compositional Variables," Corrosion, Vol. 21, p. 24, (1968).

45. Payson, P., and Harrison, N. J., "Prevention of Intergranular Corrosion in Corrosion-Resistant Chromium-Nickel Steels," Trans. Amer. Inst. Mining and Met. Engr., Vol. 100, p. 306, (1932).

46. Henthorne, M., "Intergranular Corrosion in Iron and Nickel Base Alloys," in Localized Corrosion-Cause of Metal Failure, ASTM STP 516, p. 66, ASTM, (1972).

47. Briant, C. L., Mulford, R. A., and Hall, E. L., "Sensitization of Austenitic Stainless Steels - I. Controlled Purity Alloys," Corrosion, Vol. 38, p. 468, (1982).

48. Eckenrod, J. J., and Kovach, C. W., "Effect of Nitrogen on the Sensitization, Corrosion and Mechanical Properties of 18Cr - 8Ni Stainless Steels," in Properties of Austenitic Stainless Steels and Their Weld Metals (Influence of Slight Chemistry Variations), ASTM STP 679, Brinkman, C. R., and Garvin, H. W., eds., p. 17-41, ASTM (1979).

49. Akashi, M., et al., "Evaluation of IGSCC Susceptibility of Austenitic Stainless Steels Using Electrochemical Methods," Translated from Boshoku Gijutsu (Corrosion Engr), Vol. 29, p. 163, (1980), by BTSITS.

50. Briant, C. L., "The Effects of Sulfur and Phosphorus on the Intergranular Corrosion of 304 Stainless Steel," Corrosion, Vol. 36, p. 497, (1980).

51. Babakov, A. A., et al., "Intercrystalline Corrosion of Two-Phase Steels of the Type OKh21N5," Protection of Metals, Vol. 3, p. 117, (1967).

52. Levin, I. A., and Kochergina, D. G., "Intergranular Corrosion of Ferritic-Austenitic Steels OKh21N5 and OKh21N6M2 - I. Conditions of Development of Susceptibility to Intergranular Corrosion," Protection of Metals, Vol. 1, p. 225, (1965).

53. Beck, F. H., Juppenlatz, J., and Wieser, P. F., "Effects of Ferrite and Sensitization on Intergranular and Stress-Corrosion Behavior of Cast Stainless Steels," in Stress Corrosion - New Approaches, ASTM STP 610, p. 381-398, ASTM, (1976).

54. Devine, T. M., "Mechanism of Intergranular Corrosion and Pitting Corrosion of Austenitic and Duplex 308 Stainless Steel," J. Electrochem. Soc., Vol. 126, p. 374, (1979).

55. Tedmon, C. S., Jr., and Vermilyea, D. A., "Some Observations on Carbide Precipitation and Grain Boundary Migration in a Duplex Stainless Steel," Metall. Trans. Vol. 1, p. 2043, (1970).

56. Flowers, J. W., Beck, F. H., and Fontana, M. G., "Corrosion and Age Hardening Studies of Some Cast Stainless Alloys Containing Ferrite," Corrosion, Vol. 19, p. 186t, (1963).

57. Baeslack, W. A., III, Duquette, D. J., and Savage, W. F., "The Effect of Ferrite Content on Stress Corrosion Cracking in Duplex Stainless Steel Weld Metals at Room Temperature," Corrosion, Vol. 35, p. 45, (1979).

58. Hughes, N. R., Clarke, W. L., and Delwiche, D. E., "Intergranular Stress-Corrosion Cracking Resistance of Austenitic Stainless Steel Castings," in Stainless Steel Castings, ASTM STP 756, Behal, V. G., and Melilli, A.S., eds., p. 26-47, ASTM, (1982).

59. Tedmon, C. S., Jr., Vermilyea, D. A., and Broecker, D. E., "Effect of Cold Work on Intergranular Corrosion of Sensitized Stainless Steel," Corrosion, Vol. 27, p. 104, (1971).

60. Watanabe, M., Mukai, Y., and Murata, M., "Effect of Cold Work on Intergranular Corrosion Cracking of Sensitized Stainless Steel," Trans. JWRI, Vol. 5, p. 57, (1976).

61. Briant, C. L., and Ritter, A. M., "The Effect of Martensite on the Sensitization of Low Carbon 304 Stainless Steel," Metall. Trans. A., Vol. 12A, p. 910, (1981).

62. Solomon, H. D., and Lord, D. C., "Influence of Strain During Cooling on the Sensitization of Type 304 Stainless Steel," Corrosion, Vol. 36, p. 395, (1980).

63. Solomon, H. D., "Variables Influencing Weld Sensitization of Austenitic Stainless Steel," in Weldments: Physical Metallurgy and Failure Phenomenon, Proceedings, 5th Boltan Landing Conference; G.E. Co., p. 149-64, (1978).

64. Adachi, T., Kanamaru, T., and Maekita, T., "Study of Sensitization of Heat Affected Zone of SUS 304 by EPR Method," Nisshin Steel Tech. Report, Vol. 45, p. 9,(1981) (Abstract only in English, body in Japanese.)

65. Streicher, M., "General and Intergranular Corrosion of Austenitic Stainless Steels in Acids," J. Electrochem. Soc., Vol. 109, p. 161, (1959).

66. Povich, M. J., "Low Temperature Sensitization of Type 304 Stainless Steel," Corrosion, Vol. 34, p. 60, (1978).

67. Solomon, H. D., "Continuous Cooling Sensitization of Type 304 Stainless Steel," Corrosion, Vol. 34, p. 183, (1978).

68. Dayal, R. K., and Gnanamoorthy, J. B., "Predicting Extent of Sensitization During Continuous Cooling from TTS Diagram," Corrosion, Vol. 36, p. 104, (1980).

69. Loria, E. A., "Perspective on Intergranular Corrosion of Type 304 Stainless Steel," J. of Metals, p. 16, (Oct. 1982).

70. Hodges, R. J., "Intergranular Corrosion in High Purity Ferritic Stainless Steels: Effect of Cooling Rate and Composition," Corrosion, Vol. 27, p. 119, (1971).

71. Nichol, T. J., and Davis, J. A., "Intergranular Corrosion Testing and Sensitization of Two High Chromium Ferritic Stainless Steels," in Intergranular Corrosion of Stainless Alloys, ASTM STP 656, Steigerwald, R. F., ed., p. 179-196, ASTM (1978).

72. Sweet, A. J., "Detection of Susceptibility of Alloy 26-1S to Intergranular Attack," in Intergranular Corrosion of Stainless Alloys ASTM STP 656, Steigerwald, R. F., ed., p. 197-232, ASTM, (1978).

73. Holzworth, M. L., Beck, F. H., and Fontana, M. G., "The Mechanism of Knife-Line Attack in Welded Type 347 Stainless Steel," Corrosion, Vol. 7, p. 441, (1951).

74. Brown, M. H., "Behavior of Austenitic Stainless Steels in Evaluation Tests for the Detection of Susceptibility to Intergranular Corrosion," Corrosion, Vol. 30, p. 1, (1974).

75. France, W. D., and Greene, N. D., "Interpretation of Passive Current Maxima During Polarization of Stainless Steels," Corrosion, Vol. 24, p. 403, (1968).

76. Rockel, M. B., "Interpretation of the Second Anodic Current Maximum on Polarization Curves of Sensitized Chromium Steels in 1N H_2SO_4," Corrosion, Vol. 27, p. 95, (1971).

77. General Electric Report GEAP-24888 and U.S.N.R.C. NUREG/CR-1095, (May 1981).

78. Cihal, V., "A Potentiokinetic Reactivation Method for Predicting the I.C.C. and I.G.S.C.C. Sensitivity of Stainless Steels and Alloys," Corr. Sci., Vol. 20, p. 737, (1980).

79. Majidi, A., and Striecher, M. A., "Potentiodynamic Back-Scan Method for Detecting Sensitization in Types 304 and 304L Stainless Steels,: Paper 183 presented at NACE Conf. Houston, (April 1982).

80. Mignone, A., Borello, A., and LaBarbera, A., "The Electrochemical Potentiokinetic Reactivation Method - An Analysis of Different Treatments of Experimental Data," Corrosion, Vol. 38, p. 390, (1982).

81. Loria, E. A., "Intergranular Corrosion and End-Grain Pitting in Type 304 Stainless Steel by Various Test Methods," Corrosion, Vol. 37, p. 481, (1981).

82. Novak, P., Stefec, R., and Franz, F., "Testing the Susceptibility of Stainless Steel to Intergranular Corrosion by a Reactivation Method," Corrosion, Vol. 31, p. 344, (1975).

83. Vyas, B., and Isaacs, H. S., "Detecting Susceptibility to Intergranular Corrosion of Stainless Steel Weld Heat-Affected Zones," in Intergranular Corrosion of Stainless Alloys, ASTM STP 656, Steigerwald, R. F., ed., p. 133-145, ASTM,(1978).

84. AWS A4.2-74, "Standard Procedure for Calibrating Magnetic Instruments to Measure the Delta Ferrite Content of Austenitic Stainless Steel Weld Metal," (April 1974).

85. Greene, N. D., "The Classical Potentiostat: Its Application to the Study of Passivity," Corrosion, Vol. 15, p. 369t, (1959).

86. Nippes, E. F., Wawrousek, H., and Fleischman, W. L., "Some Properties of the Heat Affected Zone in Arc Welded Type 347 Stainless Steel," Weld. J., Vol. 34, p. 169s, (1955).

VITA

Steven J. Pawel was born in Dayton, Ohio on June 3, 1958. He attended high school in Oak Ridge, Tennessee and graduated from Oak Ridge High School in June 1976. The following Fall he entered The University of Tennessee, Knoxville and received a B.S. in Metallurgical Engineering in June 1980. Study toward an M.S. in Metallurgical Engineering at The University of Tennessee began in the Fall of 1980. This degree was awarded in June 1983. He plans on continuing his education toward a Ph.D. at The University of Tennessee. Career goals include applied research and an eventual teaching position.

The author is a student member of the American Society for Metals, the Metallurgical Society of AIME and the National Association of Corrosion Engineers.